Oxidative and nitrosative stress induced by the mineralocorticoid aldosterone

Mechanism of induction and role of signal transduction pathways and transcription factors

Dissertation zur Erlangung des

naturwissenschaftlichen Doktorgrades

der Bayerischen Julius-Maximilians-Universität Würzburg

vorgelegt von

Nina Queisser

aus Ludwigsburg

Würzburg 2010

Eingereicht am: 28.09.2010………………………………………………………………..

Mitglieder der Promotionskommission:

Vorsitzender: Prof. Dr. Roy Gross……..………………………………………………..

Gutachter: Prof. Dr. Helga Stopper……………………………………………………….

Gutachter: Prof. Dr. Ricardo Benavente…..……………………………………………...

Tag des Promotionskolloquiums: 08.12.2010…………………………………………

Doktorurkunde ausgehändigt am: …………………………………………………..

INDEX

ABBREVIATIONS

A	adenine
ABC	avidin biotin complex
ACE inhibitors	angiotensin converting enzyme inhibitors
Ald	aldosterone
ANOVA	analysis of variance
2-APB	2-aminoethoxydiphenyl borate
ARE	antioxidant responsive element
AT_1 receptor	angiotensin II type 1 receptor
Bcl-2	B-cell lymphoma 2
Bcl-XL	B-cell lymphoma-extra large
BH_4	tetrahydrobiopterin
BN	binucleated
BrdU	bromodesoxyuridine
BSA	bovine serum albumin
C	cytosine
Ca-	calcium free medium
cAMP	cyclic adenosine monophosphate
CAT	catalase
CBPI	cytokinesis block proliferation index
cIAP1	cellular inhibitor of apoptosis 1
CO	carbon monoxide
CREB	cAMP-responsive element
DAB	diaminobenzidin
DABCO	diazabicyclo octane
DAF	diaminofluorescein
DAG	diacylglycerol
DAPI	diamidino phenylindole
DCF	dichlorofluorescein
dG	dihydroguanine
DHE	dihydroethidium
DTT	dithiothreitol
DMEM	Dulbecco modified Eagle's minimal essentail medium
DMSO	dimethyl sulfoxide
DNA	deoxyribonucleic acid
DOCA	deoxycorticosterone acetate
DPI	diphenyleneiodonium chloride
DSB	double strand break
EDTA	ethylenediamine-tetraacetic acid disodium salt
EGTA	ethylene glycol tetraacetic acid
EMSA	electromobility shift assay
EpRE	electrophile responsive element
ERK1/2	extracellular signal-regulated kinase
EtOH	ethanol
FAD	flavin adenine dinucleotide
FBS	fetal bovine serum
Fe^{2+}	ferrous ion
FITC	fluorescein isothiocyanat
FPG	formamidopyrimidine DNA glycosylase
FRAP	ferric reducing ability plasma

Fura 2-AM	Fura 2-acetoxymethyl ester
γ-H2AX	phosphorylated histone 2AX
G	guanine
GCL	glutamate-cysteine ligase
GCLC	glutamate-cysteine ligase, catalytic subunit
GCLM	glutamate-cysteine ligase, modifier subunit
GPx	glutathione peroxidase
GR	glucocorticoid receptor
GSH	glutathione, reduced form
GSSG	glutathione, oxidized form
GST	glutathione S-transferase
h	hour
HCl	hydrochloric acid
HClO	hypochlorous acid
H_2DCF-DA	2',7'-dichlorofluorescein diacetate
HEPES	4-(2-hydroxyethyl)-1-piperazineethanesulfonic acid
HO-1	hemeoxygenase-1
H_2O_2	hydrogen peroxide
hOGG1	8-oxodG DNA glycosylase 1
HPLC	high performance liquid chromatography
HRP	horse radish peroxidase
IgG	immunoglobulin G
IKK	IκB kinase
IL	interleukin
IP_3	inositol triphosphate
JNK	c-Jun N-terminal kinase
KCl	potassium chloride
Keap1	kelch-like ECH-associated protein 1
KH_2PO_4	monopotassium phosphate
KOH	potassium hydroxide
LA	($\pm$)-α-lipoic acid
LC-MS	liquid chromatography-mass spectrometry
LLC-PK1	porcine kidney cell line
L-NAME	N-nitro-L-arginine methyl ester
M	mol per liter
μM	micromole per liter
MAPK	mitogen-activated protein kinase
MCB	monochlorobiamine
MDCK	Madin-Darby canine kidney cell line
MEK	mitogen-activated protein kinase kinase
min	minute
MN	micronuclei
MR	mineralocorticoid receptor
NAC	N-acetyl-L-cysteine
NaCl	sodium chloride
MSK	mitogen- and stress activated protein kinase
NADH	nicotinamide adenine dinucleotide, reduced form
NADPH	nicotinamide adenine dinucleotide phoshate, reduced form
NaOH	sodium hydroxide
NF-κB	nuclear factor kappa-B
8-NitroG	8-nitroguanine

nm	nanometer
nM	nanomole per liter
NOX	NAD(P)H oxidase
NO	nitric oxide
NO˙	nitric oxide radical
NOS	nitric oxide sythase
NQO1	NAD(P)H:quinone oxidoreductase-1
Nrf2	nuclear factor-erythroid-2-related factor 2
$^1O_2$	singulet oyxgen
O_2	molecular oxygen
$O_2^{˙-}$	superoxide anion
˙OH	hydroxyl radical
$ONOO^-$	peroxynitrite
8-oxodG	8-hydroxydeoxyguanosine
PBS	phosphate buffered saline
PBST	phosphate buffered saline containing Tween
PCR	polymerase chain reaction
PI	propidium iodide
PI3K	phosphoinositide-3 kinase
PKC	protein kinase C
PLC	phospholipase C
pM	picomol per liter
PMSF	phenylmethanesulfonyl fluoride
Prx	peroxiredoxin
Rac	member of a family of hydrolases that bind and hydrolyze GTP
Ras	member of a family of hydrolases that bind and hydrolyze GTP
RAAS	renin-angiotensin-aldosterone system
RNA	ribonucleic acid
RNS	reactive nitrogen species
ROS	reactive oxygen species
rpm	rounds per minute
RPMI	Roswell Park Memorial Institute medium
RSK	ribosomal s6 kinase
SEM	standard error of the mean
SOD	superoxide dismutase
Sp-1	specificity protein-1
STAT	signal transducer and activator of transcription
T	thymidine
TBS	tris buffered saline
TG	thapsigargin
TNF-α	tumor necrosis factor alpha
Tris	trishydroxymethylaminomethane
Trx	thioredoxin
UbL	ubiquitin ligase
W7	N-(6-aminohexyl)-5-chlor-1-naphthalinsulfonamid
XIAP	X-linked inhibitor of apoptosis protein

1   INTRODUCTION

1.1   *Increased cancer incidence of hypertensive individuals and involvement of the renin-angiotensin-aldosterone system*

Epidemiological studies detected an increased cancer incidence in hypertensive individuals [1-2]. A meta-analysis of ten longitudinal studies including approximately 50.000 patients found a 23 % higher cancer mortality of hypertensives [3]. Especially increased (75 % higher for all and 85 % higher for women) was their risk to develop renal cell carcinoma [3-4]. Several mechanisms have been described for the association between hypertension and cancer. Increased levels of cytosolic calcium and inositol triphosphate (IP$_3$) are probably involved in the pathogenesis of hypertension and in the early events of cell proliferation. Calcium levels and IP$_3$ are activated by endogenous mitogens and oncogenes [5] or by mitogenic effects of hormones which are known to be implicated in the development of high blood pressure like angiotensin II, catecholamines, vasopressin, insulin, mineralo- and glucocorticoids [5]. Furthermore, abnormalities in the apoptosis process that have been observed in hypertension could contribute to cancer development, since reduced apoptosis could possibly lead to cellular overgrowth [6]. Another reason is lipid peroxidation, which has been found to be elevated in hypertensive patients and might be partially responsible for the increased risk of renal cell carcinoma [7]. Hypertension and cancer share to some extent similar cellular and molecular characteristics [8-10] and genetic predisposition both to hypertension and to cancer might be another reason [11]. Finally, the association between hypertension and malignancy could be related to factors like age, smoking, alcohol consumption, and obesity, which affect both disorders [3].

The link between renal cell cancer and hypertension is not fully understood. It has been hypothesized that hypertension might be associated with functional and metabolic changes in the renal tubules that increase the susceptibility to carcinogens [12]. Various antihypertensive therapies were associated with an increased cancer risk; especially potential carcinogenic mechanisms of diuretics were in the focus of interest of many investigators. However, based on the totality of the clinical trial literature, commonly used antihypertensive drugs are not associated with increased odds of developing cancer [13]. Furthermore, the fact that different therapies were associated with an increased cancer risk is in disfavor of an explanation that specific

effects of the drugs are the cause of the elevated cancer risk and suggests the hypertension itself as the trigger [4, 11, 14]. This is underlined by the observation that also hypertensive individuals who never were under antihypertensive therapy have a higher incidence of renal cell carcinoma [15]. After finding an association between high blood pressure and renal tumors, Lee [16] was able to show that blood pressure returned to normal levels after elimination of the tumors. Others have observed that the risk of renal cell carcinoma in hypertensive patients was related to the duration of hypertension [17-18]. These observations hint at a contribution of hypertension to the pathogenesis of renal cell carcinoma rather than being a consequence of the malignancy.

Hyperaldosteronism, contrary to former understanding, is a frequent cause of arterial hypertension. The prevalence in newly diagnosed hypertensive patients remains uncertain, but a survey of 18 recent studies showed a wide range from 1.4% to 32% (median 8.8%). The plasma concentration of aldosterone in these patients ranges from 0.5 to 6.3 nM, with patients suffering from congestive heart failure reaching 8 nM [19-20]. Normal plasma aldosterone levels in humans range from 0.1 to 0.4 nM [20]. One criterion to screen for primary aldosteronism in hypertensive patients is when this level is exceeded [21]. In the adrenal vein far higher concentrations are reached, in patients with aldosterone-producing adenomas up to 405 nM and in patients with bilateral idiopathic hyperaldosteronism up to 585 nM [22-23].

1.2 Aldosterone signaling

The steroid hormone aldosterone (Figure 1) is synthesized from cholesterol in the zona glomerulosa of the adrenal glands upon stimulation by angiotensin II, potassium or the adrenocorticotropic hormone [24].
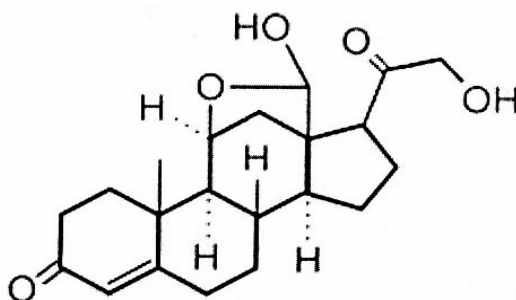
Figure 1: Structure of aldosterone.

Together with angiotensin II, it is the major effector of the renin-angiotensin-aldosterone system. Classically, it regulates sodium excretion, fluid balance and blood pressure homeostasis [25]. This regulation is achieved through binding of aldosterone to the cytosolic mineralocorticoid receptor (MR). The MR belongs to the larger family of nuclear receptors consisting of a DNA binding domain, a ligand binding domain and a N-terminal domain [26]. Hormone binding results in a conformational change and the activated receptor translocates into the nucleus, where it binds to hormone-responsive elements of target gene promotors and modulates their expression [24-25]. Consequently, the expression of various proteins like the epithelial sodium channel, Na-K-ATPase, the serum- and glucocorticoid-regulated protein kinase and the epidermal growth factor receptor is initiated [27]. These, so-called genomic actions of aldosterone occur through changes in gene expression and subsequent protein expression, which can be suppressed by inhibitors of transcription and translation.

Beside the classical genomic actions, aldosterone also exerts rapid, nongenomic effects, which are most probably mediated by the classical intracellular MR utilizing second messengers [28-29]. By this pathway aldosterone causes an increase of the intracellular calcium concentration and is associated with stimulation of phospholipase C (PLC), liberation of IP_3 and diacylglycerol (DAG), activation of protein kinase C (PKC), and of sodium–proton exchange in the kidney [26, 30]. Further reports show an activation of other kinases like extracellular signal-regulated kinase (ERK1/2), or phosphoinositide-3 kinase (PI3K) and protein kinase B (Akt) [31-32]. Nongenomic effects of aldosterone have been observed in many different epithelial and nonepithelial tissues and they are characterized by an insensitivity to inhibitors of transcription and translation, and a rapid time course (seconds to a few minutes), that is incompatible with gene regulation and de novo protein synthesis. This rapid onset of action is a sufficient but not a necessary criterion for a nongenomic effect. There also exist nongenomic effects with a slower time course [33]. Although nongenomic effects of aldosterone are clearly established, the receptor mechanisms responsible remain unclear (Figure 2). Two general mechanisms are discussed: 1) activation of nonclassical receptors, possibly membrane-associated and 2) rapid activation of the classical MR [30, 34-35]. Evidence for the latter includes i.e. that those nongenomic effects can be inhibited by the MR antagonists spironolactone or eplerenone. There are indications for an

interaction between nongenomic and genomic aldosterone signaling with the tendency that nongenomic effects enhance or support genomic effects [33-34].
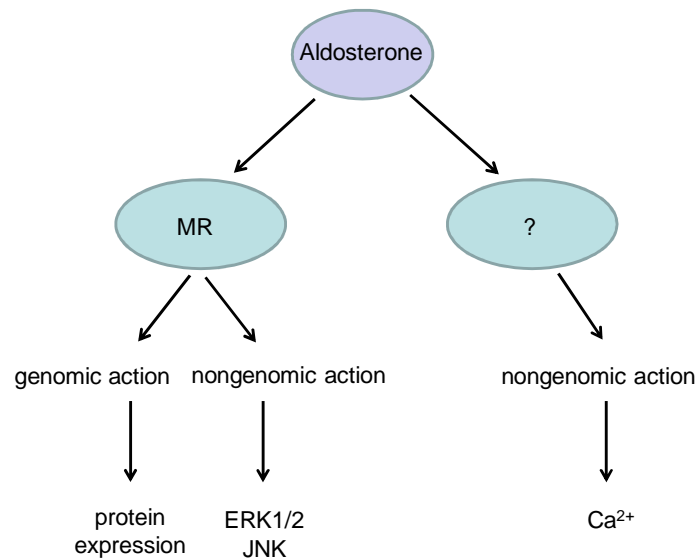
Figure 2: Scheme of the hypothesis of cellular aldosterone signaling.
There seem to exist three pathways of aldosterone signaling: 1) the classical, MR-dependent, genomic pathway, which leads to the expression of aldosterone-induced proteins; 2) a rapid, nongenomic but MR-dependent pathway leading to the activation of ERK1/2 and JNK; 3) a nongenomic, MR-independent pathway, leading to an increase of cytosolic calcium. © Modified after Grossmann *et al*. [27].

1.3 *Aldosterone induces cardiovascular complications and renal damage*

Studies demonstrating the effectiveness of MR antagonism in patients with resistant hypertension support the above mentioned high prevalence of hyperaldosteronism among this population [25]. Moreover, it is now recognized that primary aldosteronism implies excessive organ damage to the heart, vessels and kidney [21], resulting in more profound tissue damage than in age-, sex- and blood pressure-matched controls [36-37], and therefore causes severe cardiovascular, renal and metabolic complications. The cardiovascular complications can be ameliorated with MR antagonists, as was convincingly shown in two large clinical studies: In the RALES study, patients with severe heart failure received spironolactone in addition to an ACE inhibitor, diuretics and digoxin. This treatment regime reduced mortality by 30 % [38]. In the EPHESUS study, the MR antagonist eplerenone, together with ACE inhibitors, AT_1 receptor antagonists, β-blockers, digoxin and diuretics reduced all-cause and cardiovascular mortality in post-myocardial infarction patients with left ventricular dysfunction by 15 % [39]. Furthermore, elevated aldosterone levels

contribute to the development and progression of chronic kidney diseases [40-41]. Animal experiments have shown that chronically increased aldosterone causes severe glomerular and tubulointerstitial injury [42]. Protective effects of the MR blocker spironolactone against tubular damage and interstitial renal fibrosis, already reported for animal models [40], were shown in patients with proteinuric nondiabetic chronic kidney disease [43]. Multiple aldosterone-mediated mechanisms have been identified which might lead to these deleterious effects: involvement of growth factors or reactive oxygen species (ROS), potentiation of the pressor effects of angiotensin II and others [40, 44]. As a consequence, blockade of the MR reduces proteinuria and nephrosclerosis in the spontaneously hypertensive, stroke-prone rat and controls proteinuria in the subtotally nephrectomized rat model [44]. There is also evidence that aldosterone is a key factor in mediating renal injury in humans: plasma aldosterone levels are positively correlated with urinary protein excretion and negatively with glomerular filtration rates [45-47].

It is now acknowledged that one of the most important pathways by which aldosterone exerts its negative effects on the kidney is by generation of ROS [26]. The most important source of ROS is superoxide ($O_2^{\cdot-}$) generated by nicotinamide adenine dinucleotide phosphate (NAD(P)H) oxidase, which is activated via the MR [48-49].

1.4 Oxidative/nitrosative stress and DNA damage

ROS play a leading role in physiological and cellular processes. ROS and free radicals influence pathways involved in innate immunity, cell and tissue growth, angiogenesis, cell signaling, salt and fluid homeostasis, biochemical reactions, apoptosis, etc [50]. ROS are reactive chemical entities consisting of two major groups: Free radicals, e.g $O_2^{\cdot-}$ or hydroxyl moiety ($^{\cdot}OH$) and nonradical derivates of O_2 like hydrogen peroxide (H_2O_2) or peroxynitrite ($ONOO^-$) [51], that are either oxidizing agents and/or easily converted into radicals. Furthermore, free radicals can generally be subdivided in ROS, such as $O_2^{\cdot-}$ or $^{\cdot}OH$, and reactive nitrogen species (RNS) like the NO radical (NO) or $ONOO^-$. ROS or RNS are constantly generated in cells as important signaling molecules or as unwanted by-products of aerobic metabolism [52] (Figure 3). Free radicals are short-lived and after their role in the routine cellular maintenance is fulfilled, they are scavenged by several antioxidant

enzymes. An imbalance between the generation of ROS/RNS and the cellular antioxidant capacity turns into the state of "oxidative or nitrosative stress". In pathological conditions, ROS are involved in endothelial dysfunction, inflammation, cell proliferation, fibrosis, angiogenesis, etc [51].
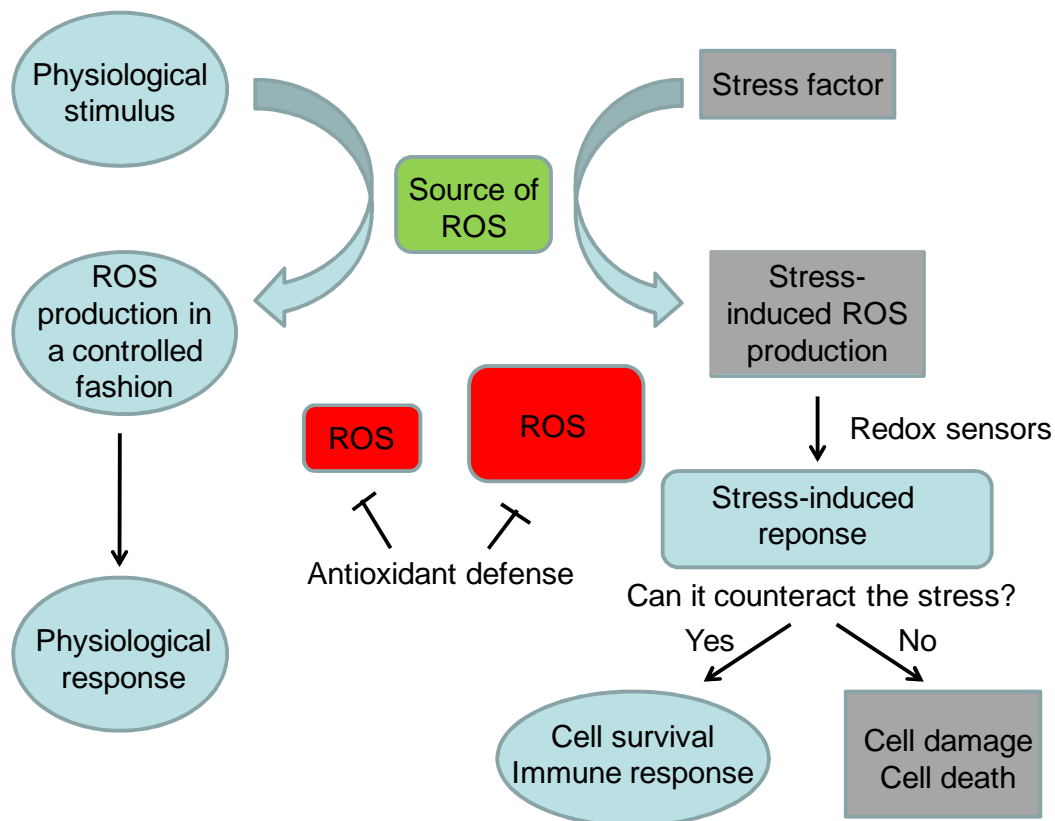
Figure 3: ROS in physiological and pathophysiological processes.
In response to various physiological stimuli, very low concentrations of ROS are produced in a controlled manner. Such generation is important and sometimes necessary for life. A number of stress factors induce an increase in ROS levels in a noncontrolled manner. This increase in the ROS levels can be counteracted (cell survivals) or can lead to cell death. © Modified after Pourova *et al.* [53].

Four endogenous processes significantly lead to DNA damage: oxidation, methylation, deamination and depurination, while the DNA damage produced by oxidative stress appears to be the most relevant endogenous damage [54]. About 10^5 oxidative lesions are formed per cell per day in rats and 10^4 in humans. ROS can directly produce single or double strand breaks, purine, pyrimidine or desoxyribose modifications and DNA cross-links [55]. Persistant DNA damage can result amongst others in replication errors or genomic instability, which is seen in cancer. Oxidative stress contributes to tumorigenesis by either directly attacking DNA to cause genetic alterations or through epigenetic mechanisms i.e. by modulating downstream

signaling pathways, such as transcription factors, tyrosine kinases/phosphatases, ion channels, mitogenic factors, and cytokines [56]. ROS can insert structural changes in cancer-related genes like chromosomal aberrations and point mutations. The most frequent genetic changes in human malignancies are point mutations in the ras-family of protooncogenes and in the p53 tumor suppressor gene, and at least some of them may be caused by oxidants [57]. Oxidative DNA damage is a major source of mutations in living cells, with more than one hundred oxidative DNA adducts having been identified [58]. The most prominent DNA modification 8-oxo-7,8-dihydro-2´-deoxyguanosine (8-oxodG) results from the oxidation of guanine at the C8 position. 8-oxodG can pair with both cytosine and adenine. If the A:G mismatch is not repaired, a G:C to T:A transversion will occur, widely found in mutated oncogenes and tumor suppressor genes [59]. Numerous studies have demonstrated that 8-oxodG levels are elevated in various human cancers [60-63]. Permanent modification of genetic material resulting from this "oxidative damage" represents the first step involved in mutagenesis, carcinogenesis and ageing.

1.5 Prooxidant enzymes

The predominant radicals in biological regulation are $O_2^{\cdot-}$ and NO. Both radicals are rapidly converted by enzymes or nonenzymatic chemical reactions into reactive nonradical species such as H_2O_2, singulet oxygen ($^1O_2$) or $ONOO^-$. Thus, most of the regulatory effects are not directly mediated by $O_2^{\cdot-}$ but rather by its ROS/RNS derivates [51, 64]. $O_2^{\cdot-}$ and NO are mainly formed by two groups of enzymes: the NAD(P)H oxidase and the nitric oxide synthase (NOS) isoforms, respectively [64].

1.5.1 NAD(P)H oxidase

NAD(P)H oxidase is a multi-enzyme complex which catalyzes the production of $O_2^{\cdot-}$ by the one-electron reduction of O_2 using NADPH or NADH as the electron donor [65]. The complex is made up of both membrane and cytosolic components. The membrane complex is composed of two subunits: gp91^{phox} (91-kDa protein), now termed Nox2 and p22^{phox} (22-kDa protein), which together form a heterodimeric flavohemoprotein known as cytochrome b_{558}. The cytosolic components include p40^{phox} (40-kDa protein), p47^{phox} (47-kDa protein), which is considered as an organizer subunit, p67^{phox} (67-kDa protein), the activator subunit and Rac [66-67].

The activation of the NAD(P)H oxidase requires the recruitment of the main membrane integral subunit gp91^{phox} with other membrane (p22^{phox}) and cytosolic components (p47^{phox}, p67^{phox}, p40^{phox} and Rac), requiring phosphorylation of the cytosolic component p47^{phox} which enables the entire cytosolic complex to migrate to the membrane, where it is associated with cytochrome b$_{558}$ to form the active oxidase (Figure 4).
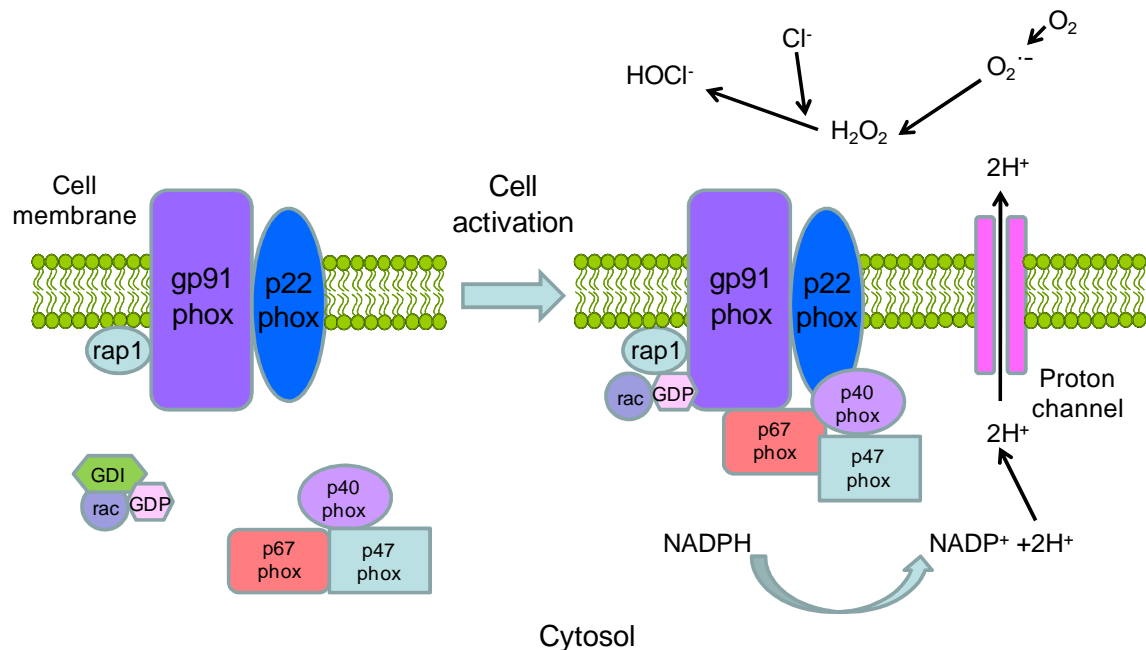
Figure 4: Schematic representation of the NAD(P)H oxidase enzyme and its activation.
NAD(P)H oxidase consists of the membrane subunits gp91phox and p22phox, forming a heterodimeric flavohemoprotein known as cytochrome b$_{558}$ and of the cytosolic subunits p40phox, p47phox and p67phox, that translocate to the membrane upon cell activation to form the NAD(P)H oxidase complex, which generates O$_2$$^{\cdot-}$. © Modified after www.medimmunol.com /content/5/1/4/ figure/F1

Although NAD(P)H oxidase was initially described in the hematopoietic system, it was subsequently also discovered in other cell types. NAD(P)H oxidase is an ubiquitous enzyme that plays an important role in signaling. The binding of different ligands to receptors that trigger the activation of signaling cascades is often associated to NAD(P)H oxidase activation [68]. Thus, long-term NAD(P)H oxidase activation could lead to a constant activation of signals that although initially protective, could lead to cellular damage and transformation. While the activation of kidney NAD(P)H oxidase has been described in hyperaldosteronism, the underlying cause remains unknown. Although the exact mechanisms of NAD(P)H oxidase activation are not fully described, it is known that calcium is a critical NAD(P)H oxidase regulator, activating the enzyme either directly or indirectly [69].

1.5.2 Nitric oxide synthase (NOS)

There are three isoforms of NOS, designated neuronal NOS (nNOS or NOS1), inducible NOS (iNOS or NOS2) and endothelial NOS (eNOS or NOS3) [70]. Expression of all three NOS isoforms has been reported in the kidney, but their distribution and regulation differs and there remains some controversy over the specific expression of functional protein for the NOS isoforms in specific renal cell populations. The regulation of nNOS and eNOS is complex and involves several post-translational steps including multi-site phosphorylation, protein-protein interactions and subcellular translocation [71]. NOS enzymes catalyze the synthesis of NO via a five electron oxidation of a guanidine group in L-arginine. Because of the high chemical reactivity and high diffusibility of NO, its production by each of the three NOS isoforms is regulated tightly at multiple levels from gene transcription to spatial proximity near intended targets to covalent modification and allosteric regulation of the enzyme itself [72]. Both, nNOS and eNOS are historically regarded as constitutive enzymes with low basal activity, which are activated by calcium and then cause binding of calmodulin as cofactor. Calmodulin serves as an allosteric modulator of the NOS isoforms and as intracellular calcium concentrations fall, calmodulin dissociates from eNOS [71]. Availability of substrate and cofactors as limiting factor of NOS activity has been primarily attributed to pathophysiological situations. However, cofactor availability may also be a physiological regulator of NOS activity [73].

NO is a very important molecule in cell signaling regulating important physiological processes. NO regulates sodium and water homeostasis via numerous mechanisms and appropriate levels of NO production are important in protecting an organ from damage. However sustained levels of NO production result in direct tissue toxicity and contribute to the vascular collapse associated with septic shock, whereas chronic expression of NO is associated with various carcinomas [74]. NO normally regulates vasodilation resulting in a decrease in blood pressure, therefore, impaired renal NO synthesis is implicated in the pathogenesis of hypertension [75]. NO can chemically modify lipids and proteins, and its reaction with $O_2^{\cdot-}$ generates the highly reactive species $ONOO^-$ (Figure 5), which thereby restricts the half-life, diffusion distance and bioactivity of NO in tissues [76]. The interplay NAD(P)H oxidase – calcium – NOS is considered very relevant in redox signaling [77].
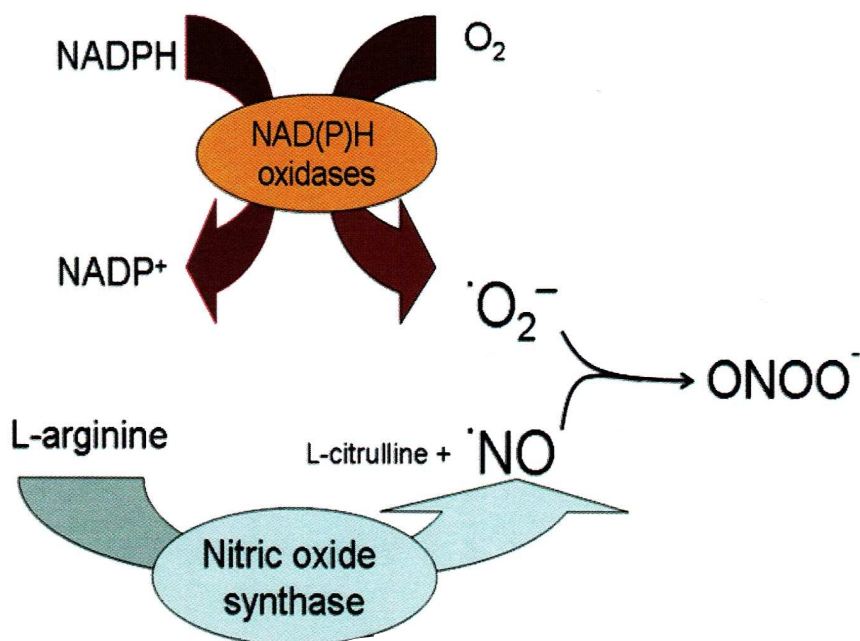
Figure 5: Induction of oxidative stress through activation of NAD(P)H oxidase and NOS.
Stimulation of the activation of NAD(P)H oxidase and NOS resulting in the formation of $O_2^{\cdot-}$ and $NO^{\cdot}$, respectively. The highly reactive $ONOO^-$ is formed, which can damage the DNA more severely than the parent radicals. © Modified after Marney and Brown [25].

1.6 Antioxidants

Exposure to free radicals from a variety of sources has led organisms to develop a series of defense mechanisms [78] (Figure 6). These defense mechanisms include: 1) preventive mechanisms, 2) repair mechanisms, 3) physical defenses, and 4) antioxidant defenses. The latter can be split into 1) enzymatic antioxidant defenses including antioxidant enzymes like superoxide dismutase (SOD), glutathione peroxidase (GPx) and catalase (CAT) (Figure 6) or detoxification enzymes (phase II enzymes) such as NAD(P)H:quinone oxidoreductase-1 (NQO1) or glutathione S-transferase (GST) and 2) nonenzymatic antioxidant defences represented by ascorbic acid, α-tocopherol, flavonoids, thioredoxin (Trx), glutathione (GSH) and other antioxidants [79].
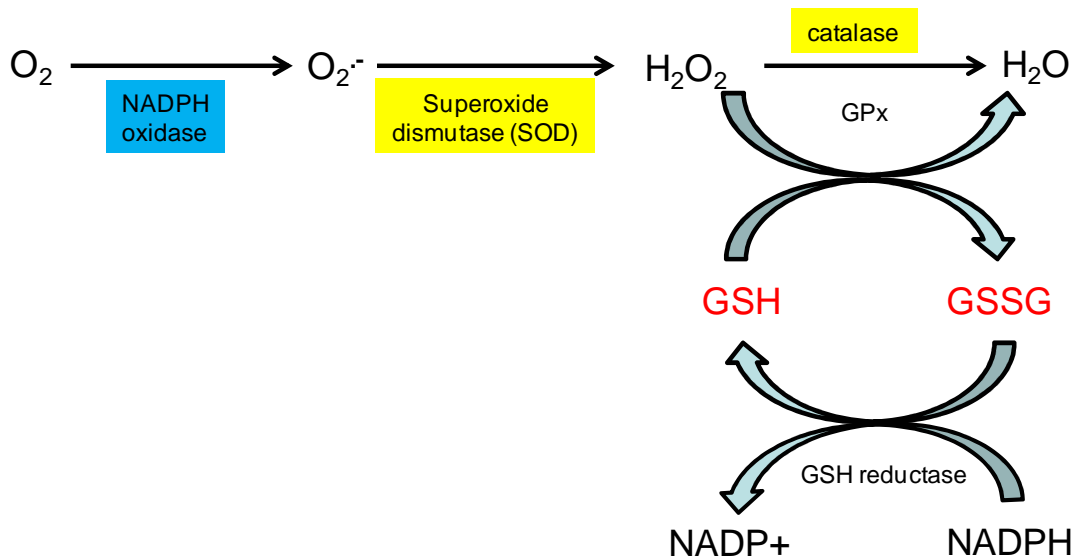
Figure 6: Pathways of ROS production and clearance.
$O_2^{.-}$ is formed by enzymes such as NAD(P)H oxidase. SOD converts superoxide enzymatically into H_2O_2 and thus, the enzymes catalase or GPx can convert H_2O_2 into water. In the GPx reaction GSH is oxidized to GSSG, which can be converted back to GSH by GSH reductase in a NADPH-consuming process. © Modified after Dröge [64].

The tripeptide glutathione, which is the most abundant thiol in mammalian cells, is synthesized in the cytosol by the sequential action of glutamate-cysteine ligase (GCL) and glutathione synthetase. GCL, the rate-limiting enzyme in GSH biosynthesis, exists as a heterodimer comprising a large catalytic subunit (GCLC) and a small modifier subunit (GCLM). Glutathione is present in a reduced (GSH) and an oxidized (GSSG) form [80]. GSH is 10- to 100-fold higher than GSSG. The ratio GSH/GSSG is normally closely regulated and a minor elevation of the oxidation of GSH to GSSG can result in a significant elevation in intracellular GSSG levels. The GSSG content increases under enhanced oxidative stress conditions and may damage many enzymes oxidatively. Therefore, the ratio GSH/GSSG is a good indicator of oxidative stress of an organism. GSSG can be reduced to GSH by the NADPH dependent GSH reductase as well as via the thioredoxin system [55, 81]. GSH exerts its protective functions via different mechanisms: 1) GSH is a cofactor of several detoxifying enzymes against oxidative stress e.g. GPx; 2) GSH participates in amino acid transport through the plasma membrane; 3) GSH is a direct scavenger of $^{.}OH$ and $^1O_2$; 4) GSH can regenerate the most important antioxidants vitamin C and E back to their active forms. Depletion of cellular GSH levels and suppression of its synthesis have been implicated in the pathogenesis of human diseases like cancer. Another ubiquitiously expressed antioxidant is Trx. It acts as reductase in redox control, protects proteins from oxidative aggregation and

inactivation, helps the cells to overcome various environmental stresses (ROS, $ONOO^-$ and arsenate) and regulates programmed cell death via denitrosylation [82-83]. The antioxidant enzyme heme oxygenase 1 (HO-1) is induced in response to oxidative stress. It catabolizes prooxidant heme into ferrous iron (Fe^{2+}), carbon monoxide (CO), and biliverdin which is quickly converted into bilirubin. These endproducts have antioxidative capacity and are therefore able to protect the cells from oxidative stress [84] (Figure 7). There are reports that bilirubin may directly inhibit NAD(P)H oxidase by interrupting the assembly and activation of the enzyme in endothelial cells and *in vivo* [85-86].
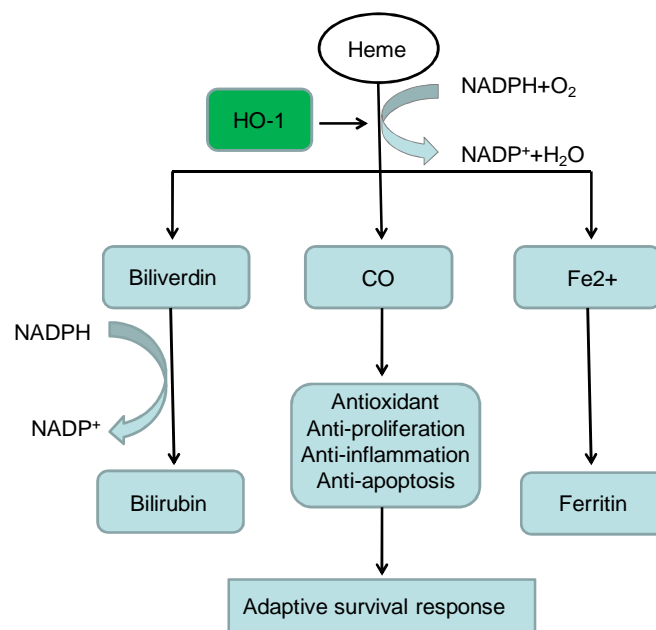
Figure 7: Adaptive cellular survival response through induction of HO-1.
HO-1 catalyzes equimolar production of biliverdin, Fe^{2+} and CO in the course of degrading and eliminating the potentially toxic free heme. © Modified after Surh *et al.* [87].

1.7 ROS modulation of gene expression

The biological mechanisms through which cells communicate with each other or react on external stimuli are called cell signaling or signal transduction [88]. Signal transduction is a process allowing information to be transferred from the outside of a cell to diverse functional elements inside the cell. ROS-induced alteration of gene expression can occur through a modulation of various signaling pathways including cyclic adenosine monophosphate (cAMP)-mediated cascades, calcium-calmodulin pathways and intracellular signaling transducers such as NO [89-90]. All cell types

are somehow dependent on the generation of cytoplasmic calcium signals to regulate cell function, or to trigger specific responses. Normally, these signals involve a combination of release of calcium from intracellular stores and influx of calcium across the plasma membrane [91]. Several studies have demonstrated that ROS can release calcium from intracellular stores, resulting for example in the activation of PKC, which regulates proliferation, cell cycle, differentiation, cytoskeletal organization, cell migration and apoptosis [92]. While high levels of ROS production may lead to the induction of apoptosis or necrosis, increasing evidence indicates that low or transient ROS exposure induces cell proliferation, likely through altered expression of growth factors and proto-oncogenes [93]. Signals sent to the transcriptional machinery responsible for expression of defined genes are generally transmitted to the cell nucleus by different transcription factors, a specific class of proteins. The effects of ROS have been related to the activation of transcription factors. The most significant effects of ROS have been observed on the signaling pathways of nuclear factor-erythroid-2-related factor 2 (Nrf2) [94], nuclear factor-κB (NF-κB) [95] and mitogen-activated protein (MAP) kinase/extracellular signal-regulated kinase (ERK) [96].

1.7.1 Transcription factor Nrf2

The induction of the expression of antioxidant enzymes involved in the deactivation of ROS/RNS and in the elimination or detoxification of electrophiles [97], is achieved among others by activating the transcription factor Nrf2. Nrf2 is a member of the Cap'n'Collar subfamily of the basic leucine zipper transcription factors, and is essential for the coordinated induction of genes encoding many stress-responsive or cytoprotective enzymes and related proteins, such as NQO1, SOD, GST, GPx, HO-1, GCL, CAT, Trx and peroxiredoxin (Prx). Besides its role in regulating carcinogen detoxification and the cellular antioxidant defense, Nrf2 also has antiinflammatory functions [98]. In resting cells, Nrf2 is sequestered in the cytoplasm as an inactive complex with the repressor Kelch-like ECH-associated protein 1 (Keap1). Upon exposure of cells to oxidative/nitrosative stress, Keap 1 undergoes a conformational change, liberating Nrf2. Nrf2 translocates into the nucleus, where it forms heterodimers with small Maf proteins and binds to the antioxidant responsive element (ARE) sequences or the electrophile responsive element (EpRE)

sequences present in the promotor/enhancer regions of genes encoding many antioxidant and detoxifying enzymes [97-100] (Figure 7).
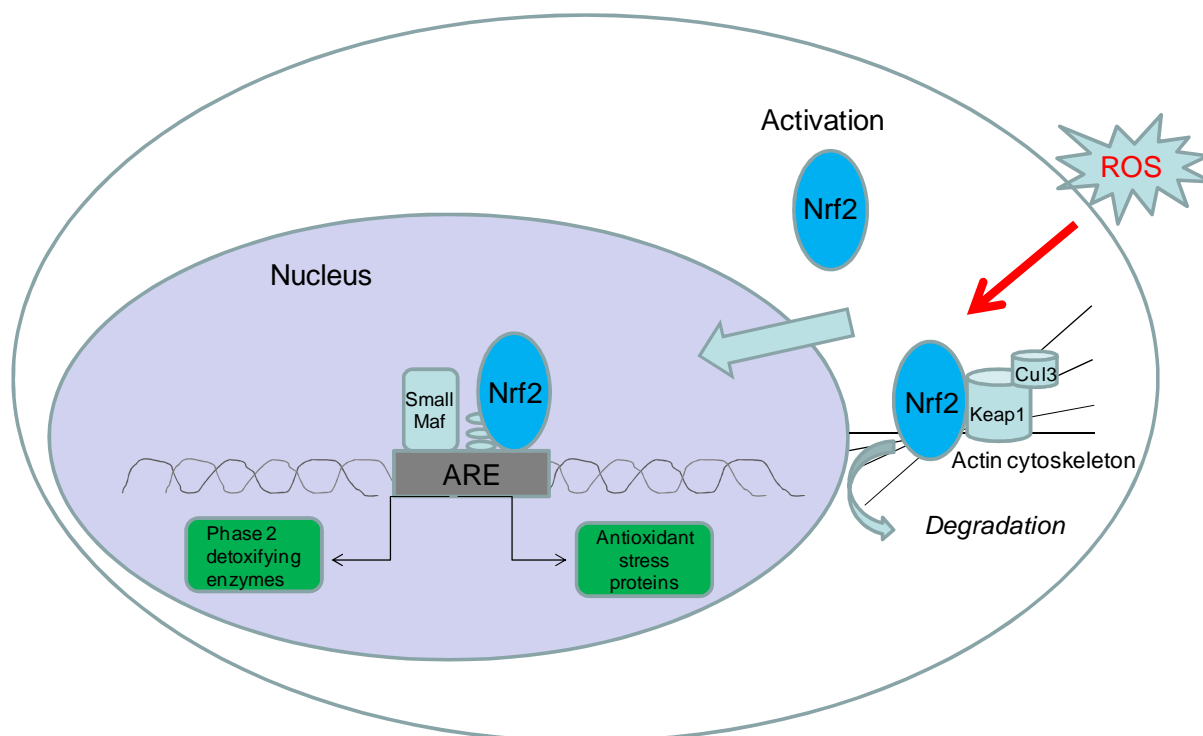
Figure 8: Schematic illustration of the transcriptional activation by Nrf2.
In resting conditions, Nrf2 is bound onto actin fibers in the cytoplasm through Keap1 and degraded by proteasomes. In this state, the transcription levels of target genes are low. Upon exposure to electrophiles and/or oxidative stress, Nrf2 translocates into the nucleus, heterodimerizes with its obligatory partner Maf and binds to the ARE, leading to the transcriptional activation of phase II enzyme genes and antioxidant stress protein genes. Keap1 interacts with Cul3, which seems to attack the sulfhydryl group of Keap1 and interferes with the interaction between Nrf2 and Keap1 or with the integrity of Keap1 and the ubiquitination machinery, resulting in the release of Nrf2 from Keap1 or the shutdown of Nrf2 degradation. © Modified after Motohashi and Yamamoto [100].

Low levels of Nrf2 activity appear to increase ROS production and DNA damage and predispose cells to tumorigenesis [93]. Based on the function of Nrf2 target genes, one can easily conclude that activation of Nrf2 may protect cells from various stresses of toxic exposure. Indeed, the Nrf2-mediated antioxidant response is one of the major cellular defense mechanisms that facilitate cell survival under toxic insults [101].

1.7.2 Transcription factor NF-κB

The transcription factor NF-κB is ubiquitiously expressed and regulates various cellular processes, including inflammation, immunity, cell proliferation and apoptosis [102]. NF-κB is composed of homo- or heterodimers of the Rel protein family,

including p50 (NF-κB1), p52 (NF-κB2), c-Rel, v-Rel, Rel A (p65), and Rel B, with the p50/p65 heterodimer being the classic and most common form. The nature of the dimer dictates its transcriptional activity on each promotor [103].
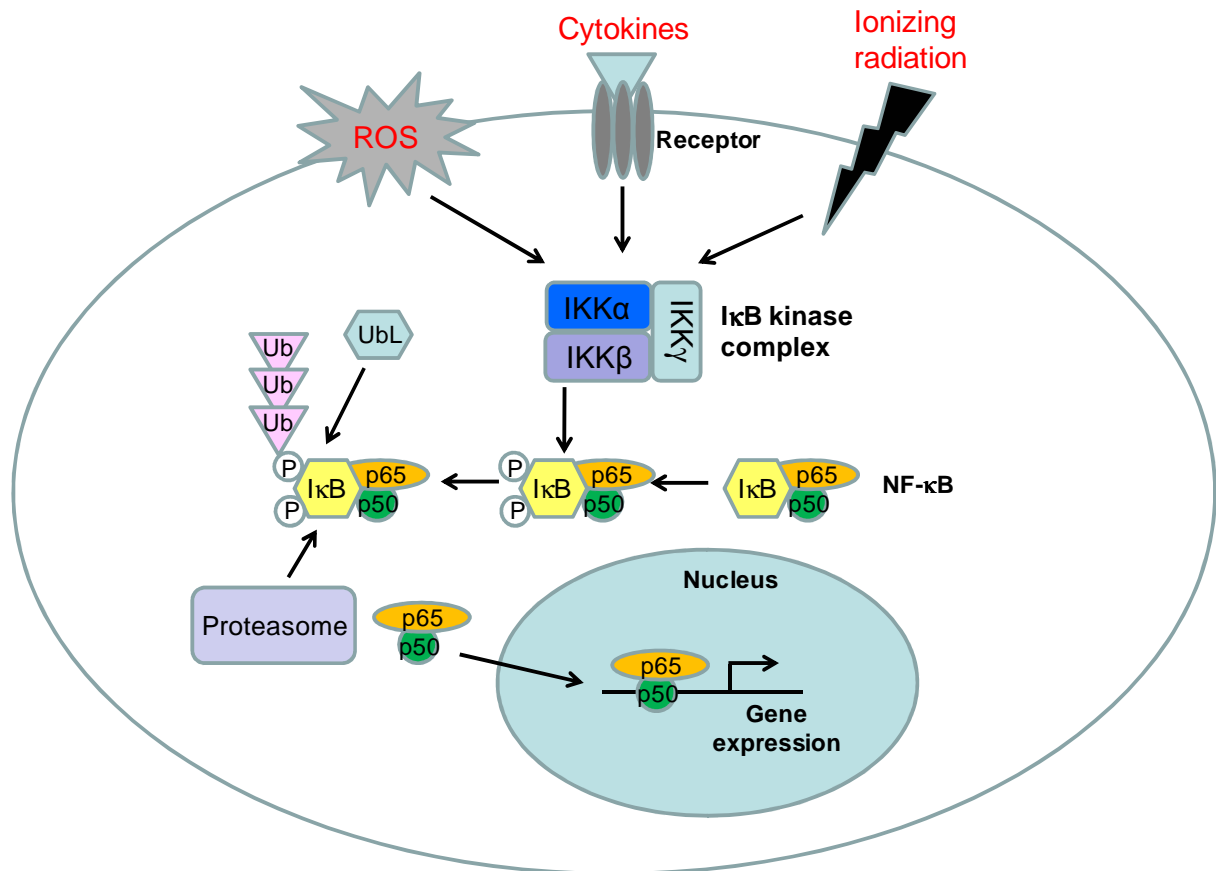
Figure 9: Pathway of NF-κB activation.
Cytokines, ROS and environmental hazards such as ionizing radiation trigger the nuclear translocation of NF-κB by activating the IκB kinase complex (IKK). IKK phosphorylates the inhibitor protein of NF-κB, IκB, marking it for ubiquitination by an ubiquitin ligase (UbL) and its degradation by the proteasome, which in turn results in the release of NF-κB. NF-κB is free and can be translocated into the nucleus where it binds to a defined DNA sequence and activates the transcription of target genes. © Modified after Haefner [104].

Inhibitors of NF-κB (IκB family of proteins) regulate NF-κB-activity by directly interacting with the transcription factor, masking the nuclear localization signal and thereby retaining NF-κB in the cytoplasm. NF-κB is activated by a large variety of stimuli: cytokines, bacterial lipopolysaccharides, phorbol myristate acetate, virus, oxidative stress, ultraviolet and ionizing radiation and genotoxic drugs [105]. Upon cell stimulation, the phosphorylation and degradation of the IκB proteins, a process that depends on the IκB kinase (IKK) complex, releases the active NF-κB which translocates into the nucleus, where it binds to the promoter or enhancer regions of several hundred genes, including cytokines/chemokines, immunoreceptors, cell-

adhesion molecules, acute phase proteins, stress-response genes, apoptosis regulators, transcription factors, and others [102, 106] (Figure 9). The prosurvival activity of NF-κB is exerted through several antiapoptotic proteins including B-cell lymphoma 2 (Bcl-2), B-cell lymphoma-extra large (Bcl-XL), cellular inhibitor of apoptosis (cIAP) and X chromosome-linked inhibitor of apoptosis (XIAP) [107]. Bcl-2 and Bcl-XL prevent apoptosis by inhibiting the permeability transition and the depolarization of mitochondria and subsequent cytochrome c release [108-109]. cIAP and XIAP directly bind and inhibit effector caspases, acting downstream of initiator caspases.

When deregulated, NF-κB activity may contribute to pathological events like chronic inflammatory diseases and various cancers [104]. In this regard, NF-κB plays a key role in different aspects of cancer biology, including malignant transformation, tumor progression, and cancer chemoresistance [110-111].

1.7.3 MAP kinase/ERK pathway

ROS have been shown to activate several signaling protein kinases, such as ERK1/2 [112-114]. The MAPK/ERK1/2 pathway is a ubiquitous signaling module that forms a link between extracellular signals and effector molecules in the cytoplasm and the nucleus, contributing to cell differentiation, proliferation and survival [115]. MAPKs are conserved proteins which represent a cascade of phosphorylation events including three crucial kinases, namely Raf, MEK (MAP kinase kinase), and ERK (MAP kinase) [116]. Raf phosphorylates and thus activates MEK1/2, which in turn culminates in the activation of ERK1/2 (Figure 10). Most experimental data suggest that ERK1 and ERK2 are functionally equivalent and both MEK and ERK isoforms are usually co-expressed [117-118]. MEK1 and MEK2 are the only commonly accepted downstream substrates of Raf [119-120] and ERK1 and ERK2 are the only identified substrates of MEK1/2 [121]. Studies demonstrated that ERK activation, which can be elicited by aldosterone, is involved in renal damage [122] and thus is likely to have a pathophysiological significance. Furthermore, the ERK signaling cascade plays an important role in cancer pathogenesis. Numerous solid tumors are known to express constitutive levels of phosphorylated ERK1 and 2 and the ERK pathway has been validated as target for novel anticancer therapies [123]. Constitutive activation of MEK has been shown to result in cellular transformation

[124]. Additionally, rapid MAPK activation influences gene transcription through phosphorylation of transcription factors, leading to changes in protein expression profiles with biological consequences [125-127].
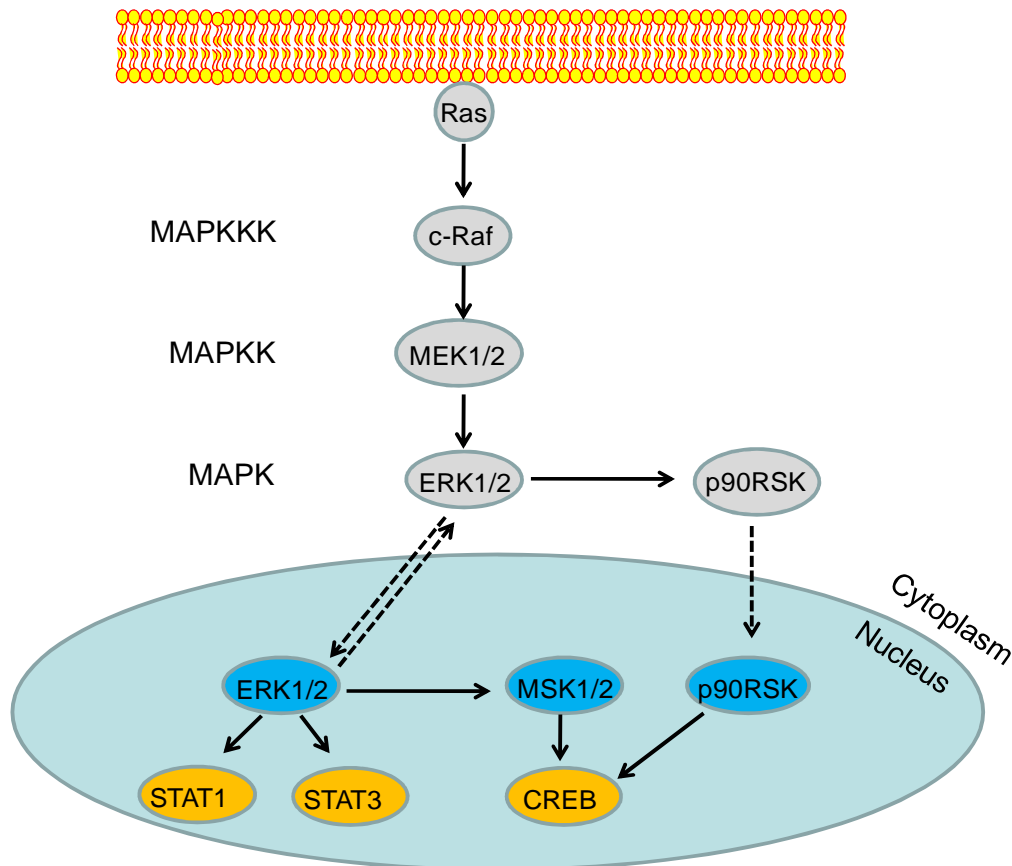
Figure 10: Schematic representation of the MAPK/ERK pathway.
The basic arrangement of this signal cascade includes the G-protein Ras working upstream of a core module consisting of 3 kinases: Raf (MAPKKK) that phosphorylates and thus activates MEK1/2 (MAPKK), which in turn results in the activation of ERK1/2 (MAPK). ERK1/2 phoshorylates and activates a variety of transcription factors such as STAT1 and STAT3 or CREB via MSK1/2 or p90RSK. MAPKs are largely characterized as serine/threonine kinases which are impicated in cell survival. © Modified after www.cellsignal.com.

ERK is a serine/threonine kinase with more than 50 identified substrates [128]. Three classical targets of ERK are e.g. the transcription factors cAMP-response element binding (CREB) protein and signal transducer and activator of transcription 1 and 3 (STAT1/3) [129] (Figure 10).

1.7.3.1 Transcription factor CREB

CREB is a transcription factor with multiple functions [130] and it is important in the survival of a variety of cell types under different stress conditions including DNA

damage [131-133]. ERK phosphorylates CREB through p90 ribosomal S6 kinases (p90RSK) [134] or through MSK (mitogen- and stress-activated protein kinase) 1 and MSK2 [135]. RSKs catalyze the phosphorylation of CREB at the Ser133 site that leads to CREB activation [131]. The activated CREB regulates the transcription of several genes that have the CREB binding site in their promotor region, including those with survival function. Thus, the activation of ERK and the subsequent induction of CREB-mediated transcription are essential for the survival of mouse proximal tubule cells during oxidant injury [136-137]. Arany *et al*. found that moderate (nonlethal) oxidative stress activates signaling via ERK to CREB and facilitates survival of renal cells, while during severe oxidative stress cells undergo necrotic death in the absence of ERK/CREB activation [136].

1.7.3.2 STAT transcription factors

The signal transducer and activator of transcription (STAT) proteins comprise a family of transcription factors consisting of seven different members: STAT1, 2, 3, 4, 5A, 5B and 6. STATs are activated by a series of extracellular signaling proteins such as growth factors or hormones and they are involved in normal physiological processes such as proliferation, apoptosis and differentiation [138]. STATs (STAT1, STAT3 and STAT4) get phosphorylated at a specific serine/threonine residue which is mediated amongst others by ERKs [129, 139]. Normally, activation of STAT proteins is transient and under tight control, while abberrant constitutive activation of STAT signaling is associated with uncontrolled growth and is frequently observed in cancers [140]. Several studies have shown the activation of STAT1 and STAT3 in renal cell carcinoma [141-143]. Although they do not directly regulate cell cycle checkpoints or contribute to the repair of DNA damage, they take part in tumorigenesis by deregulating signaling pathways in which they are implicated [144]. Potential prosurvival effects of STAT1 under stress conditions have been described earlier [145-146]. STAT3 assumes the role of a true protooncogene [147]. The oncogenic potential of STAT3 derives from the fact that it is able to promote the expression of antiapoptotic (e.g. Bcl-xl) and proproliferative (e.g. c-myc) proteins [148]. STAT1 and STAT3 might be considered as molecular markers for early detection of certain types of cancers and also prognostic indicators for determining tumor aggressiveness.

2 OBJECTIVES

Oxidative stress appears to be the most relevant endogenous damage and is involved in many diseases like hypertension or cancer. ROS contribute to tumorigenesis by directly attacking DNA to cause genetic alterations or through epigenetic mechanisms i.e. by modulating downstream signaling pathways or transcription factors. An increased risk to develop renal cancer was found in a subgroup of hypertensive individuals. Since hyperaldosteronism is a frequent cause of arterial hypertension, this work was dedicated to characterize the genomic damage caused by the blood pressure-regulating hormone aldosterone. Several mechanisms have been proposed for the pathological actions of aldosterone, including the stimulation of ROS formation via NAD(P)H oxidase.

The objectives of this thesis were to investigate the effects of aldosterone on cellular damages in two kidney cell lines, LLC-PK1 and MDCK, and in kidneys of deoxycorticosterone acetate (DOCA)/salt-treated rats. Furthermore, the underlying mechanisms of aldosterone signaling *in vitro* were elucidated and discussed. For this purpose the effects of aldosterone on the following parameters were evaluated:

- Oxidative stress: measurement of ROS formation semiquantitatively by flow cytometry and quantitatively by fluorimetry. $O_2^{\cdot-}$ generation was detected by dihydroethidium (DHE) staining.

- Nitrosative stress: detection of NO formation fluorimetrically and microscopically.

- DNA damage: assessment of DNA single and double strand breaks and micronuclei by comet assay and micronucleus test, respectively. Double strand breaks were further specifically detected by staining cells and tissue with anti-γ-H2AX antibody.

- Oxidative DNA damage: detection of 8-oxodG lesions by liquid chromatography-mass spectrometry (LC-MS), formamidopyrimidine DNA glycosylase (FPG) comet assay and immunocytochemistry.

- Nrf2 activation: measurement the Nrf2-DNA binding activity by electromobility shift assay (EMSA) and the expression of Nrf2-regulated antioxidative genes by western blot. Furthermore, the consequences of Nrf2 activation on DNA damage were investigated.

- NF-κB activation: measurement of the NF-κB-DNA binding activity by EMSA and expression of NF-κB-regulated antiapoptotic genes by western blot.

- ERK activation in the cytosol and nucleus: assessment of the activation state of the upstream and downstream kinases of the signaling cascade by western blot.

- CREB/STAT1/STAT3 activation by ERK: measurement CREB/STAT-DNA binding activity by EMSA and western blot.

- Involvement of oxidants in DNA damage and the activation of Nrf2, NF-κB, ERK, CREB, STAT1 and STAT3, by use of antioxidants.

- Involvement of the MR, intracellular calcium levels, NAD(P)H oxidase and NOS in oxidative stress, DNA damage, activation of ERK and transcription factors, by use of appropriate inhibitors.

3 MATERIALS AND METHODS

3.1 Materials

3.1.1 Cell lines and cell culture reagents

Two kidney cell lines with different characteristics were used: LLC-PK1 cells from pig kidney, which resemble proximal tubule cells and MDCK cells from dog kidney which resemble distal tubule cells.

LLC-PK1 and MDCK cells were obtained from the American Type Culture Collection (Manassas, VA, USA). Cell culture media and reagents were obtained from PAA Laboratories GmbH (Pasching, Austria) and Invitrogen Life Technologies (Carlbad, USA).

3.1.2 Animals

Sprague-Dawley rats were obtained from Charles River Laboratories, Research Models and Services, Germany GmbH (Sulzfeld, Germany).

3.1.3 Chemicals and Reagents

If not mentioned otherwise, all chemicals were purchased from Sigma Aldrich (Taufkirchen, Germany or St. Louis, MO, USA), Biomol (Hamburg, Germany) or Invitrogen Life Technologies (Darmstadt, Germany and Carlsbad, CA, USA).

(R)-BR-4628 (ethyl(4R)-5-acetyl-2,6-dimethyl-4-(2-methyl-4-oxo-4H-chromen-8-yl)-1,4-dihydropyridine-3-carboxylate), a potent and selective nonsteroidal mineralocorticoid antagonist [149] and its less active (S)-enantiomer were provided by Bayer HealthCare AG (Wuppertal, Germany). VAS2870 was kindly donated by Vasopharm BIOTECH GmbH (Würzburg, Germany). The reagents for the electro mobility shift assay (EMSA) were obtained from Promega (Madison, WI, USA). PVDF membranes were obtained from BIO-RAD (Hercules, USA) and Chroma Spin-10 columns were obtained from Clontech (Palo Alto, USA). The ECL plus western blotting system was from Amersham Pharmacia Biotech Inc. (Piscataway, USA).

3.1.4 Antibodies

The antibodies against ß-Tubulin (sc-9104), ERK (sc-93), γ-Gclc (sc-22755), γ-Gclm (sc-22754), hnRNP (sc-32301), IκBα (sc-371), NQO1 (sc-25591), Nrf2 (sc-722), p47-phox (sc-14015), phospho-ERK (sc-7383) and Trx1 (sc-13526) were obtained from Santa Cruz Biotechnology (Santa Cruz, CA, USA), cleaved caspase-3 (9661), cRaf (9422), MEK1/2 (9122), phospho-CREB (9191), the phospho-ERK1/2 pathway sampler kit (9911), phospho-IκBα (9246), phospho-MSK1 (9595), phospho-STAT1 (Ser727) (9177) and phospho-STAT3 (Ser727) (9134) were purchased from Cell Signaling Technology Inc (Beverly, USA) and α-Tubulin (T6199) was purchased from Sigma (St. Louis, MO). BrdU (ab1893) was obtained from Abcam (Cambridge, UK), HO-1 (SPA-896) was purchased from Stressgen (St. Louis, MO, USA), 8-oxoG (SQP003.1) was obtained from Squarix (Marl, Germany), γ-H2AX (AP07419PU-N) was obtained from Acris Antibodies GmbH (Herford, Germany). Secondary antibodies were from Santa Cruz Biotechnology (sc-2004, sc-2005, sc-2010, sc-2072, sc-2073, sc-2089, sc-2090, sc-2476). The secondary antibody Cy3-conjugated AffiniPure F(ab')$_2$ fragment goat anti-rabbit IgG (111-166-045) was purchased from Jackson Immunoresearch (West Grove, PA, USA).

3.1.5 Oligonucleotides

The oligonucleotides for the EMSA containing the consensus sequence for NF-κB, HO-1, CREB, STAT1, STAT3 and SP-1 were obtained from Promega (Madison, WI, USA). The oligonucleotide primers for PCR were designed with the program Primer3 [150] and purchased from MWG Biotech (Ebersberg, Germany).

3.2 Methods

3.2.1 Cell culture

LLC-PK1 cells were cultured at 37°C, 5% (v/v) CO_2 in Dulbecco's Modified Eagle Medium (DMEM) low glucose (1g/l) supplemented with 10 % (v/v) fetal bovine serum (FBS), 1% (w/v) L-glutamine, 2.5% (w/v) 4-(2-hydroxyethyl)-1-piperazineethanesulfonic acid (HEPES) and 0.2 % antibiotics (50 U/ml penicillin, 50

µg/ml streptomycin). MDCK cells were cultured at $37^{o}C$, 5% (v/v) CO_2 in MEM with Earle's Salts supplemented with 10% (v/v) FBS, 1% L-glutamine (w/v) and 0.2 % antibiotics (50 U/ml penicillin, 50 µg/ml streptomycin). All cells were split routinely twice a week to ensure exponential growth and were cultured for no more than 10 (LLC-PK1) and 40 (MDCK) passages after thawing them from stock.

LLC-PK1 and MDCK cells were cultured for 24 h in control medium. Cells were subsequently treated with aldosterone (5-100 nM) for 5 min up to 48 h depending on the assay and with different compounds as described for each experiment.

3.2.2 Animal treatment

Sixtyeight male Sprague-Dawley rats (Charles River) at the age of 8 weeks (250 to 300 g body weight) were randomly divided into 5 groups (20 in the placebo group and 12 in the other groups): group 1 = sham, the animals were anesthesized with 1.5-2% isofluran in 66% N_2O and 33% O_2 and operated but not uninephrectomized, while groups 2 to 5 were anesthesized and uninephrectomized. Seven days after the operation groups 2 to 5 received DOCA (30 mg/kg BW in sesame oil) once a week subcutaneously for 6 weeks together with 1 % NaCl added to drinking water, plus daily gavage of the following: group 2 = DOCA/salt, vehicle application (10 % ethanol, 40 % solutol, 50 % water); group 3 = DOCA-spironolactone, spironolactone (steroidal MR antagonist, 50 mg/kg) and group 4 = DOCA-BR-4628, (R)BR-4628 (selective, nonsteroidal MR antagonist, 10 mg/kg) (Figure 11). One week before the end of the experiment, 2 animals of each group received bromodesoxyuridine (BrdU) via an osmotic pump (Alzet 2 ml, 20 mg BrdU/ml). At the end of the experiment 11 animals were left in the sham group, 17 in the placebo-group and 12 in the other groups. All animals were sacrificed after six weeks of treatment by overdosing them with CO_2.

Induction of arterial hypertension, myocardial fibrosis and diastolic heart failure by DOCA/salt
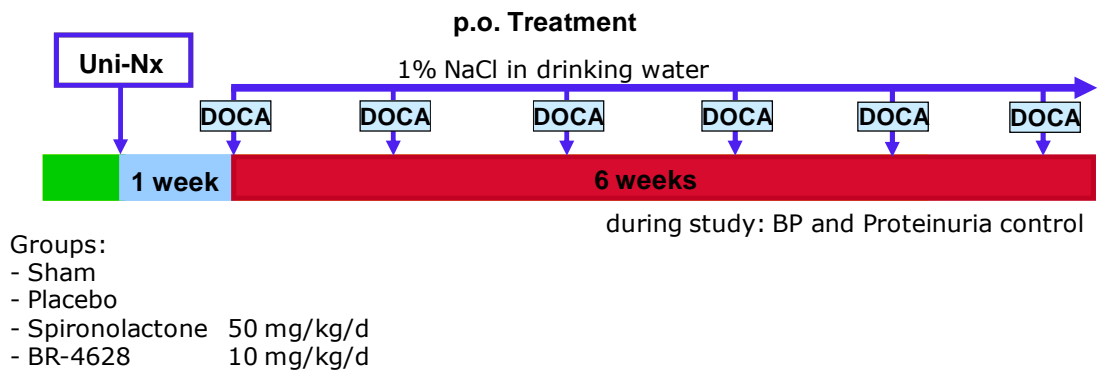
Figure 11: Animal treatment scheme

After taking out the kidney, it was divided into two parts. One part was immediately used for extraction of primary kidney cells for the comet assay and flow cytometric measurements and the other part was again separated in three sections: 1) stored in -80°C for further experiments (e.g. frozen sections), 2) fixed in 10% neutral buffered formalin and embedded in paraffin for immunohistochemistry stainings (2.2.4.3), and 3) extract primary kidney cells for the micronucleus test. Freshly obtained rat kidneys were minced on ice to small pieces, which were suspended in 3 ml buffer consisting of RPMI 1640, 15 % DMSO, 1.8 % (w/v) NaCl. The extracted primary rat kidney cells were sifted through a cell strainer with a mesh pore size of 100 μm (Becton Dickinson), centrifuged for 5 minutes at 1000 rpm and at 4°C and were finally resuspended in 1 ml buffer. Cells were counted and kept on ice until the experiments started.

All animal experiments were performed in accordance with the European Community guidelines for the use of experimental animals and with the German law for the protection of animals. The investigation conforms to the Guide for the Care and Use of Laboratory Animals" published by the US National Institutes of Health (NIH, Publication No. 85-23, revised 1996). The treatment of the animals was done by Bayer Health Care (Wuppertal, Germany).

3.2.3 Genotoxicity tests

3.2.3.1 Vitality assay

To be sure to have true genotoxic effects in the genotoxiciy test, possible cytotoxic effects of aldosterone were ruled out by vitality staining.The fluorescein-ethidium bromide assay involves staining cells with fluorescein diacetate and ethidium bromide. Fluorescein diacetate is an indicator of membrane integrity and cytoplasmic esterase activity [151]. Enzymatic hydrolysis of the fluorogenic ester substrate of fluorescein diacetate results in the intracellular accumulation of the green flourescent product flourescein in cells with intact plasma membranes. Ethidium bromide has been shown to penetrate only cells with damaged membranes and forms a red complex with nuclear DNA [152].
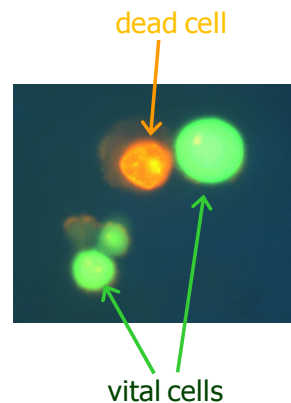
Figure 12: Principle of vitality staining.
The number of dead cells (stained with PI=> red) occuring during the counting of 200 vital cells (stained with fluorescein diacetate => green) was recorded.

The staining solution contained 30 µg/ml fluorescein diacetate and 12 µg/ml ethidium bromide. 0.35×10^6 cells were seeded in 25 cm^2 flasks for 24 h in control medium. After treatment cells were harvested and 35 µl of the cell suspension was stained with 15 µl staining solution. 15 µl of this mixture was applied to the slide and the fractions of green and red cells in a total of 200 cells were counted at a 500-fold magnification with a fluorescence microscope.

3.2.3.2 Comet assay

The comet assay, also known as single cell gel electrophoresis, is a method for the quantification of DNA single and double strand breaks as well as alkali labile sites. It

is a simple, sensitive, versatile, speedy and economic method to investigate nuclear structure based on the lysis of cells. The cell lysis leads to the removal of membranes, cytoplasm, and almost all histones, just remaining the nucleoid, which consists of RNA and proteins and supercoiled DNA [153]. After lysis, the nuclei are embedded in agarose to immobilize DNA for subsequent electrophoresis.

Cells (3.5×10^5) were seeded and cultured for 24 h in 25 cm^2 flasks. Cells were treated with aldosterone for 4 h and with different compounds in 5 ml medium. After treatment, cells were collected, dispersed into individual cells and suspended in molten low-melting-point agarose at 37°C. This mono-suspension was cast on a microscope slide which was coated with 1.5 % high-melting-point agarose. A glass cover slip was held at an angle and the mono-suspension applied to the point of contact between the coverslip and the slide. As the coverslip was lowered onto the slide the molten agarose spreads to form a thin layer. The coverslips were removed and the cells on the slides were immersed in lysis solution (lysis buffer: 2.5 M NaCl, 100 mM EDTA, 10 mM Tris, 1% Na-sarcosinate, pH 10; lysis solution: 66.5 ml lysis buffer stock solution, 7.5 ml DMSO, 0.75 ml Triton X-100) for 1 h at 4°C in the dark. After lysis the slides were left for 20 min in the cold electrophoresis solution (300 mM NaOH, 1 mM EDTA). In alkaline conditions the DNA double helix is denatured and the nucleoid becomes single stranded. Then, the slides were exposed to an electrical field for 20 min (25V, 300mA).
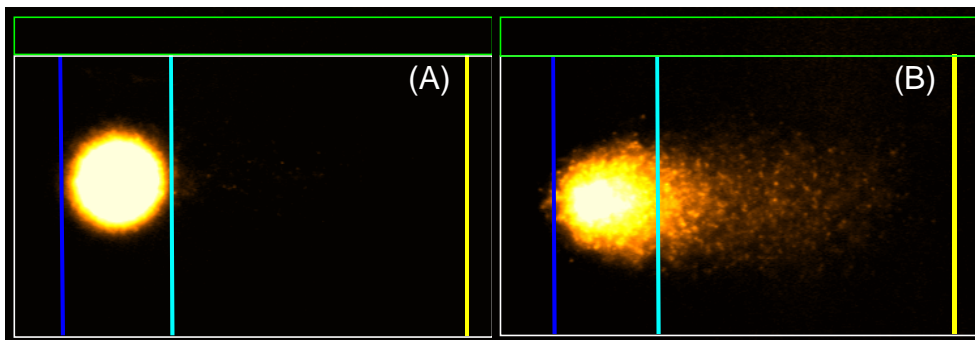
Figure 11: LLC-PK1 cells are embedded in agarose and exposed to an electrical field.
From cells with damaged DNA (B) (single or double strand breaks, alkali labile sites), more DNA can migrate than from cells with intact nuclear DNA (A). A comet-like structure is formed because smaller fragments and relaxed loops move faster than larger fragments and intact DNA. Comets are quantified microscopically after appropriate DNA staining.

From cells with damaged DNA (single or double strand breaks, alkali labile sites), more DNA can migrate than from cells with intact nuclear DNA. Consequently, a

comet-like structure is formed (Figure 11). After electrophoresis, the sides were put in neutralization buffer for 5 min (0.4 M Tris, pH 7.5), fixed in ice cold methanol for 5 min and dried. For analysis, DNA was stained with propidium iodide (PI, 20 µg/ml). A fluorescence microscope at 200-fold magnification and a computer-aided image analysis system (Komet 5, Kinetic Imaging LTD, Liverpool, UK) were used. 50 cells in total (25 per slide) were analyzed and results were expressed as percentage of DNA in the tail region.

3.2.3.3 Determination of formamidopyrimidine DNA glycosylase-sensitive sites

To increase the sensitivity of the comet assay, lesion-specific enzymes can be integrated in the standard protocol. FPG-sensitive sites were determined by comet assay including an incubation step with 0.05 µg/ml formamidopyrimidine DNA glycosylase (FPG) protein, an enzyme which cleaves DNA at sites of oxidized purines and thereby detects 8-oxodG [153]. After treatment with test substances, embedding the cells in agarose and lysis of the cell membranes, the slides were washed 3 times for 5 min in cold enzyme buffer (40 mM HEPES-KOH, 100 mM KCl, 0.5 mM Na_2EDTA and 0.2 mg/ml BSA) to remove the lysis solution. The FPG-sensitive sites were detected by incubation of the nuclei embedded in agarose with 0.005 µg/ml FPG protein (kindly donated by Professor Bernd Epe, Institute for Pharmacy, University of Mainz, Germany) for 60 min at 37°C. Afterwards, the comet assay was carried out as described above. In this case, ethidium bromide (20 µg/ml) was used for DNA staining. The net level of FPG-sensitive sites was obtained as the difference in score between samples incubated with FPG protein and samples incubated with enzyme buffer.

3.2.3.4 Micronucleus frequency test

The micronucleus test detects different kinds of chromosomal damage induced by various mechanisms [154]. Micronuclei (MN) are expressed in dividing cells that either contain chromosome breaks (resulting from unrepaired double strand breaks) and/or whole chromosomes that are unable to travel to the spindle poles during mitosis. Therefore, MN provide a convenient and reliable index of both chromosome breakage and chromosome loss. They are observed in cells with completed nuclear

division and are scored in the binucleated stage of the cell cycle by using the cytokinesis inhibitor cytochalasin B.

(A)   (B)
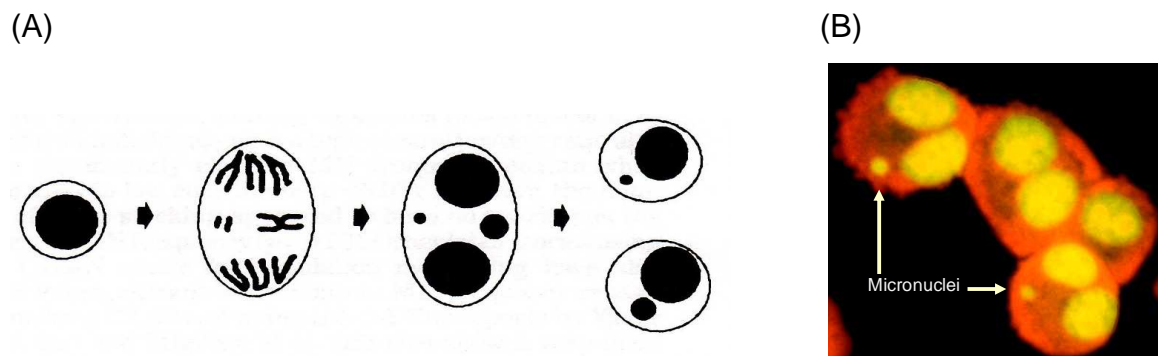
Figure 12: Micronuclei in a dividing nucleated cell.
A: Micronuclei developed from either lagging chromosomes or chromosome fragments. B: Image of cells stained with acridine orange. The cells were incubated with cytochalasin B which prevents the cytokinesis resulting in binucleated cells after one nuclear division. © Modified after Fenech [155].

The induction of MN by an agent can be considered as a biological relevant effect, since the relation between MN and carcinogenesis is strongly supported. The MN frequency is known as an early cancer risk biomarker in lymphocytes [156]. This is confirmed by the observation that many mechanisms involved in MN formation (e.g. chromosomal rearrangements, changes in gene expression, aneuploidy or altered DNA repair) enhance genomic instability associated with tumorigenesis.

The day before treatment, 3.5×10^5 cells were seeded in 25 cm^2 flasks. Cells were incubated with test substances in 5 ml medium. After 4 h treatment the medium was removed, cells were washed with phosphate buffered saline (PBS) and fresh medium was added containing 3 µg/ml cytochalasin B. This inhibitor of actin polymerisation blocks the separation of daughter cells but not of daughter nuclei, yielding binucleated cells. By limiting analysis to such binucleated cells, it can be ensured that these cells have actively divided since the treatment. After 24 h, cells were harvested, applied onto glass slides by cytospin centrifugation and fixed in methanol (-20 °C) for at least two hours. Before counting, cells were stained for 1 min with 62.5 µg/ml acridine orange (stock solution: 0.1 % acridine orange hydrochloride hydrate in H$_2$O) in Sørensen buffer (15 mM NaHPO$_4$ x H$_2$O, 15 mM KH$_2$PO$_4$ x H$_2$O, pH 6.8), washed with Sørensen buffer and mounted for microscopy. The frequency of micronuclei was obtained after scoring 1000 BN cells on each of two slides at a 500-fold magnification. Evaluation criteria were according to Fenech [155].

3.2.3.5 Proliferation index and apoptosis

The slides prepared for the micronucleus frequency test were used to calculate the cytokinesis block proliferation index (CBPI; (number of mononucleated cells + 2 x no. binucleated cells + 3 x no. multinucleated cells)/(sum of mononucleated, binucleated and multinucleated cells) from 1000 cells of each sample. The CBPI and the proportion of binucleated cells are useful parameters for comparing the mitogenic response of cells and cytostatic effects of agents examined in the assay.

During the analysis of the slides prepared for the micronucleus frequency test, also cells with nuclei which show characteristics of advanced apoptotic nuclei (highly condensed chromatin) (Figure 13) were counted relative to 1000 BN cells.
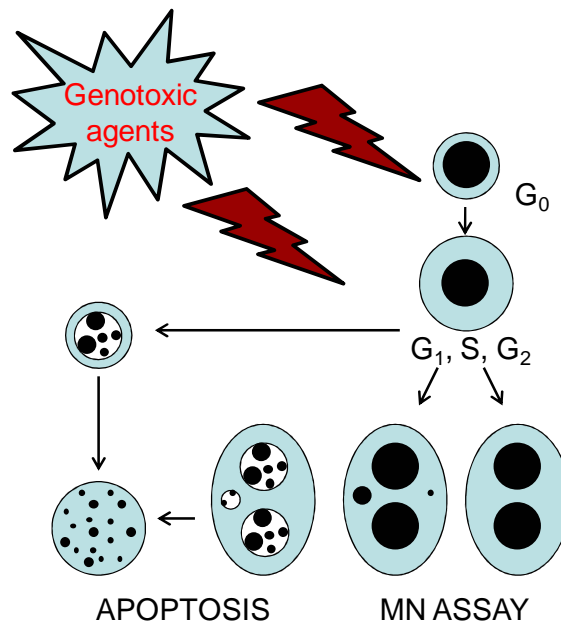
Figure 13: Possible fates of cultured cytokinesis-blocked cells exposed to cytotoxic/genotoxic agents.
Nuclei which showed characteristics of advanced apoptosis (left) were counted relative to 1000 BN cells. © Modified after Fenech [157].

3.2.4 Microscopy

3.2.4.1 Detection of fluorescent dyes

3.2.4.1.1 Evaluation of the cellular superoxide anion concentration

To detect oxidative activities in viable cells, the cell-permeable fluorogenic probe dihydroethidium (DHE) was used. Cytosolic DHE is oxidized mainly by $O_2^{\cdot-}$ to ethidium which intercalates to the DNA resulting in a bright red fluorecence ($\lambda_{ex}\backslash\lambda_{em}$:

518/605 nm). 0.2 x 10^5 cells were seeded on $\varnothing$12 mm coverslips in 6-well plates in 3 ml control medium the day before treatment. After treatment the medium was removed and cells were washed twice with PBS. Fresh medium was added containing 5 μM DHE (Merck Biosciences GmbH, Schwalbach, Germany) and the cells were incubated for 30 min at room temperature in the dark while gently shaking. After washing with PBS, pictures of the cells were taken using an Eclipse 55i microscope (Nikon GmbH, Düsseldorf, Germany) and a Fluoro Pro MP 5000 camera (Intas Science Imaging Instruments GmbH, Göttingen, Germany) at 200-fold magnification. Quantification was done by measuring grey values of 200 cells per treatment with ImageJ 1.40g (http://rsb.info.nih.gov/ij/) [158].

3.2.4.1.2 Evaluation of intracellular calcium levels by laser scanning confocal microscopy

Fura 2-acetoxymethyl ester (Fura 2-AM) is an UV light–excitable, ratiometric calcium indicator. When added to cells, Fura 2-AM crosses cell membranes and once inside the cell, the acetoxymethyl groups are removed by cellular esterases. Removal of the acetoxymethyl esters regenerates "Fura-2", the pentacarboxylate calcium indicator. Upon binding calcium, Fura 2-AM exhibits an absorption shift that can be observed by scanning the excitation spectrum between 300 and 405 nm, while monitoring the emission at ~510 nm. Cells (7 x 10^5 cells) were plated in 6-well plates on $\varnothing$12 mm coverslips. At confluence cells were treated in medium with or without 10 nM aldosterone and the appropriate substances for 30 min. At the end of the treatment the cells were loaded with 5 μM Fura 2-AM for 15 min and kept at 37℃ in the dark. After loading, the media was remo ved and the cells were washed twice with PBS. Confocal images were obtained by measuring the fluorescence at 510 nm (λexc 405 nm) using a TCS SP5 laser scanning confocal microscope (Leica Microsystems GmbH, Wetzlar, Germany).

3.2.4.1.3 Evaluation of cellular NO by scanning laser confocal microscopy

The fluorescent reagent diaminofluorescein (DAF-FM) has been widely used for specific and quantitative detection and imaging of NO in biological tissues based on its sensitivity, noncytotoxicity, and specificity. In the presence of O_2, NO and NO-

related RNS react with DAF-FM to yield the highly fluorescent benzotriazole. DAF-FM is not quite as cell-permeable as the diacetate derivate, but it does not need to be activated by cytosolic enzymes (Figure 13). Approximately 2×10^5 cells were plated in 6-well plates on $\varnothing$12 mm coverslips the day before treatment. Cells were treated with or without aldosterone and the NOS inhibitors L-NAME and W7 for 30 min. After the end of the treatment the medium was removed and cells were washed once with PBS. Fresh medium was added containing 10 µM DAF-FM and the cells were incubated for 15 min at room temperature in the dark while gently shaking. After washing with PBS, pictures of the cells were obtained measuring the fluorescence at 515 nm (λex: 495) using a TCS SP5 laser scanning confocal microscope (Leica Microsystems GmbH, Wetzlar, Germany).
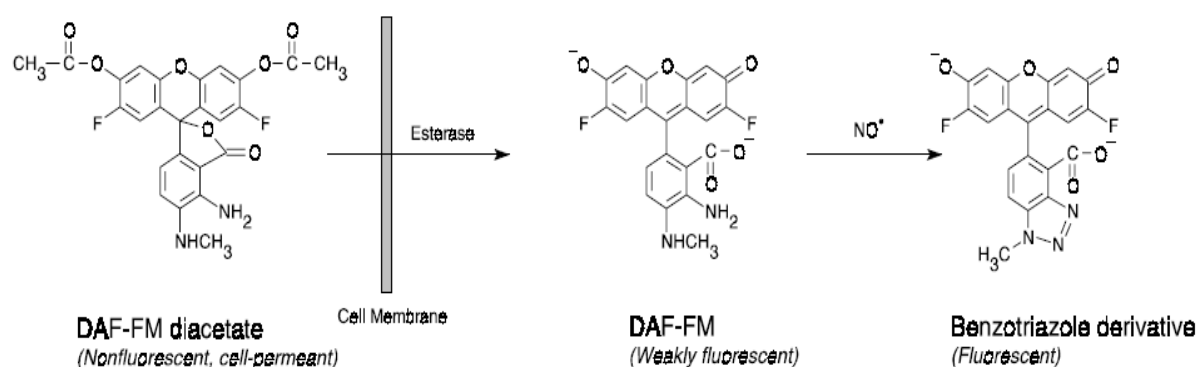
Figure 14: Reaction scheme for the detection of NO.
NO can be detected by DAF-FM and DAF-FM diacetate (www.probes.com).

3.2.4.1.4 Detection of apoptotic cells

Early apoptotic cells were quantified with the NucView[TM] 488 Caspase-3 Assay Kit for Live Cells (Biotium, Inc., Hayward, USA). The NucView[TM] 488 Caspase-3 substrate is a nonfluorecent and nonfunctional DNA dye, which rapidly crosses the cell membrane to enter the cytoplasm, where it is cleaved by caspase-3 to form a high-affinity DNA dye. The released DNA dye migrates to the cell nucleus to stain the nucleus of apoptotic cells bright green.

Cells (3.5×10^5) were seeded and cultured for 24 h in 25 cm^2 flasks in control medium. After treatment with the test substances, cells were harvested and 50 µl of the kidney cell suspension was centrifuged at 1000 rpm for 5 min in a microfuge. The cells were resuspended in 200 µl PBS and 5 µl caspase-3 substrate was added. After

30 min incubation at room temperature, the cells were washed twice with PBS (4000 rpm, 5 min, microfuge) and resuspended in 20 µl PBS. The cell suspension was put on a slide and covered by a coverslip. The number of apoptotic cells was determined counting caspase-3 positive cells under a fluorescent microscope at a 200-fold magnification in a total of 200 cells observed under transmitted light.

3.2.4.2 Immunocytochemistry

3.2.4.2.1 Detection of phosphorylated γ-H2AX sites

H2AX is a member of the histone H2A family, one of the five families of histones that pack and organize eucaryotic DNA into chromatin. H2AX undergoes phosphorylation on Ser 139, then named γ-H2AX, in response to DNA damage, particularly if the damage involves the formation of DNA double strand breaks (DSBs). During 30 min after DSB formation, large amounts of γ-H2AX molecules accumulate in the chromatin around the break site, thereby creating a focus where proteins involved in DNA repair and chromatin remodelling agglomerate. This amplification makes it possible to detect single DSBs with an antibody against γ-H2AX. LLC-PK1 cells (1×10^6) were seeded the day before in 25 cm^2 culture flasks and subsequently treated with the test substances for 24 h, harvested, brought onto glass slides by cytospin centrifugation and fixed in ice cold methanol for 24 h. The slides were washed twice with PBS and incubated over night at 37℃ with anti- γ-H2AX antibody (1:100), then nonbound antibody was removed by extensive washing with PBS containing 0.2% Tween (PBST). The slides were incubated for 30 min at 37℃ in the dark with the corresponding fluorescein isothiocyanate (FITC)-conjugated secondary antibody (donkey anti-rabbit IgG-FITC, 1:100). After thoroughly rinsing with PBST, nuclei were counterstained with 0.01 mg/ml Hoechst 33258. The slides were rinsed twice with PBS and were mounted with 1,4-diazabicyclo[2.2.2]octan (DABCO). Images were visualized and captured using a Nikon Eclipse 55i fuorescence microscope (Nikon GmbH, Düsseldorf, Germany) with a 40-fold lens. Quantification was done by measuring gray values of 150 cells per treatment with ImageJ 1.40g (http://rsb.info.nih.gov/ij/) [158].

3.2.4.2.2 Detection of 8-oxodG by immunofluorescent staining

8-oxodG is one of the predominant forms of free radical-induced oxidative lesions, and has therefore been a pivotal marker for measuring the effect of endogenous oxidative damage to DNA and a factor of initiation and promotion of carcinogenesis [159]. LLC-PK1 cells (0.35×10^5) were seeded the day before in 25 cm^2 culture flasks and subsequently treated with aldosterone for 4, 24 and 48 h. Cells were harvested and brought onto glass slides by cytospin centrifugation and fixed in ice cold methanol for 24 h. Cells were washed in PBS for 10 min, followed by RNA digestion (200 µg/ml RNAse A, 50 U/ml RNAse T1) for 1 h at 37℃ and cells were washed again in PBS. After incubating the cells with alkali solution (60% 70 mM NaOH, 140 mM NaCl and 40% methanol) for 5 min at 0°C, cells were washed in PBS and proteolyzed in 0.1% trypsin for 30 sec at 37℃. Proteinase K (2 µg/ml in 20 mM Tris/HCl and 2 mM CaCl$_2$, pH 7.5) was added for 10 min at 37℃ and cells we re washed in PBS and 0.2% glycin/PBS. Then, cells were blocked in 1% BSA/PBS for 30 min at room temperature and subsequently incubated with the primary 8-oxodG antibody (1:100) over night at 4℃. The next day, c ells were washed in 0.05% Tween/PBS and the Cy3-labeled goat anti-rabbit IgG secondary antibody (1:700) was added for 1 h at room temperature. After washing, cells were stained with 0.01 mg/ml DAPI for 30 min and mounted with confocal matrix (Micro Tech Lab, Graz, Austria). Confocal images were obtained by measuring the fluorescence at 570 nm (λexc 550 nm) and 660 nm (λexc 633 nm) using a sequential scan with the TCS SP5 laser scanning confocal microscope (Leica Microsystems GmbH, Wetzlar, Germany). Quantification was done by measuring gray values of approximately 100 cells per treatment with ImageJ 1.40g (http://rsb.info.nih.gov/ij/) [158].

3.2.4.2.3 Detection of proliferation

Cell proliferation is an important and highly studied cellular function. In 1982, Gratzner *et al.* reported an approach to the detection of cells in S (synthetic) phase of the cell cycle, based on the use of antibodies against BrdU, a thymidine analog [160] (Figure 15). Cells (0.35×10^5) were seeded the day before in 25 cm^2 culture flasks and subsequently treated with the test substances. Cells were harvested and brought onto glass slides by cytospin centrifugation and fixed in ice cold methanol for at least 2 h. After washing with PBS, DNA was denatured for 30 minutes with 1.5 M HCl at

room temperature in the dark, neutralized with 0.1 M sodium borate and washed again. Cells were blocked for 1 h in blocking solution (1 M glycine, 5% donkey serum, 0.1% tritonX100, 0.01 M PBS). Anti-BrdU antibody was added (1:130) and incubated overnight at room temperature.
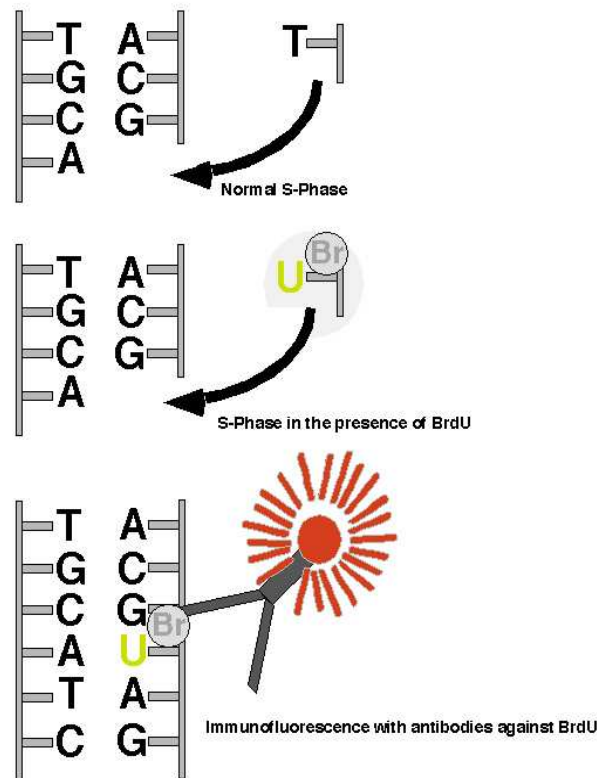
Figure 15: Labeling of mitotic cells with BrdU.
The upper part shows the normal phase of synthesis: In the S-phase of the cell cycle thymidine (T) pairs with adenine (A). In the presence of BrdU, it gets incorporated in the newly synthesized DNA strand instead of T (middle part of the figure), which can be detected and visualized by anti-BrdU antibodies (lower part of the figure). © http://edoc.hu-berlin.de/habilitationen/kempermann-gerd-2002-01-29/HTML/Kempermann_html_2a114872

After washing, the secondary donkey anti-sheep IgG-FITC antibody was added (1:100) for 1 hour. After staining the nucleus with 0.01 mg/ml Hoechst 33258, the slides were mounted with Antifade Gold (Invitrogen). BrdU-positive i.e. green fluorescent cells were scored within 500 to 800 cells seen in the brightfield of an Eclipse 55i microscope (Nikon) at 400-fold magnification.

3.2.4.3 Immunohistochemistry

3.2.4.3.1 Detection of apoptosis

Caspases are crucial mediators of programmed cell death (apoptosis). Among them, caspase-3 is a frequently activated death protease, catalyzing the specific cleavage of many key cellular proteins. Caspase-3 is required for some typical hallmarks of apoptosis, and is indispensable for apoptotic chromatin condensation and DNA fragmentation. Antibodies against cleaved caspase-3 offer an efficient way of detecting caspase-3 processing and activation. For cleaved caspase-3 staining on tissue, cryosections (5 μm thick) were fixed in 4 % paraformaldehyde at 4°C for 15 min at room temperature and subsequently washed with PBS. Afterwards, cyrosections were incubated with 0.2% Nonidet P40 for 10 min at room temperature to solubilize membrane proteins and to reduce levels of unwanted peroxides and carbonyl compounds or salts. Cryosections were blocked in 10% donkey serum for at least 1 h at room temperature and subsequently stained with anti-cleaved caspase-3 (1:100, diluted in blocking solution) antibody at 4°C in the dark over night. The tissues were washed for 30 min with PBS and thus incubated with the secondary donkey anti-rabbit IgG-FITC antibody (1:300, diluted in blocking solution) for 1 h in the dark at room temperature. After washing the sections for 30 min, 0.01 mg/ml DAPI was used to stain the nucleus. Sections were washed again and mounted with Vectashield (Linaris GmbH) and pictures were taken with a Biozero 8000 (Keyence) at 200-fold magnification. For quantification, percentage of cells positive for cleaved caspase-3 were scored within 1200 to 1700 cells seen in 2 to 3 pictures of one section.

3.2.4.3.2 Detection of oxidative stress on cryosections

DHE is the chemically reduced form of the commonly used DNA dye ethidium bromide. The probe is useful to detect oxidative activities in viable cells. Immediately after preparing cryosections, superoxide production on unfixed frozen tissue sections were detected after staining for 30 min with 10 µM DHE at room temperature in the dark. Pictures of the cells were taken using an Eclipse 55i microscope (Nikon GmbH, Düsseldorf, Germany) and a Fluoro Pro MP 5000 camera (Intas Science Imaging Instruments GmbH, Göttingen, Germany) at 200-fold magnification. Quantification

was done by measuring grey values of 500 cells per treatment with ImageJ 1.40g (http://rsb.info.nih.gov/ij/) [158].

3.2.4.3.3 Detection of phosphorylated γ-H2AX sites

The number of γ-H2AX foci formed in a cell appears to be directly related to the number of DNA double strand breaks. Phosphorylation of γ-H2AX has been identified by binding of antibodies to phoshorylated Ser-139 at the C-terminus of histone H2AX. Paraffin kidney sections (4 μm) were mounted on glass slides, heated at 60℃ for 1 h, deparaffinized (3 x 4 min Roti-Histol, 2 x 3 min 100% EtOH, 1 x 2 min 70% EtOH) and washed with PBS. Afterwards, the slides were put in a pressure cooker and the tissues were boiled in citrate buffer (10 mM citric acid, 2 M NaOH) for 4 min on the highest level. Citrate buffer is one of the most popularly used antigen retrieval solution to improve the demonstration of the antigen. It breaks the protein cross-links formed by formalin fixation and thereby uncovers hidden antigenic sites. To cool down, the slides were rinsed with cold water and washed with PBS. The sections were blocked in 5% donkey serum for 1 h at room temperature in the dark, washed and subsequently incubated with 3% H_2O_2 for 15 min at room temperature, which is commonly used to deplete endogenous peroxidase activity. In the next step, the sections were washed and incubated with 0.001% avidin solution for 15 min at room temperature, followed by a brief rinse in PBS and incubation with 0.001% biotin. Avidin is an egg-white derived glycoprotein with an extraordinarily high affinity for biotin. Kidney sections usually contain high levels of endogenous biotin resulting in a nonspecific background staining. To reduce the nonspecific background the tissues were pretreated with avidin/biotin blocking reagents prior to the incubation of biotinylated antibody. Avidin binds to any avidin binding sites on biotin in the tissue and the incubation with biotin is to saturate all the biotin-binding sites left open on the avidin. Afterwards, the sections were incubated with the primary anti-γ-H2AX antibody in a 1:25 dilution overnight at 4℃, follo wed by washing steps and a 45-minute incubation with the biotin-conjugated secondary antibody in a 1:200 dilution. The avidin biotin complex (ABC) reagent (Vectastain-Elite ABC reagent: 10 mM sodium phoshate, 0.9% NaCl, pH 7.5; mixed with two drops of reagent A and two drops of reagent B) was prepared and after washing the tissues with PBS, sections were incubated with ABC reagent for 30 min at room temperature, washed again and

incubated with diaminobenzidin (DAB) chromogen (Kit, Vector Laboratories, Servion, Switzerland) for a few seconds to minutes. In the presence of H_2O_2, DAB is converted to a brown chromogen substrate by the enzyme horse radish peroxidase (HRP) (Figure 16). In the following, the slides were washed in pure water and stained with hematoxylin for 5 min and rinsed thoroughly in water for 10 min. At the end, the sections were dehydrated (1 x 1 min 70% EtOH, 4 x 2 min 100% EtOH, 2 x 3 min Roti-Histol) and mounted with Eukitt (Fluka). Pictures were taken with an Eclipse 55i microscope (Nikon) at 200-fold magnification. The percentage of positive cells was assessed for tubules, by scoring approximately 290 tubules.
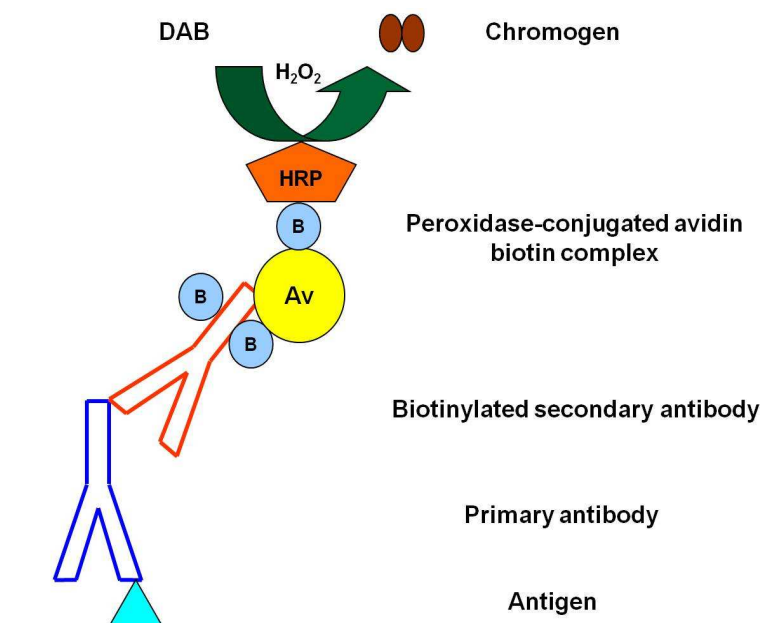
Figure 16: ABC-DAB reaction to visualize the binding of antibodies to antigens.
The primary antibody binds to the antigen of interest and the corresponding biotinylated secondary antibody binds to the primary antibody. Avidin is a basic glycoprotein which has a high affinity for the small water soluble vitamin biotin. To amplify the reaction, avidin and biotinylated HRP are simply mixed at appropriate concentrations for at least 30 minutes at room temperature to form the complex. The preformed complex is then attached to the biotinylated secondary antibody. Finally, HRP catalyzes the formation of chromogen in the presence of H_2O_2.

3.2.4.3.4 Detection of proliferation

BrdU is a synthetic thymidine analog that gets incorporated into the DNA of a cell when the cell is dividing (during the S-phase of the cell cycle, see 3.2.4.2.3). Antibodies against BrdU that are conjugated to fluorescent markers can be used to label these cells, thereby providing visual evidence of cell division. For detection of proliferating cells in kidney paraffin-embedded sections, the tissue of the BrdU-

treated animals was processed as described in the BrdU In-Situ Detection Kit (BD Pharmingen). Tissues were deparaffinized (2 x 5 min xylene, 2 x 3 min 100% EtOH, 1 x 3 min 95% EtOH) and then treated with 3% H_2O_2 for 10 min to block endogenous peroxidase activity. After rinsing the slides in PBS, they were placed in a coplin jar containing the working solution of the BD antigen retrieval solution, which mediates the unwinding of the DNA to expose the incorporated BrdU for antibody staining, and were heated in a microwave oven to 89°C for 10 min. Afterwards the slides were cooled down for 20 min, were washed in PBS for 3 x 5 min and subsequently incubated with the biotinylated anti-BrdU antibody (1:10, diluted in diluent uffer) in a humidified chamber for 1 h. Slides were rinsed in PBS, DAB substrate solution was added for seconds to minutes until the desired color intensity has developed and slides were rinsed in water (3 x 2 min). After counterstaining with hematoxylin for 5 min and rinsing thoroughly in water for 10 min, tissues were dehydrated through four changes of alcohol (2 x 95% and 2 x 100%) for 5 min each time and cleared in 3 changes of xylene. Finally, sections were mounted with Eukitt and pictures were taken with an Eclipse 55i microscope (Nikon) at 200-fold magnification. The percentage of positive cells was assessed for tubules, by scoring 250 tubules.

3.2.5 Analytics

3.2.5.1 *Quantification of 8-oxodG by liquid chromatography-mass spectrometry*

Liquid chromatography-mass spectrometry (LC-MS) is an analytical chemistry technique that combines the physical separation capabilities of liquid chromatography with the mass analysis capabilities of mass spectrometry. LC-MS is a powerful technique used for many applications which has very high sensitivity and specificity. Cells were seeded in 3 x 175 cm^2 flasks until a cell number of approximately 20 x 10^6 per concentration was reached. As positive control, 25 μg methylenblue was added and the cells were illuminated for 10 min on ice. Cells were scraped, harvested and centrifuged. Afterwards, cells were washed with PBS, centrifuged again and shock-frozen in nitrogen. The cell pellet was stored at -80°C until DNA isolation. Genomic DNA was isolated from cells as reported previously by Oli *et al* [161]: cultured cell pellets were homogenized with 3 ml of buffer A (320 mM sucrose, 5 mM MgCl2, 10 mM Tris/HCl, pH 7.5, 0.1 mM deferoxamine, and 1% (v/v) Triton X-100). After homogenization, the samples were centrifuged at 1500g for 10

min, washed with 1.5 ml of buffer A and centrifuged again (1500g for 10 min). A total of 600 µl of buffer B (10 mM Tris/HCl, pH 8, 5 mM EDTA–Na2, 0.15 mM deferoxamine) and 35 µl of 10%(w/v) sodium dodecyl sulfate were added, and the samples were agitated vigorously. After 30 µl of RNase A (1 mg/ml) in RNase buffers (10 mM Tris/HCl, pH 7.4, 1 mM EDTA, and 2.5 mM deferoxamine) and 8 µl of RNase T1 (1U/µl in RNase buffer) were added, the samples were incubated at 37℃ for 1 h to remove contaminating RNA from the D NA. Then, 30 µl of proteinase K (20 mg/ml) was added and the samples were incubated at 37℃ for 1 h. Subsequently, 1.2 ml of sodium iodide solution (7.6 M NaI, 40 mM Tris/HCl, pH 8.0, 20 mM EDTA–Na$_2$, 0.3 mM deferoxamine) and 2 ml of 2-propanol were added. The samples were gently shaken until the DNA had precipitated completely and then centrifuged at 5000g for 15 min. The DNA pellets were washed with 1 ml of 40% (v/v) 2-propanol. After centrifugation (5000g for 15 min) the DNA pellets were washed with 1 ml of 70% (v/v) ethanol. Finally, the DNA pellets were collected by centrifugation and dissolved in 0.1 mM deferoxamine overnight. DNA concentration was measured by the absorbance at 260 nm. Protein contamination was checked using the absorbance ratio A260/A280; an absorbance ratio over 1.6 was acceptable. DNA concentration was calculated by measuring the absorbance at 260 nm. DNA hydrolysis of approximately 20 µg DNA spiked with 2.82 pmol of [^{15}N5] 8-oxodG was performed as described by Oli *et al* [161] and Chao *et al* [162].100 µL of the DNA samples were loaded on the trap column using an auto sampler (Agilent 1100 series) and analyzed.

3.2.5.2 Quantification of GSH by high-performance liquid chromatography

High-performance liquid chromatography (HPLC) is a chromatographic technique that can separate a mixture of compounds, and is used in biochemistry and analytical chemistry to identify, quantify and purify the individual components of the mixture. Cells (1 x 10^6) were seeded in 60 mm dishes for 24 h. After treatment with aldosterone, cells were washed with 1 ml of 100 µM EGTA. The procedure was performed as described by Jones *et al* [163]. Cells were scraped in 200 µl of 0.1% Igepal and 50 µl were put aside for protein determination. The rest (150 µl) was put into a 1.5 ml tube containing 100 µl of perchloric acid solution (10% (w/v) perchloric acid, 0.2 M boric acid, and 10 µM gamma-glutamylglutamate. For derivatization, cells were centrifuged for 3 min at 3000 rpm and 150 µl of the supernatant was transferred

to a new 1.5 ml tube. 30 µl of iodoacetic solution (7.4 mg/ml water) and appoximately 140 µl KOH/tetraborate solution (1.6 M $K_2B_4O_7 \cdot 4H_2O$, 1 M KOH) were added to adjust the pH to 9. After 20 min, 150 µl of freshly prepared dansyl chloride solution (200 mg/ 10 ml acetone) was loaded. Samples were mixed and placed in the dark at room temperature for approximately 24 h. Then, 250 µl of chloroform was added to extract unreacted dansyl chloride. For the HPLC measurement, samples were centrifuged for 3 min at 3000 rpm and the supernatant was transferred to the HPLC (3-aminopropyl column, size 25 cm x 4.6 mm, 5 µm particle size) and analyzed. The fluorescence spectrum was 510-650 nm (λexc 395) and the retention time for GSH was 26 min and for GSSG 29 min.

3.2.5.3 Fluorimetric determination of GSH levels

LLC-PK1 cells (0.18×10^5) were seeded the day before in medium in 25 cm^2 culture flasks and subsequently treated with the test substances for 4, 24 and 48 h. Cells were washed with ice cold 1 x PBS and culture flasks were placed on ice. Cells were incubated with 1 ml of lysis buffer (0.2 M mannitol, 50 mM saccharose, 0.01 M HEPES, pH 7.5) for 10 min on ice. Afterwards, cells were scraped, transferred into a microcentrifuge tube and centrifuged at 12.000 x g for 10 min at 4°C. Meanwhile, the GSH standard curve was prepared. Therefore, a 50 mM reduced L-glutathione (15 mg GSH/ml PBS) stock solution was prepared, which was further diluted with PBS to make a dilution series (endconcentrations 1, 5, 10, 25, 50, 75, 100 µM). Then, the cell lysates were collected into a new microcentrifuge tube and 90 µl of the samples were added to a 96-well plate (Fluotrac 200, black, Greiner Bio-One GmbH, Frickenhausen, Germany). The standards (10 µl) were also transferred to the wells and mixed with PBS (80 µl). Finally, 10 µl of 17.65 mM monochlorobimane (MCB) (4 mg/ml PBS) was loaded to all wells. MCB is a dye with high affinity to GSH. The unbound dye is almost nonfluorescent, whereas the GSH-bound dye fluoresces blue. The samples and the standards were inbubated with MCB for 1-2 hours in the dark while gently shaking at room temperature. Fluorescence was recorded using a fluorescence plate reader with a 355/460 nm filter set. Protein content was determined by Bradford [164]. Results are expressed as the ratio DCF fluorescence/protein content.

3.2.5.4 Fluorimetric evaluation of intracellular calcium levels

Intracellular calcium levels were determined using the probe Fura 2-AM, which is a UV-excitable fluorescent dye binding to free intracellular calcium. Hydrolysis by nonspecific esterases traps the indicator in the cytosol. 0.5×10^4 cells were seeded in control medium in 96-well plates for 24 h. At confluence they were incubated in medium with or without aldosterone or the appropriate substances. Afterwards, the medium was removed and cells rinsed with PBS. Fresh medium was added and cells were incubated with 10 μM Fura 2-AM for 30 min at room temperature in the dark while gently shaking. Cells were washed again in PBS and fluorescence was measured by plate reader at 510 nm (λexc 340). Results are expressed as the fluorescence emission (λem: 510 nm) at λexc 340 nm.

3.2.5.5 FRAP assay: Method to measure the antioxidant capacity of substances

Total antioxidant activity of a substance is measured by ferric reducing antioxidant power (FRAP) assay of Benzie and Strain [165]. The FRAP assay measures the ferric to ferrous ion reduction at low pH in the presence of antioxidants resulting in a colored ferrous-tripyridyltriazine complex. FRAP values are obtained by comparing the absorbance change at 593 nm in test reaction mixtures with those containing ferrous ions in known concentrations. Absorbance changes are linear over a wide concentration range with antioxidant mixtures. First, a calibration curve was pipetted as follows:

Table 1: Calibration curve FRAP assay.

FeSO$_4$*7 H$_2$O (10 mM)	H$_2$O
7 μM: 0.7 μl	199.3 μl
14 μM: 1.4 μl	198.6 μl
21 μM: 2.1 μl	197.9 μl
28 μM: 2.8 μl	197.2 μl
35 μM: 3.5 μl	196.5 μl

20 μl of the substance of interest (triplicates) and the standards (triplicates) were mixed with 600 μl of FRAP reagent (300 mM sodium acetate buffer, 10 mM ferric-tripyridyltriazine and 20 mM FeCl$_3$* 6 H$_2$O) and 180 μl water for 2 min. Fluorescence

was measured by photometry at 593 nm for 20 seconds (three time points: 0 s, 10 s, 20 s).

3.2.5.6 Fluorimetric quantification of intracellular oxidants

The concentration of intracellular oxidants was estimated using the probe 2´,7´-dichlorodihydrofluorescein diacetate (H_2DCF-DA). The cell permeable H_2DCF-DA is nonfluorescent until the acetate groups are removed by intracellular esterases and oxidation occurs within the cell, leading to the fluorescent product dichlorofluorescein (DCF) (Figure 17). Oxidation of this probe can be detected by monitoring the increase in fluorescence using a plate reader with filters appropriate for fluorescein (FITC).

nonfluorescent   fluorescent
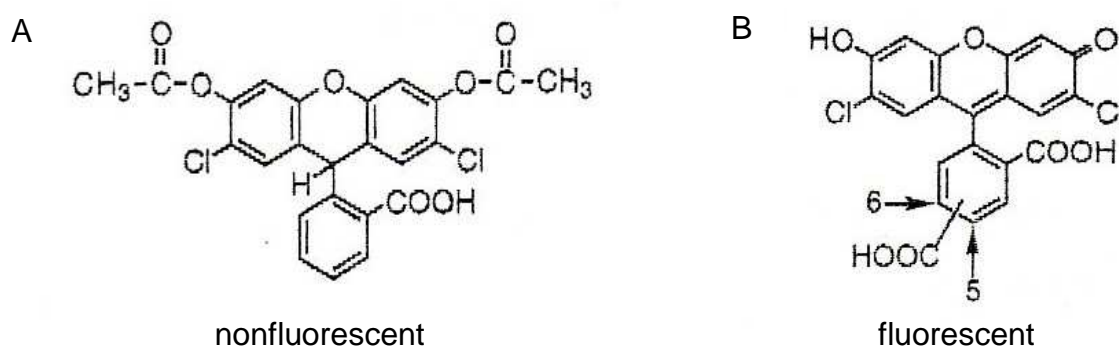
Figure 17: Structures of H$_2$DCF-DA and DCF.
The structures of the nonfluorescent and cell permeable H_2DCF-DA (A) and the oxidized and thus fluorescent product DCF (B) are shown.

Cells (1.5×10^4) were seeded in 96-well plates and at confluence cells were incubated in medium with or without 10 nM aldosterone. At the end of the treatment, 40 µM H_2DCF-DA was additionaly loaded for approximately 30 min. Afterwards the medium was removed, cells were rinsed with PBS and 200 µl of PBS was added per well. Fluorescence was measured at λexc: 475 nm; λem: 525 nm. To determine the DNA content, samples were subsequently incubated with 0.1 % (v/v) Igepal and 50 µM PI, incubated for 20 min at room temperature, and the fluorescence (λexc: 538 nm, λem: 590 nm) was measured. Results are expressed as the ratio DCF fluorescence/PI fluorescence.

3.2.5.7 Fluorimetric quantification of intracellular NO

The concentration of intracellular nitrogen species was estimated using DAF-FM, which is a very sensitive probe for the detection of nitric oxide (NO). This compound is essentially nonfluorescent until it reacts with NO to form a fluorecent benzotriazole. Cells (1.5 x 10^4) were seeded in 96 well plates and at confluence were incubated with or without aldosterone. After the end of the treatment cells were washed once in PBS and fresh medium was added. Cells were loaded with 10 µM DAF-FM for 30 min at room temperature in the dark. Afterwards the medium was removed, cells were rinsed with PBS and 200 µl of PBS was added per well. Fluorescence was measured at λexc: 495 nm; λem: 515 nm. To determine the DNA content, samples were subsequently incubated with 0.1 % (v/v) Igepal and 50 µM PI, incubated for 20 min at room temperature, and the fluorescence (λexc: 538 nm, λem: 590 nm) was measured. Results are expressed as the ratio DAF-FM fluorescence/PI fluorescence.

3.2.5.8 Flow cytometric analysis of oxidative stress

Flow cytometry is a technique for counting and examining microscopic particles, such as cells and chromosomes, by suspending them in a stream of fluid and passing them by an electronic detection apparatus. It allows simultaneous multiparametric analysis of the physical and/or chemical characteristics of up to thousands of particles per second. H_2DCF-DA was used to detect ROS production in cells. H_2DCF-DA is a nonflourescent probe that enters the cell where it is oxidized to a fluorescent derivate (DCF) by endogenous oxidants. 0.5 x 10^6 cells were seeded and cultured for 24 h in control medium in 25 cm^2 flasks. Substances were added to the cells for 30 min and at the end of the treatment cells were additionally loaded with 10 µM H_2DCF-DA for 5 min at 37℃. As a positive control 100 µM H_2O_2 was used. After treatment, the cells were harvested, washed twice with cold PBS/1% BSA and analyzed (3 x 10^5 cells/sample) by flow cytometry using a FACS LSR I (Becton-Dickinson, Mountain View, USA) after incubation for 10 min on ice with 1 µg/ml PI. Fluorescence intensities of 30,000 cells were recorded. The shift to the right of the fluorescent histograms indicates an increase of ROS.

3.2.6 Proteinchemical methods

3.2.6.1 Electromobility shift assay

The most widely applied method to establish the binding of proteins to the DNA is the electromobility shift assay (EMSA). It is the core technology underlying a wide range of qualitative and quantitative analysis for the characterization of interacting systems. In the classical assay, solutions of protein and nucleic acid are combined and the resulting mixtures are subjected to electrophoresis under native conditions through a polyacrylamide gel. After electrophoresis, the distribution of probes containing nucleic acid is determined, usually by autoradiography of ^{32}P-labeled nucleic acid. The assay is based on the observation that the electrophoretic mobility of a protein-nucleic acid complex is typically less than that of the free nucleic acid (Figure 18). Cells (5 x 10^6) were seeded and cultured in 100 mm dishes for 24 h in control medium. After treatment cells were washed with PBS and scraped in 1 ml PBS. Nuclear fractions were isolated as follows: cells were transferred to a 1.5 ml tube and centrifuged at 3000 rpm for 10 min at 4℃. Afterwards, the supernatant was removed, the pellet was resuspended in 150-200 μl of ice-cold lysis buffer (1 M HEPES, 1 M KCl, 100 mM dithiothreitol (DTT), 25 x protein inhibitor cocktail, 1 M MgCl$_2$ and 50 mM EDTA), incubated for 10 min on ice and centrifuged at 14,000 rpm for 2 min at 4℃. The result is a pellet of nuclei. The supernatant (cytosolic fraction) was collected and stored at -80℃. The nuclear pellet was resuspended in 75-100 μl of an ice-cold extraction buffer (1 M NaCl, 1 M HEPES, 100 mM DTT, 50% glycerol, 25% protease inhibitor cocktail, 1 M MgCl$_2$ and 50 mM EDTA). To facilitate the extraction of the nuclear proteins, the nuclear suspension was shaken every 5 min for a total period of 20 min on ice. The nuclear lysates were centrifuged at 10,000 rpm for 10 min at 4℃ and the supernatant, containing the nuclear proteins, was collected and stored immediately at -80℃ until further use. The protein concentrations were determined according to the method of Bradford [164], yielding sample concentrations of approximately 1 μg/ml. For the EMSA, the oligonucleotides containing the consensus sequence for NF-κB, HO-1, STAT1, STAT3, CREB or SP-1 were end labeled with [γ-^{32}P] ATP in the presence of T4 polynucleotide kinase at 37℃ for 20 min and purified using Chroma Spin-10 columns. Samples were incubated with the labeled oligonucleotide (20,000-30,000 cpm) for 20 min at room temperature in 1x binding buffer (5x binding buffer: 50 mM

Tris-HCl buffer, pH 7.5, containing 20 % (v/v) glycerol, 5 mM $MgCl_2$, 2.5 mM EDTA, 2.5 mM DTT, 250 mM NaCl and 0.25 mg/ml poly(dI-dC)). The products were separated by electrophoresis in a 6 % (w/v) nondenaturing polyacrylamide gel for approximately 3 h using 0.5 x TBE (Tris/borate 45 mM, EDTA 1mM) as the running buffer. The gels were dried for 1 h and the radioactivity was quantified in a Phosphoimager 840 (Amersham Pharmacia Biotech. Inc. Piscataway, NJ).
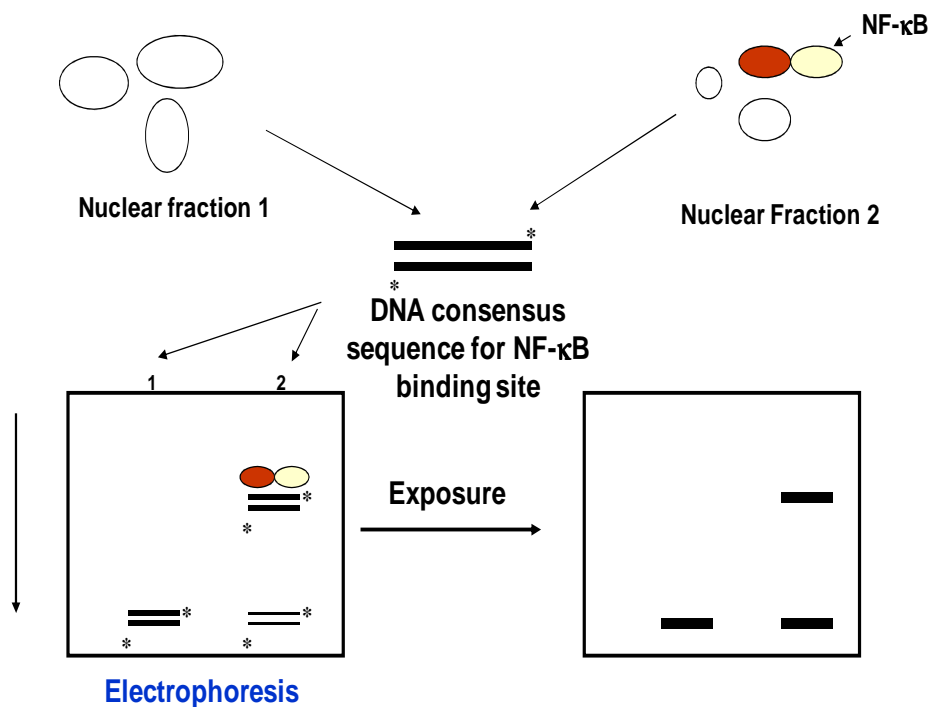
Figure 18: Schematic representation of electrophoretic mobility shift assay.
The evaluation of NF-κB binding activity to the DNA is demonstrated.

3.2.6.2 Western blot analysis

The western blot is an analytical technique used to detect specific proteins in a given sample of tissue homogenate or extract. It uses gel electrophoresis to separate native or denatured proteins by the length of the polypeptide (denaturing conditions) or by the 3-D structure of the protein (native/ nondenaturing conditions). The proteins are then transferred to a membrane (typically nitrocellulose or PVDF), where they are detected using antibodies specific to the target protein. For the preparation of total cell extracts, cells (5 x 10^6 cells) were cultured in 60 mm dishes for 24 h in control medium and subsequently treated with test substances. Cells were rinsed with PBS, scrapped and centrifuged at 1000 x g for 5 min at 4°C. The pellet was resuspended in approximately 80 µl (depending on the pellet size) of lysis solution (100 µM sodium

fluoride, 1 mM sodium pervanadate, 50 mM PMSF, phosphatase inhibitors I and II, protein inhibitor cocktail including 1 mg/l leupeptin, 1 mg/l pepstatin, 1.5 mg/l aprotinin, 2 mg/l bestatin and lysis buffer consisting of 100 mM Tris, 300 mM NaCl, 0.2% TritonX-100, 2% Igepal, 4 mM EDTA and 4 mM EGTA). Samples were incubated on ice for 30 min and centrifuged at 10,000 x g for 20 min at 4°C. The supernatant was transffered into a new tube and the protein concentration was measured by Bradford [164]. To isolate cytosolic fractions, cells were treated with 150 µl lysis buffer (10 mM HEPES, 1.5 mM $MgCl_2$, 5 mM KCl, 0.5 mM DTT, 0.2% Igepal and 0.5 mM PMSF) and incubated on ice for 10 min. Cells were centrifuged for 2 min at 14,000 rpm at 4°C. The supernatant was tra nsferred into a new tube and protein concentration was determined using Bradford [164]. Aliquots of total, nuclear or cytosolic fractions containing 25-40 µg protein were mixed with 4x sample buffer (0.2 M Tris, 0.2 M sodium dodecyl sulfate, 80% glycerol, 0,005% bromphenol blue, 10% mercaptoethanol) and heated to 95°C for 5 min. Afterwards, samples were loaded and separated by reducing 10% or 12.5% (w/v) polyacrylamide gel electrophoresis (80-100 V for 90 min) in running buffer (25 mM Tris, 0.2 M glycine, 3 mM sodium dodecyl sulfate) and electroblotted for 90 min at 100 V to PVDF membranes in 1 x transfer buffer (100 ml transfer buffer 10x (0.25 M Tris, 2 M glycine), 200 ml methanol, 700 ml water). Colored molecular weight standards (5 µl) (Amersham, Piscataway, USA) were ran simultaneously. Then, membranes were stained with Ponceau S, a dye for rapid reversible staining of protein bands and erased with 0.1 M NaOH. Membranes were washed with tris buffered saline (TBS), blocked for at least two hours in 5% (w/v) milkpowder at room temperature, and incubated in the presence of corresponding primary antibodies overnight at 4°C or for β-tubulin (1:1000) for 90 min at 37°C. After washing (2 x quickly with TBS, 1 x 15 min 0.1% TBS-Tween and 2 x 5 min 0.1% TBS-Tween), membranes were incubated for 90 min at room temperature in the presence of the secondary antibody (HRP-conjugated) (1:10,000 dilution) and washed again (2 x quickly with 0.1% TBS-Tween, 1 x 15 min 0.1% TBS-Tween, 1 x 5 min 0.1% TBS-Tween and 2 x 5 min TBS). Finally, the conjugates were visualized by chemiluminescence detection in a Phosphoimager 840.

3.2.7 Molecular biological methods

3.2.7.1 RT-PCR experiments

The reverse transcription polymerase chain reaction (RT-PCR) allows the analysis of RNA by PCR. cDNA is synthesized from RNA templates using reverse transcriptases (RNA-dependent DNA polymerases) isolated from a variety of retroviral sources. The expression of the mineralocorticoid receptor mRNA was detected using RT-PCR. 5×10^6 cells were seeded and cultured in 75 cm^2 flasks in control medium. The next day, cells were harvested, washed twice with PBS and kept on ice. Total RNA was isolated with the RNeasy Mini Kit 50 (Qiagen, Hilden, Germany) and 2.5 µg of RNA was used for cDNA synthesis using the RevertAid First Strand cDNA Synthesis Kit (Fermentas GmbH, St. Leon-Rot, Germany). cDNA was amplified by PCR using REDTaq^{TM} ReadyMix^{TM} PCR Reaction Mix (Sigma-Aldrich, Taufkirchen, Germany) for 35-40 cycles with an annealing temperature of 52°C (MR pig/MR dog). The following primers with the respective GenBank accession number and predicted size were used for amplification: mineralocorticoid receptor pig (U88893; 303 bp) 5'-TGCACCAGTCTGCCATGTAT-3' (sense), 5'-ATTCCAACAAGTCGCTCACC-3' (antisense) and mineralcorticoid receptor dog (DG195096; 244 bp) 5'-ACAGGATTGGTGCTCAAGGT-3' (sense), 5'-TGCAGTCGAACGAACTGAAG' (antisense). All primers were designed with the program Primer3 [150].

3.2.8 Statistical analysis

For comet assay, micronucleus frequency test, and O$_2$$^{\cdot-}$ quantification results, Mann-Whitney test was used to determine significance between two groups. Kruskal-Wallis test was used to determine significance between multiple groups. For calculations SPSS 17.0 was used. Values are given as means ± SEM or as means ± standard deviation. The quantification of 8-oxodG by LC-MS was done once. Here the mean of two serial measurements of the same sample is shown.

For the results of EMSA and fluorimetric measurements of oxidative stress, one way analysis of variance (ANOVA) with subsequent post hoc comparisons by Scheffe, were performed using Statview 5.0.1 (Brainpower Inc., Calabazas CA). A p value ≤ 0.05 was considered statistically significant. Values are given as means ± SEM.

Except for 8-oxodG quantification all experiments were done at least three times.

For the *in vivo* study, data from at least 5 animals ± SEM are depicted.

Results were considered significant if p values were ≤ 0.05.

For the evaluation of proliferation only two animals were treated with BrdU, here the mean value alone is shown.

4 RESULTS

4.1 *Oxidative stress and DNA damage caused by aldosterone* in vitro

4.1.1 Aldosterone induces oxidative stress

It is known that one of the most important pathways by which aldosterone exerts its negative effects on the kidney is by generation of ROS. This hypothesis was tested in two kidney cell lines: LLC-PK1 cells from pig kidney, which resemble proximal tubule cells and MDCK cells from dog kidney which resemble distal tubule cells. H_2DCF-DA is a nonfluorescent probe that enters the cell where it is oxidized to a fluorescent derivative (DCF) by endogenous oxidant (RNS and ROS) species, with particular reactivity towards $ONOO^-$. Flow cytometric measurements using the probe H_2DCF-DA showed that 100 nM aldosterone caused a significant production of ROS in LLC-PK1 and MDCK cells (Figure 19).
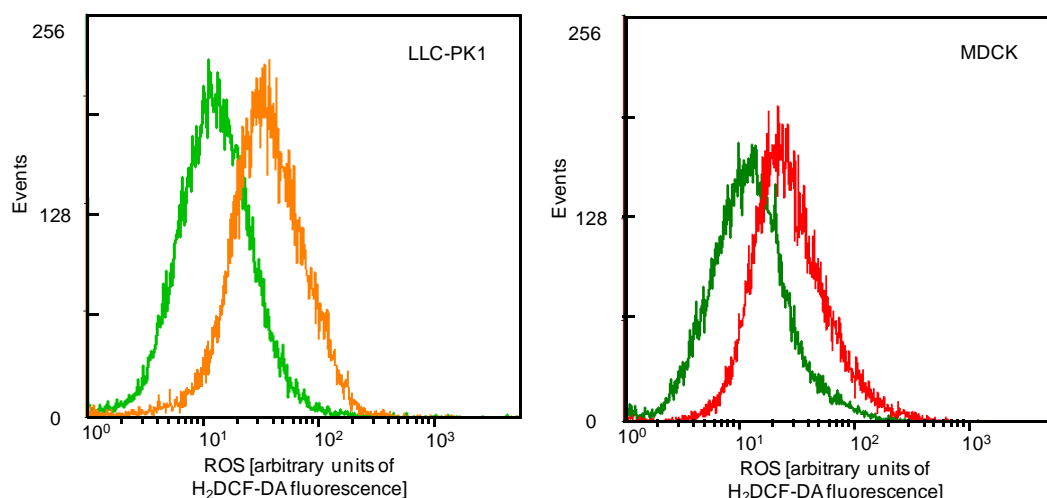
Figure 19: Flow cytometric analysis of aldosterone-induced ROS formation in LLC-PK1 and MDCK cells.
Shown are representative frequency histograms of the green flourescence of DCF-positive cells in control cells (green lines) and cells after 30 min aldosterone treatment with 100 nM aldosterone (red lines).

Results of fluorimetrical measurements, using the probe H_2DCF-DA showed that 10 nM aldosterone triggers a significant induction of DCF fluorescence in LLC-PK1 cells which reached a maximum after 30 min and 4 h incubation and stayed high until the last time point measured (24 h) (Figure 20).
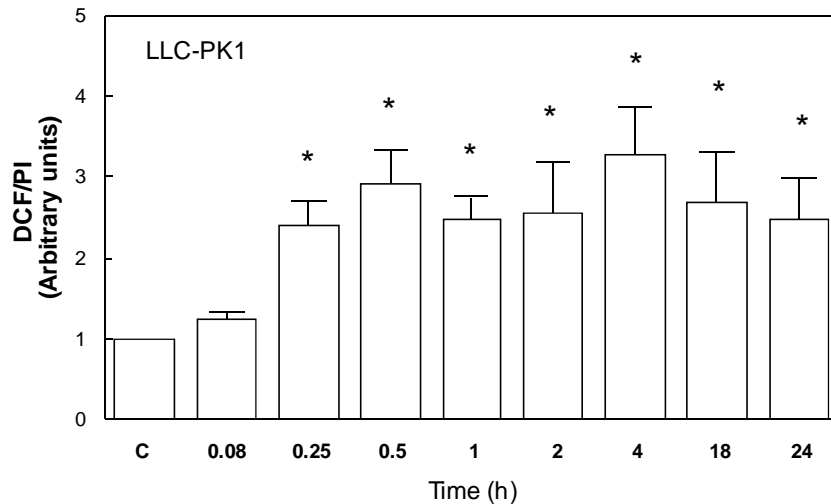
Figure 20: Kinetics of oxidant production caused by aldosterone in LLC-PK1 cells.
ROS production was observed by using the probe H_2DCF-DA. LLC-PK1 cells were treated for the indicated time periods with 10 nM aldosterone. Oxidation of H_2DCF-DA was detected by monitoring the increase in fluorescence fluorimetrically with appropriate filters for fluorescein. Results are presented as mean ± SEM of 3 independent experiments. * p≤0.05 vs. control

$O_2^{\cdot-}$ production was monitored by staining LLC-PK1 and MDCK cells with DHE, a fluorescent dye, changing its emission wavelength upon oxidation by ROS, mainly by $O_2^{\cdot-}$. As can be seen in Figure 21A, 10 nM aldosterone caused a significant increase in red fluorescence compared to control cells (Figure 21). The quantification of the DHE fluorescence by ImageJ is shown in Figure 22.
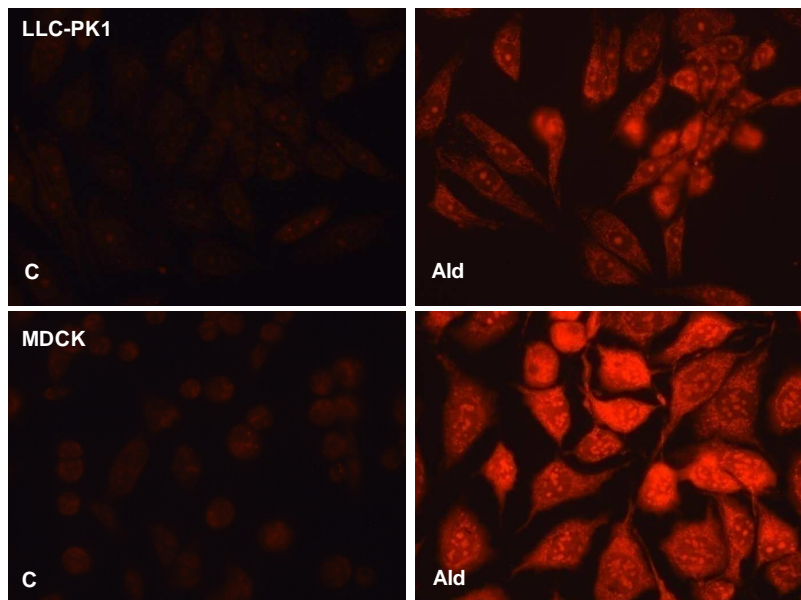
Figure 21: Aldosterone-induced superoxide production in LLC-PK1 and MDCK cells.
Representative pictures of LLC-PK1 and MDCK cells are shown, incubated with 10 nM aldosterone for 4 h and oxidants evaluated with the $O_2^{\cdot-}$-reactive probe DHE. Pictures were taken at 200-fold magnification.
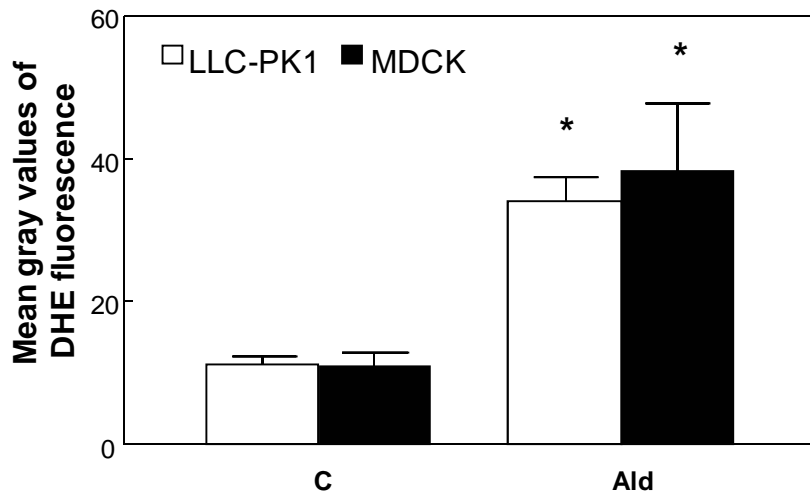
Figure 22: Quantification of aldosterone-induced superoxide production in LLC-PK1 and MDCK cells.
Quantification of DHE fluorescence by measurement of mean gray values of 200 LLC-PK1 and MDCK cells per treatment without (C) or with 10 nM aldosterone (Ald) by ImageJ. Results are presented as mean ± SEM of 3 independent experiments. * $p \leq 0.05$ vs. control.

4.1.2 Aldosterone induces DNA damage

To ensure the observation of genotoxic effects, a possible influence of cytotoxicity of aldosterone was eliminated by monitoring several endpoints of cell vitality. Aldosterone in concentrations up to 1 µM after 4 and 24 h incubation did not decrease the number of viable LLC-PK1 and MDCK cells (Table 2). A marker for early apoptosis (% caspase-3 positive cells) was significantly increased in LLC-PK1 cells only at 1 µM aldosterone and in MDCK cells at 500 nM and 1 µM aldosterone (Table 2). Nevertheless, the increase in the number of late apoptotic cells observed under the microscope after 24 h recovery did not reach significance in both cell lines (Table 2).

Table 2: Effects of aldosterone on cell viability, proliferation and apoptosis.
Percentage of viable cells was assessed after 4 and 24 h incubation with aldosterone. The proliferation index was calculated after 4 h incubation with aldosterone, followed by a 24 h recovery period. Early apoptosis was detected fluorimetrically with an antibody against active caspase-3 after a 4 h aldosterone incubation (caspase-3 positive cells) and late apoptotic cells (cells with condensed chromatin) were counted after 4 h incubation with aldosterone, followed by a 24 h recovery period. Shown are mean values ± SEM of three independent experiments.

	Treatment	LLC-PK1	MDCK
% vital cells (after 4 h)	Control	96.01 ± 0.25	98.61 ± 1.40
	100 nM Ald	95.81 ± 0.11	98.79 ± 1.43
	500 nM Ald	95.62 ± 0.24	99.56 ± 0.19
	1.0 µM Ald	96.60 ± 0.25	99.34 ± 0.44
% vital cells (after 24 h)	Control	95.67 ± 0.39	98.82 ± 0.28
	100 nM Ald	95.47 ± 0.34	98.97 ± 0.29
	500 nM Ald	95.45 ± 0.50	98.64 ± 0.51
	1.0 µM Ald	93.79 ± 0.53	98.50 ± 0.33
Proliferation index	Control	2.00 ± 0.01	1.74 ± 0.06
	100 nM Ald	2.00 ± 0.01	1.72 ± 0.08
	500 nM Ald	2.01 ± 0.01	1.73 ± 0.08
	1.0 µM Ald	2.01 ± 0.01	1.71 ± 0.08
Caspase-3 positive cells/500 cells	Control	6.00 ± 1.00	10.00 ± 2.00
	100 nM Ald	10.00 ± 1.53	13.70 ± 3.21
	500 nM Ald	8.67 ± 1.45	17.30 ± 2.08*
	1.0 µM Ald	14.00 ± 2.08*	20.00 ± 3.61*
Cells with condensed chromatin/1000 BN cells	Control	8.33 ± 1.85	10.67 ± 3.06
	100 nM Ald	6.67 ± 2.87	8.67 ± 4.04
	500 nM Ald	7.00 ± 3.27	12.67 ± 6.03
	1.0 µM Ald	11.33 ± 1.89	10.67 ± 1.53

To investigate the genotoxic potential of aldosterone, two different genotoxicity tests were employed. In the comet assay a significant increase of DNA strand breaks was observed over the whole range (1-100 nM) of aldosterone concentrations tested (Figure 23A). The significant formation of micronuclei, a subset of chromosomal aberrations monitored in the micronucleus frequency test, started at aldosterone concentrations of 5 nM and 10 nM for LLC-PK1 and MDCK cells, respectively (Figure 23B).

A

B
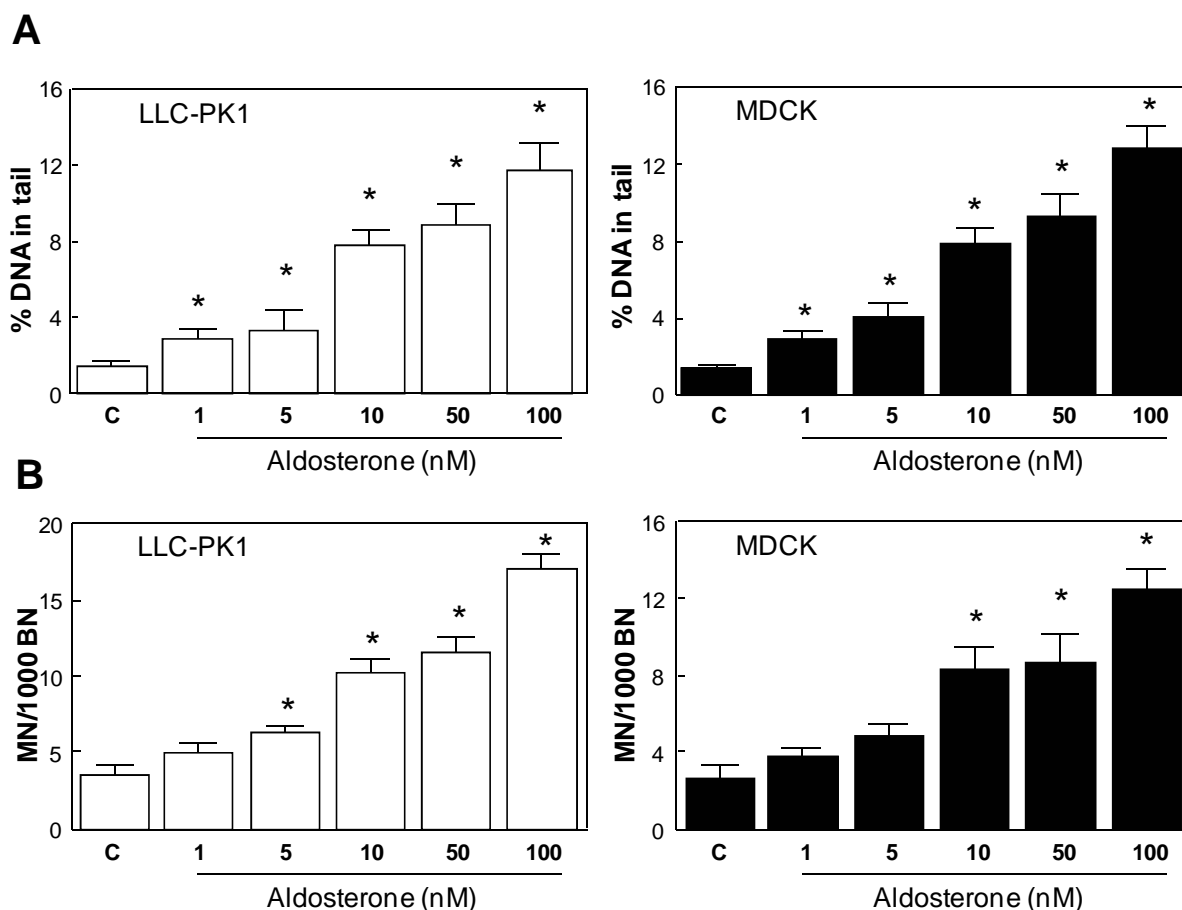
Figure 23: Dose-dependency of the DNA damaging effects of aldosterone.
LLC-PK1 and MDCK cells were incubated in the presence of 1-100 nM aldosterone for 4 h. A: DNA-strand breaks quantified with the comet assay. Results are shown as the percentage of DNA in tail. B: Micronuclei formation induced in LLC-PK1 and MDCK cells treated for 4 h with aldosterone, followed by 24 h incubation with 3 µg/ml of the cytokinesis blocker cytochalasin B. Data are presented as mean of micronuclei containing cells (MN) per 1000 binucleated cells (BN) ± SEM of 3 independent experiments. * p≤0.05 vs. control.

4.1.2.1 Aldosterone induces oxidative DNA damage

To further characterize the DNA damage caused by aldosterone, the comet assay was performed with an additional incubation in the presence of the DNA repair enzyme FPG. The oxidative base modification 8-oxodG is the main DNA lesion recognized by FPG. While the normal alkaline comet assay detects strand breaks and abasic sites, the addition of FPG allows the quantification of 8-oxodG. The enzyme incises the DNA at the site of the lesion, thereby generating additional strand breaks [153]. Treatment with aldosterone significantly increased the occurrence of FPG-sensitive sites in LLC-PK1 and MDCK cells (Figure 24).
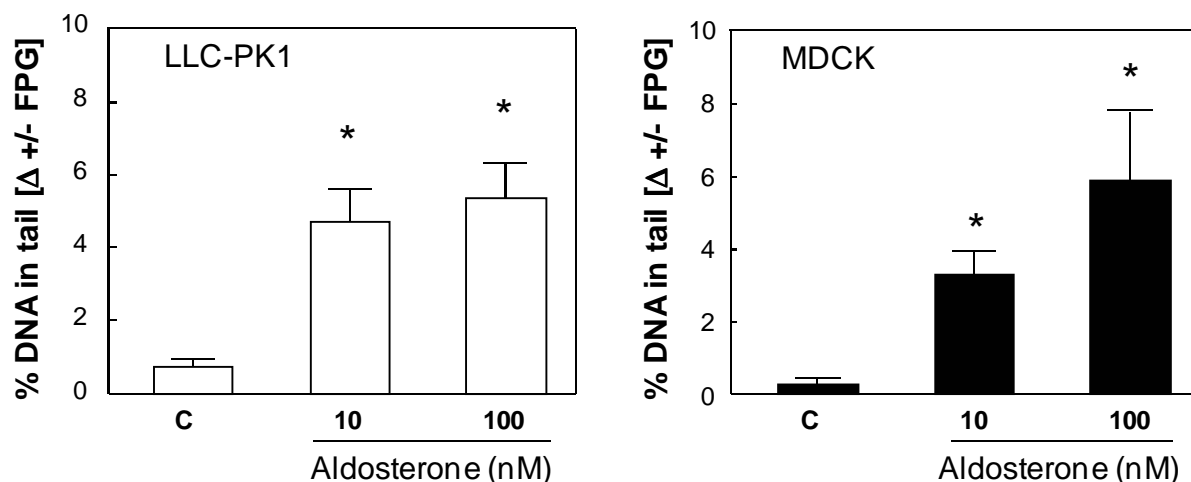
Figure 24: Oxidative DNA damage induced by aldosterone measured by the FPG-modified comet assay.
DNA damage in LLC-PK1 and MDCK cells after 4 h treatment with the indicated aldosterone concentrations. Depicted is the mean of the difference (Δ) in the percentage of DNA in tail between nuclei treated and untreated with FPG enzyme. Results are shown as mean ± standard deviation of 3 independent experiments. * p≤0.05 vs. control.

Additionally, aldosterone-triggered 8-oxodG formation was quantified by mass spectrometry in both cell lines. This very sensitive method showed that 10 nM aldosterone caused an approximately 4-fold and 5-fold 8-oxodG increase in LLC-PK1 and MDCK cells, respectively (Figure 25).
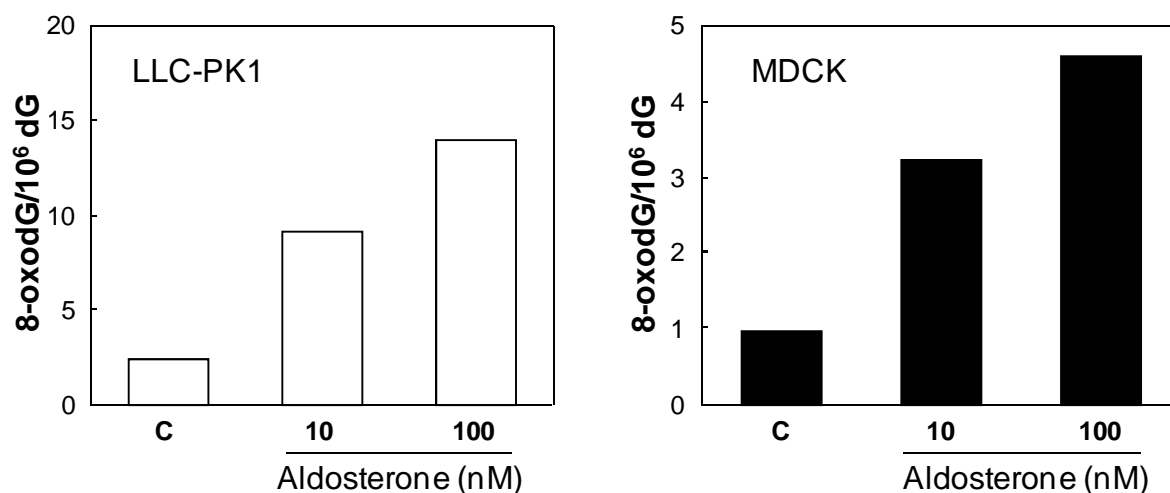

Figure 25: Oxidative DNA damage induced by aldosterone measured by mass spectrometry.
Quantification of 8-oxodG in LLC-PK1 and MDCK cells treated with aldosterone in the indicated concentrations by mass spectrometry. Data are presented as the amount of 8-oxodGs per 10^6 dihydroguanines (dG) from one experiment.

4.1.2.2 Aldosterone induces oxidative stress and DNA damage nongenomically

Besides the classical genomic effects, aldosterone exerts fast nongenomic effects via signaling cascades. To classify the DNA damaging effects of aldosterone, which most probably are caused by oxidative stress, the time-dependent increase of $O_2^{\cdot-}$ cell levels (evaluated with the probe DHE) and the induction of DNA strand breaks and micronuclei was examined. A cellular $O_2^{\cdot-}$ increase was detected after 5 min incubation with 10 nM aldosterone in LLC-PK1 cells (Figure 26A), that continuously rose up to the last time point tested (4 h). The quantification of the DHE fluorescence images revealed a significant fluorescence increase (35 %) in LLC-PK1 cells after 5 min treatment with 10 nM aldosterone (Figure 26B). In MDCK cells, DHE fluorescence increase (42%) was significant starting at 30 min incubation with 10 nM aldosterone.
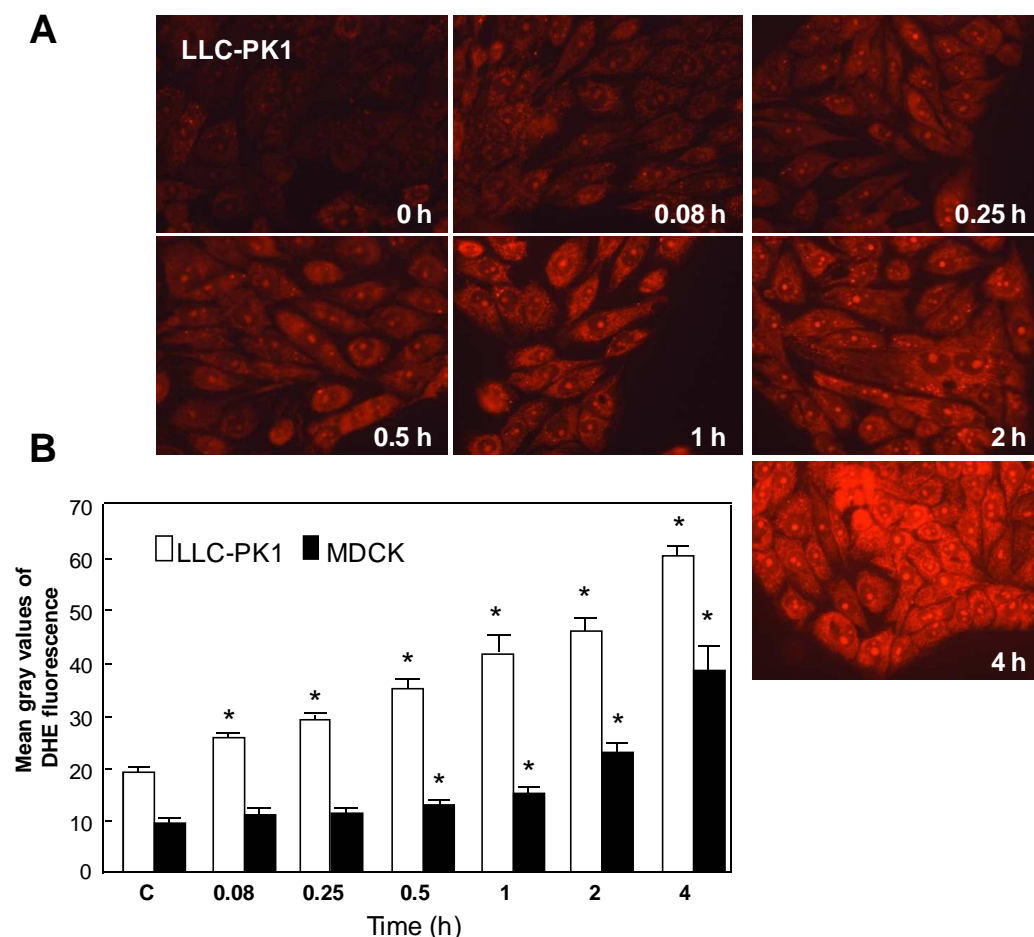
Figure 26: Kinetics of superoxide increase caused by aldosterone.
A: Representative pictures of LLC-PK1 cells incubated for the indicated times with 10 nM aldosterone and oxidants evaluated with the $O_2^{\cdot-}$-reactive probe DHE. Pictures were taken at 200-fold magnification. B: Quantification of fluorescence by measurement of mean gray values of 200 LLC-PK1 and MDCK cells per treatment with ImageJ. Results are presented as mean ± SEM of 3 independent experiments. * p≤0.05 vs. control.

The induction of DNA strand breaks was detectable and significant in both cell lines after only 5 min incubation with 10 nM aldosterone and continued rising up to the last time point tested (4 h) (Figure 27A). Formation of micronuclei needed a slightly longer time to become significant. After 30 min incubation with aldosterone this subset of chromosomal aberrations could be detected in LLC-PK1 and MDCK cells (Figure 27B).
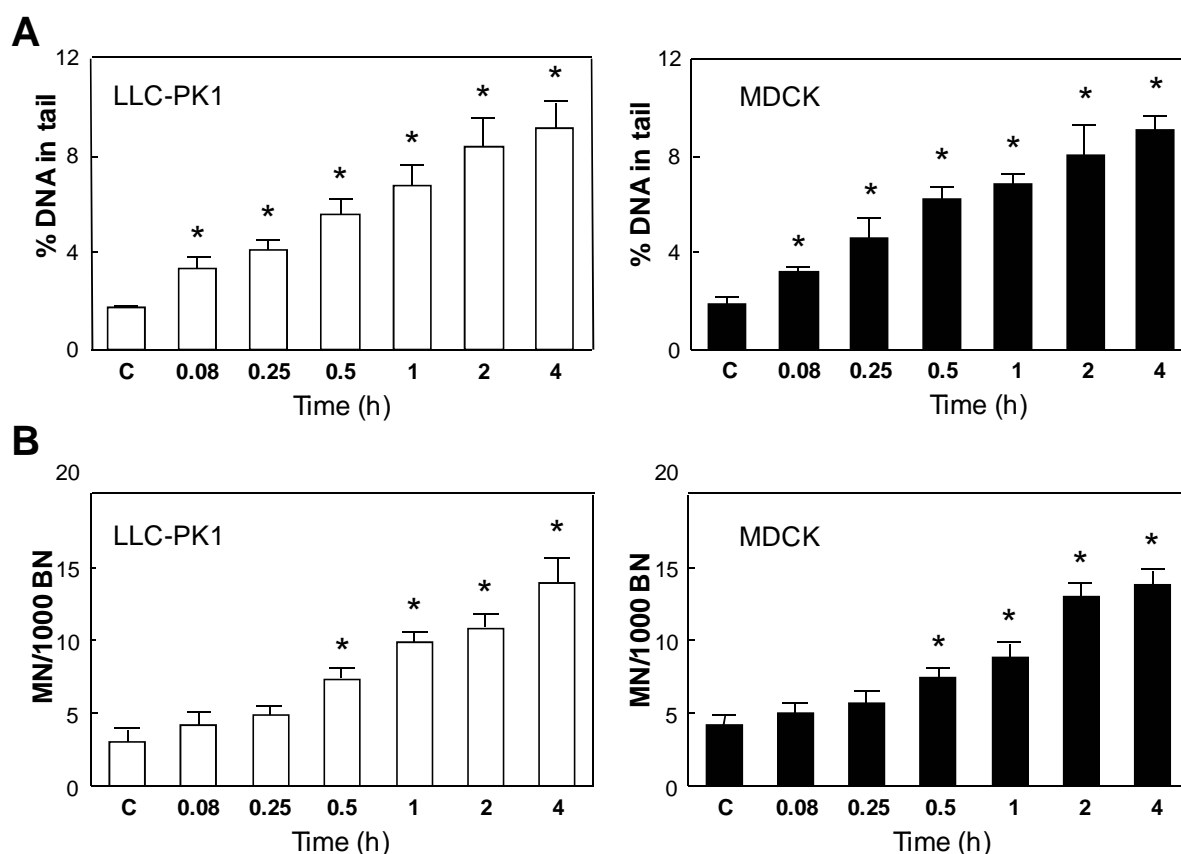
Figure 27: Kinetics of DNA damage caused by aldosterone.
A: DNA strand breaks induced by 10 nM aldosterone quantified with the comet assay in LLC-PK1 and MDCK cells incubated for the indicated times. Shown is the percentage of DNA in tail. B: Micronuclei formation induced by 10 nM aldosterone quantified with the micronucleus test in LLC-PK1 and MDCK cells incubated for the indicated times with aldosterone, followed by 24 h incubation with 3 µg/ml of cytochalasin B. Shown are micronuclei containing cells (MN) per 1000 binucleated cells (BN). Results are presented as mean ± SEM of 3 independent experiments. * p≤0.05 vs. control.

4.1.3 Aldosterone-induced oxidative stress and DNA damage are prevented by antioxidants

To strengthen the hypothesis that aldosterone-induced DNA damage occured as a consequence of increased cell oxidants, the production of oxidants and the influence of selected antioxidants was next investigated. Cell oxidants were evaluated with the probe H_2DCF-DA. Aldosterone caused a significant increase in

DCF fluorescence in LLC-PK1 and MDCK cells (Figure 28). This increase in cell oxidants was partially or totally prevented by the simultaneous incubation of cells with the cell permeable antioxidants (±)-α-lipoic acid (LA), N-acetyl cysteine (NAC) and tempol. LA acts as an antioxidant through different mechanisms including glutathione reduction, free radical scavenging, and metal chelation [166-167]. NAC provides the cysteine required for GSH synthesis, a critical molecule in the defense of cells against oxidative stress. NAC can also increase other thiol pools and can directly scavenge ROS and RNS [168] and tempol scavenges mainly $O_2^{\cdot-}$ and, to some extent, other radicals [169].

Figure 28: Aldosterone-induced oxidant production is inhibited by antioxidants.
LLC-PK1 and MDCK cells were incubated in the absence (C) and the presence of aldosterone (Ald). Aldosterone-treated cells were simultaneously incubated with either 0.5 mM (±)-α-lipoic acid (LA), 0.5 mM N-acteyl-cysteine (NAC) or 50 μM tempol (Tem). Cells were incubated with 100 nM aldosterone and cellular oxidant levels were measured fluorimetrically with the probe H_2DCF-DA after 30 min and 120 min incubation in the combinations described above for LLC-PK1 and MDCK cells, respectively. DCF fluorescence data are shown normalized to the PI fluorescence. Results are shown as mean ± SEM of 3 independent experiments. * p≤0.05 vs. control, °p ≤0.05 vs. aldosterone treatment.

The DNA damaging effects of aldosterone measured with the comet assay (Figure 29A) and with the micronucleus frequency test (Figure 29B) were also prevented by the addition of the three different antioxidants LA, NAC and tempol, in both LLC-PK1 and MDCK cells. NAC was the less effective antioxidant in both cell lines.

A

B

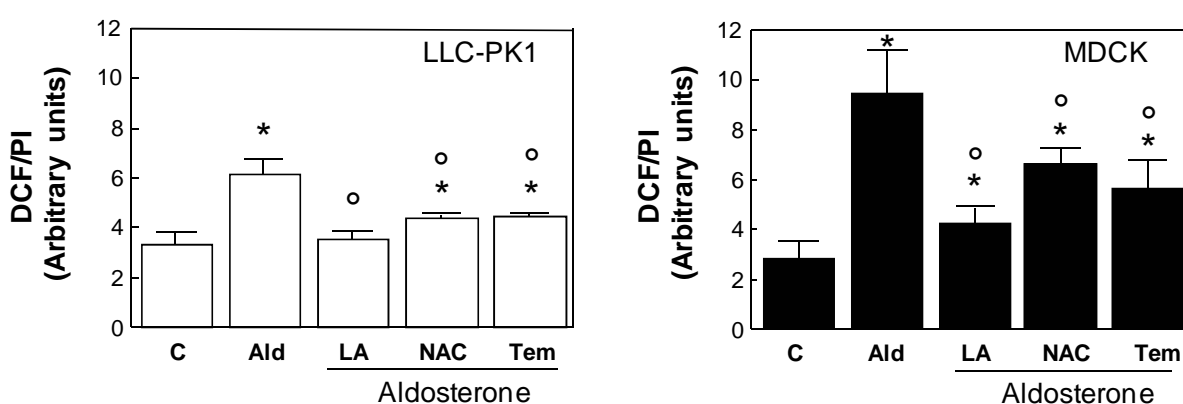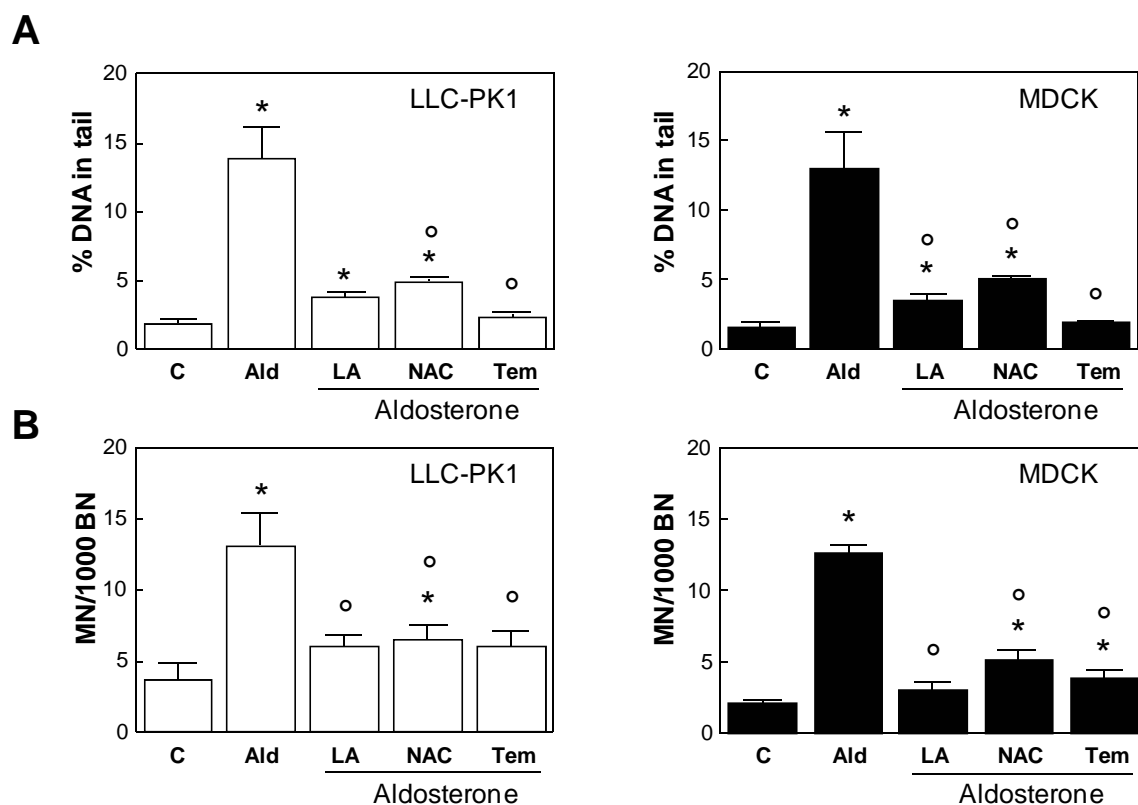**Figure 29: Aldosterone-induced DNA damage is inhibited by antioxidants.**
LLC-PK1 and MDCK cells were incubated in the absence (C) and the presence of aldosterone (Ald). Aldosterone-treated cells were simultaneously incubated with either 0.5 mM (±)-α-lipoic acid (LA), 0.5 mM N-acteyl-cysteine (NAC) or 50 µM tempol (Tem) A: DNA strand breaks quantified with the comet assay after 4 h incubation with 10 nM aldosterone in the combinations described above. Shown is the percentage of DNA in tail. B: Micronuclei formation quantified after 4 h incubation with 10 nM aldosterone in the combinations described above, followed by 24 h incubation with 3 µg/ml cytochalasin B. Shown are micronuclei containing cells (MN) per 1000 binucleated cells (BN). Results are shown as mean ± SEM of 3 independent experiments. * p≤0.05 vs. control, ° p≤0.05 vs. aldosterone treatment.

4.2 Aldosterone causes oxidative stress and DNA damage in kidneys of DOCA-salt rats mediated by the mineralocorticoid receptor

To investigate the possible DNA damaging effect of aldosterone *in vivo*, rats were treated with desoxycorticosterone acetate (DOCA), a precursor of aldosterone, and salt, to induce a mineralocorticoid-dependent hypertension.

4.2.1 DOCA/salt-treatment leads to oxidative stress

Since aldosterone is known to induce oxidative stress, ROS were measured in kidney cells of the rats by flow cytometry. Compared to the sham group, DOCA/salt-treatment induced a significant release of ROS. Treatment with the MR antagonists spironolactone or BR-4628 resulted in a significant decrease of oxidative stress-

induced fluorescence (Figure 30) (Data from the dissertation of Ursula Schmid, University of Würzburg, 2007).
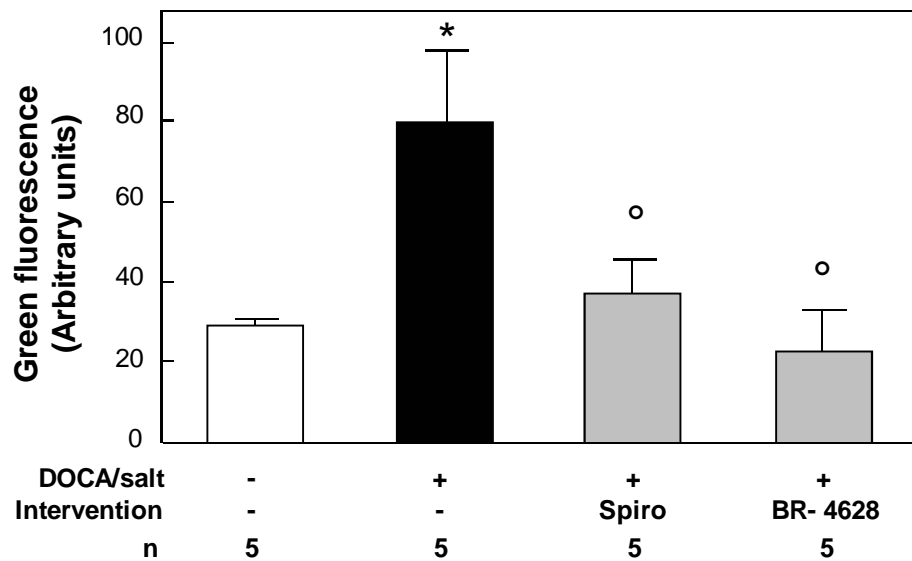
Figure 30: Oxidative stress measurements in rat kidneys by flow cytometry.
Flow cytometrical quantification of ROS in rat kidney cells from sham-operated, DOCA/salt-treated, spironolactone-treated and BR-4628-treated rats after 6 weeks of treatment. Shown is the mean of arbitrary units of green fluorescence ± SEM. Quantification * $p \leq 0.05$ vs. control, ° $p \leq 0.05$ vs. DOCA/salt

Staining of cryosections of rat kidneys with the dye DHE showed a much higher $O_2^{\cdot -}$ formation in the DOCA/salt group than in the sham, spironolactone and BR-4628 group (Figure 31A). Treatment with spironolactone and BR-4628 significantly reduced the DHE fluorescence quantified with ImageJ (Figure 31B).

A
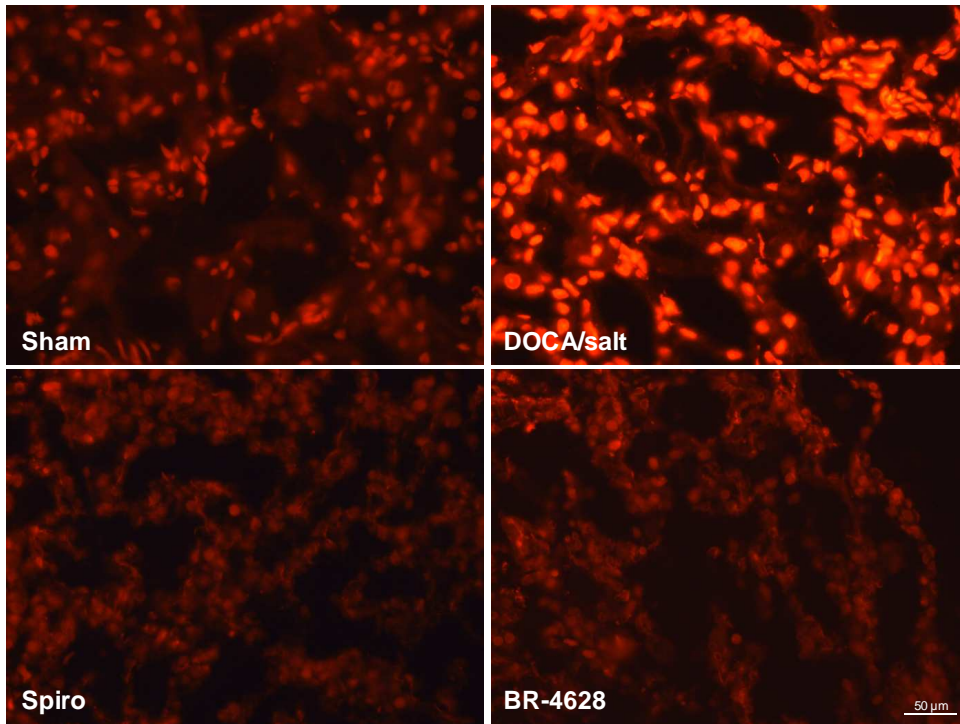
B
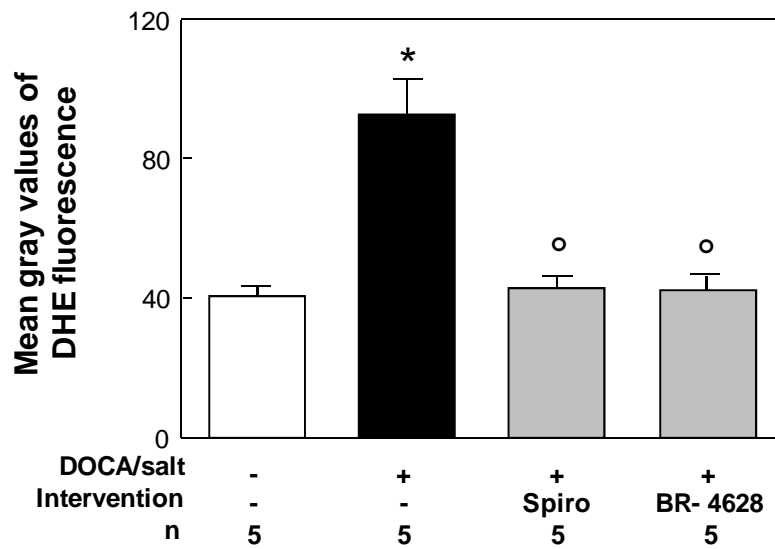
Figure 31: Detection of superoxide in rat kidneys by DHE staining.
A: Visualisation of $O_2^{\cdot-}$ formation with help of the dye DHE on cryosections of kidneys from sham-operated, DOCA/salt-treated, spironolactone-treated and BR-4628-treated rats after 6 weeks of treatment. B: Quantification of fluorescence by measurement of mean gray values of rat kidney cells with ImageJ. Quantification * p≤0.05 vs. control, °p ≤0.05 vs. DOCA/salt.

4.2.2 DOCA/salt-treatment leads to structural DNA damage

Measurements of the amount of DNA strand breaks subsequent to DOCA/salt-treatment, assessed by the comet assay, showed that DOCA/salt alone induced a significant formation of DNA damage compared to the untreated sham animals. After co-treatment of the DOCA/salt-animals with spironolactone or BR-4628, a significant decrease in the incidence of DNA strand breaks could be observed (Figure 32) (Data from the dissertation of Ursula Schmid, University of Würzburg, 2007).

DOCA/salt	-	+	+	+
Intervention	-	-	Spiro	BR-4628
n	5	5	5	5
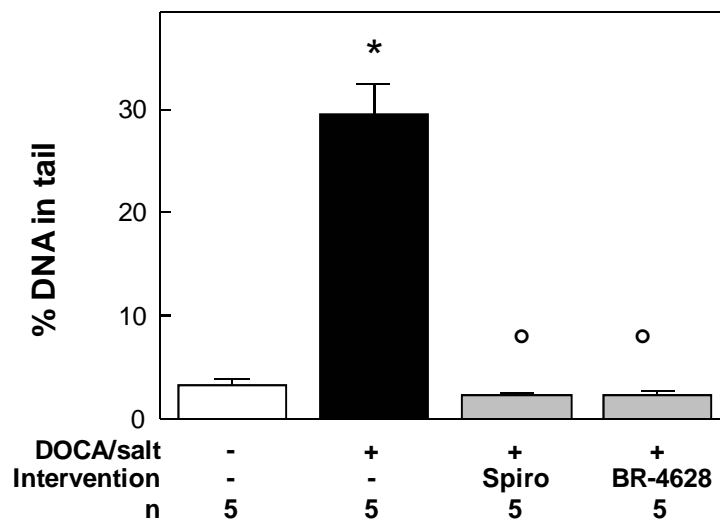
Figure 32: DNA damage in rat kidney cells extracted out of kidneys measured by the comet assay.
DNA damage in male Sprague Dawley rats as measured by the comet assay after 6 weeks of DOCA-treatment with or without co-treatment with spironolactone or BR-4628. Shown is the mean of DNA damage ± SEM as % DNA in tail. * $p \leq 0.05$ vs. control, °$p \leq 0.05$ vs. DOCA/salt treatment.

Immunohistochemical staining for the double strand break marker γ-H2AX and scoring of the positive stained cells showed a significant induction of double strand breaks in the DOCA/salt-treated animals compared to the sham, spironolactone and BR-4628 animals (Figure 33).

A
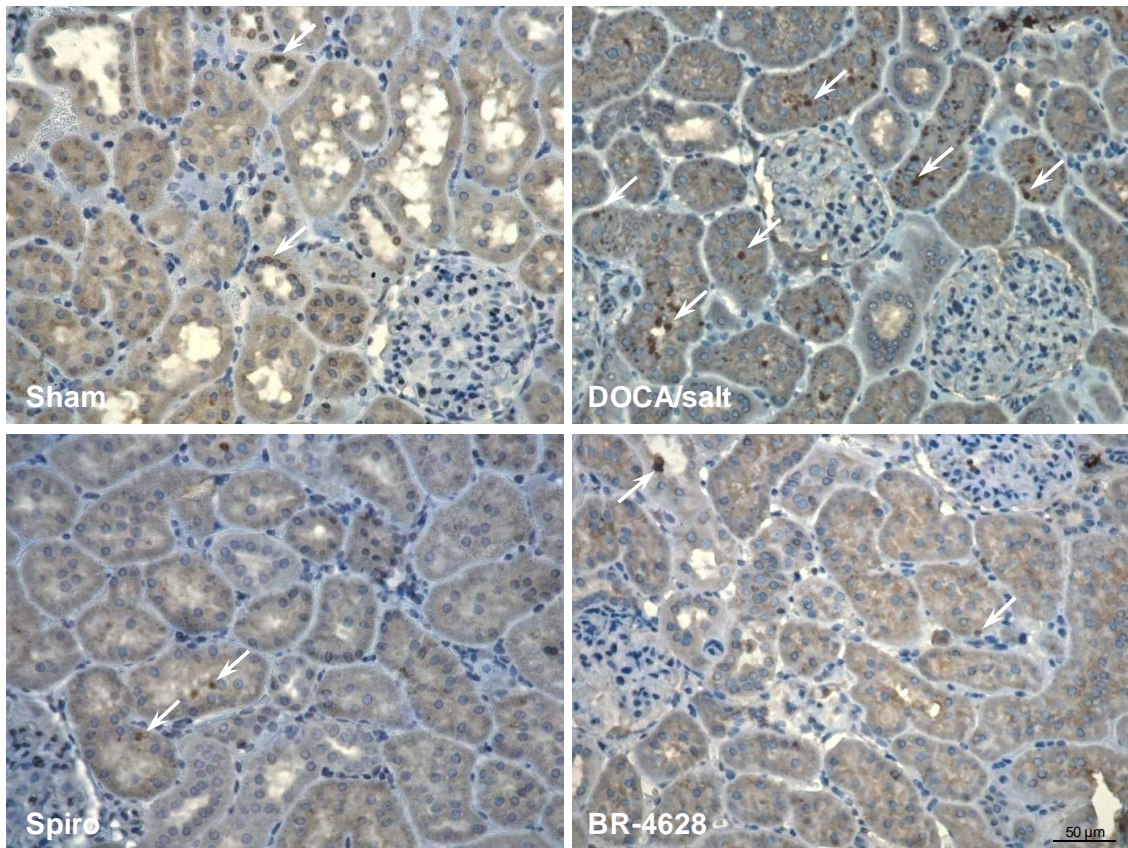
B
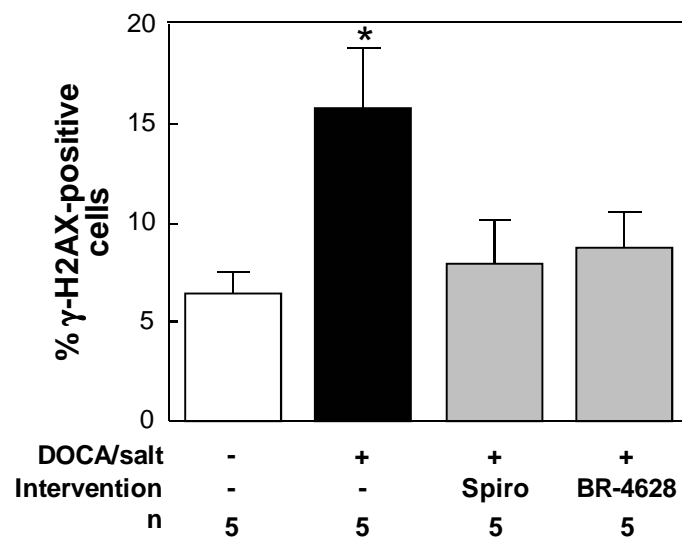
Figure 33: Immunohistochemical detection of the DNA double strand break marker γ-H2AX.
A: Representative pictures of γ-H2AX antibody (1:25) staining on paraffin embedded kidney sections from sham-operated, DOCA/salt-treated, spironolactone-treated and BR-4628-treated rats after 6 weeks of treatment. Some examples of positive stained nuclei are marked with white arrows. B: Mean percentage of γ-H2AX positive cells ± SEM was assessed for tubules by scoring approximately 290 tubules.

4.2.3 DOCA/salt-treatment causes oxidative DNA damage

Mass spectrometrical analysis of DNA isolated out of the kidneys of sham and DOCA/salt-treated animals revealed a significant increase of the oxidatively formed mutagenic base modification 8-oxodG in the DOCA/salt group (Figure 34).
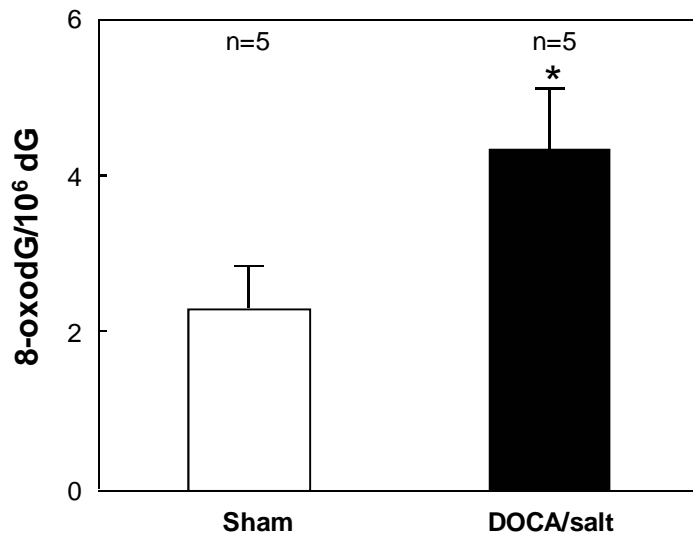
Figure 34: Detection of 8-oxodG in rat kidneys by mass spectrometry.
Mean amount of 8-oxodG $\pm$ SEM per 10^6 dG in the DNA of kidneys of sham-operated rats and DOCA/salt-treated rats after 6 weeks of treatment. * $p \leq 0.05$ vs. sham rats

4.2.4 Assessment of apoptosis after DOCA/salt-treatment

To estimate a possible artefactual impact of apoptosis in the kidney on the results of DNA damage and double strand breaks, the levels of cleaved caspase-3 was investigated. Immunofluorescent staining of cleaved caspase-3 on kidney slices showed no significant increase of apoptosis in the DOCA/salt-treated animals compared to the sham animals (Figure 35A and B), but slightly lower occurrence of apoptotic cells in kidneys of BR-4628- treated animals.

A
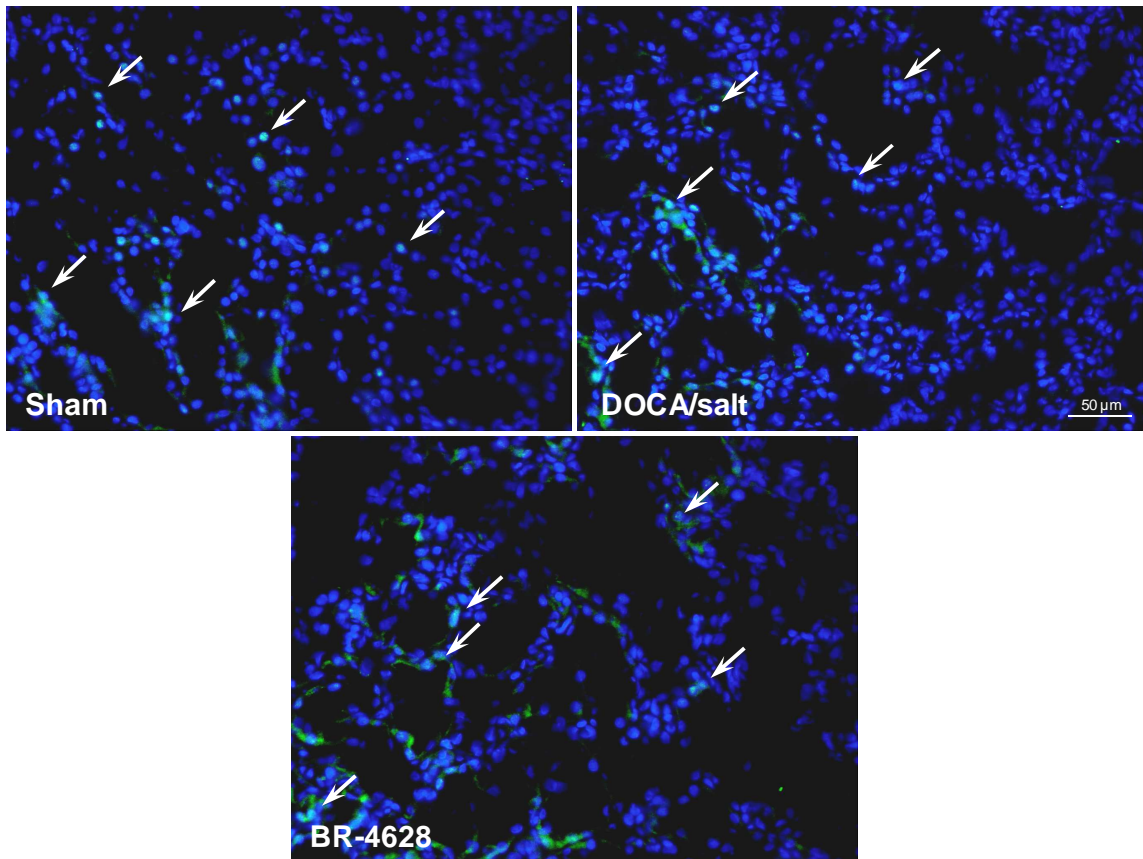
B
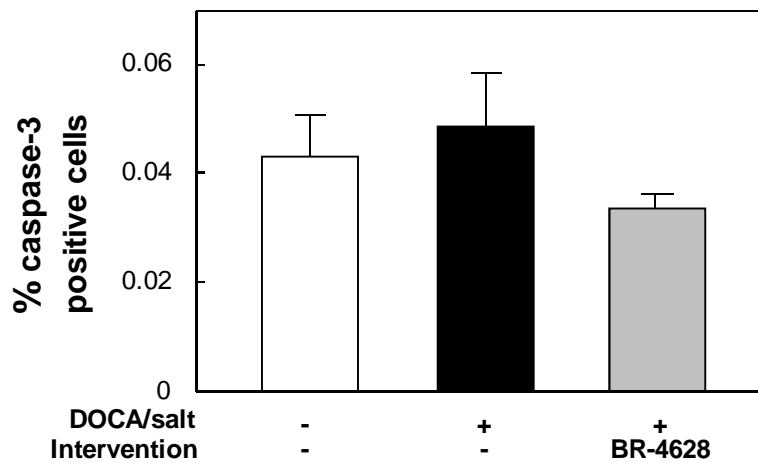
Figure 35: Detection of cleaved caspase-3 on cyrosections.
A: Representative pictures of the immunohistochemical detection of the apoptotic marker, cleaved caspase-3 (1:100) on kidney cryosections from sham operated, DOCA/salt-treated and BR-4628-treated rats after 6 weeks of treatment. Some examples of positive stained cells are marked with white arrows. Green fluorescence: caspase-3, blue fluorescence: nuclei stained with DAPI, B: Percentage of cells positive for cleaved caspase-3, scored within 1200 to 1700 cells seen in 2 to 3 pictures of one section from sham-operated rats and DOCA/salt-treated rats with and without BR-4628 medication after 6 weeks of treatment.

4.2.5 Assessment of proliferation after DOCA/salt-treatment

In this study an increased weight of the kidneys were observed under DOCA/salt-treatment (data not shown). This suggests an elevated kidney cell proliferation. To evaluate this possibility, cells on cytospins, as well as tissue sections from two rats of each group equipped with BrdU-pumps were stained with an antibody against BrdU (Figure 36A).
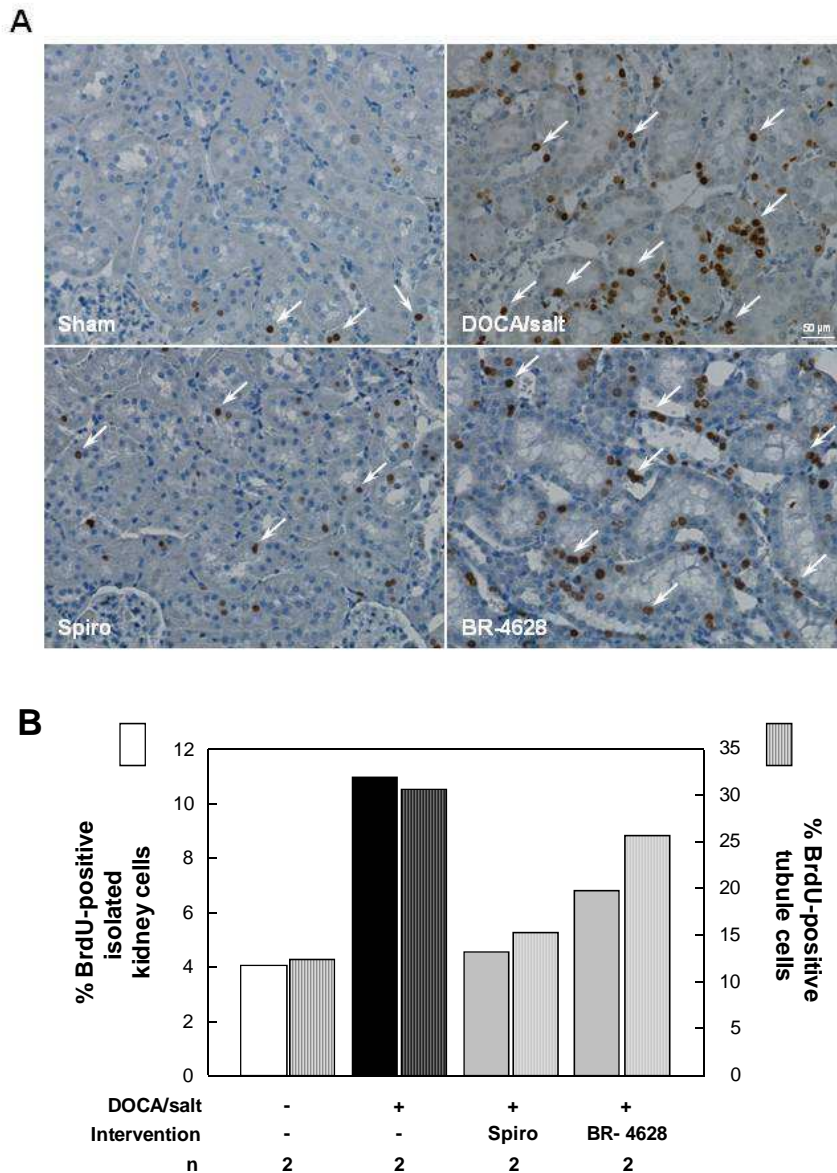
Figure 36: Detection of BrdU-positive cells on paraffin embedded kidney sections.
A: Representative pictures of the immunohistochemical detection of proliferating cells (1:10 anti-BrdU) on paraffin embedded kidney sections from sham-operated, DOCA/salt-treated, spironolactone-treated and BR-4628-treated rats after 6 weeks of treatment, including BrdU-exposure during the last week of the experiment. B: Percentage of BrdU-positive cells either scored within 500 to 800 isolated kidney cells on cytospin slides or scored in approximately 290 tubules on paraffin embedded kidney sections after immunohistochemical staining for BrdU of two sham-operated, two DOCA/salt-treated, two spironolactone-treated and BR-4628-treated rats after 6 weeks of treatment including BrdU-treatment during the last week of the experiment. Shown is the mean of the two BrdU-treated animals.

BrdU, a chemical analogue of thymidin, is incorporated into the DNA during the S-phase of proliferating cells. The DOCA/salt-treatment indeed led to an increase of BrdU-positive cells. To analyze the tissue slices, only cells of the highly affected cortical tubules were included in the scoring. Therefore, the increase of proliferating cells is more pronounced here, while on the cytospins cells extracted out of all kidney regions are represented (Figure 36B).

4.3 Aldosterone activates transcription factors and signaling pathways in vitro

Since aldosterone produces oxidative stress, we next investigated the activation of the redox-sensitive transcription factors Nrf2 and NF-κB, the activation of the redox-sensitive ERK signaling pathway and the subsequent activation of the transcription factors CREB, STAT1 and STAT3.

4.3.1 Transcription factor Nrf2

Nrf2 is activated by oxidative and nitrosative stress and is essential for the coordinated induction of genes encoding many stress-responsive enzymes and related proteins. The activation of Nrf2, the induction of Nrf2-regulated genes and the resulting consequences for LLC-PK1 cells were investigated.

4.3.1.1 Aldosterone activates the potentially protective transcription factor Nrf2

The activation of Nrf2 by aldosterone was evaluated in the pig kidney cell line LLC-PK1, measuring the Nrf2-DNA binding in nuclear fractions by EMSA. The incubation of LLC-PK1 cells with 100 nM aldosterone caused an increase in nuclear Nrf2-binding, which reached a maximum after 30 min and 4 h incubation and afterwards went down gradually (Figure 37A). The specificity of the Nrf2-DNA complex in the EMSAs was assessed by competition with a 100-fold molar excess of unlabeled consensus oligonucleotides (cold), displacing all radiolabeled oligonucleotides (hot), resulting in the disappearence of the Nrf2-DNA complexes. Furthermore, the specificity of the Nrf2-DNA complex in the EMSAs was ascertained by competition with a 100-fold molar excess of unlabeled specificity protein-1 (SP-1), which does not displace the hot Nrf2 oligonucleotides, resulting in the Nrf2-DNA complexes

(Figure 37A). Induction of Nrf2 expression, also representing Nrf2 activation was observed after treatment with 100 nM aldosterone for 4 h by measuring the appearence of Nrf2 in nuclear fractions by western blot (Figure 37B).
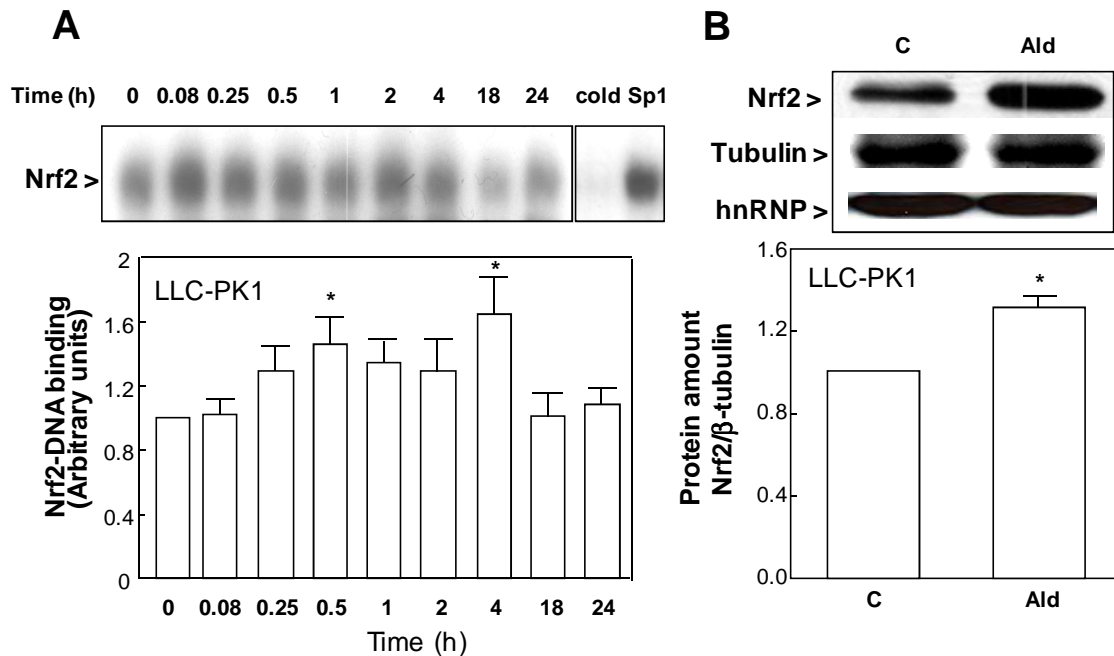
Figure 37: Aldosterone-induced activation of Nrf2.
A: Kinetics of aldosterone-mediated Nrf2 activation by 100 nM aldosterone measured in nuclear fractions by EMSA. Shown is the intensity of Nrf2-DNA binding after the indicated incubation times. * $p \leq 0.05$ vs. time point 0. To determine the specificity of the Nrf2-DNA complex, the control nuclear fraction (0 h incubation) was incubated in the presence of 100-fold molar excess of unlabeled oligonucleotide containing the consensus sequence for either Nrf2 (cold) or SP-1 (SP-1) before the binding assay. B: Western blot for Nrf2 (1:1000 in milk powder) in LLC-PK1 cells incubated with 100 nM aldosterone for 4 h. The housekeeping proteins hnRNP (1:1000 in 5% BSA for 1h at 37°C) and ß-tubulin (1:1000 in BSA for 1h at 37°C) were run as loading controls. Results are shown as mean ± SEM of 3 independent experiments. * $p \leq 0.05$ vs. control.

The activation of Nrf2 in LLC-PK1 cells evaluated by EMSA was dependent on the aldosterone concentration (5-100 nM). A slight increase of Nrf2-DNA binding was already observed at 10 nM aldosterone, while significance was reached at 50 and 100 nM aldosterone treatments for 30 min (Figure 38).
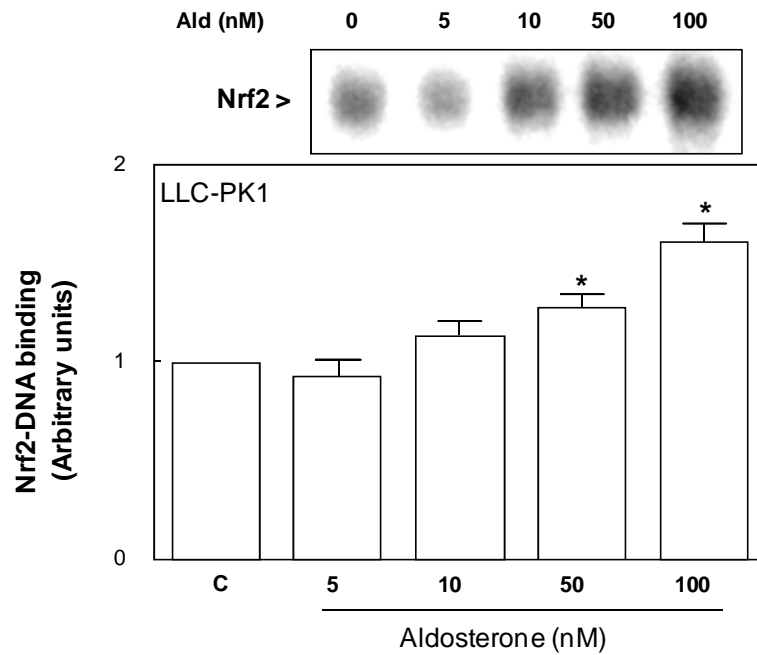
Figure 38: Dose-dependency of Nrf2 activation.
LLC-PK1 cells were incubated with the indicated aldosterone concentrations for 30 min. The intensity of the bands corresponding to the Nrf2-DNA complexes was measured. Results are shown as mean ± SEM of at least 5 independent experiments. * $p \leq 0.05$ vs. control.

4.3.1.2 Cellular oxidants are involved in aldosterone-induced activation of Nrf2

To follow the hypothesis that Nrf2 activation occured as a consequence of increased cell oxidants, the influence of selected antioxidants was tested by EMSA. The Nrf2-DNA binding was partially or totally prevented by the simultaneous incubation of cells with the cell permeable antioxidants LA, NAC and tempol (Figure 39). These findings strongly suggest that aldosterone induces Nrf2 in LLC-PK1 cells through an increase in the cellular production of ROS and/or RNS.
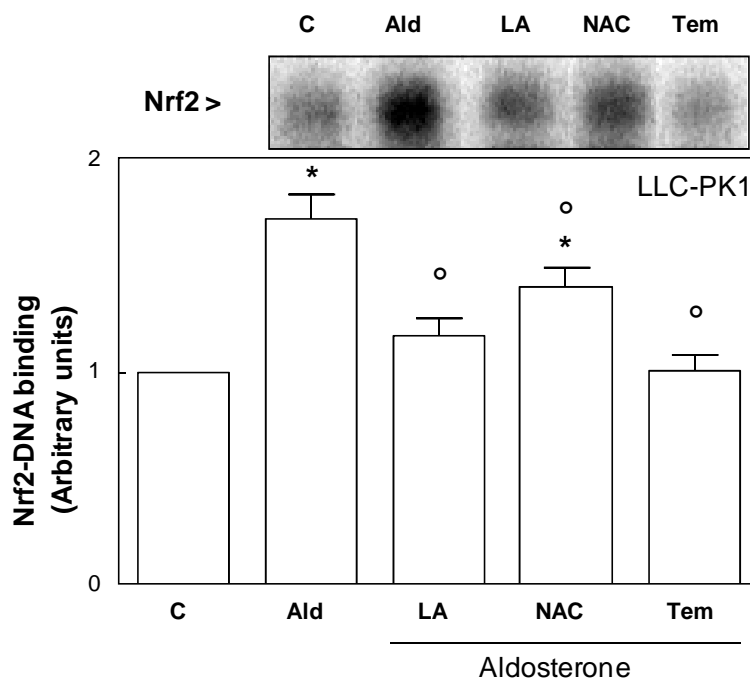
Figure 39: Aldosterone-induced activation of Nrf2 is prevented by antioxidants.
LLC-PK1 cells were incubated in the absence (C) and the presence of 100 nM aldosterone (Ald) for 30 min. Aldosterone-treated cells were simultaneously incubated with either 0.5 mM LA (LA), 0.5 mM NAC (NAC) or 50 µM tempol (Tem). Nuclear fractions were isolated and analyzed by EMSA. The intensity of the bands corresponding to the Nrf2-DNA complexes was measured. Results are shown as mean ± SEM of at least 3 independent experiments. * p≤0.05 vs. control, °p ≤0.05 vs. aldosterone treatment.

4.3.1.3 Aldosterone-induced activation of Nrf2 leads to an increased expression of Nrf2-regulated genes

The downstream targets of Nrf2, the genes of GCLM, GCLC, Trx, HO-1 and NQO1 were analyzed for their increased expression, by detection of their protein products in western blots. GCLC is the catalytic and GCLM the modulator subunit of the rate-limiting enzyme glutamate cysteine ligase (GCL) in GSH biosynthesis. Trx, a selenoprotein, is important in regulating the redox status of the cell and protects against oxidative stress. The enzyme NQO1 catalyzes the reduction and detoxification of highly reactive quinones and might be involved in the stabilization of the tumor suppressor gene p53 [101]. The antioxidant enzyme HO-1 is responsible for the elimination of excess free heme, since it catalyzes the initial and rate-limiting step in heme catabolism, the oxidative cleavage of the porphyrin ring to generate biliverdin with the release of the heme iron and CO [170] (see 1.6).

After 4 h of incubation with 100 nM aldosterone a significant upregulation of all studied proteins were observed in LLC-PK1 cells (Figure 40).
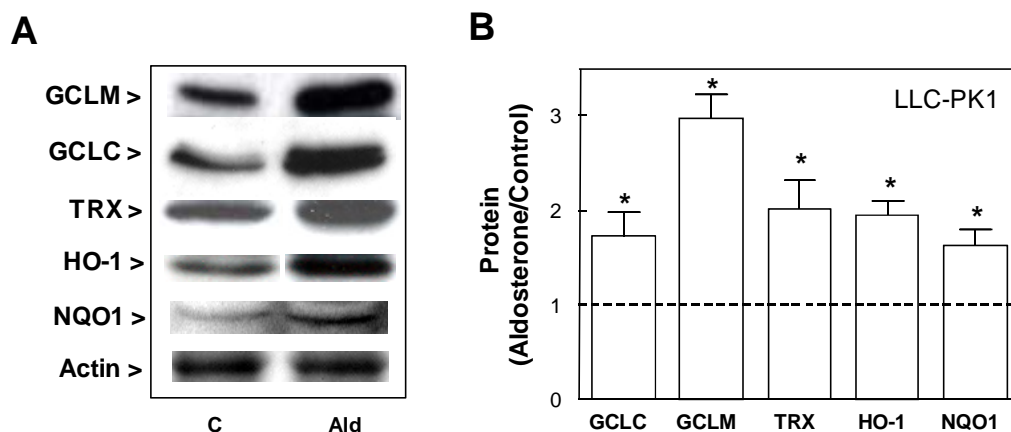
Figure 40: Expression of Nrf2-regulated proteins.
The expression of Nrf2-regulated proteins was detected by western blot in LLC-PK1 cells (all primary antibodies 1:1000 in 5% milk powder). Cells were incubated with 100 nM aldosterone for 4 h. A: Respresentative pictures of the obtained bands by western blot are shown. B: Quantification of the bands. Results are shown as mean ± SEM of 3 independent experiments. * p≤0.05 vs. control.

4.3.1.4 The activation of Nrf2 is not sufficient to protect the cells against aldosterone-induced oxidative stress and oxidative DNA damage

To investigate whether the activation of Nrf2 is successful in protecting the cells against aldosterone-induced oxidative stress and oxidative DNA damage or whether it is transient and prone to be overwhelmed by excess amount of ROS/RNS, GSH levels were determined after 24 h incubation without or with 100 nM aldosterone by HPLC. Results show that GSH levels are significantly reduced in aldosterone-treated cells after 24 h (Figure 41).
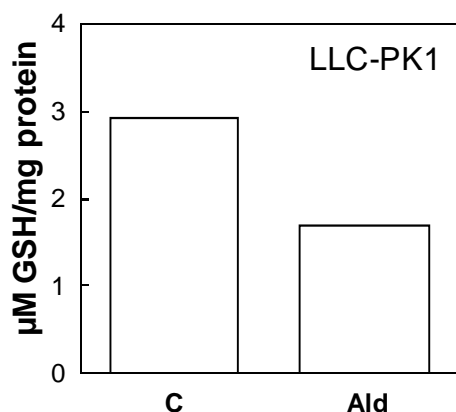
Figure 41: Determination of GSH levels in LLC-PK1 cells by HPLC.
GSH levels were evaluated by treating LLC-PK1 cells without (C) or with 100 nM aldosterone (Ald) for 24 h and samples were measured by HPLC. Data are presented as µM GSH per mg protein from one experiment.

GSH levels were also determined fluorimetrically. Cells were treated for 4, 24 and 48 h with 10 nM aldosterone and subsequently analyzed with a filter appropriate for fluorescein. Results indicate that GSH levels significantly increase after 4 h aldosterone treatment, while after 24 und 48 h GSH levels decrease compared to the respective controls (Figure 42).
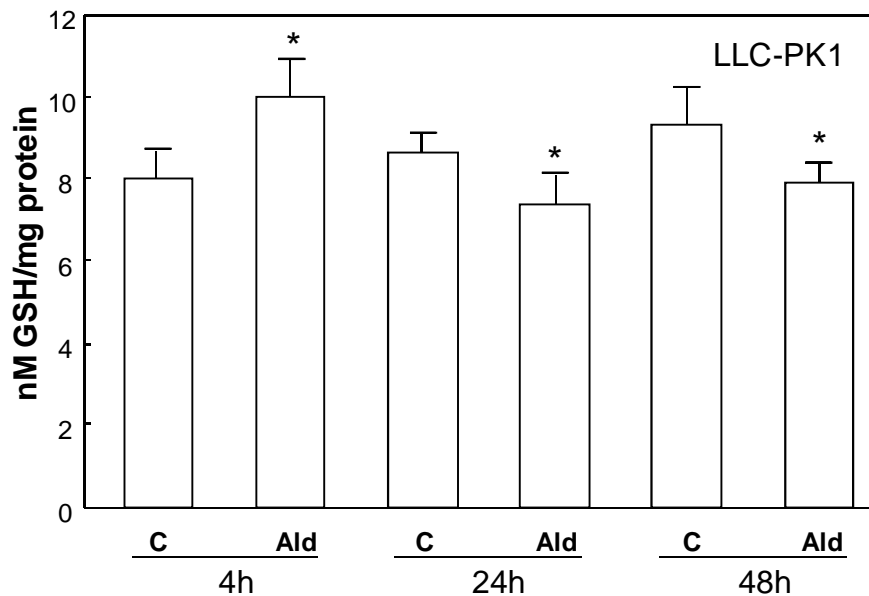
Figure 42: Fluorimetric determination of GSH levels in LLC-PK1 cells.
Cell were incubated without (C) or with 10 nM aldosterone (Ald) for the indicated times and fluoresence was measured fluorimetrically at 460 nm (λexc 355 nm). Results are expressed as the fluorescence emission (λem 460 nm) at λexc 355 nm and referred to the protein content. Results are shown as mean ± SEM of 5 independent experiments. * p≤0.05 vs. control.

The occurence of double strand breaks induced by aldosterone was next investigated. Shown are representative pictures of immunofluorescence staining of γ-H2AX-foci (Figure 43A). The quantification of the fluorescence showed that treatment with 10 nM aldosterone for 30 min resulted in a slight increased frequency of γ-H2AX-foci, which became significant after 4, 24 and 48 h. The frequency of γ-H2AX rose up dose-dependently. Genistein was used as positive control (Figure 43B).

A

B
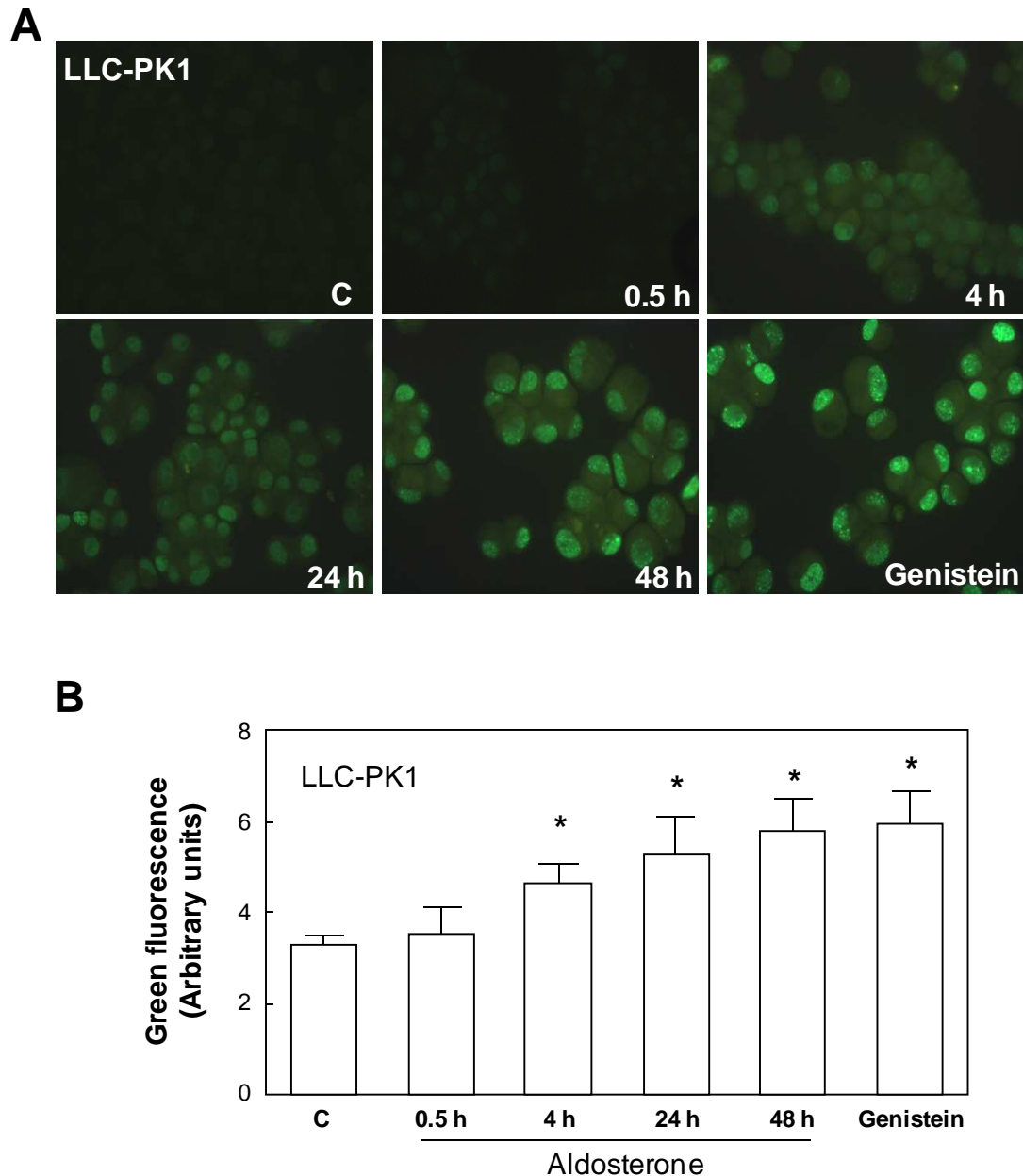
Figure 43: Detection of γ-H2AX-foci in LLC-PK1 cells.
LLC-PK1 cells were treated for 0.5, 4, 24 and 48 h with 10 nM aldosterone, and subsequently brought onto glass slides by cytospin centrifugation and stained for γ-H2AX-foci (primary antibody 1:100). Genistein was used as positive control. A: Shown are representative pictures of control cells and aldosterone-treated cells after the indicated time points as well as genistein-treated positive control cells. Pictures were taken using a fluorescence microscope. B: Quantifications were done by measuring gray values of approximately 150 cells per treatment with ImageJ. Results are shown as mean ± SEM of 3 independent experiments. * p≤0.05 vs. control.

Furthermore, the most prominent DNA modification caused by oxidative stress, 8-oxodG, was observed by confocal microscopy in LLC-PK1 cells after 4, 24 and 48 h incubation with 10 nM aldosterone (Figure 44A). Quantifications revealed that the induction of 8-oxodG was significant after 4 h, but the amount of 8-oxodG lesions increased steadily up to 48 h (Figure 44B).

A
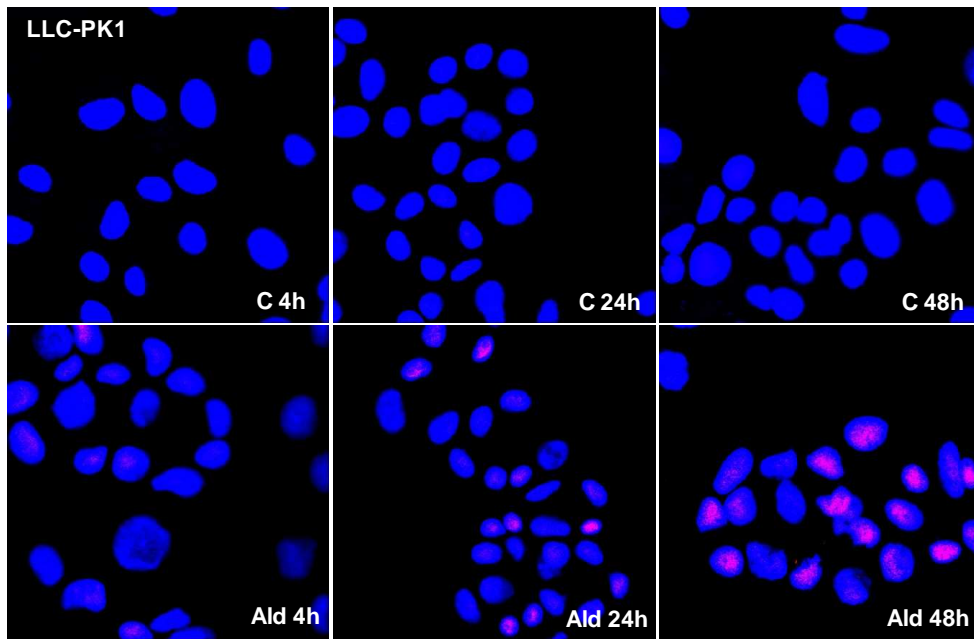
B
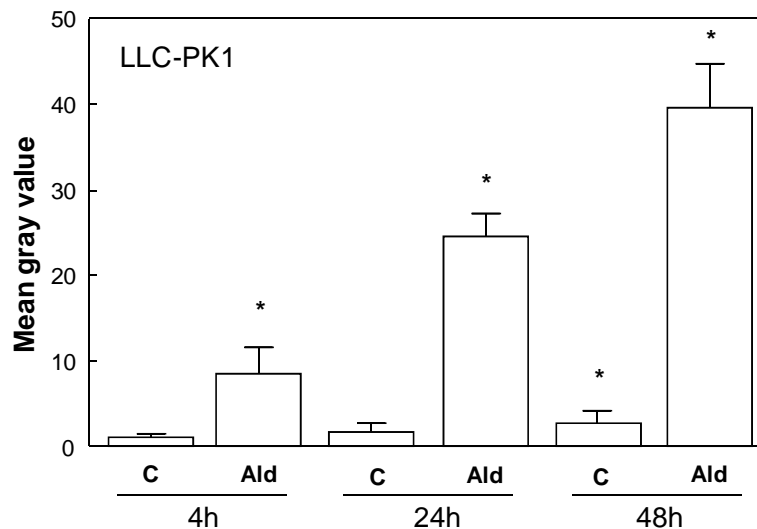
Figure 44: Detection of 8-oxodG modifications in LLC-PK1 cells.
LLC-PK1 cells were treated with 10 nM aldosterone for 4, 24 and 48 h and subsequently brought onto glass slides by cytospin centrifugation and stained for 8-oxodG lesions (primary antibody 1:100). A: Shown are representative pictures of control cells and aldosterone-treated cell after the indicated time points. Pictures were taken by TCS SP5 laser scanning confocal microscope. B: Quantifications were done by measuring gray values of approximately 100 cells per treatment with ImageJ. Results are shown as mean ± SEM of 3 independent experiments. * p≤0.05 vs. control.

All these results provide a first hint that Nrf2 activation as an adaptive survival response in LLC-PK1 cells is not sufficient to protect the cells against the increased amounts of aldosterone-induced ROS/RNS and oxidative DNA damage.

4.3.2 Transcription factor NF-κB

The activation of the potentially prosurvival transcription factor NF-κB was investigated, since it is known that NF-κB is redox-sensitive and therefore might be activated by aldosterone in LLC-PK1 and MDCK cells.

4.3.2.1 Aldosterone activates transcription factor NF-κB

The activation of transcription factor NF-κB by aldosterone was evaluated measuring the NF-κB-DNA binding in nuclear fractions by EMSA. The specificity of the NF-κB-DNA complex in EMSAs was assessed by competition with a 100-fold molar excess of unlabeled oligonucleotide (cold) containg the consensus sequence for either NF-κB or SP-1 (Figure 45A).

The incubation of LLC-PK1 and MDCK with 100 nM aldosterone caused an increase in nuclear NF-κB-DNA binding, which reached a maximum after 30 and 120 min for LLC-PK1 and MDCK cells, respectively (Figure 45A). NF-κB activation in both cell lines was also observed when measuring the upstream phosphorylation of IκBα and the associated decreased levels of unphosphorylated IκBα, as evaluated by western blot (Figure 45B).

A

B
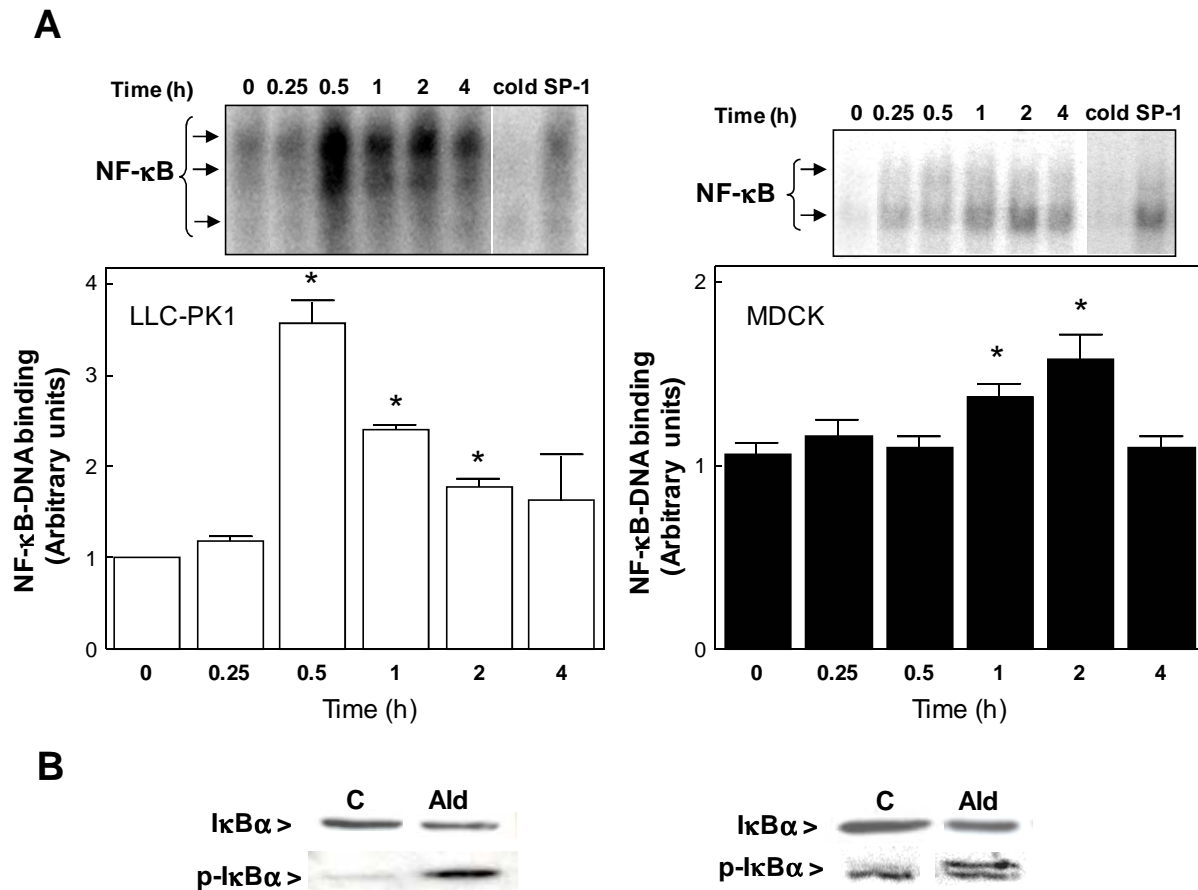
Figure 45: Aldosterone-induced activation of NF-κB in LLC-PK1 and MDCK cells.
A: Kinetics of aldosterone-mediated NF-κB activation by 100 nM aldosterone measured in nuclear fractions by EMSA. Shown is the intensity of NF-κB-DNA binding after the indicated incubation times. * $p \leq 0.05$ vs. time point 0. To determine the specificity of the NF-κB-DNA complex, the control nuclear fraction (0 h incubation) was incubated in the presence of 100-fold molar excess of unlabeled oligonucleotide containing the consensus sequence for either NF-κB (cold) or SP-1 (SP-1) before the binding assay. B: Western blot for phosphorylated (1:500) and non-phosphorylated (1:500) IκB in LLC-PK1 and MDCK cells incubated with 100 nM aldosterone for 4 h. Results are shown as mean ± SEM of at least 3 independent experiments. * $p \leq 0.05$ vs. control.

The activation of NF-κB in LLC-PK1 and MDCK cells evaluated by EMSA was dependent on the aldosterone concentration (5-100 nM). Although significance was not reached under 50 and 100 nM in LLC-PK1 cells and only at 100 nM in MDCK cells (Figure 46), a positive and significant ($p < 0.05$) correlation was calculated for NF-κB activation and aldosterone in the range of concentrations tested (5-100 nM) (r^2: 0.95 (LLC-PK1), r^2:0.97 (MDCK)).
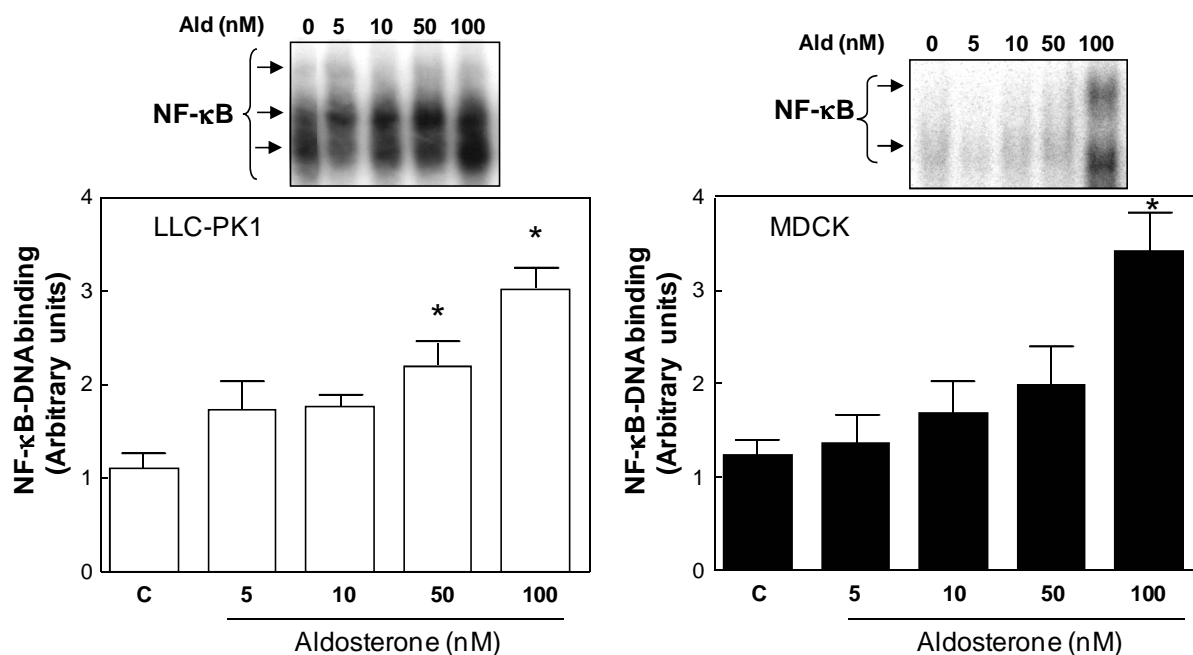
Figure 46: Dose-dependency of NF-κB activation.
LLC-PK1 and MDCK cells were incubated with the indicated aldosterone concentrations for 30 (LLC-PK1) or 120 (MDCK) min and nuclear fractions were evaluated by EMSA. The intensity of the bands corresponding to the NF-κB-DNA complexes was measured. Results are shown as mean ± SEM of at least 5 independent experiments. * p≤0.05 vs. control.

4.3.2.2 Cellular oxidants are involved in aldosterone-induced activation of NF-κB

To follow the hypothesis that NF-κB activation occured as a consequence of increased cell oxidants, the influence of selected antioxidants was next investigated. The NF-κB-DNA binding was prevented by the simultaneous incubation of LLC-PK1 and MDCK cells with the cell permeable antioxidants LA, NAC and tempol (Figure 47). As observed for DNA damage, NAC was the less effective antioxidant in both cell lines. These findings strongly support the hypothesis that aldosterone-induced NF-κB activation occured through an increase in the cellular ROS and/or RNS production.
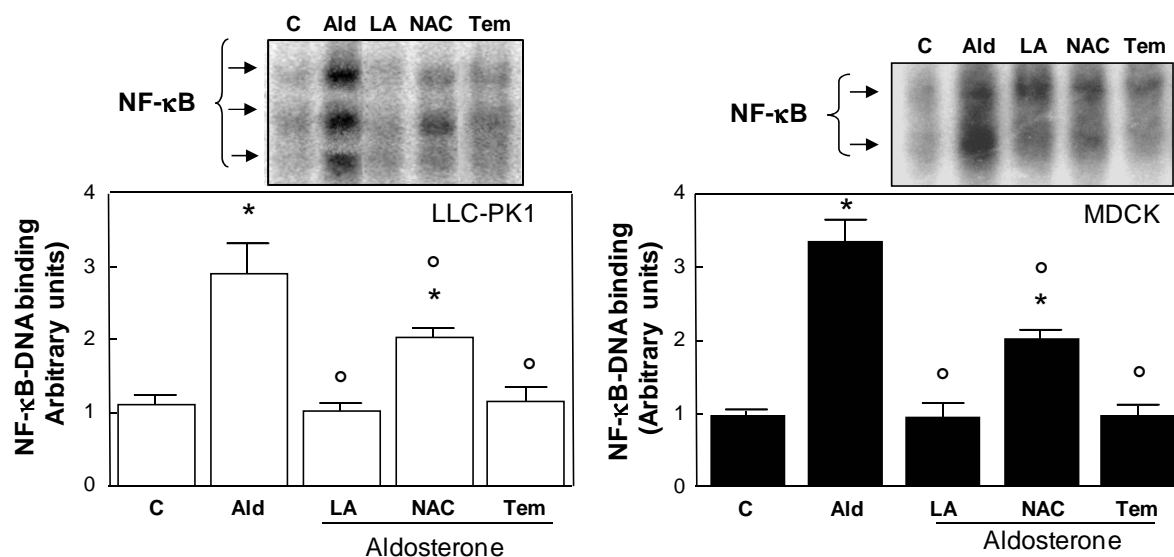
Figure 47: Aldosterone-induced activation of NF-κB is prevented by antioxidants.
LLC-PK1 and MDCK cells were incubated in the absence (C) and the presence of 100 nM aldosterone (Ald) for 30 min. Aldosterone-treated cells were simultaneously incubated with either 0.5 mM LA (LA), 0.5 mM NAC (NAC) or 50 µM tempol (Tem). Nuclear fractions were isolated and analyzed by EMSA. The intensity of the bands corresponding to the NF-κB-DNA complexes was measured. Results are shown as mean ± SEM of at least 3 independent experiments. * p≤0.05 vs. control, ° p ≤0.05 vs. aldosterone treatment.

4.3.2.3 Aldosterone-induced activation of NF-κB leads to an increased expression of NF-κB-regulated genes

The expression of the NF-κB-regulated genes Bcl-2, Bcl-xL, xIAP and cIAP was analyzed by detection of their proteins products in western blots. Bcl-2 is the founding member of the Bcl-2 family of apoptosis regulator proteins and plays a role in the pathogenesis of cancer, since it decreases apoptosis. Also Bcl-xL is known to be antiapoptotic, belongs to the Bcl-2 family of proteins and has been implicated in the survival of cancer cells. XIAP and cIAP1 are members of the inhibitor of apoptosis family of proteins (IAP). After 4, 18 and 24 h incubation with 100 nM aldosterone a clear upregulation of of all studied proteins were observed in LLC-PK1 cells (Figure 48).
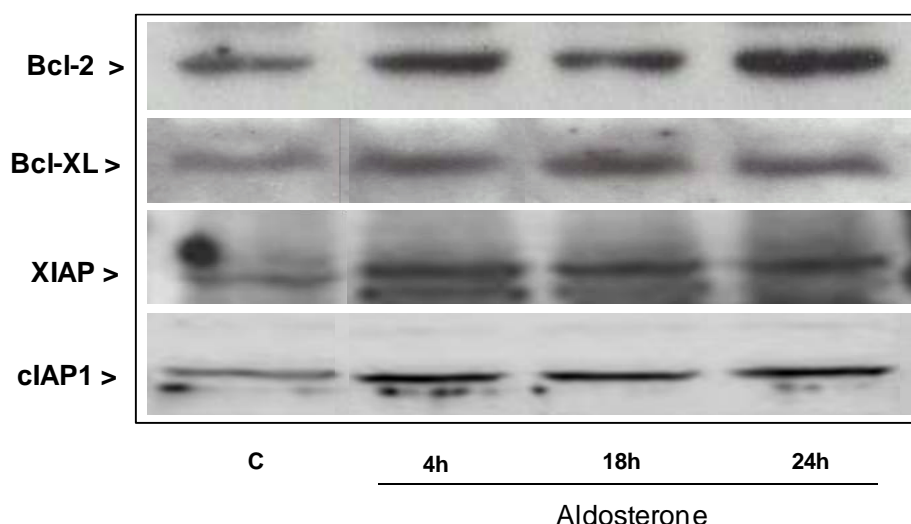
Figure 48: Expression of NF-κB-regulated proteins.
The expression of NF-κB-regulated proteins was detected by western blot in LLC-PK1 cells (all primary antibodies 1:1000 in 5% milk powder). Cells were incubated with 100 nM aldosterone for 4, 18 and 24 h. Shown are pictures of the obtained bands by western blot from one or two experiment/s.

4.3.3 The ERK signaling pathway and CREB/STAT transcription factors

ROS have been shown to activate several signaling protein kinases, such as ERK1/2 and aldosterone has been shown to phosphorylate ERK1/2 in different cell lines. Therefore, in the following we investigated whether aldosterone activates ERK1/2 also in LLC-PK1 cells and whether ERK1/2 is responsible for the subsequent activation of prosurvival transcription factors like CREB, STAT1 and STAT3.

4.3.3.1 Aldosterone activates the ERK signaling pathway

To first investigate a possible activation of ERK in the cytosol, western blots were performed. As depicted in Figure 48, 10 nM aldosterone caused the activation of ERK. At 30 min and 4 h incubation, ERK phosphorylation reached significance (Figure 49A). Furthermore, the phosphorylation of the upstream kinases of the signaling cascade, c-Raf and MEK1/2, was analyzed by western blot in total fractions. Both kinases were significantly upregulated in aldosterone-treated cells compared to control cells (Figure 49B).
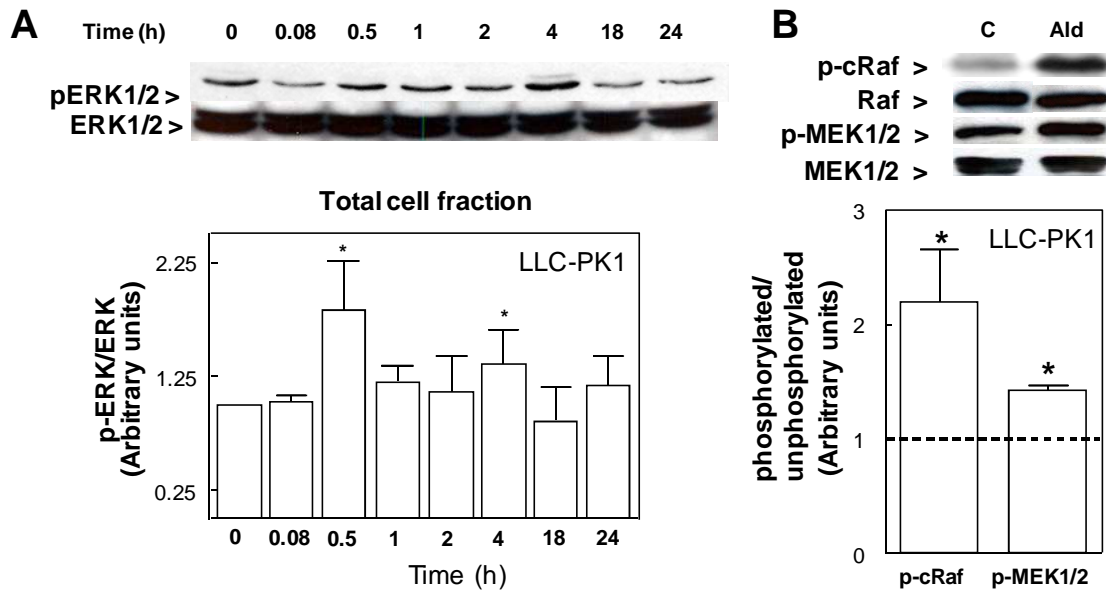
Figure 49: Aldosterone-mediated cytosolic ERK, c-Raf and MEK1/2 phosporylation in total fractions of LLC-PK1 cells.
LLC-PK1 cells were incubated with 10 nM aldosterone for the indicated time points (A) or for 4 h (B) and total fractions were isolated and p-ERK activation was analyzed by western blot. Shown is p-ERK related to ERK, p-cRaf to Raf and p-MEK1/2 to MEK1/2 (all primary antibodies 1:1000 in 5% BSA). Results are shown as mean ± SEM of 3 independent experiments. * p≤0.05 vs. control.

To investigate whether activated ERK translocates into the nucleus to phosphorylate nuclear substrates, nuclear fractions were analyzed by western blot.
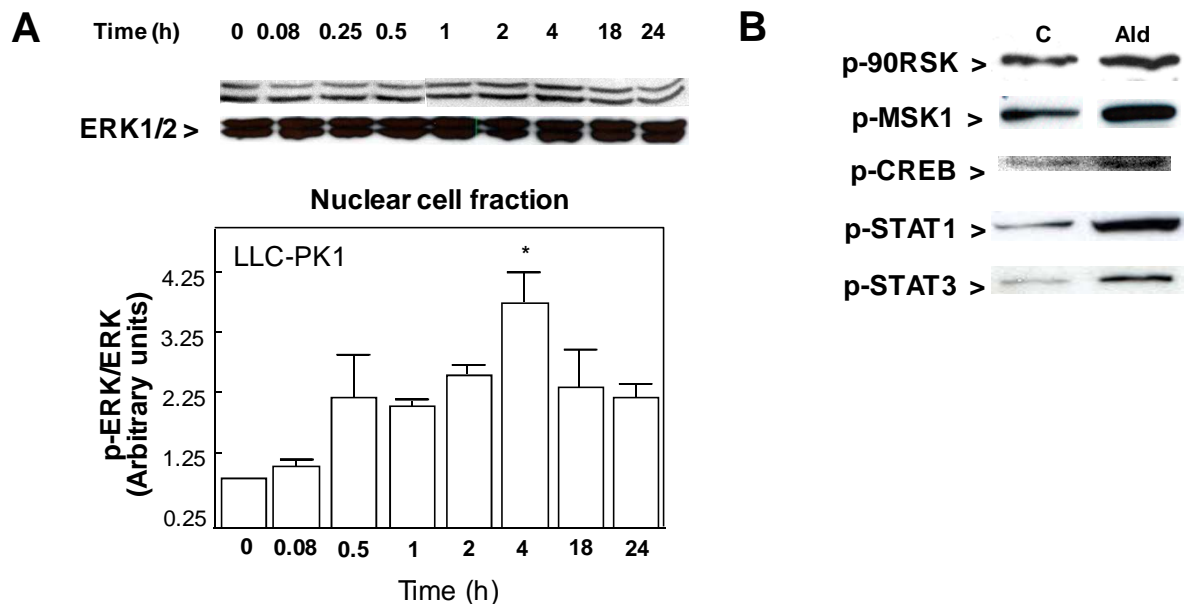
Figure 50: Aldosterone-mediated nuclear ERK activation and subsequent phosphorylation of downstream kinases and transcription factors in LLC-PK1 cells.
A: LLC-PK1 cells were incubated with 10 nM aldosterone for the indicated time points (A) or 4 hours (B) and nuclear fraction were isolated and p-ERK, p-90RSK, p-MSK1, p-CREB, p-STAT1 and p-STAT3 activation was analyzed by western blot (all primary antibodies 1:1000 in 5% BSA) Shown is p-ERK related to ERK. Results are shown as mean ± SEM of 3 independent experiments. * p≤0.05 vs. control.

In fact, the results demonstrate that ERK is activated by 10 nM aldosterone in the nucleus with a maximum at 4 hours (Figure 50A) and subsequently phosphorylates downstream targets namely 90-RSK, MSK1 and transcription factors like CREB, STAT1 and STAT3 (Figure 50B).

4.3.3.2 Aldosterone-induced ERK activation leads to the activation of transcription factors

Since the expression of downstream targets of ERK1/2 like transcription factors CREB, STAT1 and STAT3 could already be observed by western blot, the DNA-binding of these transcription factors was investigated by EMSA in LLC-PK1 cells.

4.3.3.2.1 Aldosterone-induced ERK activation leads to the activation of transcription factor CREB

The transcription factor CREB is known as a downstream target of ERK. To confirm this hypothesis, the activation of CREB by aldosterone was evaluated measuring the CREB-DNA binding in nuclear fractions by EMSA. The incubation of LLC-PK1 with 10 nM aldosterone caused an increase in nuclear CREB-DNA binding, which reached significance starting at 30 min lasting up to 8 h (Figure 51).
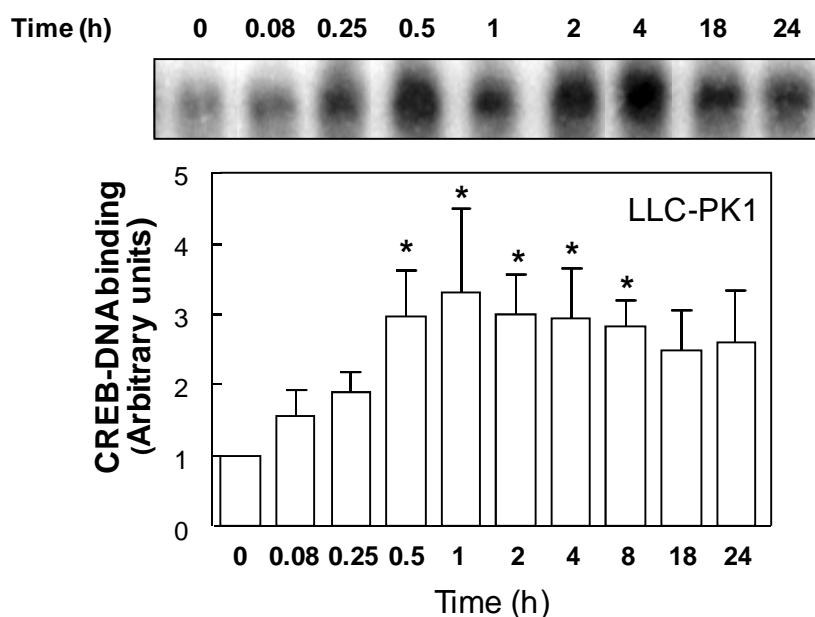
Figure 51: Aldosterone-mediated activation of CREB in LLC-PK1 cells.
Kinetics of aldosterone-mediated CREB activation by 10 nM aldosterone measured in nuclear fractions by EMSA. Shown is the intensity of CREB-DNA binding after the indicated incubation times. Results are shown as mean ± SEM of 3 independent experiments * $p \leq 0.05$ vs. time point 0.

The activation of CREB in LLC-PK1 cells evaluated by EMSA was dependent on the aldosterone concentration (5-100 nM). Significance was reached at 10 nM aldosterone (Figure 52).
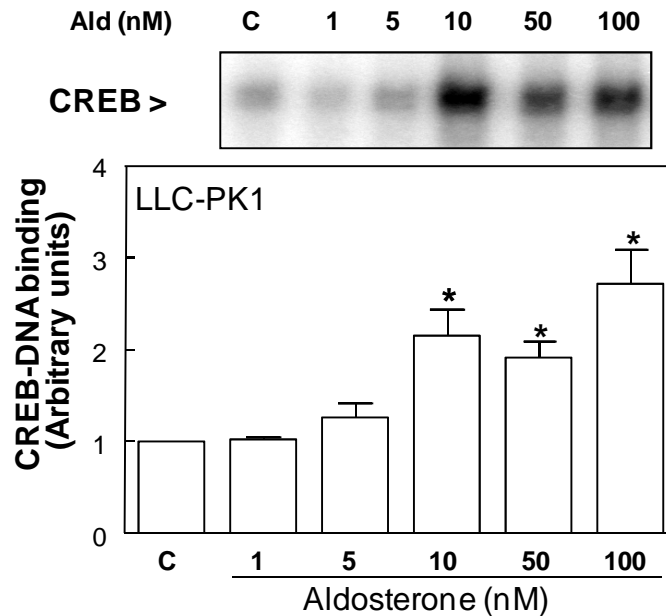
Figure 52: Dose-dependency of CREB activation.
LLC-PK1 cells were incubated with the indicated aldosterone concentrations for 30 min. The intensity of the bands corresponding to the CREB-DNA complexes was measured. Results are shown as mean ± SEM of at least 4 independent experiments. * p≤0.05 vs. control.

4.3.3.2.2 Aldosterone-induced ERK activation leads to the activation of STAT transcription factors

Amongst others, the transcription factors STAT1 and STAT3 are phosphorylated by ERK. To investigate whether ERK activates these transcription factors in LLC-PK1 cells the STAT-DNA binding in nuclear fractions was evaluated by EMSA. The maximum of STAT1-DNA binding and STAT3-DNA binding was reached after 4 hours incubation with 10 nM aldosterone (Figure 53A, B).

A

B
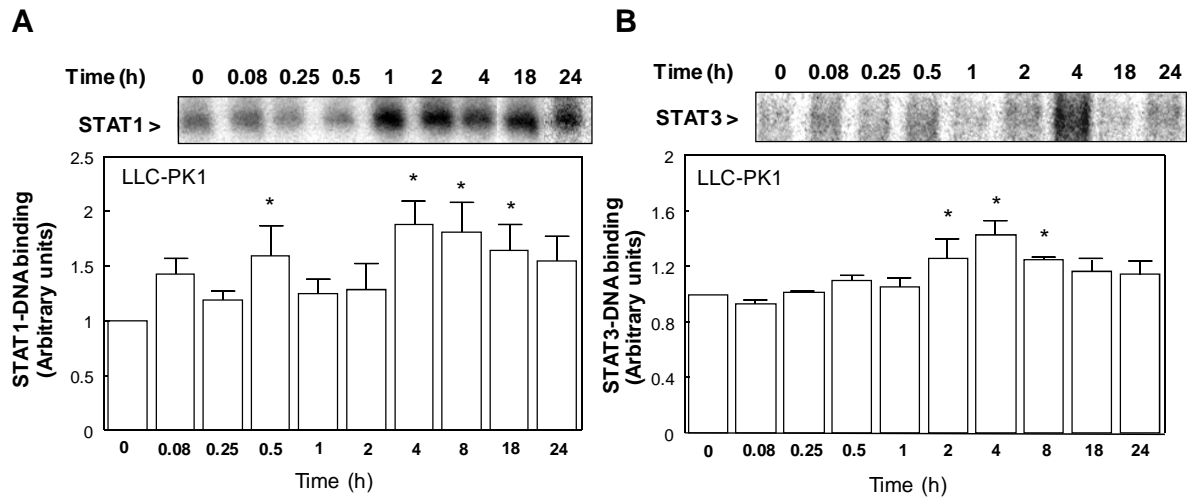
Figure 53: Aldosterone-mediated activation of STAT1 and STAT3 in LLC-PK1 cells.
Kinetics of aldosterone-mediated A: STAT1 and B: STAT3 activation by 10 nM aldosterone measured in nuclear fractions by EMSA. Shown is the intensity of STAT-DNA binding after the indicated incubation times. Results are shown as mean ± SEM of 3 independent experiments * $p \leq 0.05$ vs. timepoint 0.

The activation of STAT1 and STAT3 was dependent on the aldosterone concentration (5-100 nM) in LLC-PK1 cells evaluated by EMSA. Significance was reached at 10 nM aldosterone for both transcription factors (Figure 54A, B), although STAT1 activation was already upregulated at 1 nM aldosterone (Figure 54A).

A

B
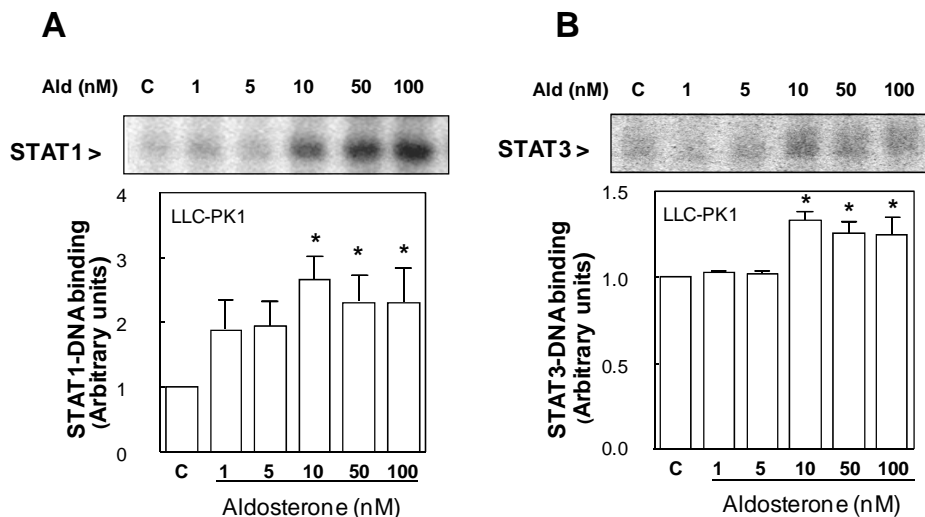
Figure 54: Dose-dependency of STAT activation.
LLC-PK1 cells were incubated with the indicated aldosterone concentrations for 4 h. Nuclear fractions were isolated and the A: STAT1- and B: STAT3-DNA binding was analyzed by EMSA. The intensity of the bands corresponding to the STAT-DNA complexes was measured. Results are shown as mean ± SEM of at least 4 independent experiments. * $p \leq 0.05$ vs. control.

4.3.3.2.3 Cellular oxidants are involved in aldosterone-induced activation of ERK and the subsequent activation of transcription factors

To follow the hypothesis that ERK activation and the subsequent activation of CREB, STAT1 and STAT3 occured as a consequence of increased cell oxidants, the influence of the antioxidant tempol was next investigated. The aldosterone-induced activation of ERK and of the transcription factors was prevented by the simultaneous incubation of LLC-PK1 cells with the cell permeable antioxidant tempol (Figure 55). These findings lead to the conclusion that aldosterone-induced ERK activation and subsequent activation of CREB, STAT1 and STAT3 occured through an increase in the cellular production of ROS, especially $O_2^{\cdot-}$.
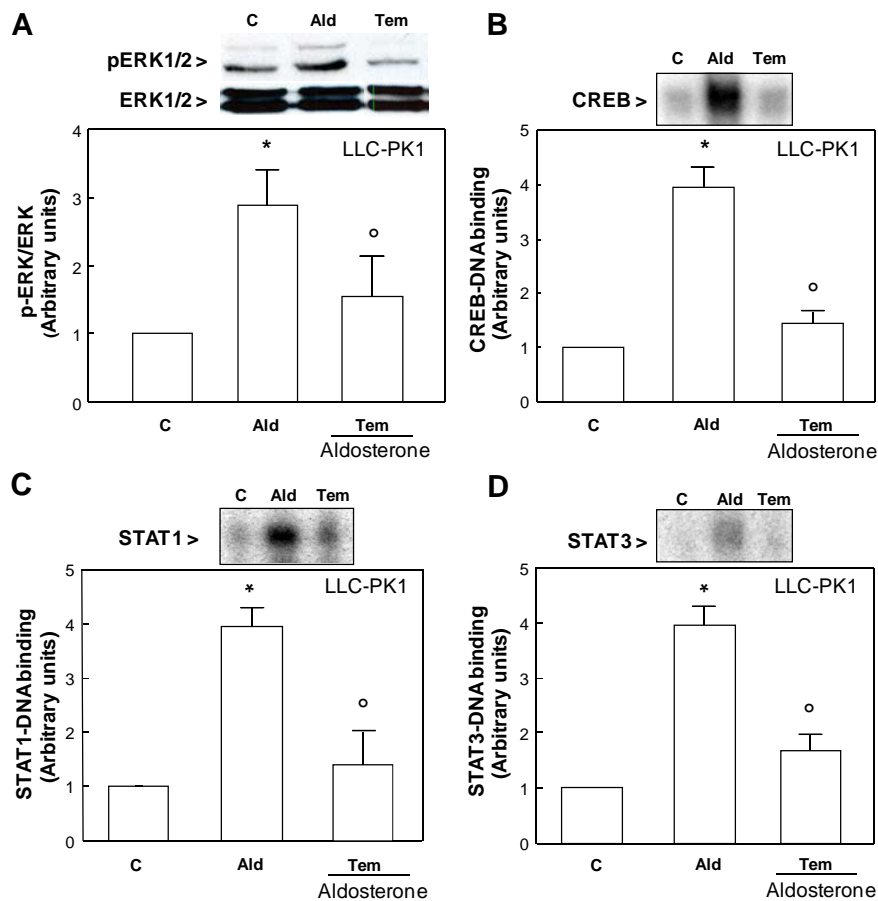
Figure 55: Aldosterone-induced activation of ERK and the subsequent activation of CREB, STAT1 and STAT3 are prevented by antioxidants.
LLC-PK1 cells were incubated for 30 min in the absence (C) and the presence of 100 nM aldosterone (Ald). Aldosterone-treated cells were simultaneously incubated with 50 µM tempol (Tem). A: Total fractions were isolated and analyzed by western blot (primary antibody 1:1000 in 5% BSA). Nuclear fractions were isolated and B: CREB-, C: STAT1-, and D: STAT3-DNA binding was analyzed by EMSA. The intensity of the bands corresponding to the CREB/STAT-DNA complexes was measured. Results are shown as mean ± SEM of at least 3 independent experiments. * p≤0.05 vs. control, ° p≤0.05 vs. aldosterone treatment.

4.3.3.2.4 Aldosterone-induced ERK activation is responsible for CREB, STAT1 and STAT3 activation

Since the transcription factors CREB, STAT1 and STAT3 can also be activated by other pathways, the specific activation by ERK was investigated using an inhibitor of the ERK signaling pathway. The MEK inhibitor U0126 was tested in the western blot and EMSA. U0126 clearly inhibited ERK phosphorylation in western blot and the subsequent activation of the transcription factors CREB, STAT1 and STAT3 in the EMSA, suggesting that phosphorylated ERK is responsible for their activation (Figure 56).
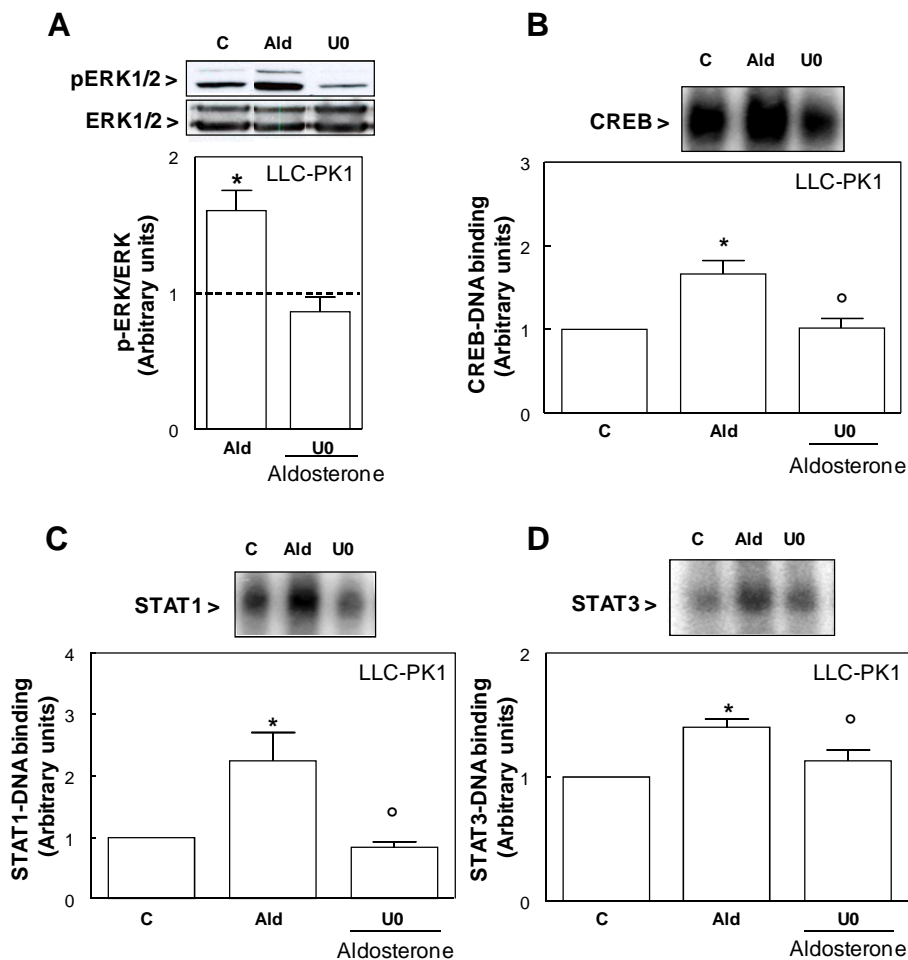
Figure 56: Effects of the MEK inhibitor U0126 on aldosterone-mediated ERK phosphorylation and subsequent activation of transcription factors.
LLC-PK1 cells were incubated without (C) or with 10 nM aldosterone (Ald). Aldosterone-treated cells were simultaneously incubated with 10 µM U0126 (U0). A: LLC-PK1 cells were treated as described above for 4 h, total cell fractions were isolated and analyzed by western blot (primary antibody 1:1000 in 5% BSA). B, C, D: LLC-PK1 cells were treated as described above for 4 h, nuclear fractions were isolated and measured by EMSA. Results are shown as mean ± SEM of 3 independent experiments. * $p \leq 0.05$ vs. control, °$p \leq 0.05$ vs. aldosterone treatment.

4.4 Mechanisms of aldosterone-induced cellular damages in vitro

To understand the underlying mechanisms of oxidant production, DNA damage and the activation of transcription factors and signaling pathways, the involvement of the MR, intracellular calcium levels and the prooxidant enzymes NAD(P)H oxidase and NOS in aldosterone-induced cellular damages were investigated in LLC-PK1 and MDCK cells.

4.4.1 The mineralocorticoid receptor

Since aldosterone is known to act via the MR, first, the presence of the expression of the MR in LLC-PK1 and MDCK cells was verified by RT-PCR (Figure 57). The obtained sequences of the respective MRs is 99 % identical to the partial codons of *Sus scrofa mineralocorticoid receptor mRNA* and 98% identical to the partial codons of *canis mineralocorticoid receptor mRNA* available in GenBank (U88893, DG195096).
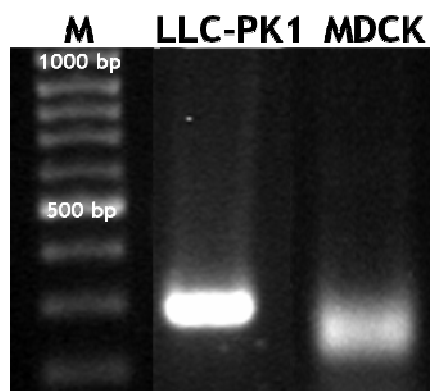
Figure 57: Expression of the mineralocorticoid receptor.
The expression of the MR in LLC-PK1 and MDCK cells was verified by RT-PCR.

4.4.1.1 Aldosterone-induced oxidant production and DNA damage is mediated via the MR

To investigate if the aldosterone-triggered increase in cellular oxidants and DNA damage is mediated exclusively via the MR and not via the glucocorticoid receptor (GR), antagonists of the MR and GR were used: eplerenone and mifepristone, respectively. Cell oxidants were evaluated with the probe H_2DCF-DA. Eplerenone significantly inhibited aldosterone-induced DCF fluorescence increase in LLC-PK1 and MDCK (67 and 86%, respectively), while mifepristone had no effect (Figure 58).
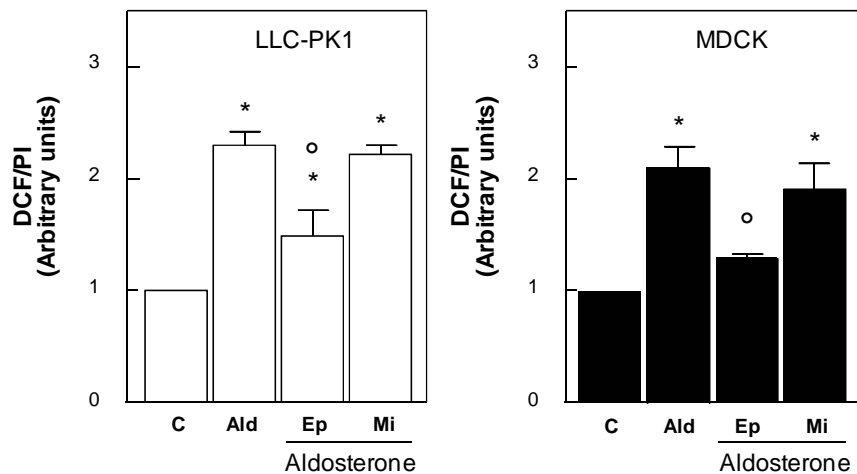
Figure 58: Aldosterone-induced oxidative stress is mediated via the MR.
LLC-PK1 and MDCK cells were incubated in the absence (C) and the presence of 100 nM aldosterone (Ald). Aldosterone-treated cells were simultaneously incubated with either 500 nM eplerenone (Ep) or 500 nM mifepristone (Mi). Cells were treated with aldosterone and cellular oxidant levels were measured with the probe H_2DCF-DA after 30 min and 120 min incubation in the combinations described above for LLC-PK1 and MDCK cells, respectively. DCF fluorescence data are shown normalized to the PI fluorescence. Results are presented as mean ± SEM of 3 independent experiments. * $p \leq 0.05$ vs. control, °$p \leq 0.05$ vs. aldosterone treatment.

As for oxidative stress, DNA strand breaks observed in the comet assay were significantly reduced by eplerenone, but not by the GR antagonist mifepristone (Figure 59).
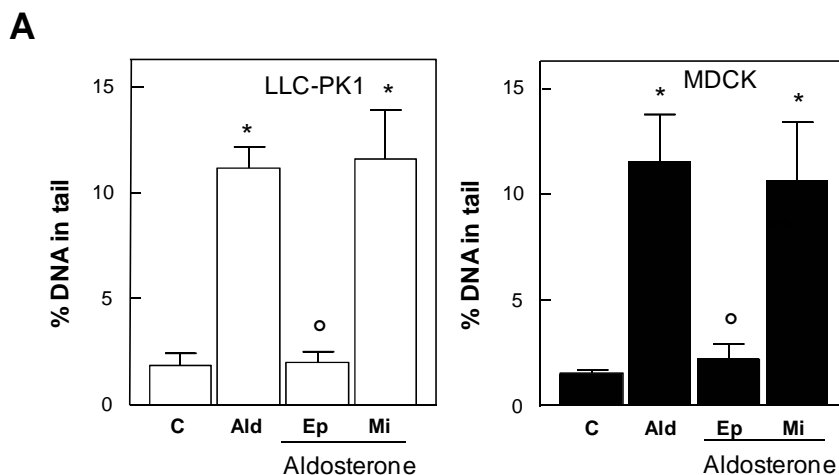
Figure 59: Aldosterone-induced DNA strand breaks are mediated via the MR.
LLC-PK1 and MDCK cells were incubated in the absence (C) and the presence of 10 nM aldosterone (Ald). Aldosterone-treated cells were simultaneously incubated with either 500 nM eplerenone (Ep) or 500 nM mifepristone (Mi). DNA strand breaks induced by aldosterone quantified with the comet assay in LLC-PK1 and MDCK cells incubated for 4 h. Shown is the percentage of DNA in tail. Results are presented as mean ± SEM of 3 independent experiments. * $p \leq 0.05$ vs. control, ° $p \leq 0.05$ vs. aldosterone treatment.

The observed results were confirmed with the micronucleus test. Eplerenone, but not mifepristone significantly reduced micronuclei formation in LLC-PK1 and MDCK cells (Figure 60), suggesting that both oxidative stress and DNA damage is mediated exclusively via the MR.

B
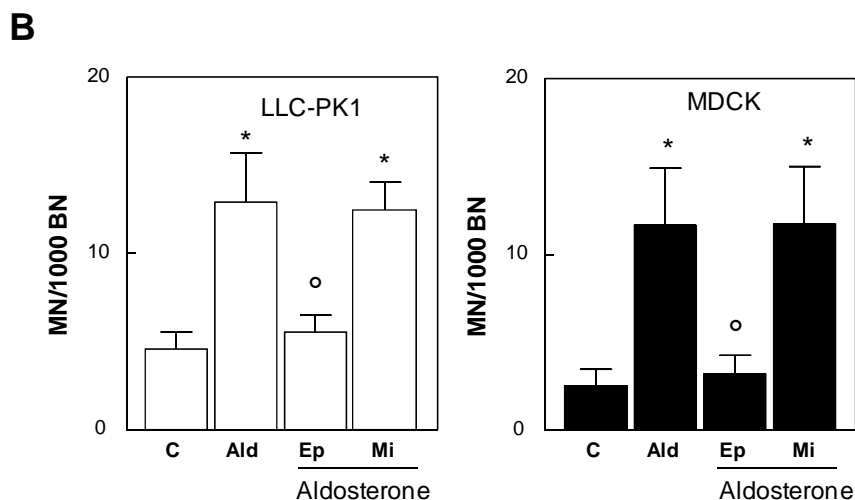
Figure 60: Aldosterone-induced micronuclei formation is mediated via the MR.
LLC-PK1 and MDCK cells were incubated in the absence (C) and the presence of 10 nM aldosterone (Ald). Aldosterone-treated cells were simultaneously incubated with either 500 nM eplerenone (Ep) or 500 nM mifepristone (Mi). Micronuclei formation quantified with the micronucleus test in LLC-PK1 and MDCK cells incubated for 4 h with aldosterone, followed by 24 h incubation with 3 µg/ml of cytochalasin B. Shown are micronuclei containing cells (MN) per 1000 binucleated cells (BN). Results are presented as mean ± SEM of 3 independent experiments. * p≤0.05 vs. control, ° p ≤0.05 vs. aldosterone treatment.

This hypothesis was further strengthened by testing two more MR antagonists: the steroidal antagonist spironolactone and the novel nonsteroidal MR antagonist (R)-BR-4628 [171]. These MR inhibitors were tested in LLC-PK1 cells in regard to oxidative stress and DNA damage. (R)-BR-4628 is a dihydropyridine-based drug candidate which is as potent as spironolactone at human MR but much more selective than spironolactone in functional cell-based transactivation assays *in vitro* [171-172]. $O_2^{\cdot -}$ production was monitored by staining the cells with DHE. As can be seen in Figure 61A, 10 nM aldosterone caused an increase in red fluorescence compared to control cells. The quantification of the intensity of the fluorescence formed from intracellular $O_2^{\cdot -}$ showed a significant increase of $O_2^{\cdot -}$ production by aldosterone treatment (Figure 61B). In a next step it was tested whether this $O_2^{\cdot -}$ production can be prevented by the addition of the MR antagonists spironolactone and (R)-BR-4628. The (S)-enantiomer of (R)-BR-4628, which is about 100-fold less active at the MR was used as a control. (S)-BR-4628 had no effect on the aldosterone-induced production of $O_2^{\cdot -}$ (Figure 61).

A
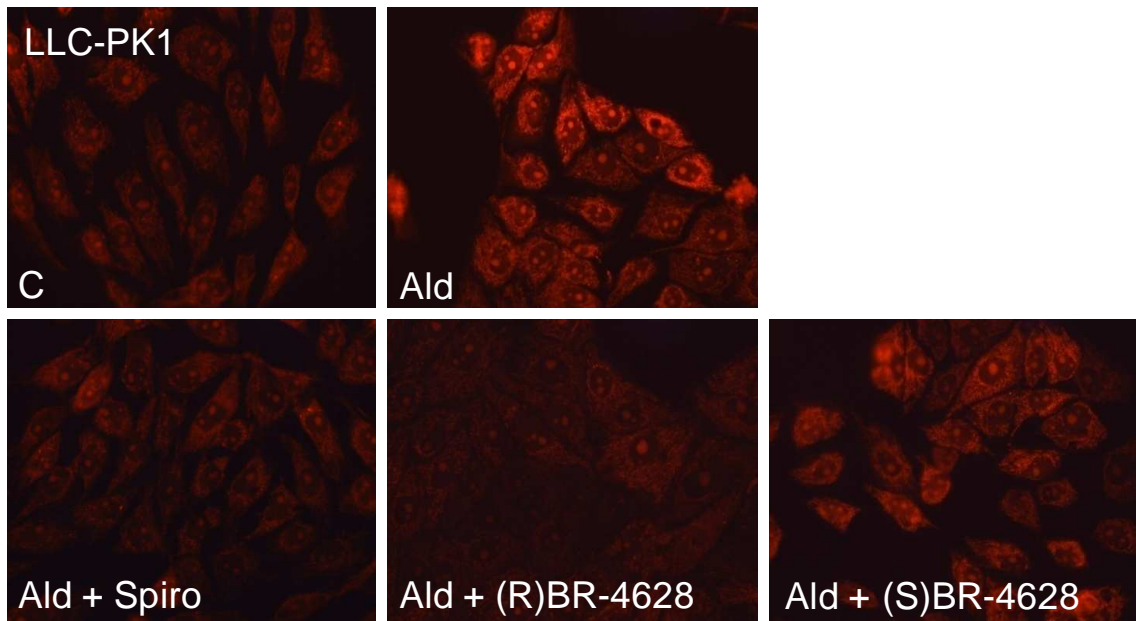
B
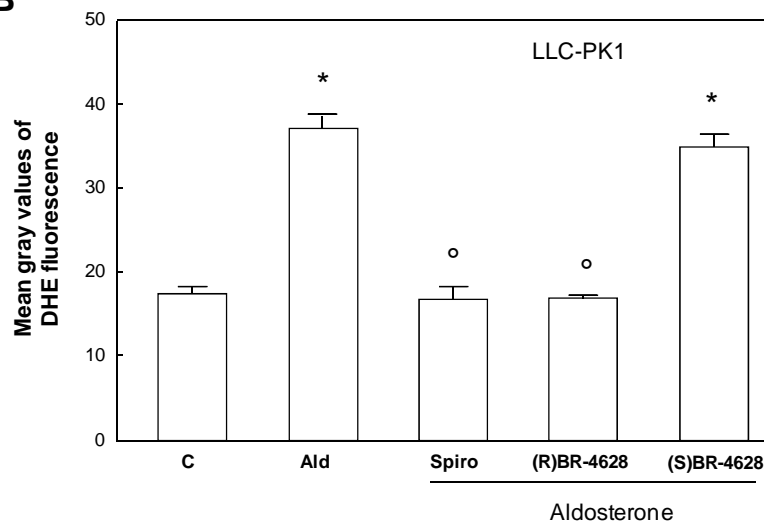
Figure 61: Effects of MR antagonists on the aldosterone-induced formation of superoxide.
A: control cells (C),10 nM aldosterone (Ald)-treated cells and cells incubated with the combination of 10 nM aldosterone and 500 nM spironolactone (Spiro), 10 nM aldosterone and 500 nM (R)-BR-4628 ((R)-BR-4628) and 10 nM aldosterone and 500 nM (S)-BR-4628 ((S)-BR-4628). B: Quantification of $O_2^{\cdot-}$ production by measuring mean gray values of 200 cells per treatment, done in triplicates, with ImageJ. *p≤0.05 vs. control, °p ≤0.05 vs. aldosterone treatment.

Also the DNA damage was prevented by the addition of the MR antagonist spironolactone, which was applied to reassess the involvement of the MR. As can be seen in Figure 62A, spironolactone was also able to reduce the damaging effect of aldosterone down to control level in the comet assay and to a certain extent in the micronucleus frequency test (Figure 62D). (R)-BR-4628 was also effective in protecting the cells from aldosterone-induced DNA damage (Figure 62B, D). Levels

of DNA strand breaks and micronuclei not significantly different from the control were reached at 50-fold higher concentrations of (R)-BR-4628 than aldosterone. (S)-BR-4628 influenced aldosterone-induced DNA damage in the comet assay only slightly, not reaching a significant decrease (Figure 62C). Inexplicably, (S)-BR-4628 reduced the micronucleus frequency significantly, although not as pronounced as (R)-BR-4628 did (Figure 62D).
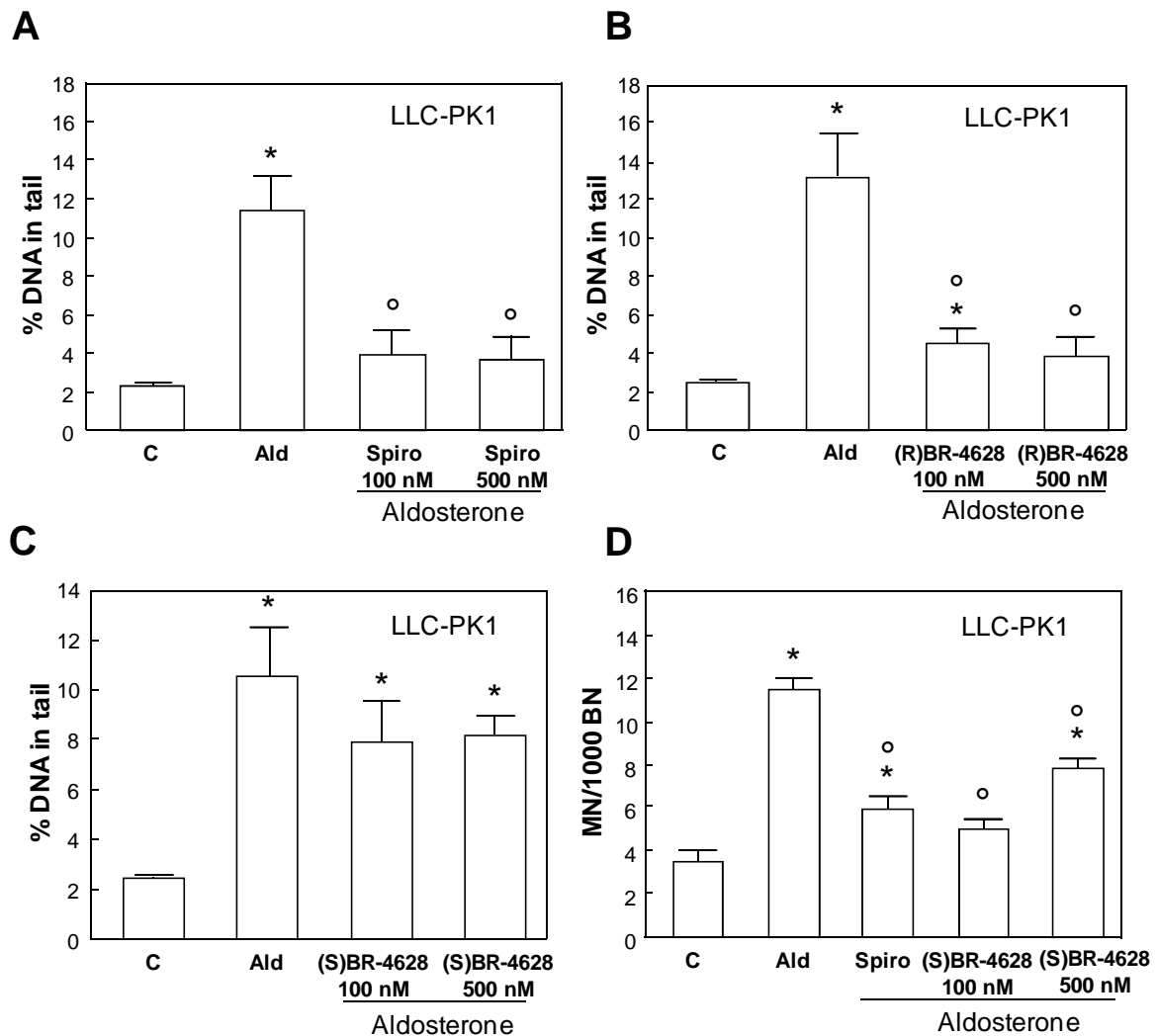
Figure 62: Effect of the MR antagonists spironolactone and (R)-BR-4628 on aldosterone-induced DNA damage.
Effects of the MR antagonists spironolactone (Spiro), (R)-BR-4628 and its less active enantiomer (S)-BR-4628 in two different concentrations (100 and 500 nM) on aldosterone (Ald)-induced DNA damage measured by the comet assay (A, B, C), and in one concentration (500 nM) on the micronucleus frequency (D) in LLC-PK1 cells. Shown is the percent of DNA in the tail region (A, B, C) and the number of micronuclei per 1000 binucleated cells (D). * $p \leq 0.05$ vs. control, ° $p \leq 0.05$ vs. aldosterone treatment.

4.4.1.2 Aldosterone-induced activation of transcription factors and signaling pathways are mediated via the MR

To investigate if the aldosterone-triggered activation of Nrf2, NF-κB, ERK, CREB, STAT1 and STAT3 is mediated exclusively via the MR, the two antagonists of the MR and GR, eplerenone and mifepristone, respectively, were used.

The nuclear Nrf2-binding and NF-κB-binding was significantly reduced by the simultaneous incubation with aldosterone and eplerenone, but not by aldosterone combined with mifepristone (Figure 63A, B)
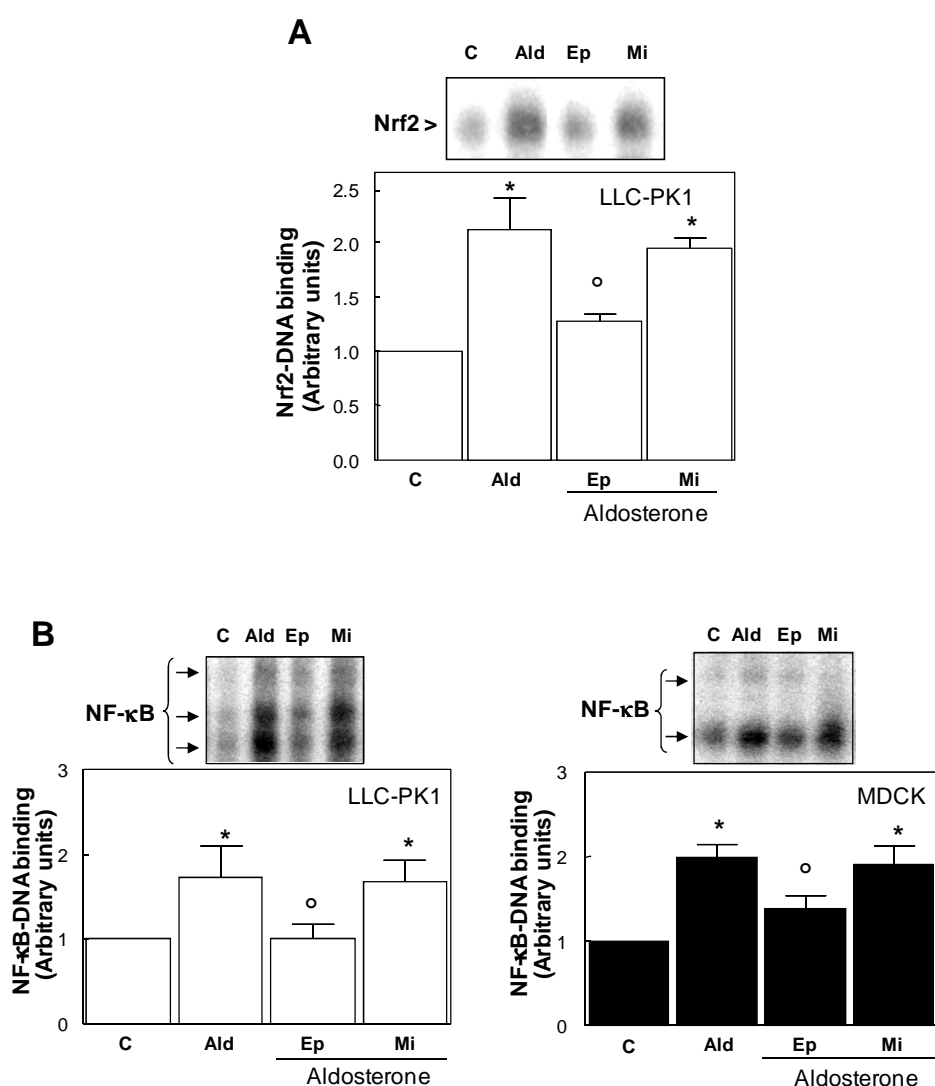
Figure 63: The activation of Nrf2 and NF-κB requires the interaction with the MR.
LLC-PK1 and MDCK cells were incubated in the absence (C) and the presence of 100 nM aldosterone (Ald). Aldosterone-treated cells were simultaneously incubated with either 500 nM eplerenone (Ep) or 500 nM mifepristone (Mi). A: Analysis of Nrf2-DNA binding by EMSA. B: Analysis of NF-κB-DNA binding by EMSA. Results are shown as mean ± SEM of at least 3 independent experiments. * p≤0.05 vs. control, °p ≤0.05 vs. aldosterone treatment.

Furthermore, ERK activation and the subsequent activation of CREB, STAT1 and STAT3 was significantly reduced by eplerenone, but not by mifepristione (Figure 64)
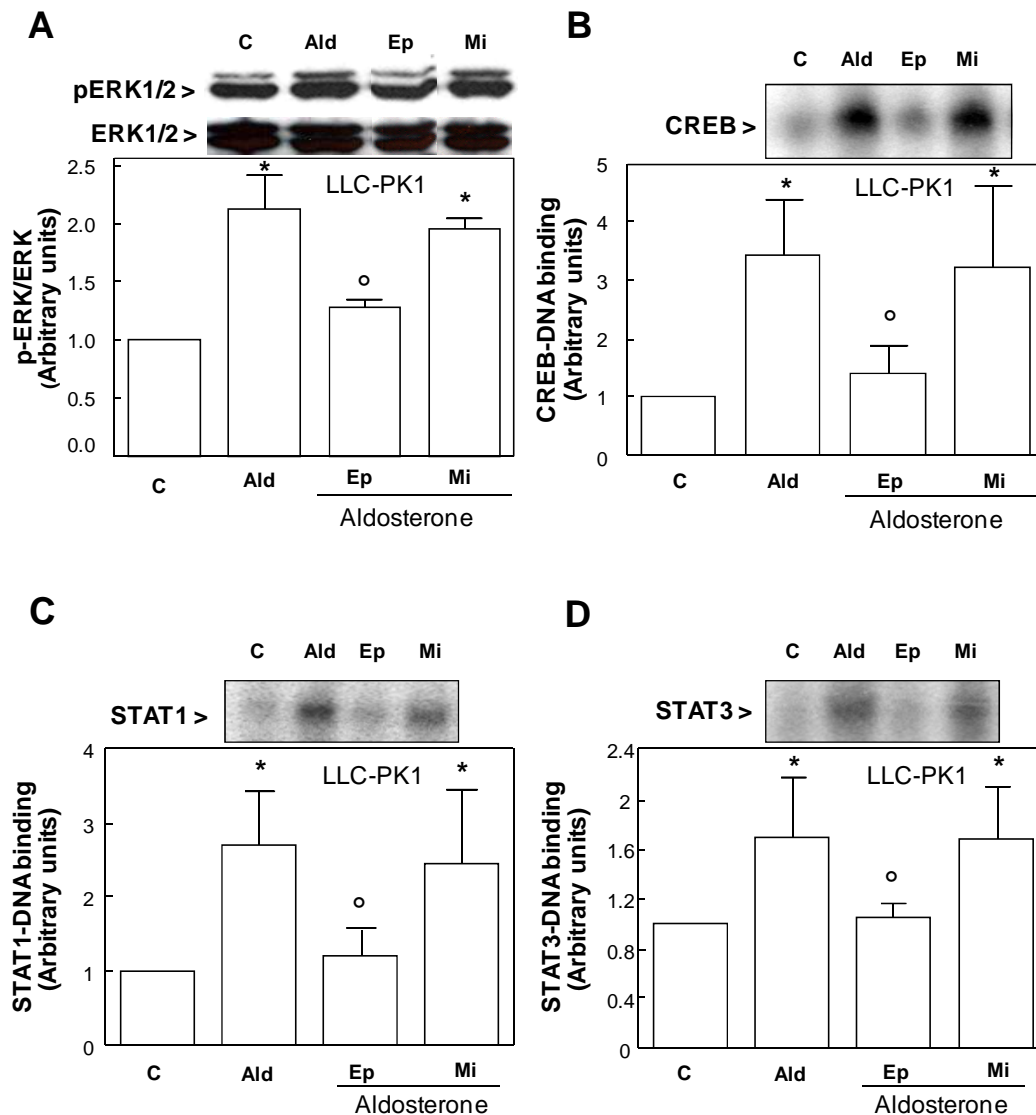
Figure 64: The activation of ERK and the CREB/STAT transcription factors require the interaction with the MR.
LLC-PK1 cells were incubated in the absence (C) and the presence of 10 nM aldosterone (Ald). Aldosterone-treated cells were simultaneously incubated with either 500 nM eplerenone (Ep) or 500 nM mifepristone (Mi). A: Analysis of ERK activation by western blot (primary antibody 1:1000 in 5% BSA). B: CREB-, C: STAT1-, D: STAT3-DNA binding was analyzed by EMSA. Results are shown as mean ± SEM of at least 3 independent experiments. * p≤0.05 vs. control, ° p ≤0.05 vs. aldosterone treatment.

These results suggest that the activation of Nrf2, NF-κB, ERK, CREB, STAT1 and STAT3 in LLC-PK1 and NF-κB in MDCK cells only requires the interaction with the MR and not with the GR.

4.4.2 Intracellular calcium levels

Since it is known that intracellular calcium is an important signaling molecule, the possibility that aldosterone could trigger an increase in cellular calcium was next investigated (see 1.2). Intracellular calcium was measured in LLC-PK1 and MDCK cells using the cell permeable calcium probe Fura 2-AM by confocal microscopy. The images in Figure 65 show that the increase in calcium was completely prevented by intracellular calcium blockers (bapta, 2-aminoethoxydiphenyl borate (2-APB) and thapsigargin) as well as by calcium free medium. These findings suggest the involvement of the release of calcium from intracellular stores and influx of calcium across the plasma in aldosterone signaling.
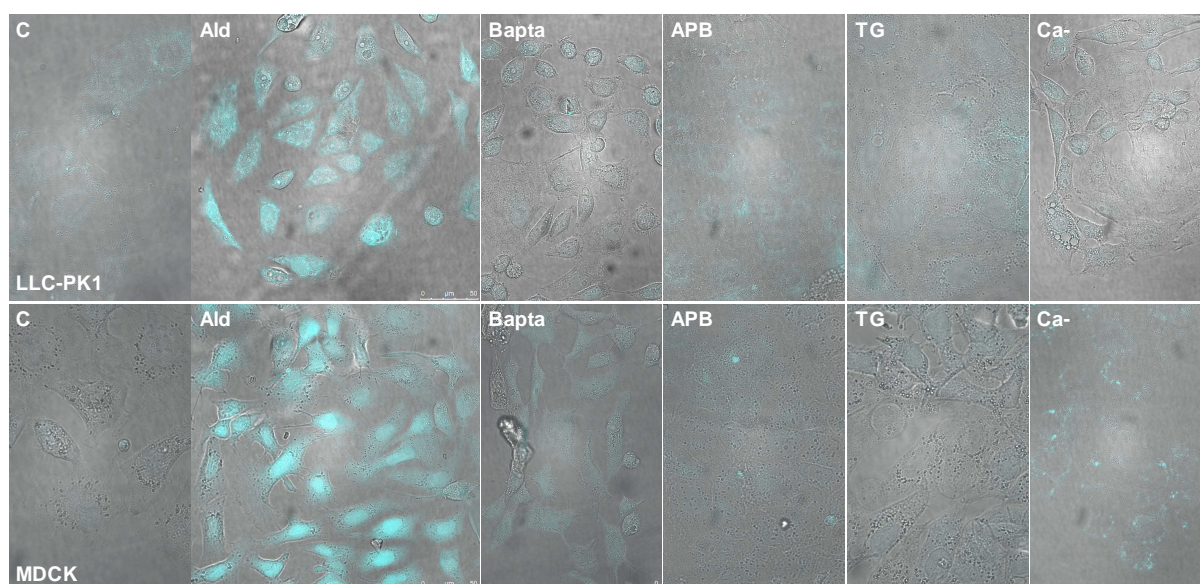
Figure 65: Confocal microscopy of intracellular calcium levels in LLC-PK1 and MDCK cells.
LLC-PK1 and MDCK cells were incubated in the absence (C) and the presence of 10 nM aldosterone (Ald). Aldosterone-treated cells were simultaneously incubated with either 10 µM bapta (Bapta), 5 µM 2-APB (APB) or 200 nM thapsigargin (TG) or were treated with aldosterone in calcium free medium (Ca-). Cells were treated for 30 min (LLC-PK1) or 120 min (MDCK) and subsequently incubated with 10 µM Fura 2-AM for 30 min. Confocal images were obtained by measuring the fluorescence at 510 nm (λexc 405 nm). Representative pictures out of three independent experiments are shown.

Intracellular calcium levels were further determined fluorimetrically using Fura 2-AM. The obtained results support the data of the cofocal microscopy. The calcium chelator bapta, thapsigargin and 2-APB as well as calcium free medium inhibited the increase of intracellular calcium in both cell lines. Interestingly, eplerenone inhibited the aldosterone-induced calcium signal in LLC-PK1 cells, but not in MDCK cells. These results indicate the involvement of the MR in the aldosterone-induced calcium

signal in LLC-PK1 cells whereas in MDCK cells calcium signaling seems to be independent of the MR. This was the only observed different effect of LLC-PK1 and MDCK cells in aldosterone signaling. Mifepristone did not show any effect in both cell lines, indicating that the GR is not involved in the aldosterone-mediated calcium signal (Figure 66).
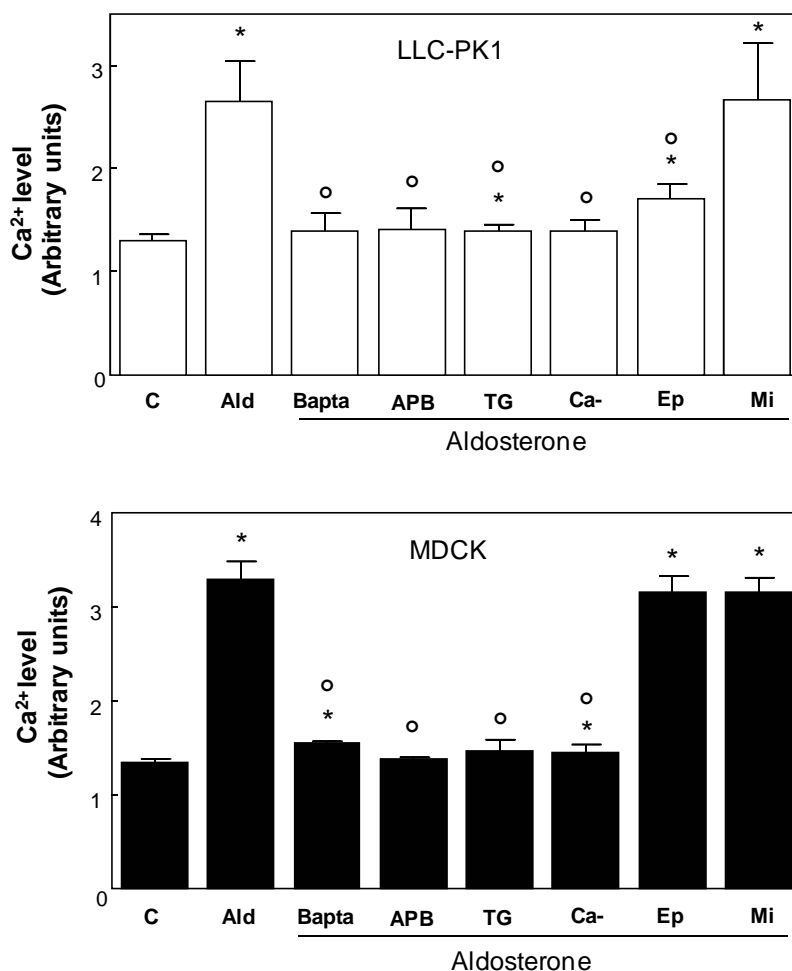
Figure 66: Effects of intracellular calcium blockers and calcium free medium on aldosterone-mediated calcium levels.
LLC-PK1 and MDCK cells were incubated in the absence (C) and the presence of 10 nM aldosterone (Ald). Aldosterone-treated cells were simultaneously incubated with either 10 µM bapta (Bapta), 5 µM 2-APB (APB), 200 nM thapsigargin (TG), 500 nM eplerenone (Ep) or 500 nM mifepristone (Mi) or were treated with aldosterone in calcium free medium (Ca-). Cells were treated for 30 min (LLC-PK1) or 120 min (MDCK) and subsequently incubated with 10 µM Fura 2-AM for 30 min. Fluorescence was measured fluorimetrically at 510 nm (λexc 340 nm). Results are expressed as the fluorescence emission (λem 510 nm) at λexc 340 nm. Results are shown as mean ± SEM of 3 independent experiments. * p≤0.05 vs. control, °p ≤0.05 vs. aldosterone treatment.

4.4.2.1 Intracellular calcium levels are involved in aldosterone-mediated oxidative stress and DNA damage

To investigate the consequences of increased intracellular calcium levels on oxidative stress and DNA damage, fluorimetrical measurements using DCF and

genotoxicity tests were performed. Oxidative stress was significantly reduced using the calcium chelator bapta in LLC-PK1 and MDCK cells (Figure 67).

Figure 67: Cellular calcium levels are involved in aldosterone-induced oxidative stress.
LLC-PK1 and MDCK cells were incubated in the absence (C) and the presence of 100 nM aldosterone (Ald). Aldosterone-treated cells were simultaneously incubated with 10 µM bapta (Bapta). Cells were treated with aldosterone and cellular oxidant levels were measured with the probe H_2DCF-DA after 30 min and 120 min incubation in the combinations described above for LLC-PK1 and MDCK cells, respectively. DCF fluorescence data are shown normalized to the PI fluorescence. Results are presented as mean ± SEM of 3 independent experiments. * $p \leq 0.05$ vs. control, ° $p \leq 0.05$ vs. aldosterone treatment.

As depicted in Figure 68, DNA strand breaks were clearly reduced in the comet assay by all intracellular calcium inhibitors (bapta, 2-APB and thapsigargin) and by calcium free media in LLC-PK1 and MDCK cells.
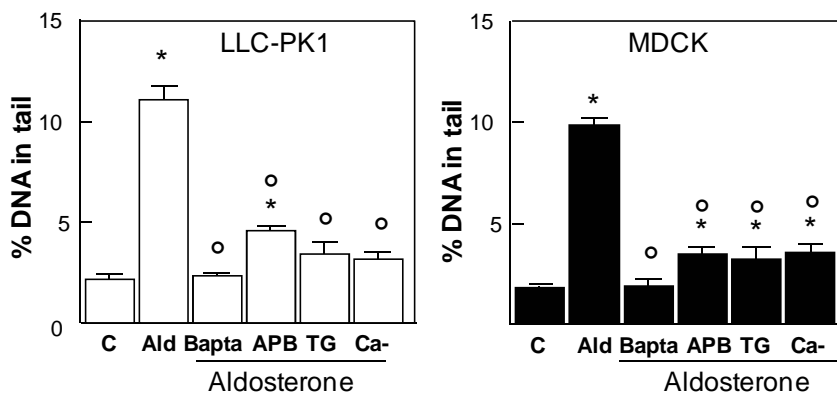
Figure 68: Intra- and extracellular calcium is involved in aldosterone-induced DNA strand breaks.
LLC-PK1 and MDCK cells were incubated in the absence (C) and the presence of 10 nM aldosterone (Ald). Aldosterone-treated cells were simultaneously incubated with either 10 µM bapta (Bapta), 5 µM 2-APB (APB), 200 nM thapsigargin (TG) or were treated in calcium free medium (Ca-). DNA strand breaks quantified with the comet assay in LLC-PK1 and MDCK cells incubated for 4 h. Shown is the percentage of DNA in tail. Results are shown as mean ± SEM of 3 independent experiments.* $p \leq 0.05$ vs. control, ° $p \leq 0.05$ vs. aldosterone treatment.

Furthermore, the micronucleus frequency was significantly reduced by all calcium inhibitors and calcium free medium (Figure 69), indicating that intra- and extracellular calcium is involved in aldosterone-induced DNA damage. Bapta was the most effective calcium inhibitor in the comet assay, whereas it could not be used in the micronucleus test, since it inhibited cellular proliferation.
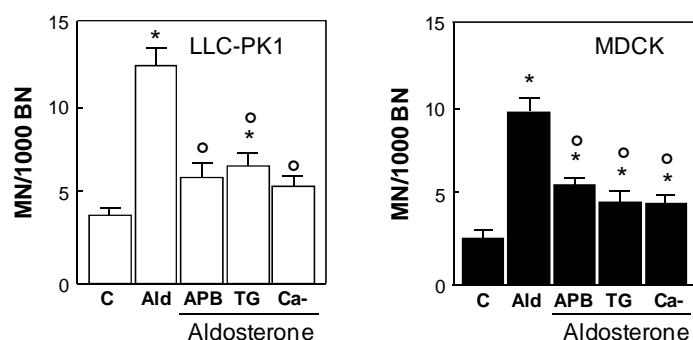
Figure 69: Intra- and extracellular calcium is involved in aldosterone-induced in micronuclei formation.
LLC-PK1 and MDCK cells were incubated in the absence (C) and the presence of 10 nM aldosterone (Ald). Aldosterone-treated cells were simultaneously incubated with either 10 μM bapta (Bapta), 5 μM 2-APB (APB), 200 nM thapsigargin (TG) or were treated in calcium free media (Ca-). Micronuclei formation quantified with the micronucleus test in LLC-PK1 and MDCK cells incubated for 4 h with aldosterone, followed by 24 h incubation with 3 μg/ml of cytochalasin Shown are micronuclei containing cells (MN) per 1000 binucleated cells (BN). Results are presented as mean ± SEM of 3 independent experiments. * $p \leq 0.05$ vs. control, °$p \leq 0.05$ vs. aldosterone treatment.

Since calcium release is often triggered by an activation of PLC, we investigated the involvement of PLC in aldosterone-induced DNA damage in the comet assay. In LLC-PK1 cells, the PLC inhibitor U73122 significantly reduced aldosterone-induced DNA damage (Figure 70), revealing first evidence of the involvement of PLC in the signaling cascade.
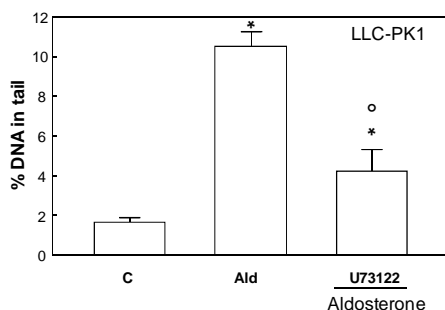
Figure 70: Involvement of PLC in aldosterone-induced DNA strand breaks in LLC-PK1 cells.
Cells were incubated in the absence (C) and presence of 10 nM aldosterone (Ald). Aldosterone-treated cells were simultaneously incubated with 1 μM U73122. DNA strand breaks quantified with the comet assay in LLC-PK1 cells incubated for 4 h. Shown is the percentage of DNA in tail. Results are shown as mean ± SEM of 3 independent experiments.* $p \leq 0.05$ vs. control, °$p \leq 0.05$ vs. aldosterone treatment.

4.4.2.2 Elevated intracellular calcium levels are involved in the activation of Nrf2 and NF-κB

The influence of intracellular calcium on the DNA binding of the transcription factors Nrf2 and NF-κB was measured by EMSA. Aldosterone-induced Nrf2 and NF-κB activity was significantly reduced by bapta (Figure 71A, B) showing the importance of intracellular calcium in the activation of Nrf2 and NF-κB.
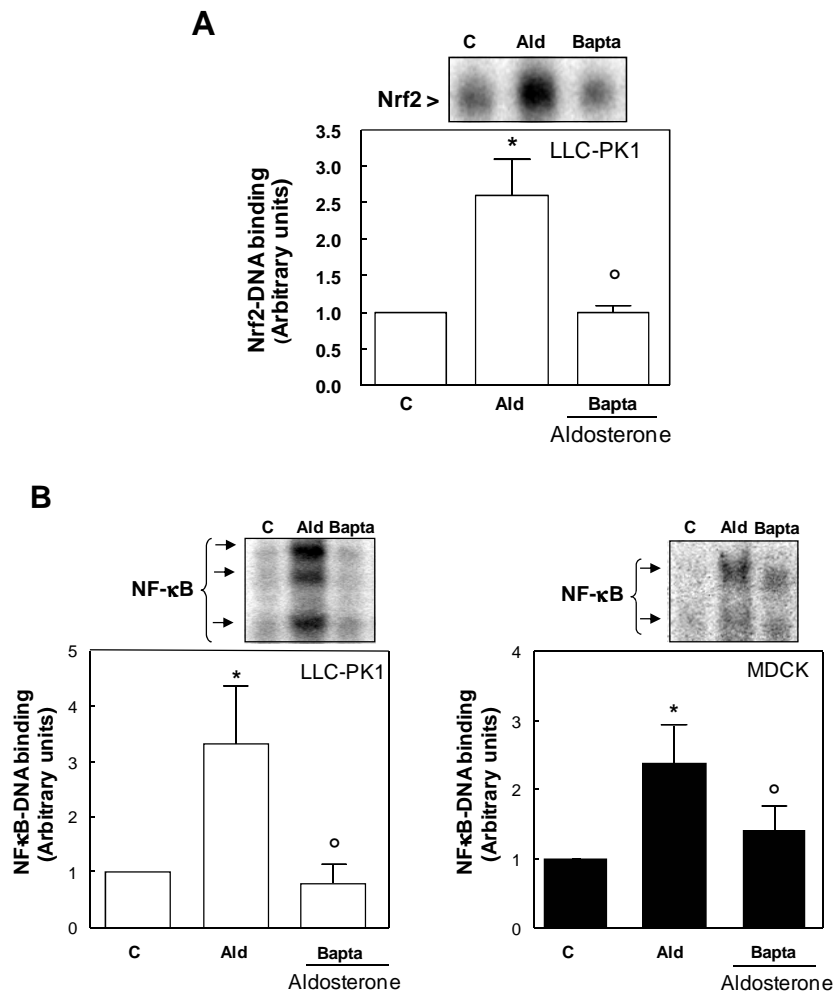
Figure 71: Intracellular calcium levels are involved in the activation of Nrf2 and NF-κB.
LLC-PK1 and MDCK cells were incubated in the absence (C) and the presence of 100 nM aldosterone (Ald). Aldosterone-treated cells were simultaneously incubated with 10 µM bapta (Bapta) for 30 and 120 min respectively. A: Analysis of Nrf2-DNA binding by EMSA. B: Analysis of NF-κB-DNA binding by EMSA. Results are presented as mean ± SEM of 3 independent experiments. * p≤0.05 vs. control, ° p≤0.05 vs. aldosterone treatment.

4.4.3 NAD(P)H oxidase

Since it is known that NAD(P)H oxidase gets activated by calcium and that aldosterone produces oxidative stress via the NAD(P)H oxidase, the activation of this enzyme by aldosterone was investigated, measuring the translocation of the cytosolic

subunit p47phox to the membrane, an event that is required for the activation of NAD(P)H oxidase. As depicted in Figure 72, p47phox levels in cytosolic fractions, as measured by western blot, were significantly lower in LLC-PK1 and MDCK cells incubated with 100 nM aldosterone for 30 min and 120 min cells, respectively, than in control cells.
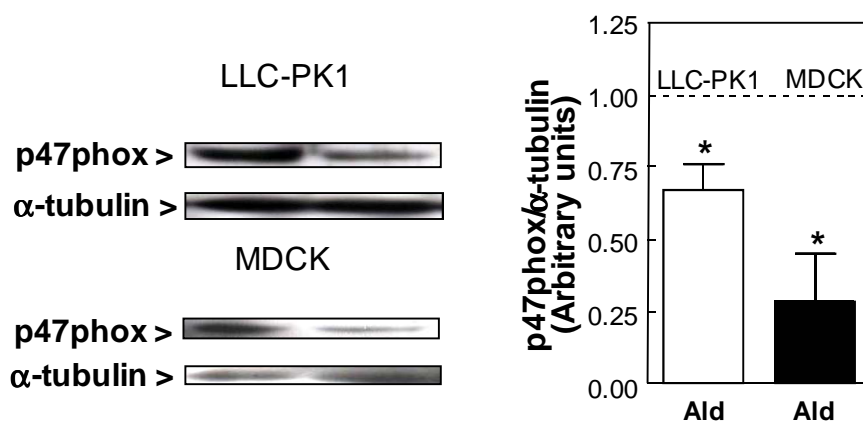
Figure 72: Aldosterone-induced activation of NAD(P)H oxidase.
The translocation of the cytosolic subunit p47phox (1:500 in 5% BSA) to the membrane and therefore the activation of NAD(P)H oxidase was measured by western blot. LLC-PK1 and MDCK cells were incubated with 100 nM aldosterone for 30 or 120 min, respectively, cytosolic fractions were isolated and western blots were performed. Results are presented as mean ± SEM of 3 independent experiments. * p≤0.05 vs. control.

4.4.3.1 NAD(P)H oxidase and PKC are involved in aldosterone-induced oxidative stress and DNA damage

The effects of the NAD(P)H oxidase inhibitors diphenyleniodonium (DPI), apocynin (Apo) and VAS2870 (VAS) and the PKC inhibitor Ro320432 (Ro) on oxidative stress and DNA damage were next investigated. DPI is a flavoprotein inhibitor which inhibits the NAD(P)H oxidase by blocking the reduction of its co-factor flavin adenine dinucleotide (FAD). Apocynin interferes with the serine phosphorylation and intracellular translocation of the cytosolic p47phox/p67phox subunits to the membrane [173]. VAS2870 was identified as a potent NAD(P)H oxidase inhibitor by NAD(P)H oxidase specific high-throughput screeing. The exact acting site of the compound remains elusive, but it seems not to be involved in translocation of the p47phox subunit [174]. The possibility that NAD(P)H oxidase activation occurs via PKC activation was assessed using the PKC inhibitor Ro. All three NAD(P)H inhibitors and the PKC inhibitor Ro caused a clear inhibition of the aldosterone-mediated increase in DCF fluorescence in LLC-PK1 and MDCK cells (Figure 73).
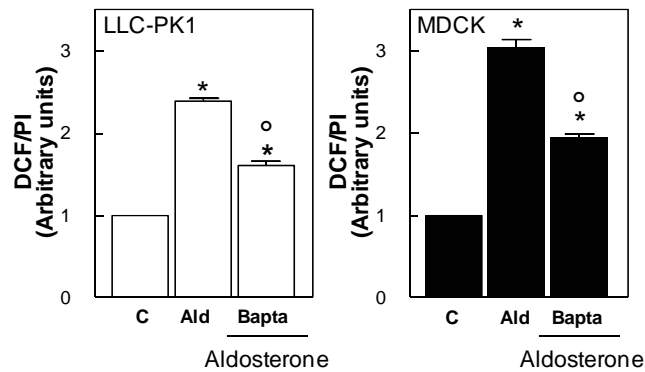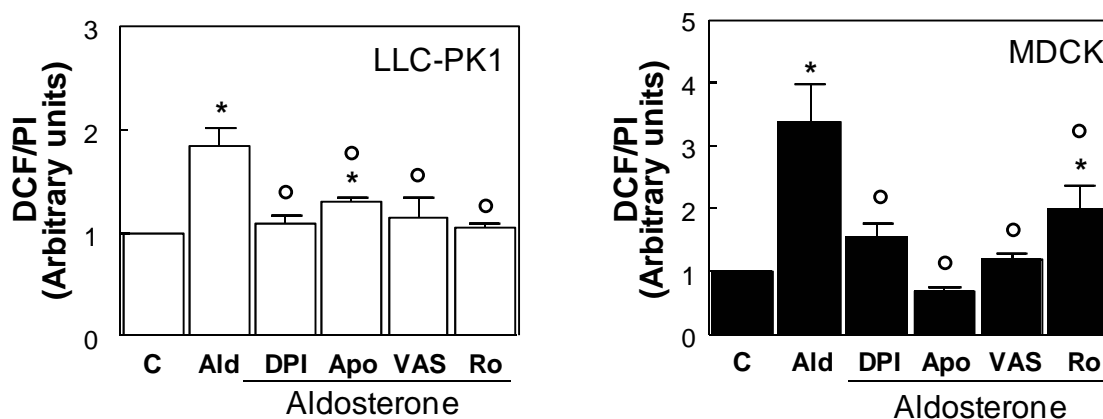
Figure 73: NAD(P)H oxidase and PKC are involved in aldosterone-induced oxidative stress.
LLC-PK1 and MDCK cells were incubated in the absence (C) and the presence of 100 nM aldosterone
(Ald). Aldosterone-treated cells were simultaneously incubated with either 1 µM DPI (DPI), 50 µM
apocynin (Apo), 1 µM VAS2870 (VAS) or 1 µM Ro320432 (Ro). Cellular oxidant levels were measured
using the probe H_2DCF-DA after 30 min and 120 min incubation in LLC-PK1 and MDCK cells,
respectively. DCF fluorescence data are shown normalized to the PI fluorescence. Results are
presented as mean ± SEM of 3 independent experiments. * p≤0.05 vs. control, ° p ≤0.05 vs.
aldosterone treatment.

NAD(P)H oxidase is a major source of $O_2^{\cdot-}$ in cells. To further strengthen the
hypothesis that aldosterone-mediated production of ROS is mediated via NAD(P)H
oxidase, the increase in $O_2^{\cdot-}$ cell levels and the potenial inhibition by NAD(P)H
oxidase inhibitors was investigated using the probe DHE. DHE fluorescence was 2.6-
and 2.3-fold higher after 30 min and 120 min incubation with 10 nM aldosterone in
LLC-PK1 and MDCK cells, respectively (Figure 74). Similarly, like observed with
DCF, this increase was completely prevented by the simultaneous incubation of cells
with the NAD(P)H oxidase inhibitors DPI, apocynin and VAS, and the PKC inhibitor
Ro.

A

B

Figure 74: NAD(P)H oxidase and PKC are involved in aldosterone-induced DNA damage.
LLC-PK1 and MDCK cells were incubated in the absence (C) and the presence of 10 nM aldosterone (Ald). Aldosterone-treated cells were simultaneously incubated with either 1 µM DPI (DPI), 50 µM apocynin (Apo), 1 µM VAS2870 (VAS) or 1 µM Ro320432 (Ro). A: Representative pictures of cells incubated in the combinations above using 10 µM DHE for 30 min (LLC-PK1) or 120 min (MDCK). B: Quantification of $O_2^{·-}$ production by measuring mean gray values of 200 cells per treatment with ImageJ. Results are presented as mean ± SEM of 3 independent experiments. * p≤0.05 vs. control, ° p≤0.05 vs. aldosterone treatment.

Aldosterone-induced DNA damage was assessed by comet assay and micronucleus test using the NAD(P)H inhibitors DPI, apocynin and VAS, and the PKC inhibitor Ro. As was observed for aldosterone-induced oxidative stress, all inhibitors significantly dimished aldosterone-induced genotoxicity (Figure 75A, B).

Figure 75: NAD(P)H oxidase and PKC are involved in aldosterone-induced DNA damage.
LLC-PK1 and MDCK cells were incubated in the absence (C) and the presence of 10 nM aldosterone (Ald). Aldosterone-treated cells were simultaneously incubated with either 1 μM DPI (DPI), 50 μM apocynin (Apo), 1 μM VAS2870 (VAS) or 1 μM Ro320432 (Ro). A: DNA strand breaks quantified with the comet assay in LLC-PK1 and MDCK cells incubated for 4 h. Shown is the percentage of DNA in tail. B: Micronuclei quantified with the micronucleus test in LLC-PK1 and MDCK cells incubated for 4 h with aldosterone, followed by 24 h incubation with 3 μg/ml of cytochalasin B. Shown are micronuclei containing cells (MN) per 1000 binucleated cells (BN). Results are presented as mean ± SEM of 3 independent experiments. * p≤0.05 vs. control, °p ≤0.05 vs. aldosterone treatment.

4.4.3.2 NAD(P)H oxidase and PKC are involved in aldosterone-induced activation of transcription factors and signaling pathways

To further investigate the mechanisms involved in the activation of transcription factors and the ERK signaling pathway, LLC-PK1 and MDCK cells were incubated for 30 min with or without aldosterone and simultaneously treated with DPI, apocynin, VAS and Ro. The PKC inhibitor Ro, as well as all three NAD(P)H oxidase inhibitors caused a significant inhibition of Nrf2-DNA binding activity in LLC-PK1 cells, with VAS2870 being the most potent inhibitor (Figure 76A). NF-κB-DNA binding was also inhibited by all NAD(P)H oxidase inhibitors and the PKC inhibitor Ro in LLC-PK1 and MDCK cells (Figure 76B).
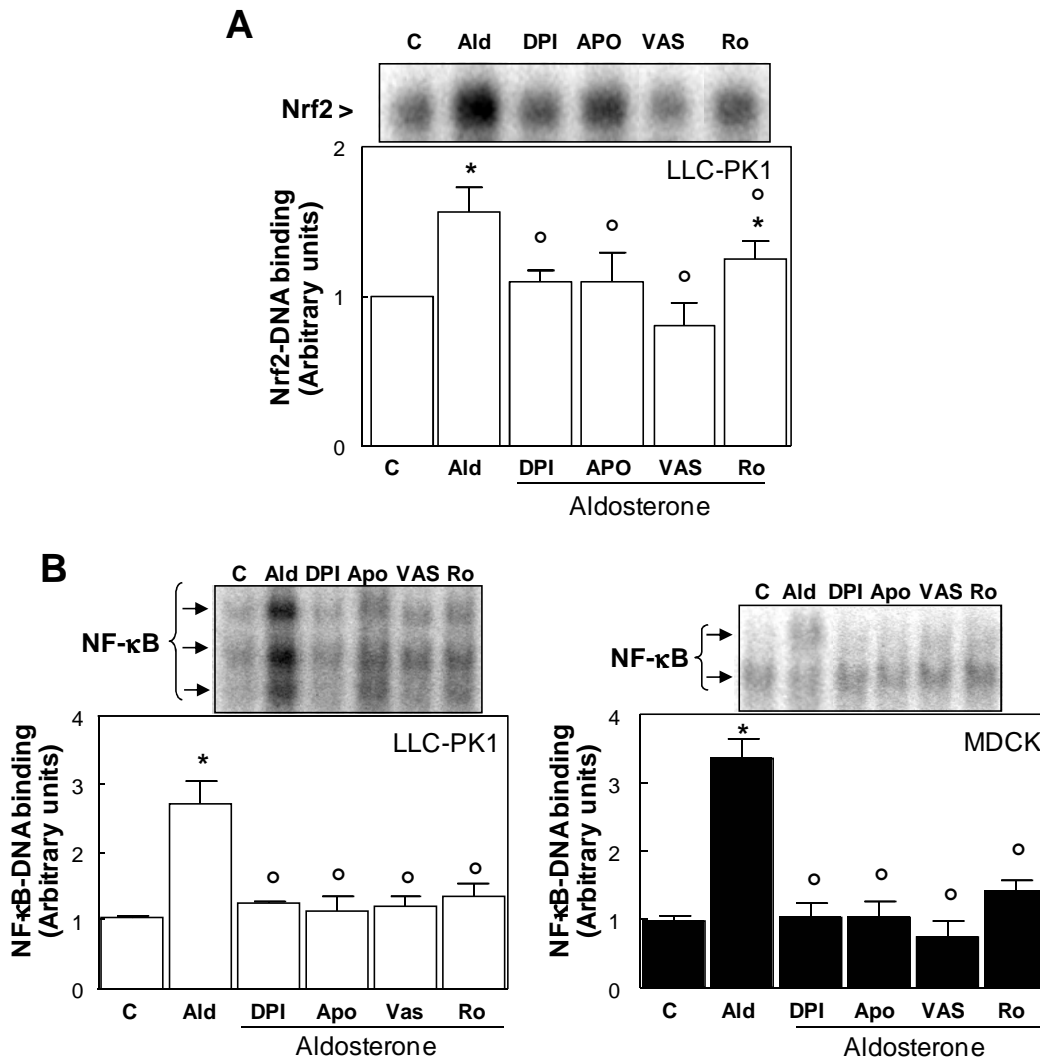
Figure 76: NAD(P)H oxidase is involved in the aldosterone-induced activation of transcription factors and signaling pathways.
LLC-PK1 and MDCK cells were incubated in the absence (C) and the presence of 100 nM aldosterone (Ald). Aldosterone-treated cells were simultaneously incubated with either 1 μM DPI (DPI), 50 μM apocynin (Apo), 1 μM VAS2870 (VAS) or 1 μM Ro320432 (Ro). A: LLC-PK1 cells were treated with aldosterone in the combination described above for 30 min and Nrf2-DNA binding was analyzed by EMSA. B: LLC-PK1 and MDCK cells were treated with aldosterone in the combination described above for 30 min and 120 min, respectively and NF-κB-DNA binding was analyzed by EMSA. Results are shown as mean ± SEM of at least 3 independent experiments. * p≤0.05 vs. control, ° p ≤0.05 vs. aldosterone treatment.

Furthermore, ERK activation and subsequent activation of CREB, STAT1 and STAT3 was significantly reduced by the NAD(P)H oxidase inhibitor VAS in LLC-PK1 cells (Figure 77).
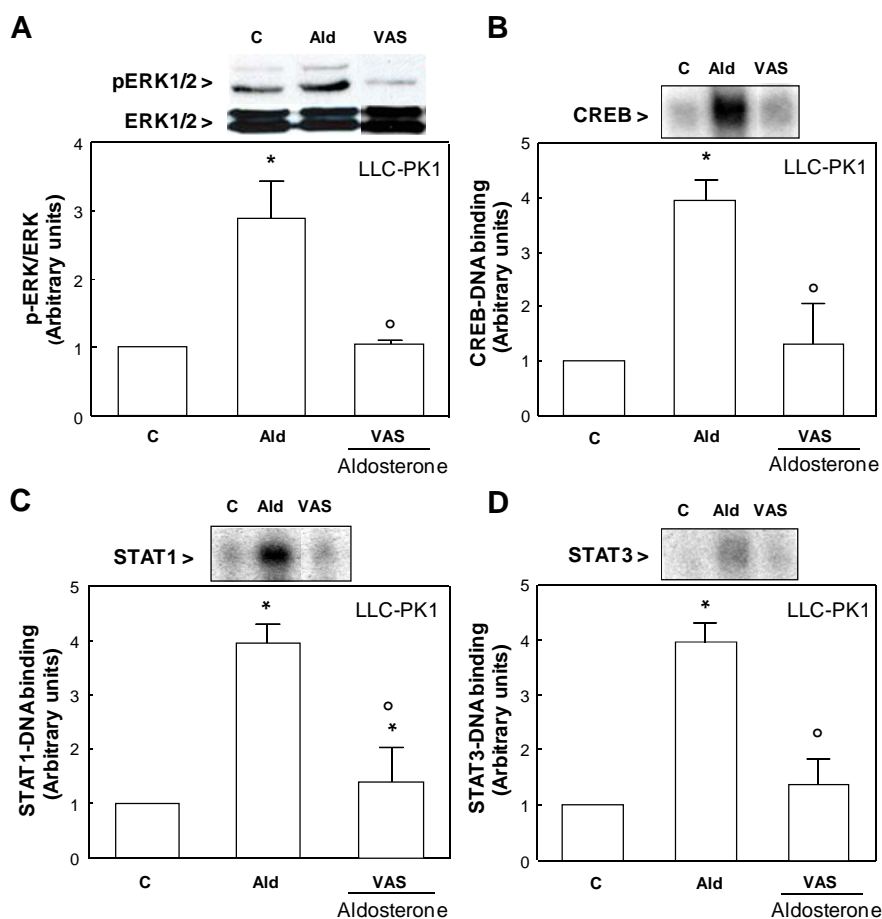
Figure 77: NAD(P)H oxidase is involved in the aldosterone-induced activation ERK and CREB/STAT transcription factors.
LLC-PK1 cells were incubated in the absence (C) and the presence of 10 nM aldosterone (Ald). Aldosterone-treated cells were simultaneously incubated with 1 µM VAS2870 (VAS). LLC-PK1 cells were treated for 30 min and A: ERK activation was analyzed by western blot (primary antibody 1:1000 in 5% BSA). B: CREB-, C: STAT1- and D: STAT3-DNA binding was analyzed by EMSA under the same conditions. Results are shown as mean ± SEM of at least 3 independent experiments. * $p \leq 0.05$ vs. control, °$p \leq 0.05$ vs. aldosterone treatment.

4.4.4 NOS

Given that the probe H_2DCF-DA can react with both ROS and RNS, and that NOS can also be activated by calcium, the next step was to investigate if aldosterone could activate NOS. NOS needs the binding of calmodulin as a cofactor to get activated. Therefore, the calmodulin inhibitor W7 was included in the experiments. NOS is the only enzyme which produces NO. For this purpose, DAF-FM was used which is a very sensitive probe for the detection of NO. Aldosterone caused a 51% and 154% increase in DAF-FM fluorescence in LLC-PK1 and MDCK cells, respectively, that was significantly inhibited by the calcium chelator bapta and by the NOS inhibitors L-NAME (LN) and W7 demonstrated by confocal microscopy (Figure

78A) and determined fluorimetrically (Figure 78B). The prevention of the increase in DAF-FM fluorescence by the NOS inhibitor L-NAME indicates that aldosterone activates NOS causing a subsequent increase in NO synthesis. The activation of NOS occurs via calcium-calmodulin given that both bapta and the calmodulin inhibitor W7 completely prevented DAF-FM fluorescence increase.

A

B
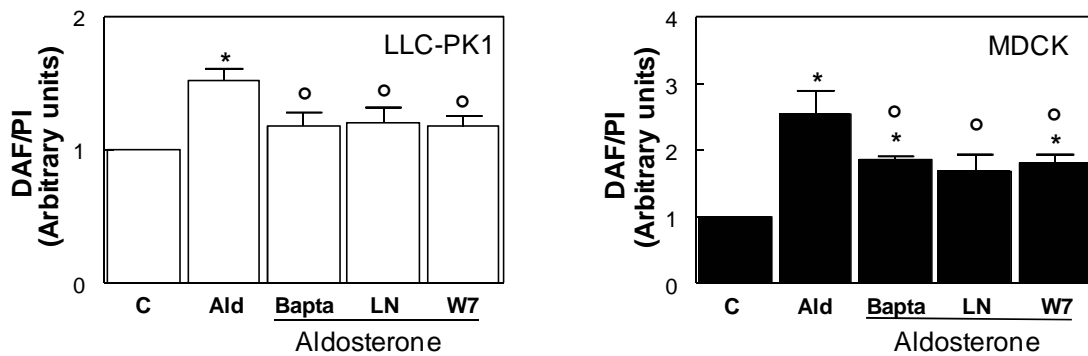
Figure 78: Detection of NO in aldosterone-treated cells using the probe DAF-FM.
LLC-PK1 and MDCK cells were incubated in the absence (C) and the presence of aldosterone (Ald). Aldosterone-treated cells were simultaneously incubated with either 10 µM bapta (Bapta), 50 µM L-NAME (LN) or 10 µM W7 (W7). A: Representative pictures of cells incubated with 10 nM aldosterone in the combinations described above using 10 µM DAF-FM for 30 min (LLC-PK1) or 120 min (MDCK). Confocal images were obtained by measuring the fluorescence at 515 nm (λexc 495 nm). B: Cells were incubated with 100 nM aldosterone for 30 (LLC-PK1) or 120 min (MDCK) and fluorescence at 515 nm (λexc 495 nm) was measured fluorimetrically. DAF fluorescence data are shown normalized to the PI fluorescence. Results are presented as mean ± SEM of 3 independent experiments. * p≤0.05 vs. control, °p ≤0.05 vs. aldosterone treatment.

4.4.4.1 NOS is involved in aldosterone-induced DNA damage

To investigate the involvement of NOS in aldosterone-mediated DNA damage, the NOS inhibitors L-NAME and W7 were tested in the genotoxicity tests. Interestingly, just W7 significantly reduced aldosterone-induced DNA damage in the comet assay, while L-NAME did not (Figure 79A). In the micronucleus test, the NOS inhibitors just slightly reduced micronuclei formation (Figure 79B).
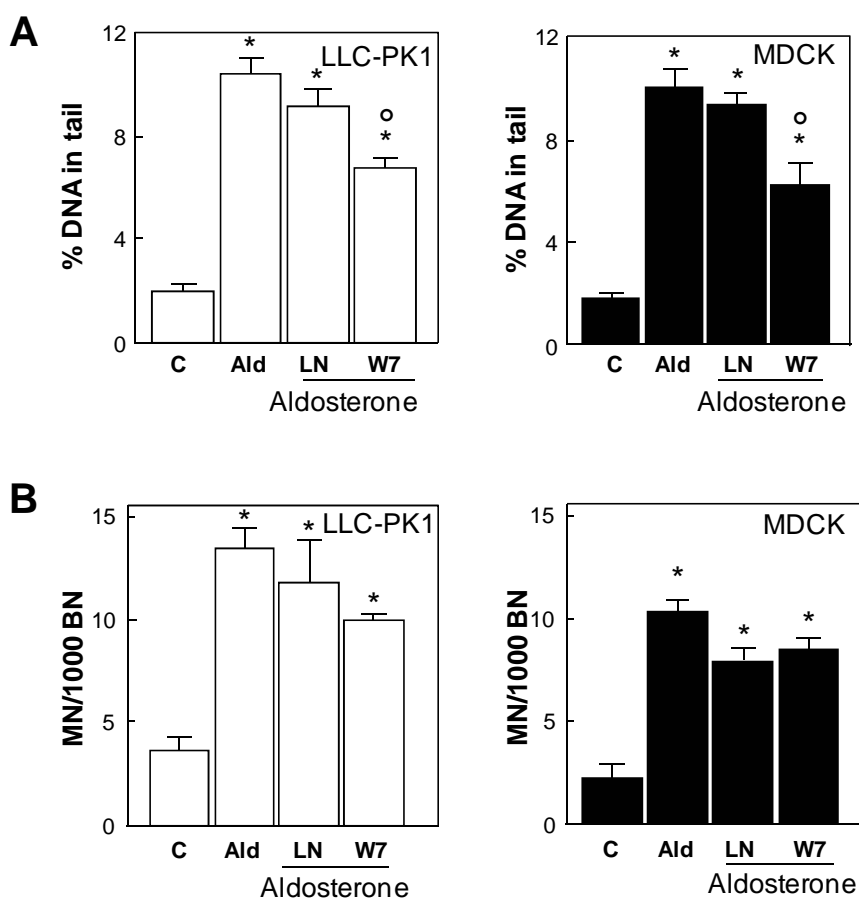
Figure 79: NOS inhibitors slightly reduce aldosterone-mediated DNA damage.
LLC-PK1 and MDCK cells were incubated in the absence (C) and the presence of 10 nM aldosterone (Ald). Aldosterone-treated cells were simultaneously incubated with either 50 µM L-NAME (LN) or 10 µM W7 (W7). A: DNA strand breaks quantified with the comet assay after 4 h in LLC-PK1 and MDCK cells. Shown is the percentage of DNA in tail. B: Micronuclei formation quantified with the micronucleus test in LLC-PK1 and MDCK cells after 4 h incubation with aldosterone, followed by 24 h incubation with 3 µg/ml of cytochalasin B. Shown are micronuclei containing cells (MN) per 1000 binucleated cells (BN). Results are presented as mean ± SEM of 3 independent experiments. * p≤0.05 vs. control, °p ≤0.05 vs. aldosterone treatment.

To check the possibility that NOS is involved in oxidative DNA damage, FPG comet assays were performed. Lesion-specific enzymes can be integrated in the standard protocol to increase the sensitivity of the comet assay. FPG cleaves DNA at sites of oxidized purines and thereby detects 8-oxodG (see 3.2.3.3). The net level of FPG-

sensitive sites was obtained as the difference in score between samples inbubated with FPG protein and samples incubated just with enzyme buffer. Indeed, NOS seems to be involved in oxidative DNA damage, since both NOS inhibitors, L-NAME and W7, significantly reduced FPG-sensitive sites (Figure 80).
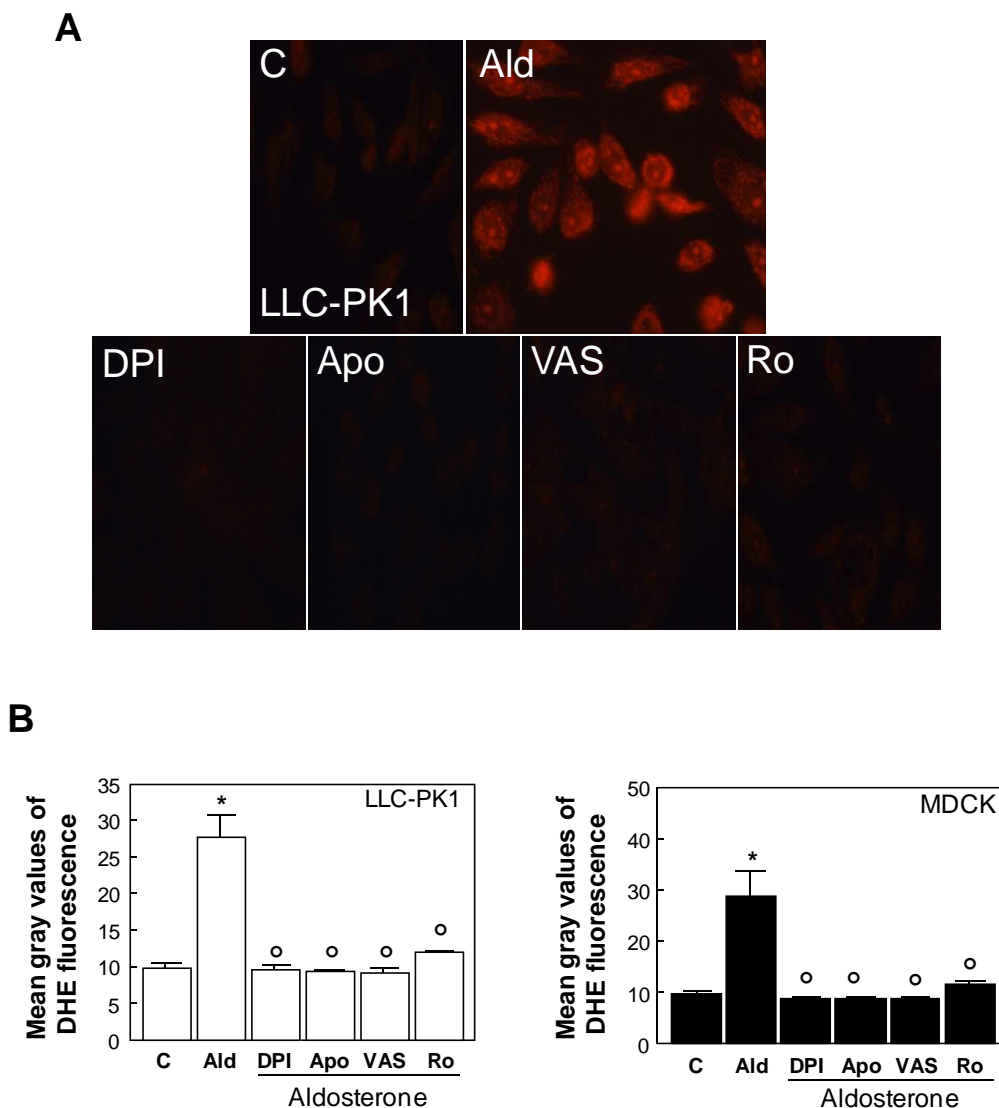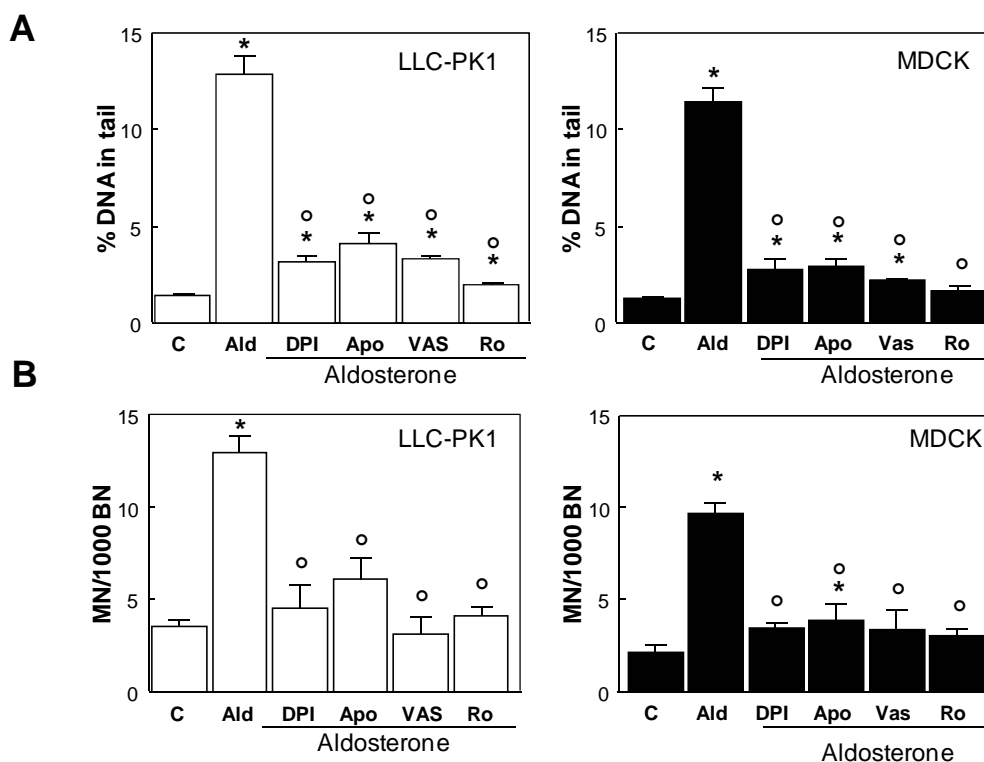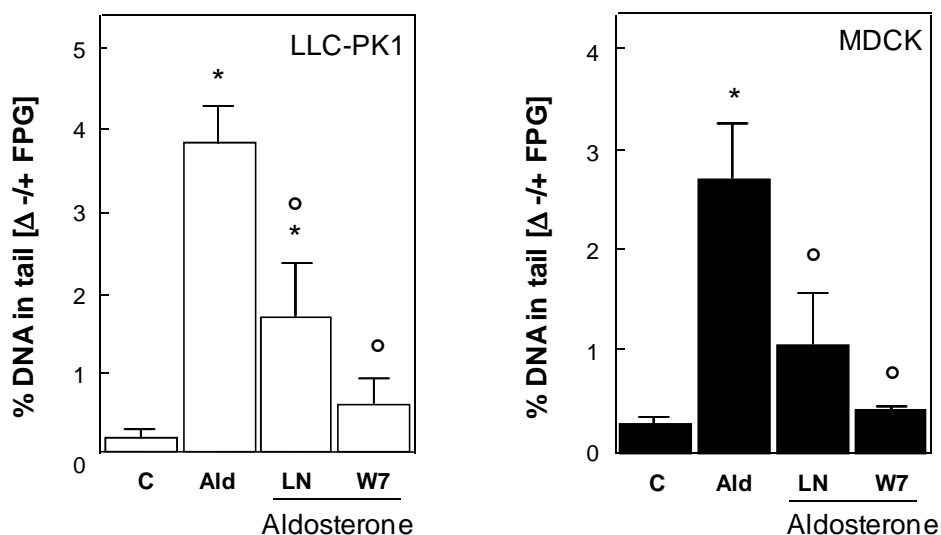

Figure 80: NOS is involved in aldosterone-inducded oxidative DNA damage.
LLC-PK1 and MDCK cells were incubated in the absence (C) and the presence of 10 nM aldosterone (Ald). Aldosterone-treated cells were simultaneously incubated with either 50 µM L-NAME (LN) or 10 µM W7 (W7). DNA damage was assessed after 4 h treatment with aldosterone. Depicted is the mean of the difference (Δ) in the percentage of DNA in tail between nuclei treated and untreated with FPG enzyme. Results are shown as mean ± SEM of 3 independent experiments. * p≤0.05 vs. control, ° p≤0.05 vs. aldosterone treatment.

4.4.4.2 NOS is involved in aldosterone-induced activation of transcription factors and signaling pathways

To investigate the possibility that NOS is involved in the aldosterone-induced activation of Nrf2, NF-κB, ERK, CREB, STAT1 and STAT3, NOS inhibitors were included in the EMSA and the western blot. As shown in Figure 81A, Nrf2-DNA binding was significantly reduced by L-NAME and W7 in LLC-PK1 cells after incubation with 100 nM aldosterone for 30 min. NF-κB-DNA binding was also inhibited by both NOS inhibitors in LLC-PK1 and MDCK cells (Figure 81B).

A

B
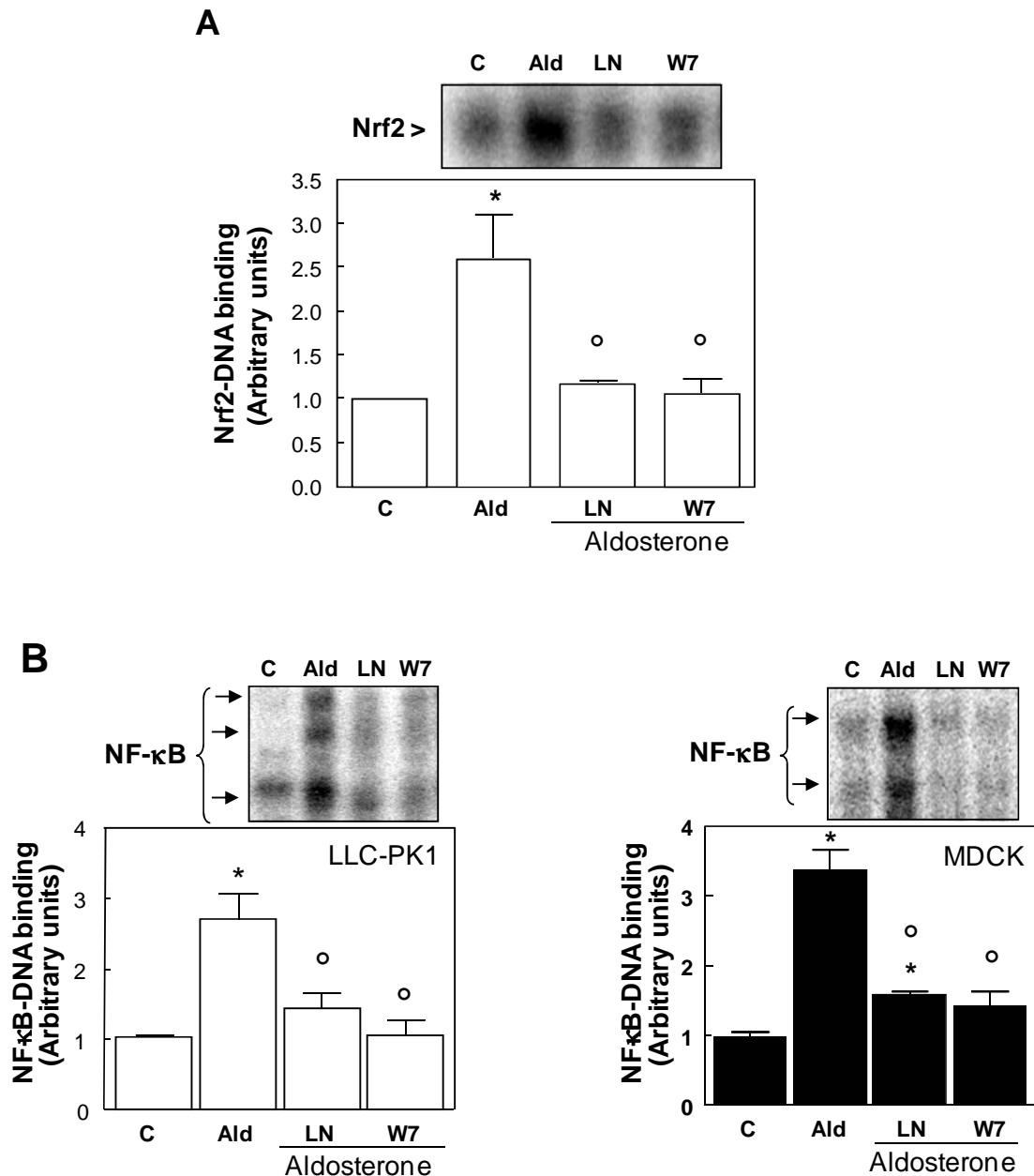
Figure 81: NOS is involved in the aldosterone-induced activation of Nrf2 and NF-κB.
LLC-PK1 and MDCK cells were incubated in the absence (C) and the presence of 100 nM aldosterone (Ald). Aldosterone-treated cells were simultaneously incubated with either 50 μM L-NAME (LN) or 10 μM W7 (W7). A: LLC-PK1 cells were treated with aldosterone in the combination described above for 30 min and Nrf2-DNA binding was analyzed by EMSA. B: LLC-PK1 and MDCK cells were treated with aldosterone in the combination described above for 30 min and 120 min, respectively and NF-κB-DNA binding was analyzed by EMSA. Results are shown as mean ± SEM of at least 3 independent experiments. * p≤0.05 vs. control, °p ≤0.05 vs. aldosterone treatment.

As depicted in Figure 82, the phosphorylation of ERK and the subsequent phosphorylation of CREB, STAT1 and STAT3 were also prevented by the NOS inhibitor L-NAME.
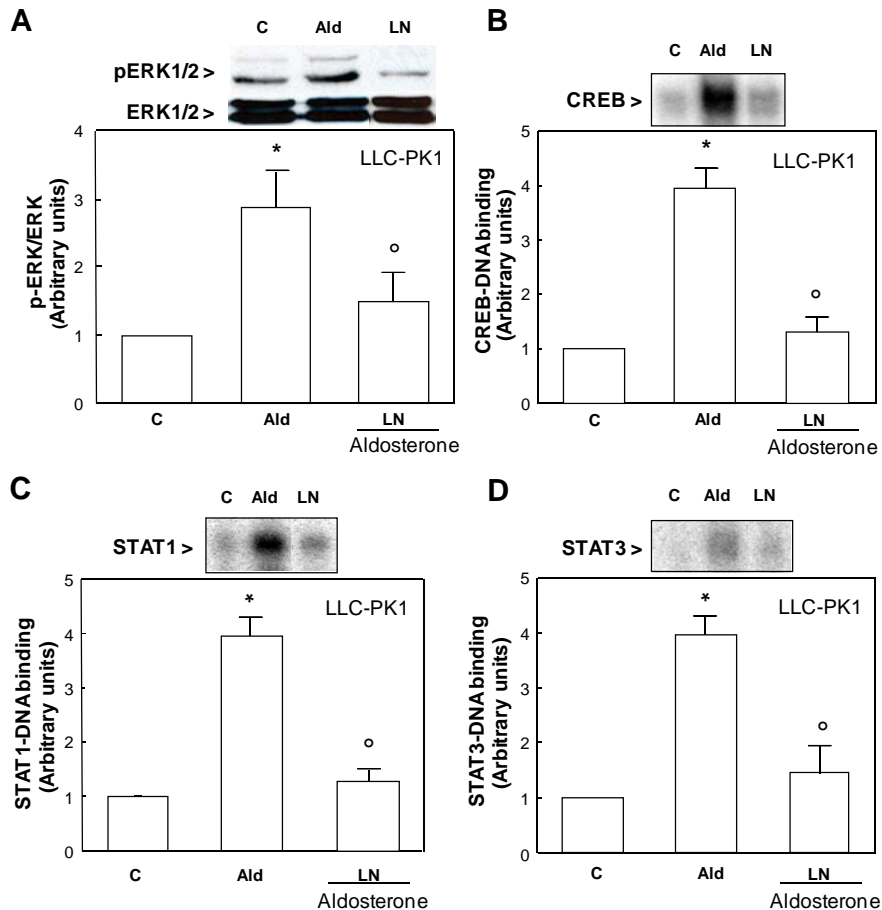
Figure 82: NOS is involved in the aldosterone-induced activation of transcription factors and signaling pathways.
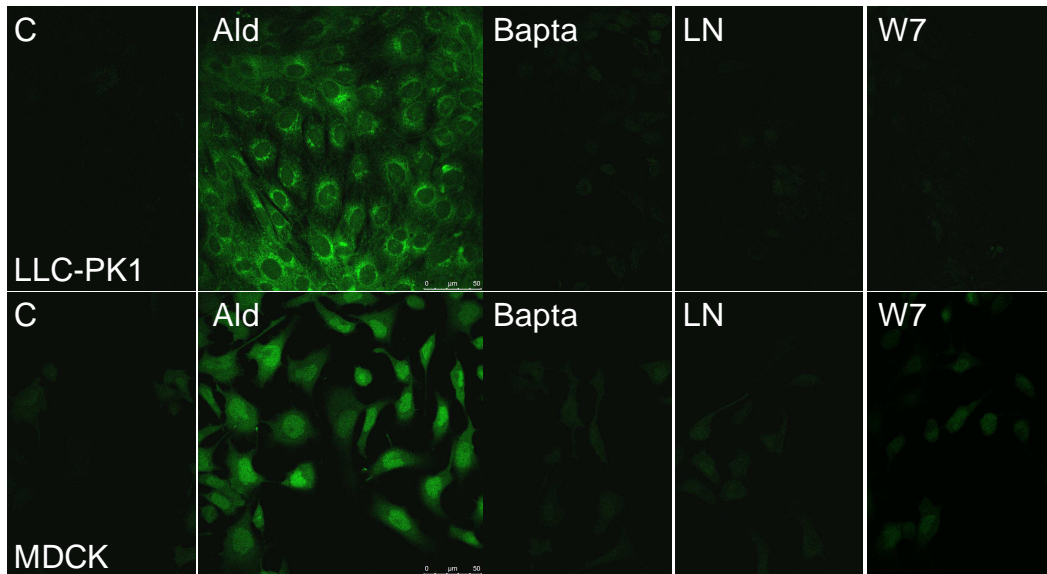LLC-PK1 cells were incubated in the absence (C) and the presence of 10 nM aldosterone (Ald). Aldosterone-treated cells were simultaneously incubated with 50 µM L-NAME (LN). LLC-PK1 cells were treated with aldosterone in the combinations described above for 30 min and A: ERK activation was analyzed by western blot (primary antibody 1:1000 in 5% BSA). B: CREB- C: STAT1- and D: STAT3-DNA binding was analyzed by EMSA under the same conditions. Results are shown as mean ± SEM of at least 3 independent experiments. * $p \leq 0.05$ vs. control, °$p \leq 0.05$ vs. aldosterone treatment.

4.4.5 Assessment of potential antioxidant capacity of substances

It is assumed that all inhibitor substances used in this study inhibit oxidative stress, DNA damage and the activation of transcription factors and signaling pathways due to their inhibitor function and not by an intrinsic antioxidative capacity. This was confirmed in the photometric FRAP assay, which shows, with the limitation that the reaction takes place under acidic conditions, that the antioxidant tempol, but none of the other substances (bapta, DPI, apocynin, VAS2870, Ro320432, L-NAME and W7) are able to reduce the ferric-tripyridyltriazine comlex to its ferrous, colored form (Table 3).

Table 3: NAD(P)H oxidase, PKC and NOS inhibitors do not show antioxidative capacity in the FRAP assay.
Ferric reducing ability of cell-free solutions of bapta, DPI, apocynin, VAS2870, Ro320432, L-NAME, W7 and tempol in the concentrations used above assessed by utilisation of the photometric FRAP assay. Shown are means ± standard deviation.

Substance	Equiv of Fe(II)/L (µM)
Bapta	0.000 ± 3.654
DPI	0.000 ± 4.278
Apocynin	48.99 ± 7.079
VAS	0.000 ± 0.000
Ro320432	9.610 ± 6.342
L-NAME	0.000 ± 1.218
W7	0.230 ± 4.239
Tempol	2200.42 ± 164.268

5 DISCUSSION

5.1 Aldosterone induces oxidative stress and DNA damage in vitro

Aldosterone, a steroid hormone with mineralocorticoid activity, plays a major role in blood pressure homeostasis, the regulation of circulating volume, and the maintenance of the sodium-potassium balance. Beyond these well-known actions, however, aldosterone exerts other effects on the kidney, which can have pathophysiological consequences. The renin-angiotensin-aldosterone system (RAAS) is central to the pathogenesis of hypertension, cardiovascular disease, and kidney disease. There is evidence for many pathways through which a local renal RAAS can affect kidney function, hypertension, and cardiovascular disease. A major mechanism is the loss of the redox homeostasis and the formation of excessive free radicals [175]. Free radicals such as ROS are necessary in normal physiologic processes, e.g. tubular sodium transport. However, the loss of redox homeostasis contributes to proinflammatory and profibrotic pathways in the kidney. In 1985, it was even demonstrated for the first time that exposure of mouse fibroblasts to ROS can lead to malignant transformation of cells [176]. Aldosterone is known to induce oxidative stress through several mechanisms: upregulation of the expression of NAD(P)H oxidase subunits, promotion of the "uncoupling" of NO-synthase, and inhibition of $NADP^+$ reduction by decrease of the activity of glucose-6-phosphate dehydrogenase [25]. Recently the upregulation of genes involved in the generation of ROS was shown in the tissue of a human aldosterone-producing adenoma [177].

In LLC-PK1 porcine kidney cells and MDCK canine kidney cells we could measure the formation of oxidative stress induced by 100 nM aldosterone, already after 30 minutes. Lower concentrations of aldosterone could not be measured with the flow cytometric method quantifying the fluorescence of the redox sensitive dye H_2DCF-DA, since this method is not sensitive enough. Furthermore, H_2DCF-DA was used in fluorimetric measurements to detect ROS. Already after 15 min a significant induction of oxidative stress could be observed by 100 nM aldosterone treatment. Additionally, the $O_2^{\cdot-}$-sensitive dye DHE was used to demonstrate the high production of $O_2^{\cdot-}$ in aldosterone-treated LLC-PK1 and MDCK cells. With this method $O_2^{\cdot-}$-production could be detected already at 10 nM aldosterone.

In LLC-PK1 and MDCK cells a DNA damaging potential of aldosterone was found. There were no considerable cytotoxic effects of aldosterone. It nevertheless was

important to safeguard the results against potential cytotoxicity, as cytotoxic events include DNA degradation [178]. Aldosterone was capable of inducing dose-dependent structural DNA damage starting at 1 nM aldosterone detectable in the comet assay, which may consist of single and double strand breaks as well as of alkali-labile sites [179]. Depending on the class of DNA damage, these lesions can theoretically be repaired [180], with the perpetual risk of mutation by repair errors. Aldosterone also dose-dependently induced an irreparable, inheritable form of chromosomal aberrations, micronuclei, detected in the micronucleus frequency test. In this assay, slightly higher aldosterone concentrations (5 and 10 nM for LLC-PK1 and MDCK, respectively) were needed to induce the significant formation of micronuclei. The two basic mechanisms leading to the formation of micronuclei are chromosome breakage and disturbance of the chromosome segregation machinery, leading to mutated daughter cells [180-181].

Patni *et al.* [182] observed a significant induction of apoptosis at the aldosterone concentration of 100 nM. When using an assay for induction of caspase-3 activity, we also found apoptotic cells, but LLC-PK1 cells only showed a significant increase of caspase-3 positive cells at 1 µM and MDCK cells at 500 nM and 1 µM. Interestingly, there was no significant increase of late apoptotic cells in both cell lines. This might be because the timing of the evaluation of the micronuclei did not fit to the time course of the apoptotic progression. Most probably the cells which were caspase-3 positive were already dead or deattached when the samples were prepared for the microscopic scoring.

Furthermore, we found in LLC-PK1 and MDCK cells the most prominent DNA modification caused by oxidative stress, 8-oxodG by mass spectronomy and FPG-modified comet assay. This is the first evidence of the capability of aldosterone to induce 8-oxodG formation, which has not been previously investigated neither in primary aldosteronism nor in *in vitro* experiments. 8-oxodG is now widely used as a marker of oxidative stress in various diseases. In hypertension, this marker was found to be increased in urine and a significant correlation was observed between the urinary 8-oxodG levels and those found in mitochondrial DNA [183]. 8-oxodG has a high mutagenic potential, because repair errors or unrepaired 8-oxodGs lead to G:C->T:A transversions, which are often found in genes altered in tumors [184].

In agreement with the finding of high 8-oxodG, aldosterone caused an increase in LLC-PK1 and MDCK cell oxidants, and in particular of $O_2^{\cdot-}$, as suggested when

using the probe DHE. Evidence from animal models showed that ROS have an important role in aldosterone-induced renal and heart injury [42, 185]. ROS generation by cultured renal cells exposed to aldosterone was reported for rat mesangial cells, human proximal tubular cells and murine podocytes [186-188]. We observed, in agreement with findings in human cells [187], the earliest significant oxidant increase in MDCK cells after 30 min of aldosterone exposure. In rat cardiac myocytes, similarly to the observations in LLC-PK1 cells, cell oxidants increased already after 5 min of aldosterone treatment [189]. Accordingly, we detected DNA strand breaks after 5 min in both aldosterone-treated cell lines, while the micronucleus frequency significantly rose after 30 min of aldosterone treatment. The fast time course of oxidant production and DNA strand breaks identifies them as being nongenomic actions of aldosterone, which occur between seconds and 30 min, when the earliest genomic event, the increased expression of serum glucocorticoid-activated kinase-1, can be detected [190]. Although aldosterone-induced micronuclei formation is significant at 30 min, this effect could be considered nongenomic, given that DNA double strand breaks might need a longer time to evolve than single strand breaks. What defines an effect of being nongenomic is 1) a rapid onset of action, which is a sufficient, but not necessary criterion, since some nongenomic effects occur with a slower time course and 2) an insensitivity to inhibitors of transcription and translation [33]. Thus, the final proof of having a nongenomic or genomic action of aldosterone in the micronucleus test failed, because the inhibitors of transcription and translation, actinomycin D and cycloheximide, were highly cytotoxic in our cells and therefore could not be used in the genotoxicity tests.

To strengthen the hypothesis that aldostrone-induced DNA damage occured as a consequence of increased oxidative stress, the production of oxidants and the influence of selected antioxidants were investigated. Three different cell permeable antioxidants were chosen: NAC, LA and tempol. NAC has been widely used as an antioxidant *in vitro* and *in vivo*. It is a powerful scavenger of hypochlorous acid (HClO) and it also reacts with OH$^\bullet$ [191]. The antioxidant effects of LA were demonstrated when it was found to prevent the symptoms of vitamin C and vitamin E deficiency. LA is reduced intracellularly to dihydrolipoic acid which in cell culture regenerates by reduction of antioxidant radicals, such as vitamin C and vitamin E [192]. LA is able to scavenge ROS and RNS *in vitro*. Tempol scavenges $O_2^{\bullet -}$ *in vitro*

and may act as a genuine "SOD-mimetic" [193]. Tempol also reduces the formation of OH$^{\bullet}$ either by scavenging $O_2^{\bullet-}$ or by reducing the intracellular concentrations of Fe^{2+} and, hence, the formation of OH$^{\bullet}$ via the Fenton or Haber-Weiss reactions [194]. From these antioxidants, NAC was the less effctive antioxidant. One possible reason could be that the concentration used in the study was not sufficient in totally reducing oxidative stress and DNA damage. Another reason could be that NAC mainly scavenges HClO and not, as tempol, $O_2^{\bullet-}$, which might be the most important radical in aldosterone signaling. The importance of an increase in cellular oxidants on the deleterious effects caused by aldosterone is reflected by the capacity of the antioxidants to prevent aldosterone-induced oxidative stress and DNA damage. These findings suggest the increase in oxidants as a major cause of DNA damage.

5.2 *Aldosterone induces oxidative stress and DNA damage* in vivo

In kidneys of rats with DOCA/salt-induced hypertension, a model for severe hypertension, elevated markers of oxidative stress, DNA damage and proliferation were found. Many of these adverse effects of DOCA/salt-treatment could be prevented by MR antagonism, indicating that the receptor is involved in these pathophysiological processes.

Oxidative stress in DOCA/salt-treated animals has been studied with a variety of stress markers. Subunits of the NAD(P)H oxidase were found to be markedly expressed, the oxidative stress-scavenging protein HO-1 is upregulated and also the urinary oxidative stress marker 8-isoprostane is often increased [195-197]. Both methods used in this study, flow cytometry and DHE staining, for the detection of oxidative stress in the different groups, showed a clear increase of ROS and $O_2^{\bullet-}$, in kidney cells of DOCA/salt-treated rats compared to sham operated rats. Other than in the kidney [198], increased $O_2^{\bullet-}$ production was also observed in the aortas and hearts of DOCA/salt-treated rats [199].

Against the background of several studies which report an increased cancer incidence (especially of the kidney) in individuals with hypertension [3-4], and which suggest the trigger to be the hypertension itself [4], we tried to find evidence for genotoxic effects of mineralocorticoid-dependent hypertension in kidney cells. *In vitro* we have not just found prooxidative and genotoxic effects of aldosterone, but also of

angiotensin II [200-201]. Even physiological concentrations of angiotensin II lead to DNA damage in the *ex vivo* perfused mouse kidney [202]. The question, whether hypertension might lead to DNA damage, has not yet been addressed. A single publication found an increase of chromosomal aberrations in the spontaneously hypertensive rat compared to the control Wistar-Kyoto rat [203]. In humans, two laboratories quantified DNA damage in peripheral lymphocytes with the comet assay and found an increase in the hypertensive group [204-205]. Here, a significant increase of DNA strand breaks in kidney cells of DOCA/salt-treated rats was demonstrated – an increase seen neither in the sham operated control, nor in the rats treated with interventional medications. The medication dosage in the present study was chosen in an attempt to lower the blood pressure only to minor extent, if at all. The fact that both oxidative stress and DNA damage nevertheless were reduced to the levels of the control rats by the different drugs indicates that in this model the elevated mineralocorticoid hormone – and not the hypertension itself – causes these types of damage. Exactly this observation was made in the perfused mouse kidney where we could show that DNA damage induced by angiotensin II was independent of its vasoconstrictive effects [202].

Besides performing the comet assay, double strand breaks were quantified on paraffin embedded rat kidneys. The histone H2AX has been shown to get rapidly phosphorylated after induction of double strand breaks and is thought to promote repair protein recruitment [206]. γ-H2AX can be visualized by using phospho-specific antibodies [207]. Double strand breaks are known as the most toxic form of DNA damage, leading to cell death or genetic alterations like large- or small-scale deletions, loss of heterozygousity, translocations, and chromosome loss [208]. The chromosomal rearrangements that may occur after incorrect repair are discussed as a major initiating factor in carcinogenesis [209].

However, because double strand breaks and DNA damage observed in the comet assay could nevertheless theoretically be completely repaired or could be attributed to apoptotic events, further experiments measuring the base 8-oxodG were performed. Increased amounts of the oxidative base modification 8-oxodG in the DOCA/salt-group were found. Studies in a mouse model suitable for the quantification of mutations revealed that less than one additional 8-oxodG per 10^6 base pairs is sufficient to double the mutation rate in hepatocytes of affected animals [210]. As already mentioned in 4.1, no investigation has as yet been published

regarding 8-oxodG, either in hyperaldosteronism, or in experimental mineralocorticoid-dependent hypertension. In this study first evidence is presented to induce the formation of 8-oxodG in DOCA/salt-treated rats.

The high blood pressure in the rats in the present study still provokes the observed changes in kidney weight, kidney function and kidney pathology. While in our investigation the nonsteroidal MR antagonist BR-4628 was clearly superior to spironolactone, this is not the case with regard to oxidative stress and DNA damage.

To correctly evaluate the observed DNA damage in DOCA/salt-treated animals, the occurrence of apoptosis was assessed. Apoptotic, cleaved caspase-3 positive, tubular cells were not significantly increased in the kidney after DOCA/salt-treatment, and therefore could not have influenced the amount of DNA strand breaks. If apoptosis would have been increased, as was shown in tubular cells *in vitro* [182] in mesangial cells *in vivo*, [211] in endothelial cells [212] and in cardiac myocytes, [213] it nevertheless would have had no impact on 8-oxodG formation [182].

We have found in the DOCA/salt model the induction of oxidative DNA damage. DNA lesions such as the demonstrated base modifications, single and double strand breaks can lead to mutations, but only if the affected cells proliferate. Proliferative effects of mineralocorticoids on kidney cells were reported before. By administration of the thymidin analogue BrdU elevated proliferation in the kidneys of DOCA/salt-treated rats were detected, mainly in tubular regions. This was in agreement with Pietranera *et al.* showing enhanced proliferation in brains of DOCA/salt-treated rats compared to the brains of steroid-free control animals [214]. If this prerequisite is also met in humans suffering from elevated aldosterone levels and if aldosterone as well causes DNA damage in humans, then aldosterone might indeed play a so far undescribed but important role in the increased cancer risk observed in hypertensive patients.

5.3 *Aldosterone activates transcription factors and signaling pathways* in vitro

ROS have been related to the activation of transcription factors and to signaling pathways like the ERK pathway. Since aldosterone induces oxidative stress, the activation of Nrf2, NF-κB and ERK, and the subsequent activation of CREB, STAT1 and STAT3 was observed in LLC-PK1 cells. In the following paragraph the activation

of these transcription factors and ERK as well as the consequences for the cells are discussed.

5.3.1 Transcription factor Nrf2

Nrf2 plays a leading role in the protection against oxidant- and xenobiotic-induced cellular injury. Nrf2 regulates basal activity and coordinated induction of genes encoding antioxidants and phase II detoxifying enzymes. We demonstrated that aldosterone causes oxidative stress and DNA damage in renal cells [201]. Therefore here we investigated the possible subsequent activation of Nrf2. Indeed, aldosterone treatment activated Nrf2. We could show that not only the Nrf2-DNA binding increases after treating the cells with aldosterone, but also the protein Nrf2 itself got upregulated. This is, to the best of our knowledge, the first report of the activation of Nrf2 by aldosterone in kidney tubule cells. Furthermore, we found that the Nrf2-DNA binding was partially or totally prevented by the simultaneous incubation of cells with the antioxidants NAC, LA and tempol, suggesting an increase in the aldosterone-induced production of ROS and/or RNS as cause of Nrf2 activation.

The coordinated induction of antioxidants and phase II enzymes has been shown to protect cells against toxicity, mutagenicity and carcinogenicity resulting from exposure to environmental and synthetic chemicals and drugs [215]. We investigated if the aldosterone-induced activation of Nrf2 leads to the expression of target genes encoding for antioxidants and detoxifying enzymes. We observed that the detoxifying enzyme NQO1, the antioxidant enzyme HO-1 and the selenoprotein Trx are significantly expressed in aldosterone-treated cells after 4 h, suggesting a protective role against the aldosterone-mediated oxidative and nitrosative stress in LLC-PK1 cells.

GSH is the most abundant endogenous antioxidant in eukaryotic cells and plays a leading role in the regulation of the redox state. GSH exerts potent antioxidant actions by directly scavenging ROS/RNS and by serving as the substrate in reactions catalyzed by a number of major antioxidant enzymes such as GPx. Selective inhibition of the enzymes of the glutathione redox cycle heightens the susceptibility to ROS/RNS-mediated cell injury [99]. Our study clearly showed that after 4 h treatment, aldosterone upregulates both transcripts of GCL, which would

presumably result in increased intracellular glutathione levels. Increased intracellular GSH levels have been shown to provide greater resistance of cells during acute NO stress [216] and increased oxidative stress [217]. Nevertheless, we found a significant decrease of GSH levels in LLC-PK1 cells after 24 h aldosterone treatment by mass spectronomy. This result was confirmed by fluorimetric measurements, showing an increase of GSH levels after 4 h treatment with aldosterone, but a significant decrease after 24 and 48 h. Since we also observed that ROS levels are still high in aldosterone-treated cells, but Nrf2 activation clearly decreases after 24 h, we conclude that Nrf2 activation is a transient process in LLC-PK1 cells.

Furthermore, we found a slight increase of DNA double strand breaks in aldosterone-treated kidney cells after 30 min aldosterone treatment, which became significant after 4, 24 and 48h. Double strand breaks are serious lesions that can initiate genomic instability, finally leading to cancer [218-219]. When a cluster of ROS is sufficiently close to a DNA double strand helix, multiple lesions are formed on both strands, often leading to double strand breaks. During 30 min after double strand break formation, large amounts of γ-H2AX molecules accumulate in the chromatin around the break site, thereby creating a focus where proteins involved in DNA repair and chromatin remodeling agglomerate. This amplification makes it possible to detect single double strand breaks with an antibody to γ-H2AX [220] (see 4.2). Although aldosterone-induced Nrf2 activation reached its maximum at 4 h, it was not sufficient to protect the cells against the increased amount of aldosterone-induced ROS/RNS production, leading to the formation of double strand breaks. Additionally to the above mentioned double strand breaks, we found significantly increased amounts of the base modification 8-oxodG after 4, 24 and 48 h aldosterone treatment. The amount of 8-oxodG steadily increased up to 48 h. 8-oxodG is one of the most abundant products of oxidatively damaged DNA [221]. Oxidatively damaged DNA has been recognized to be associated with the development of cancer, aging and some degenerative diseases [222]. Aoki *et al.* demonstrated that Nrf2-deficient, but not wildtype mice exposed to diesel exhaust particles had increased levels of 8-oxodG in bronchial epithelial cells [223-224]. Contrary to this, our results provide a first hint that Nrf2 activation as an adaptive survival response in LLC-PK1 cells is not sufficient to protect the cells against the increased amount of aldosterone-induced ROS/RNS and oxidative DNA damage.

In summary, our results indicate that aldosterone activates Nrf2 by enhancing intracellular ROS/RNS levels. In reponse to oxidative stress, cells attempt to fortify the antioxidant arsenal as a first line of defense. Although antioxidant or detoxifying enzymes, such as GCL, HO-1, Trx or NQO1 are rapidly induced in response to oxidative or nitrosative stress, such an adaptive survival response is normally transient and prone to be readily saturated and overwhelmed by excess amounts of ROS/RNS, which is in agreement with our findings. Additionally, we could show that Nrf2 activation is not sufficient to protect LLC-PK1 cells from the aldosterone-induced ROS/RNS and oxidative DNA damage. Therefore, Nrf2 activation seems to be a futile process in LLC-PK1 cells, which could possibly be one of the reasons for the higher cancer mortality in hypertensive patients with elevated aldosterone levels.

5.3.2 Transcription factor NF-κB

NF-κB is activated by a series of stimuli, such as cytokines, bacterial lipopolysaccharides, ultraviolet and ionizing radiation, but also by ROS and genotoxic substances [103]. Depending on the amount of ROS produced and on the kind of DNA damage induced, activation of NF-κB can lead to prolonged cell survival [102-103]. Several target genes activated by NF-κB contribute to prosurvival functions, which are essential for lymphopoiesis, osteogenesis, neuroprotection, and tissue response to injury. However, persistent NF-κB activation is associated with an increased transcription of genes that regulate cancer-associated events such as chronic inflammation, uncontrolled proliferation, resistance to apoptotic death, invasion, angiogenesis and metastasis [225]. Gene targeting studies demonstrated a complex role of the IKKß/NF-κB pathway in a variety of cancer models that are dependent on chronic inflammation [226]. Multiple proinflammatory molecules trigger the activation of NF-κB. Several studies have demonstrated that the administration of aldosterone is associated with a proinflammatory response. Therefore, aldosterone participates in renal and cardiac damage through the stimulation of inflammatory processes. The proinflammatory role of aldosterone seems to involve the system of NFκB/IκB, since the reduction of vascular inflammatory markers by MR antagonists observed in genetic hypertensive rats was accompanied by both a decrease in the expression of the transcription factor NF-κB as well as an increase in the aortic expression of its inhibitor IκB. This

supports that a reduction of the activity of the system is involved in the reduction of the inflammatory process produced by antagonism of the mineralocorticoid receptor [227]. It is speculated that NF-κB is furthermore activated by genomic damage and that NF-κB induces - as an answer to genomic damage - a signaling pathway which enables the cell to adhere the cell cycle. Consistent with the activation of NF-κB by oxidative stress and DNA damage [102, 228], aldosterone induced, in LLC-PK1 and MDCK cells, a time- and dose-dependent activation of NF-κB. The maximum of NF-κB activation was different in the cell lines: LLC-PK1 cells showed a maximum in NF-κB activation already after 30 min aldosterone treatment while in MDCK cells the maximal NF-κB activation was observed after 2 hours. In one animal experiment, a significant increase in NF-κB-DNA binding was shown, which could be prevented by administration of an antioxidant [229]. This was in agreement with our study, since the antioxidants NAC, LA and tempol prevented aldosterone-induced NF-κB activation. NAC was again the less effective antioxidant. These findings suggest the increase in oxidants as a major cause of NF-κB activation. We observed that aldosterone caused a rapid activation of NF-κB in LLC-PK1 and MDCK cells, that could be one of the first steps of the genomic effects of aldosterone, which either leads to a protection of cells against the induced DNA damage by enhancing the expression of DNA repair proteins, thereby promoting cell survival [103]. Or, as has been shown in rats with increased aldosterone levels, activation of NF-κB could contribute to the pathology by upregulating selected genes that further increase oxidative stress, like NADPH-oxidase subunits, and inflammatory mediators (tumor necrosis factor (TNF)-α, interleukin (IL)-1β, IL-6) [230]. Furthermore, we observed that aldosterone treatment up to 24 h led to an increased expression of the NF-κB-regulated antiapoptotic proteins Bcl-2, Bcl-xL, cIAP and XIAP in LLC-PK1 cells. These proteins have been implicated in cell survival and their increased expression is frequently observed in different cancers [231].

In the short term, the activation of NF-κB can be a protective response against aldosterone-induced oxidative stress and DNA damage. However, a long-term NF-κB activation by persistently high aldosterone levels could unfold the prosurvival activity of NF-κB in aldosterone-exposed cells. DNA damage caused by increased ROS might become persistent and would be inherited to daughter cells, probably initiating carcinogenesis.

5.3.3 ERK signaling pathway and CREB/STAT transcription factors

The Ras/Raf/MEK/ERK pathway is an important intracellular pathway whose activation influences many fundamental cellular processes and whose aberrancy is associated with cancer cell growth. This pathway has enormous effects on proliferation, apoptosis and differentiation. In resting conditions, ERK is anchored in the cytoplasm in association with MEK, the microtubule network, or with phosphatases. ERK is activated by upstream kinases: Raf phosphorylates MEK and MEK phosphorylates ERK. Once activated, ERKs primarily phosphorylate a multitude of target substrates on serine or threonine residues followed by a proline residue, and regulate cellular activities. Our findings of an activation of upstream kinases Raf and MEK by aldosterone are in line with previous work e.g. in smooth muscle cells [232]. Mitogens induce a biphasic activation of ERK1/2, with a rapid and strong onset of kinase activity peaking within a few minutes followed by a second wave of lower but sustained activity that persists throughout the G1 phase for up to 6 h [233]. In LLC-PK1 cells we also observed the first peak of ERK activation rapidly, after 30 min aldosterone teatment, and a slower wave after 4 h. The rapid activation of ERK could be due to nongenomic effects of aldosterone, whereas the later activation could be a genomic effect of aldosterone. Rapid ERK phosphorylation by aldosterone has been observed before in kidney cells e.g. in the mouse cortical collecting duct cell line M1 [125] or in MDCK-C11 cells [31]. Nuclear translocation of ERK1/2 can occur within 15 min of activation, persists during the entire G1 phase, and can be reversed upon removing the mitogenic stimulus. In our cells, a slight increase of nuclear phospho-ERK could be observed rapidly, reaching the maximum after 4 h incubation with aldosterone. Various mechanisms have been reported that facilitate nuclear translocation of phospho-ERK1/2. Integrin-mediated organization of the actin cytoskeleton is necessary for the proper localization and translocation of activated ERK1/2 into the nucleus [234]. Since cell cycle regulatory proteins that are activated by ERK1/2 are localized in the nucleus, access of the ERKs to their substrates is important for their regulation. We clearly demonstrated the activation of nuclear substrates by phosphorylated ERK, like RSK, MSK and the transcription factors CREB, STAT1 and STAT3. ERK activates the RSKs which catalyze the phosphorylation of the transcription factor CREB at serine 133 to promote cell survival [235]. There is strong support of CREB being a survival factor in the kidney. Contrary to Grossman *et al.* [236] we found an aldosterone-mediated

activation of CREB in LLC-PK1 cells. The activation was significant after 30 min aldosterone treatment.

Furthermore, the activation of two STAT proteins, STAT1 and STAT3, was observed by aldosterone-induced ERK phosphorylation in LLC-PK1 cells. STAT1 and STAT3 contain a consensus sequence at Serine^{727}, which can be targeted by ERK. In response to angiotensin II STAT1 and STAT2 are rapidly tyrosine-phosphorylated in rat aortic smooth muscle cells [237], but no studies concerning aldosterone and the activation of STAT proteins exist. The STAT pathway is as well as the NF-κB pathway a so-called 'oncopathway'. Although both transcription factors do not match the classical oncogen definition, they are powerful activators of the malignant transformation and control expression of target genes important for cell proliferation and survival [238]. NF-κB and STAT3 are responsible for the expression of antiapoptotic genes and for the survival of premalignant cells harboring mutations which makes these cells resistant against genotoxic insults [239]. The role of STAT1 in tumorigenesis is complex and controversal. On the one hand, upregulation of STAT1 has been found in many tumors [240], and on the other hand STAT1 deficiency has also been found in cancer [241]. Nevertheless, it was shown that STAT1 has potential proapoptotic and significant prosurvival effects by activating the expression of either proapoptotic or prosurvival proteins. Most often these transcription factors are constitutively upregulated due to upregulation of upstream signaling pathways, e.g. ERK pathway.

Furthermore, the activation of the ERK pathway and the subsequent activation of transcription factors were dependent on cellular oxidants, since the antioxidant tempol significantly reduced their phosphorylation. The involvement of oxidants in the activation of ERK has been reported before.

The Ras/Raf/MEK/ERK pathway can frequently be silenced by MEK inhibitors [242], which is an important approach in the treatment of cancer. To clearly demonstrate that ERK is responsible for the activation of the prosurvival transcription factors CREB, STAT1 and STAT3, the effects of MEK inhibitor U0126 were investigated. U0126 inhibited the aldosterone-induced ERK activation and the subsequent phosphorylation of CREB, STAT1 and STAT3.

As mentioned above for NF-κB in 4.3.2, an aberrant or long-term activation of CREB and STAT proteins via ERK (especially STAT3) by persistently high aldosterone levels could unfold the prosurvival activity of these transcription factors in

aldosterone-exposed cells and therefore contribute to the survival of cells with damaged DNA, probably initiating carcinogenesis.

5.4 Mechanisms of aldoterone-induced cellular damages in vitro

Understanding the underlying mechanisms of oxidant production, DNA damage and the activation of transcription factors and signaling pathways is essential in the development of strategies that could prevent the adverse effects of chronic aldosteronism, particularly the possibly associated increase in kidney cancer risk.

We observed that aldosterone caused an increase in ROS in LLC-PK1 and MDCK cells. Aldosterone-induced increase in $O_2^{\cdot-}$ occured as a consequence of a calcium-mediated activation of NAD(P)H oxidase. An increase of calcium by aldosterone was reported in different cell types and is involved in rapid aldosterone signaling [243-245]. The release of calcium from intracellular stores is often signaled by IP_3, and secondary by a process of calcium-induced calcium release [246]. The influx of calcium across the plasma membrane can be activated by multiple mechanisms. In most cell types, the activation of capacitative calcium entry is signaled by the depletion of intracellular calcium stores, occuring through store-operated calcium channels [91]. We used different inhibitors and conditions to evaluate the source of aldosterone-induced calcium increase. The marked decrease in aldosterone-induced calcium increase observed in cells incubated in calcium free medium indicates that aldosterone induces calcium influx. Significantly, the calcium channel blocker dihydropyridine, protects the kidney from aldosterone-induced NAD(P)H oxidase activation and injury in rats [247]. In spontaneously hypertensive rats, benidipine an inhibitor of L-type (long lasting) and T-type (transient) calcium channels protected the kidney from damage through the inhibition of NAD(P)H oxidase [248]. On the other hand, the inhibitory effect of thapsigargin points that calcium is also mobilized from thapsigargin-sensitive stores. An intracellular source of the increased cytosolic calcium in LLC-PK1 and MDCK cells exposed to aldosterone is also supported by the inhibitory action of the cell-permeable intracellular calcium chelator bapta and 2-APB, which is a blocker of inositol triphosphate (IP_3) receptors [249] and of store-operated calcium channels [250]. Generally, studies found that over the range 1-100 µM, 2-APB inhibited calcium signals due to the release of intracellular stores and subsequent calcium entry [251]. Since we used 5 µM 2-APB, calcium seems to be

released from intracellular stores. Therefore, aldosterone signaling seems to involve a combination of release of calcium from intracellular stores and influx of calcium across the plasma membrane.

As already mentioned, in renal cells it was shown that aldosterone causes the generation of $O_2^{\cdot-}$ via activation of NAD(P)H oxidase [48-49]. Furthermore, previous evidence has shown that treatment of rats with aldosterone caused oxidative stress in the kidney and the activation of NAD(P)H oxidase [247]. Therefore, the activity of this enzyme seems to be under hormonal control, since angiotensin II can also increase the expression of a catalytic subunit of NAD(P)H oxidase, gp91^{phox}, and thereby increase $O_2^{\cdot-}$ production [252]. NAD(P)H oxidase is believed to be the primary source of abnormal cellular signaling, although in terms of quantity the mitochondrial respiratory chain system may generate the most $O_2^{\cdot-}$ [50, 253]. Once activated, the enzyme complex NAD(P)H oxidase catalyzes the transfer of electrons from NADPH to molecular oxygen via their catalytic subunit to generate not only $O_2^{\cdot-}$, but also H_2O_2 as shown in some studies. We found the activation of NAD(P)H oxidase in LLC-PK1 and MDCK cells, measuring the translocation of the subunit p47phox from the cytosol to the membrane. It is currently known that at least five different isoforms of the NAD(P)H oxidase subunit Nox (1-5) and two homologous oxidases (Duox1, Duox2) exist in eukaryotic cells [254]. From them, the one present in macrophages (Nox2) is the most extensively characterized. In a cell line model of renal proximal tubule cells (human hRPT) the presence of Nox2 and Nox4 has recently been described [255]. NAD(P)H oxidase can be activated by calcium either directly or via PKC. Nox5 is the only isoform that can be directly activated by calcium. The other isoforms can be activated in an indirect form, and PKC has been shown to activate NOX in different cell types [256-257]. The finding that Ro320432 inhibited the increase in ROS caused by aldosterone indicates that the isoforms activated and present in LLC-PK1 and MDCK cells are regulated by calcium via PKC.

Aldosterone also induced an increase in RNS in LLC-PK1 and MDCK cells as evidenced using the NO-specific probe DAF-FM. This increase occurs as a consequence of the activation of NOS, the enzyme that generates NO from L-arginine in the presence of NADPH and oxygen. eNOS is dependent on cytosolic calcium and calmodulin as cofactor whereas iNOS is activated independent of calcium. NOS is considered to have protective effects on the kidney. Mice genetically deficient in eNOS are characterized by kidney damage which includes

glomerular hypoplasia, and death of tubular cells [258]. Although NOS activation and NO production are important in vasorelaxation which also involves the kidney vasculature, excess NO can lead to damage of cellular components. In this regard, iNOS activation is involved in the proximal tubular damage in sepsis, and iNOS inhibitors are being studied as a protective therapy for this injury [259]. Furthermore, NO can react with $O_2^{\cdot-}$ to the highly reactive species $ONOO^-$ which thereby restricts the half-life, diffusion distance and bioactivity of NO in tissues. The reaction rate between NO and $O_2^{\cdot-}$ is three times faster than the scavenging of $O_2^{\cdot-}$ by SOD, which catalyzes the conversion of $O_2^{\cdot-}$ to H_2O_2 and O_2 [260]. The pathophysiological role of increased $O_2^{\cdot-}$ reducing NO bioavailability has been extensively demonstrated in several disorders like hypertension. The removal of the buffering influence of NO on vasoconstrictor systems plays a key role in the development of hypertension [261]. Laursen *et al.* [262] showed that angiotensin II-induced ROS production resulted in an increased interaction of $O_2^{\cdot-}$ and NO and thus as a consequence in the interaction with $ONOO^-$ and the eNOS cofactor 5,6,7,8-tetrahydrobiopterin (BH_4). In the absence of either L-arginine or BH4, eNOS produces $O_2^{\cdot-}$ and H_2O_2 instead of NO. Therefore, this observation strongly supports the possibility that oxidation of BH_4 by ROS may be a pathologic cause of eNOS "uncoupling" [263]. In addition, increased concentrations of NO have been implicated in cancer development and progression as an endogenous mutagen, an angiogenesis factor, and/or an inhibitor of apoptosis [264].

The expression of the MR in LLC-PK1 and MDCK cells was verified by RT-PCR, but the protein of the receptor could not be detected in the pig and dog cells, since there are no appropriate antibodies for these species commercially available. Nevertheless, ROS and RNS increase, NAD(P)H oxidase and NOS activation by aldosterone are mediated by the MR. This was proven by their preventability with the highly specific MR blocker eplerenone [265-266], and the lack of effect of the GR inhibitor mifepristone. Eplerenone is a newly developed MR inhibitor that has significantly fewer adverse effects than similar doses of spironolactone. Eplerenone increases NO bioavailability and decreases oxidative stress [267]. It is important to consider the possibility of a crossreaction between aldosterone and GR, since aldosterone, especially in higher concentrations starting around 100 nM, can also activate the GR [268]. However, aldosterone binds to the MR with a much higher affinity than it does to the GR [269]. Only the calcium increase in MDCK cells was not

inhibitable by eplerenone, as observed before by Grossmann *et al.* [27]. Until now it is not known what kind of receptor mediates the nongenomic, MR-independent actions. This was the only difference of LLC-PK1 and MDCK cells in aldosterone signaling found in the course of this work.

The activation of the MR, calcium, NAD(P)H oxidase and NOS and the associated production of ROS/RNS caused by aldosterone had functional consequences in LLC-PK1 and MDCK cells. Through the above mentioned mechanisms, aldosterone induces not just oxidative stress, but also DNA damage and the activation of transcription factors and signaling pathways.

5.4.1 Mechanisms of DNA damage

Although oxidative DNA damage is implicated in the genesis of many degenerative diseases, in the ageing process and also in cancer [270-272], the exact mechanisms leading to these pathological conditions are not well known. Eplerenone was used to prove the involvement of the MR in aldosterone-induced DNA damage. Mifepristone did not have an effect suggesting an exclusion of the GR in aldosterone-mediated DNA damage. Furthermore, we used two more MR inhibitors to confirm the involvement of the MR in aldosterone signaling in LLC-PK1 cells: spironolactone and BR-4628. The structural DNA damage, but not the increased micronucleus frequency induced by aldosterone could be completely prevented by spironolactone, which is not very selective for the MR [273]. The novel, selective and nonsteroidal MR antagonist (R)-BR-4628, however, could completely ameliorate all aldosterone-induced damages at the higher concentration. The less active enantiomer of this antagonist had only minimal effects. These results prove that the induction of DNA damage is mediated by the MR. There are reports existing that aldosterone also stimulates the AT1R, resulting in oxidative stress [274]. We have already shown this effect of AT1R, when activated by angiotensin II [200]. If aldosterone is indeed able to stimulate AT1R, this could add to the damage.

We have first hints that PLC is activated in LLC-PK1 cells, since the PLC inhibitor U73122 reduced the aldosterone-induced DNA damage in LLC-PK1 cells in the comet assay. In the following, we observed that aldosterone-induced DNA damage is dependent on an increase of intracellular calcium, which can be activated by PLC. It was previously described that increased cytosolic calcium itself could be

responsible for the formation of DNA strand breaks [275]. Disruption of the calcium homeostasis is strongly correlated with micronucleus formation and the induction of mitotic disturbances [276-277]. These findings are in agreement with our results, since diverse calcium inhibitors and calcium free medium significantly reduced aldosterone-induced DNA damage in the comet assay and in the micronucleus test. In the case of aldosterone-induced DNA damage the most important consequence of calcium increase is NAD(P)H oxidase activation and the increase in $O_2^{\cdot-}$ [201, 278] which most probably causes DNA damage. The involvement of NAD(P)H oxidase in aldosterone-induced DNA damage was confirmed by using three NAD(P)H oxidase inhibitors, namely apocynin, DPI and VAS2870. DPI is an unspecific inhibitor of all flavoenzymes, which – apart from NAD(P)H oxidases – include xanthine oxidase and cytochrome P450 enzymes [279]. Apocynin, extracted from Picrorhiza kurroa, prevents the formation of the active oxidase complex [280] and is known to be a potent NAD(P)H oxidase inhibitor, but also influences other events such as the induction of AP-1 transcription factor [281]. The novel NAD(P)H oxidase inhibitor VAS2870 has been shown to be effective and specific in suppressing the activation of NAD(P)H oxidase and subsequent production of intracellular ROS in vascular smooth muscle cells (VSMC) [174]. The inhibition of comet and micronuclei formation by Ro320432 indicates that NAD(P)H oxidase activation occurs, at least in part, through the activation of PKC by aldosterone-induced cellular calcium increase.

The inhibition of NOS by the NOS inhibitors L-NAME and W7 prevented the induction of NO/RNS. L-NAME is an analog of arginine that inhibits NO production and W7 is a calmodulin antagonist, which inhibits calcium-calmodulin dependent enzymes. Interestingly, DNA damage observed in the comet assay and micronucleus test was just slightly reduced by L-NAME and W7, but FPG-sensitive sites (8-oxodG lesions) as detected by FPG comet assay were significantly reduced by these inhibitors. NO has been shown to directly react with DNA, not only causing base deamination and nitration, but also oxidation. Huang *et al.* [282] observed that NO causes nitrosative and oxidative stress, leading to the accumulation of 8-nitroguanine (8-NitroG) and 8-oxodG. Furthermore, NO has also been shown to inhibit the human enzyme repairing 8-oxodG, 8-oxodG DNA glycosylase 1 (hOGG1). This enzyme contains critical thiol moieties and thus is potentially susceptible to inactivation by nitrosylation reactions of NO. Therefore, the inhibition

of DNA repair processes and potentiation of oxidative DNA damage by NO would be expected to increase the rate of mutagenic DNA lesions [283]. In agreement with our findings, these observation suggests an integral role of NO in promoting oxidative DNA damage.

5.4.2 Mechanisms of Nrf2 signaling

In agreement with the DNA damage data, we observed the involvement of the MR in aldosterone-induced Nrf2 activation. Furthermore, we used the calcium inhibitor bapta to investigate the role of intracellular calcium in the aldosterone-mediated activation of Nrf2. Indeed, we observed a clear reduction of the Nrf2-DNA binding in LLC-PK1 cells. The importance of calcium signaling in the activation process of Nrf2 was observed before by Burdette *et al.* in in human hepatoma cells infected with hepatitis C virus [284]. We also investigated the role of NAD(P)H oxidase in the ROS-mediated activation of Nrf2. In our study VAS2870 was the most potent NAD(P)H oxidase inhibitor leading to a complete inhibition of Nrf2-DNA binding. However, NAD(P)H oxidase could act as a double-edged sword, with transient activation providing a feedback antioxidant response to ROS via Nrf2. Prolonged NAD(P)H oxidase activation may lead to depletion of intracellular NADPH and impaired ROS scavenging associated with eNOS uncoupling, mitochondrial dysfunction and diminished Nrf2-mediated antioxidant gene expression [285].

NAD(P)H oxidase can be activated by calcium either directly or via PKC. Aldosterone-induced Nrf2 activation was significantly reduced by the PKC inhibitor Ro320432, suggesting that NAD(P)H oxidase is activated via a PKC-dependent pathway. Huang *et al.* demonstrated that PKC can directly phosphorylate Nrf2 and thereby induces ARE-mediated gene expression [286].

We have shown that aldosterone treatment led to the production of NO/RNS via NOS activation in LLC-PK1 cells. Therefore, we investigated the possible involvement of NOS in the aldosterone-mediated activation of Nrf2. The two NOS inhibitors L-NAME and W7 clearly inhibited the aldosterone-mediated Nrf2 activation in LLC-PK1 cells. NOS is known to activate a battery of detoxifying enzymes and other proteins with protective functions [287]. Although NOS has generally protective effects on the kidney, excess NO is considered to damage cellular components by reacting with $O_2^{\cdot-}$ to the highly reactive $ONOO^-$ [87]. In this regard,

by inhibiting NO production with L-NAME or NOS activity with W7, ROS/RNS production is diminished and therefore the activation of Nrf2 becomes unnecessary.

5.4.3 Mechanisms of NF-κB and ERK/CREB/STAT signaling

As seen for DNA damage and Nrf2 activation, aldosterone-induced activation of NF-κB and ERK is mediated via the MR. PLC is activated via both a G protein-dependent or -independent process, leading to the production of DAG and IP$_3$. The rise in these intracellular messengers causes the activation of PKC and mobilization of intracellular calcium [288]. This is followed by the activation of NF-κB and ERK. The involvement of increased intracellular calcium levels and the activation of NF-κB and ERK have been reported earlier [289-290]. This was in agreement with our finding that the calcium chelator bapta reduced the aldosterone-induced NF-κB and ERK activation. Furthermore, NAD(P)H oxidase inhibitors reduced the aldosterone-mediated activation of NF-κB and ERK, suggesting the involvement of this enzyme complex in their activation in LLC-PK1 and MDCK cells. Since NAD(P)H oxidase produces $O_2^{\cdot-}$, NF-κB, which is redox-sensitive, is activated dependent on this enzyme. This was reported earlier by Ha *et al.* [291]. NAD(P)H oxidase has been implicated in renal cell injury by producing ROS and subsequently activating ERK in LLC-PK1 cells before. Matsunaga *et al.* [292] showed that the NAD(P)H oxidase inhibitor DPI inhibited zinc-related increase of ROS, ERK activation and renal cell injury. There exist several mechanisms of NAD(P)H oxidase-dependent ERK activation. For example the inhibition of intracellular tyrosine phosphatases may not be the only mechanism by which NAD(P)H oxidase promotes ERK activation. There is also evidence that the expression and activation of the small Rac protein upstream of ERK is affected by NAD(P)H oxidase-derived ROS [293]. Furthermore, the activation of NF-κB and ERK was dependent on NOS in LLC-PK1 and MDCK cells. As mentioned above, NOS produces NO, and NO was shown to induce the activation of NF-κB in several studies, also in one kidney cell line [294]. Similar effects were observed for ERK activation by Meini *et al.* [295] who showed that pretreatment with L-NAME antagonized ERK activation, leading to reduced proliferation in human astrocytoma U-373MG cells.

The same mechanisms were observed for the ERK-dependent activation of the transcription factors CREB, STAT1 and STAT3. The DNA-binding of all three

transcription factors was dependent on the MR, intracellular calcium, NAD(P)H oxidase and NOS. Furthermore, the DNA-binding of the transcription factors could be reduced by tempol, suggesting a role of oxidants in their activation. The involvement of intracellular calcium and NAD(P)H oxidase in the activation of CREB has been reported earlier e.g. in rat skeletal muscle cells [296]. For the STAT proteins a NAD(P)H oxidase-dependent activation by angiotensin II has been described by Schieffer *et al.* in rat aortic smooth muscle cells [297]. In this report the NAD(P)H oxidase inhibitor DPI significantly suppressed STAT1 and STAT3 activity. In our study, we used the NAD(P)H oxidase inhibitor VAS2870, which had the same effect in LLC-PK1 cells.

Aldosterone induces oxidative stress and DNA damage via the mineralocorticoid receptor *in vitro* and *in vivo*. The pathway leading to DNA damage includes a calcium signal, PKC activation and subsequent NAD(P)H oxidase and NOS activation. As a reaction to oxidative stress the transcription factors Nrf2 and NF-κB are induced. Nrf2 transiently leads to the increased expression of antioxidative enzymes, which nevertheless cannot overcome the aldosterone-induced oxidative stress. NF-κB persistently leads to the expression of several prosurvival proteins, preventing the cells to undergo apoptosis. Additional prosurvival factors like ERK, CREB and STAT proteins are activated by aldosterone, which could possibly lead to the survival of cells with DNA damage, increasing the risk of the genesis of mutated cells.

6 SUMMARY

Several epidemiological studies found that hypertensive patients have an increased risk to develop kidney cancer. Different mechanisms have been described for the correlation between hypertension and cancer, like increased cytosolic calcium levels or mitogenic effects of blood pressure controling hormones such as angiotensin II and aldosterone. Hyperaldosteronism frequently results in arterial hypertension and contributes to the development and progression of kidney injury, with reactive oxygen species (ROS) playing an important role. ROS are increasingly thought to be associated with many pathological conditions such as cancer and other disorders, like cardiovascular complications, which often come along with hypertension. The aim of the present work was to investigate whether the effects of elevated aldosterone concentrations might be involved in the increased cancer incidence in hypertensive individuals.

First, the potential capacity of aldosterone to induce oxidative stress and DNA damage was investigated *in vitro* and *in vivo*. In LLC-PK1 porcine kidney cells and MDCK canine kidney cells the significant formation of ROS, and especially of superoxide ($O_2^{\cdot-}$) was assessed. With two genotoxicity tests, the comet assay, detecting structural DNA damage, and the micronucleus frequency test, detecting a subgroup of inheritable chromosomal aberrations, the DNA damaging potential of aldosterone was quantified. In both genotoxicity tests a dose-dependent increase in aldosterone-induced structural DNA damage was observed. DNA strand breaks were already detected after 5 min aldosterone treatment, whereas the formation of micronuclei rose significantly after 30 min in both cell lines. This fast time course was also observed for oxidative stress, indicating nongenomic actions of aldosterone. Oxidative stress and DNA damage were prevented by antioxidants, suggesting ROS as a major cause of DNA damage. Furthermore, the oxidatively modified DNA lesion 8-oxo-7,8-dihydro-2´-deoxyguanosine (8-oxodG), was found to be significantly elevated.

In kidneys of rats with desoxycorticosterone acetate (DOCA)/salt-induced hypertension, which is a model of severe mineralocorticoid-dependent hypertension, elevated levels of ROS and $O_2^{\cdot-}$ were found, compared to kidneys of sham rats. Also DNA strand breaks, measured with the comet assay and double strand breaks, visualized with antibodies against the double strand break-marker γ-H2AX were

significantly elevated in kidneys of DOCA/salt-treated rats. In addition, significantly increased amounts of 8-oxodG were detected. Proliferation of kidney cells was found to be increased, which theoretically enables the DNA damage to manifest itself as mutations, since the cells divide. The mineralocorticoid receptor (MR) was involved in the DOCA/salt-induced oxidative stress and DNA damage, because the MR antagonists spironolactone and BR-4628 significantly reduced the negative effects.

Second, the effects of aldosterone on the activation of transcription factors and signaling pathways were investigated. A significant activation of the potentially protective transcription factor Nrf2 was observed in LLC-PK1 cells by electrophoretic mobility shift assay (EMSA). This activation was triggered by an increase of ROS or reactive nitrogen species (RNS). In response to oxidative stress, glutathione synthesis and detoxifying enzymes, such as the subunits of the glutathione-cysteine-ligase or heme oxygenase 1 were rapidly induced after 4 h. Nevertheless, after 24 h a decrease of glutathione levels was observed. Since ROS levels were still high after 24 h, but Nrf2 activation decreased, this adaptive survival response seems to be transient and quickly saturated and overwhelmed by ROS/RNS. Furthermore, Nrf2 activation was not sufficient to protect cells against oxidative DNA damage, because the amounts of double strand breaks and 8-oxodG lesions steadily rose up to 48 h of aldosterone treatment.

The second transcription factor that was time- and dose-dependently activated by aldosterone in LLC-PK1 and MDCK cells was NF-κB. Furthermore, a significant cytosolic and nuclear activation of ERK and the up- and downstream kinases of this pathway were detected in LLC-PK1 cells. Aldosterone induced the phosphorylation of the transcription factors CREB, STAT1 and STAT3 through ERK. By inhibition of the upstream kinase MEK it was clearly proven that the aldosterone-induced activation of ERK is responsible for the activation of these transcription factors. The activation of both NF-κB and ERK was redox-sensitive, because antioxidants prevented their activation by aldosterone.

Third, the underlying mechanisms of oxidant production, DNA damage and activation of transcription factors and signaling pathways were studied. Aldosterone exclusively acted via the MR, which was proven by the MR antagonists eplerenone, spironolactone and BR-4628, whereas the glucocorticoid receptor (GR) antagonist mifepristone did not show any effect. Furthermore, aldosterone needed cytosolic

calcium to exert its negative effects. Calcium from intracellular stores and the influx of calcium across the plasma membrane was involved in aldosterone signaling. The calcium signal activated on the one hand, the prooxidant enzyme complex NAD(P)H oxidase through PKC, which subsequently caused the generation of $O_2^{\cdot-}$. On the other hand, nitric oxide synthase (NOS) was activated, which in turn produced NO. NO and $O_2^{\cdot-}$ can react to the highly reactive species $ONOO^-$ that can damage the DNA more severely than the less reactive $O_2^{\cdot-}$.

In the short term, the activation of transcription factors and signaling pathways could be a protective response against aldosterone-induced oxidative stress and DNA damage. However, a long-term NF-κB and ERK/CREB/STAT activation by persistently high aldosterone levels could unfold the prosurvival activity of NF-κB and ERK/CREB/STAT in aldosterone-exposed cells. DNA damage caused by increased ROS might become persistent and could be inherited to daughter cells, probably initiating carcinogenesis. If these events also occur in patients with hyperaldosteronism, these results suggest that aldosterone could be involved in the increased cancer incidence of hypertensive individuals.

7 ZUSAMMENFASSUNG

Mehrere epidemiologische Studien haben ein erhöhtes Nierenkrebsrisko bei Patienten mit Bluthochdruck aufgedeckt. Es wurden verschiedene Mechanismen für die Korrelation von Krebs und Bluthochdruck beschrieben, wie zum Beispiel erhöhte cytosolische Calciumspiegel oder mitogene Effekte von blutdruckregulierenden Hormonen wie Angiotensin II und Aldosteron. Hyperaldosteronismus führt oft zu arteriellem Bluthochdruck und trägt zur Entwicklung und zum Fortschreiten von Nierenschäden bei, wobei reaktive Sauerstoffspezies (ROS) eine wichtige Rolle spielen. Immer häufiger werden ROS mit Krankheitsbildern wie Krebs und kardiovaskulären Erkrankungen, die mit Bluthochdruck einhergehen, in Verbindung gebracht. Das Ziel dieser Arbeit war es, zu untersuchen, ob erhöhte Aldosteronkonzentrationen an dem gesteigerten Krebsrisiko von hypertensiven Patienten beteiligt sein könnten.

Zunächst wurde die potentielle Kapazität von Aldosteron, oxidativen Stress und DNA-Schaden *in vitro* und *in vivo* induzieren zu können, untersucht. In der Schweine-Nierenzelllinie LLC-PK1 und der Hunde-Nierenzelllinie MDCK wurde die Entstehung von ROS und speziell die Bildung von Superoxid ($O_2^{\cdot-}$) nachgewiesen. Das gentoxische Potential von Aldosteron wurde mit zwei Genotoxizitätstests, dem Comet Assay und dem Mikrokernfrequenztest bestimmt. Der Comet Assay erfasst strukturelle DNA-Schäden und Mikrokerne sind eine irreparable, vererbbare Form chromosomaler Aberrationen. In beiden Genotoxizitätstests konnte ein dosis-abhängiger Anstieg des strukturellen DNA-Schadens beobachtet werden. DNA-Strangbrüche wurden bereits nach 5 min Aldosteronbehandlung gefunden, wohingegen die Bildung von Mikrokernen erst nach 30 min in beiden Zelllinien signifikant wurde. Der schnelle Zeitverlauf wurde auch bei der Bildung von ROS beobachtet, was auf nicht-genomische Effekte von Aldosteron hinweist. Antioxidantien konnten den oxidativen Stress und die DNA-Schäden verringern, was annehmen lässt, dass ROS die Hauptursache für die Entstehung der DNA-Schäden sind. Darüberhinaus wurden signifikant erhöhte Mengen der oxidativ modifizierten DNA Läsion 8-Oxo-7,8-dihydro-2´-deoxyguanosin (8-oxodG) gefunden.

In Nieren von Ratten mit Desoxycorticosteron-Acetat (DOCA) und Salz-induziertem Bluthochdruck, ein Modell für massiven Mineralocorticoid-induzierten Bluthochdruck, wurde ebenfalls eine erhöhte Bildung von ROS und $O_2^{\cdot-}$ in Nieren von DOCA/Salz-

Ratten im Vergleich zu Sham-Ratten beobachtet. Auch im Comet Assay erfasste DNA-Strangbrüche und Doppelstrangbrüche, die mit Hilfe von Antikörpern gegen den Doppelstrangbruchmarker γ-H2AX sichtbar gemacht wurden, waren in den Nieren der DOCA/Salz-behandelten Ratten signifikant erhöht. Weiterhin wurden erhöhte 8-oxodG-Spiegel in DOCA/Salz-Ratten beobachtet. Auch eine erhöhte Proliferationsrate in DOCA/Salz-behandelten Ratten konnte festgestellt werden, was theoretisch dazu führen könnte, dass sich die DNA-Schäden als Mutationen manifestieren, da sich die Zellen teilen. Signifikante Reduktion der schädigenden Effekte durch Mineralocorticoid-Rezeptor (MR)-Antagonisten beweist die Beteiligung des MR an dem durch DOCA/Salz-induzierten oxidativen Stress und DNA-Schaden.

Im zweiten Teil der Arbeit wurde der Einfluss von Aldosteron auf die Aktivierung von Transkriptionsfaktoren und Signalwegen untersucht. Zunächst konnte die Aktivierung des potentiell schützenden Transkriptionsfaktors Nrf2 in LLC-PK1 Zellen mittels electrophoretic mobility shift assay (EMSA) beobachtet werden. Diese Aktivierung wurde durch den Anstieg an ROS und reaktiven Stickstoffspezies (RNS) ausgelöst. Als Antwort auf den oxidativen Stress, wurde die Glutathion-Synthese und detoxifizierende Enzyme, wie die Untereinheiten der Glutathion-Cystein-Ligase oder Hämoxygenase 1, nach 4 Stunden rasch hochreguliert. Nichtsdestotrotz konnte nach 24 Stunden eine Abnahme des Glutathionspiegels festgestellt werden. Da die Konzentration an ROS nach 24 Stunden immer noch signifikant erhöht war, die Aktivierung von Nrf2 allerdings stark zurückgegangen ist, scheint diese adaptive Überlebensstrategie nur kurzfristig, und somit schnell durch ROS/RNS gesättigt zu sein. Weiterhin war die Aktivierung von Nrf2 nicht ausreichend, um die Zellen vor dem durch Aldosteron-induzierten DNA-Schaden zu schützen, da Doppelstrangbrüche, sowie 8-oxodG-Läsionen bei bis zu 48-stündiger Inkubation mit Aldosteron stetig anstiegen.

Der zweite Transkriptionsfaktor, der zeit- und dosisabhängig durch Aldosteron aktiviert wurde, war NF-κB. Ausserdem wurde die cytosolische und nukleäre Aktivierung von ERK und die Aktivierung von vor- und nachgeschalteten Kinasen des ERK-Signalweges in LLC-PK1 Zellen nachgewiesen. Aldosteron induzierte weiterhin die Phosphorylierung der Transkriptionsfaktoren CREB, STAT1 und STAT3 durch ERK. Durch die Inhibierung der MEK-Kinase, wurde bewiesen, dass tatsächlich die durch Aldosteron-induzierte ERK-Aktivierung für die anschließende Phosphorylierung

der Transkriptionsfaktoren verantwortlich ist. Die Aktivierung von NF-κB und ERK war redox-sensitiv, da Antioxidantien deren Aktivierung durch Aldosteron verhindern konnten.

Im dritten Teil dieser Arbeit wurden die zugrundeliegenden Mechanismen der Entstehung von ROS/RNS, des DNA-Schadens und der Aktivierung von Transkriptionsfaktoren untersucht. Aldosteron wirkte ausschließlich über den MR, bewiesen durch Einsatz der MR-Antagonisten Eplerenon, Spironolakton und BR-4628. Der Glucocorticoid-Rezeptor-Antagonist Mifepriston zeigte dagegen keinen Effekt. Weiterhin benötigte Aldosteron cytosolisches Calcium, um seine negativen Effekte auszuüben. Es waren intrazelluäres Calcium, sowie ein Calciuminflux über die Plasmamembran am Aldosteronsignal beteiligt. Einerseits wurde der prooxidative Enzymkomplex NAD(P)H-Oxidase von Calcium durch die Proteinkinase C (PKC) aktiviert, was wiederum zur Bildung von $O_2^{\cdot-}$ führte. Andererseits kam es durch erhöhtes cytosolisches Calcium zur Aktivierung der NO-Synthase (NOS), welche daraufhin Stickoxid (NO) produzierte. NO und $O_2^{\cdot-}$ können zu dem hochreaktiven Peroxynitrit ($ONOO^-$) reagieren, welches die DNA mehr schädigen kann als das etwas weniger reaktive $O_2^{\cdot-}$.

Kurzfristig könnte die Aktivierung der Transkriptionsfaktoren und Signalwege eine schützende Wirkung gegen den durch Aldosteron-induzierten oxidativen Stress und DNA-Schaden in den Zellen haben. Allerdings kann eine länger anhaltende Aktivierung von NF-κB und ERK/CREB/STAT durch permanent hohe Aldosteronspiegel zur Induktion einer Überlebensstrategie durch NF-κB und ERK/CREB/STAT in Aldosteron-exponierten Zellen führen. Der DNA-Schaden, der durch erhöhte ROS-Spiegel entsteht, könnte persistent und somit an Tochterzellen weitervererbt werden, was eventuell zur Entstehung von Krebs beitragen könnte. Falls diese Effekte auch in Patienten mit Hyperaldosteronismus gefunden werden können, dann könnte Aldosteron an der erhöhten Krebsinzidenz bei Bluthochdruck beteiligt sein.

8 REFERENCES

1.   Friis, S., et al., *Angiotensin-converting enzyme inhibitors and the risk of cancer: a population-based cohort study in Denmark.* Cancer, 2001. **92**(9): p. 2462-70.
2.   Moore, L.E., R.T. Wilson, and S.L. Campleman, *Lifestyle factors, exposures, genetic susceptibility, and renal cell cancer risk: a review.* Cancer Invest, 2005. **23**(3): p. 240-55.
3.   Grossman, E., et al., *Is there an association between hypertension and cancer mortality?* Am J Med, 2002. **112**(6): p. 479-86.
4.   Corrao, G., et al., *Hypertension, antihypertensive therapy and renal-cell cancer: a meta-analysis.* Curr Drug Saf, 2007. **2**(2): p. 125-33.
5.   Meyer, P., *Increased intracellular calcium: from hypertension to cancer.* J Hypertens Suppl, 1987. **5**(4): p. S3-4.
6.   Hamet, P., *Cancer and hypertension. An unresolved issue.* Hypertension, 1996. **28**(3): p. 321-4.
7.   Gago-Dominguez, M., et al., *Lipid peroxidation: a novel and unifying concept of the etiology of renal cell carcinoma (United States).* Cancer Causes Control, 2002. **13**(3): p. 287-93.
8.   Ross, R., *The pathogenesis of atherosclerosis: a perspective for the 1990s.* Nature, 1993. **362**(6423): p. 801-9.
9.   Hughes, A.D., et al., *Platelet-derived growth factor (PDGF): actions and mechanisms in vascular smooth muscle.* Gen Pharmacol, 1996. **27**(7): p. 1079-89.
10.   Abedi, H. and I. Zachary, *Signalling mechanisms in the regulation of vascular cell migration.* Cardiovasc Res, 1995. **30**(4): p. 544-56.
11.   Fryzek, J.P., et al., *A cohort study of antihypertensive treatments and risk of renal cell cancer.* Br J Cancer, 2005. **92**(7): p. 1302-6.
12.   Colli, J.L., J.E. Busby, and C.L. Amling, *Renal cell carcinoma rates compared with health status and behavior in the United States.* Urology, 2009. **73**(2): p. 431-6.
13.   Coleman, C.I., et al., *Antihypertensive medication and their impact on cancer incidence: a mixed treatment comparison meta-analysis of randomized controlled trials.* J Hypertens, 2008. **26**(4): p. 622-9.
14.   Flaherty, K.T., et al., *A prospective study of body mass index, hypertension, and smoking and the risk of renal cell carcinoma (United States).* Cancer Causes Control, 2005. **16**(9): p. 1099-106.
15.   Shapiro, J.A., et al., *Hypertension, antihypertensive medication use, and risk of renal cell carcinoma.* Am J Epidemiol, 1999. **149**(6): p. 521-30.
16.   Lee, M.R., *Renin-secreting kidney tumours. A rare but remediable cause of serious hypertension.* Lancet, 1971. **2**(7718): p. 254-5.
17.   Fraser, G.E., R.L. Phillips, and W.L. Beeson, *Hypertension, antihypertensive medication and risk of renal carcinoma in California Seventh-Day Adventists.* Int J Epidemiol, 1990. **19**(4): p. 832-8.
18.   McCredie, M. and J.H. Stewart, *Risk factors for kidney cancer in New South Wales, Australia. II. Urologic disease, hypertension, obesity, and hormonal factors.* Cancer Causes Control, 1992. **3**(4): p. 323-31.
19.   Rossi, G.P., et al., *A prospective study of the prevalence of primary aldosteronism in 1,125 hypertensive patients.* J Am Coll Cardiol, 2006. **48**(11): p. 2293-300.

20.   Weber, K.T., *Aldosterone in congestive heart failure.* N Engl J Med, 2001. **345**(23): p. 1689-97.

21.   Rossi, G.P., A.C. Pessina, and A.M. Heagerty, *Primary aldosteronism: an update on screening, diagnosis and treatment.* J Hypertens, 2008. **26**(4): p. 613-21.

22.   Young, W.F., *Primary aldosteronism: renaissance of a syndrome.* Clin Endocrinol (Oxf), 2007. **66**(5): p. 607-18.

23.   Young, W.F., et al., *Role for adrenal venous sampling in primary aldosteronism.* Surgery, 2004. **136**(6): p. 1227-35.

24.   Connell, J.M. and E. Davies, *The new biology of aldosterone.* J Endocrinol, 2005. **186**(1): p. 1-20.

25.   Marney, A.M. and N.J. Brown, *Aldosterone and end-organ damage.* Clin Sci (Lond), 2007. **113**(6): p. 267-78.

26.   Skott, O., et al., *Rapid actions of aldosterone in vascular health and disease--friend or foe?* Pharmacol Ther, 2006. **111**(2): p. 495-507.

27.   Grossmann, C., et al., *Human mineralocorticoid receptor expression renders cells responsive for nongenotropic aldosterone actions.* Mol Endocrinol, 2005. **19**(7): p. 1697-710.

28.   Boldyreff, B. and M. Wehling, *Rapid aldosterone actions: from the membrane to signaling cascades to gene transcription and physiological effects.* J Steroid Biochem Mol Biol, 2003. **85**(2-5): p. 375-81.

29.   Funder, J.W., *Minireview: aldosterone and the cardiovascular system: genomic and nongenomic effects.* Endocrinology, 2006. **147**(12): p. 5564-7.

30.   Harvey, B.J., et al., *Rapid responses to aldosterone in the kidney and colon.* J Steroid Biochem Mol Biol, 2008. **108**(3-5): p. 310-7.

31.   Gekle, M., et al., *Rapid activation of Na+/H+-exchange in MDCK cells by aldosterone involves MAP-kinase ERK1/2.* Pflugers Arch, 2001. **441**(6): p. 781-6.

32.   Liu, S.L., et al., *Aldosterone regulates vascular reactivity: short-term effects mediated by phosphatidylinositol 3-kinase-dependent nitric oxide synthase activation.* Circulation, 2003. **108**(19): p. 2400-6.

33.   Good, D.W., *Nongenomic actions of aldosterone on the renal tubule.* Hypertension, 2007. **49**(4): p. 728-39.

34.   Grossmann, C. and M. Gekle, *New aspects of rapid aldosterone signaling.* Mol Cell Endocrinol, 2009. **308**(1-2): p. 53-62.

35.   Fuller, P.J. and M.J. Young, *Mechanisms of mineralocorticoid action.* Hypertension, 2005. **46**(6): p. 1227-35.

36.   Krug, A.W. and M. Ehrhart-Bornstein, *Adrenocortical dysfunction in obesity and the metabolic syndrome.* Horm Metab Res, 2008. **40**(8): p. 515-7.

37.   Rossi, G.P., et al., *Primary aldosteronism: cardiovascular, renal and metabolic implications.* Trends Endocrinol Metab, 2008. **19**(3): p. 88-90.

38.   Pitt, B., et al., *The effect of spironolactone on morbidity and mortality in patients with severe heart failure. Randomized Aldactone Evaluation Study Investigators.* N Engl J Med, 1999. **341**(10): p. 709-17.

39.   Pitt, B., et al., *Eplerenone, a selective aldosterone blocker, in patients with left ventricular dysfunction after myocardial infarction.* N Engl J Med, 2003. **348**(14): p. 1309-21.

40.   Remuzzi, G., D. Cattaneo, and N. Perico, *The aggravating mechanisms of aldosterone on kidney fibrosis.* J Am Soc Nephrol, 2008. **19**(8): p. 1459-62.

41.   Funder, J.W., *Reconsidering the roles of the mineralocorticoid receptor.* Hypertension, 2009. **53**(2): p. 286-90.

42.   Nishiyama, A. and Y. Abe, *Molecular mechanisms and therapeutic strategies of chronic renal injury: renoprotective effects of aldosterone blockade.* J Pharmacol Sci, 2006. **100**(1): p. 9-16.

43.   Tylicki, L., et al., *Triple pharmacological blockade of the renin-angiotensin-aldosterone system in nondiabetic CKD: an open-label crossover randomized controlled trial.* Am J Kidney Dis, 2008. **52**(3): p. 486-93.

44.   Epstein, M., *Aldosterone blockade: an emerging strategy for abrogating progressive renal disease.* Am J Med, 2006. **119**(11): p. 912-9.

45.   Nishiyama, A., et al., *Drug discovery for overcoming chronic kidney disease (CKD): pharmacological effects of mineralocorticoid-receptor blockers.* J Pharmacol Sci, 2009. **109**(1): p. 1-6.

46.   Bianchi, S., R. Bigazzi, and V.M. Campese, *Antagonists of aldosterone and proteinuria in patients with CKD: an uncontrolled pilot study.* Am J Kidney Dis, 2005. **46**(1): p. 45-51.

47.   Quinkler, M., et al., *Increased expression of mineralocorticoid effector mechanisms in kidney biopsies of patients with heavy proteinuria.* Circulation, 2005. **112**(10): p. 1435-43.

48.   Iwashima, F., et al., *Aldosterone induces superoxide generation via Rac1 activation in endothelial cells.* Endocrinology, 2008. **149**(3): p. 1009-14.

49.   Yu, L., et al., *Aldosterone-induced increases in superoxide production counters nitric oxide inhibition of epithelial Na channel activity in A6 distal nephron cells.* Am J Physiol Renal Physiol, 2007. **293**(5): p. F1666-77.

50.   Nistala, R., A. Whaley-Connell, and J.R. Sowers, *Redox control of renal function and hypertension.* Antioxid Redox Signal, 2008. **10**(12): p. 2047-89.

51.   Paravicini, T.M. and R.M. Touyz, *NADPH oxidases, reactive oxygen species, and hypertension: clinical implications and therapeutic possibilities.* Diabetes Care, 2008. **31 Suppl 2**: p. S170-80.

52.   Pi, J., et al., *ROS signaling, oxidative stress and Nrf2 in pancreatic beta-cell function.* Toxicol Appl Pharmacol, 2010. **244**(1): p. 77-83.

53.   Pourova, J., et al., *Reactive oxygen and nitrogen species in normal physiological processes.* Acta Physiol (Oxf), 2010. **198**(1): p. 15-35.

54.   Ames, B.N., M.K. Shigenaga, and L.S. Gold, *DNA lesions, inducible DNA repair, and cell division: three key factors in mutagenesis and carcinogenesis.* Environ Health Perspect, 1993. **101 Suppl 5**: p. 35-44.

55.   Klaunig, J.E. and L.M. Kamendulis, *The role of oxidative stress in carcinogenesis.* Annu Rev Pharmacol Toxicol, 2004. **44**: p. 239-67.

56.   Gius, D. and D.R. Spitz, *Redox signaling in cancer biology.* Antioxid Redox Signal, 2006. **8**(7-8): p. 1249-52.

57.   Cerutti, P., et al., *The role of the cellular antioxidant defense in oxidant carcinogenesis.* Environ Health Perspect, 1994. **102 Suppl 10**: p. 123-9.

58.   Lu, A.L., et al., *Repair of oxidative DNA damage: mechanisms and functions.* Cell Biochem Biophys, 2001. **35**(2): p. 141-70.

59.   Shibutani, S., M. Takeshita, and A.P. Grollman, *Insertion of specific bases during DNA synthesis past the oxidation-damaged base 8-oxodG.* Nature, 1991. **349**(6308): p. 431-4.

60.   Miyake, H., et al., *Oxidative DNA damage in patients with prostate cancer and its response to treatment.* J Urol, 2004. **171**(4): p. 1533-6.

61.   Weiss, J.M., et al., *Polymorphic variation in hOGG1 and risk of cancer: a review of the functional and epidemiologic literature.* Mol Carcinog, 2005. **42**(3): p. 127-41.

62.   Diakowska, D., et al., *Oxidative DNA damage and total antioxidant status in serum of patients with esophageal squamous cell carcinoma.* Hepatogastroenterology, 2007. **54**(78): p. 1701-4.

63.   Tanaka, H., et al., *Hepatic oxidative DNA damage is associated with increased risk for hepatocellular carcinoma in chronic hepatitis C.* Br J Cancer, 2008. **98**(3): p. 580-6.

64.   Droge, W., *Free radicals in the physiological control of cell function.* Physiol Rev, 2002. **82**(1): p. 47-95.

65.   Lassegue, B. and K.K. Griendling, *NADPH oxidases: functions and pathologies in the vasculature.* Arterioscler Thromb Vasc Biol, 2010. **30**(4): p. 653-61.

66.   Babior, B.M., *NADPH oxidase: an update.* Blood, 1999. **93**(5): p. 1464-76.

67.   Bedard, K. and K.H. Krause, *The NOX family of ROS-generating NADPH oxidases: physiology and pathophysiology.* Physiol Rev, 2007. **87**(1): p. 245-313.

68.   Drogemuller, C., et al., *Congenital hypotrichosis with anodontia in cattle: a genetic, clinical and histological analysis.* Vet Dermatol, 2002. **13**(6): p. 307-13.

69.   Trebak, M., et al., *Interplay between calcium and reactive oxygen/nitrogen species: an essential paradigm for vascular smooth muscle signaling.* Antioxid Redox Signal, 2010. **12**(5): p. 657-74.

70.   Stuehr, D.J., *Mammalian nitric oxide synthases.* Biochim Biophys Acta, 1999. **1411**(2-3): p. 217-30.

71.   Kone, B.C., et al., *Protein interactions with nitric oxide synthases: controlling the right time, the right place, and the right amount of nitric oxide.* Am J Physiol Renal Physiol, 2003. **285**(2): p. F178-90.

72.   Kone, B.C., *Nitric oxide synthesis in the kidney: isoforms, biosynthesis, and functions in health.* Semin Nephrol, 2004. **24**(4): p. 299-315.

73.   Herrera, M. and J.L. Garvin, *Recent advances in the regulation of nitric oxide in the kidney.* Hypertension, 2005. **45**(6): p. 1062-7.

74.   Hou, Y.C., A. Janczuk, and P.G. Wang, *Current trends in the development of nitric oxide donors.* Curr Pharm Des, 1999. **5**(6): p. 417-41.

75.   Mount, P.F. and D.A. Power, *Nitric oxide in the kidney: functions and regulation of synthesis.* Acta Physiol (Oxf), 2006. **187**(4): p. 433-46.

76.   Wilcox, C.S. and W.J. Welch, *Interaction between nitric oxide and oxygen radicals in regulation of tubuloglomerular feedback.* Acta Physiol Scand, 2000. **168**(1): p. 119-24.

77.   Trebak, M., et al., *Interplay between calcium and reactive oxygen/nitrogen species: an essential paradigm for vascular smooth muscle signaling.* Antioxid Redox Signal. **12**(5): p. 657-74.

78.   Cadenas, E., *Basic mechanisms of antioxidant activity.* Biofactors, 1997. **6**(4): p. 391-7.

79.   Valko, M., et al., *Free radicals and antioxidants in normal physiological functions and human disease.* Int J Biochem Cell Biol, 2007. **39**(1): p. 44-84.

80.   Meister, A. and M.E. Anderson, *Glutathione.* Annu Rev Biochem, 1983. **52**: p. 711-60.

81.   Forman, H.J., H. Zhang, and A. Rinna, *Glutathione: overview of its protective roles, measurement, and biosynthesis.* Mol Aspects Med, 2009. **30**(1-2): p. 1-12.

82.   Brigelius-Flohe, R., *Selenium compounds and selenoproteins in cancer.* Chem Biodivers, 2008. **5**(3): p. 389-95.

83.   Collet, J.F. and J. Messens, *Structure, Function, and Mechanism of Thioredoxin Proteins.* Antioxid Redox Signal, 2010.

84.   Gozzelino, R., V. Jeney, and M.P. Soares, *Mechanisms of cell protection by heme oxygenase-1.* Annu Rev Pharmacol Toxicol, 2010. **50**: p. 323-54.

85.   Jiang, F., et al., *NO modulates NADPH oxidase function via heme oxygenase-1 in human endothelial cells.* Hypertension, 2006. **48**(5): p. 950-7.

86.   Datla, S.R., et al., *Induction of heme oxygenase-1 in vivo suppresses NADPH oxidase derived oxidative stress.* Hypertension, 2007. **50**(4): p. 636-42.

87.   Surh, Y.J., et al., *Role of Nrf2-mediated heme oxygenase-1 upregulation in adaptive survival response to nitrosative stress.* Arch Pharm Res, 2009. **32**(8): p. 1163-76.

88.   Poli, G., et al., *Oxidative stress and cell signalling.* Curr Med Chem, 2004. **11**(9): p. 1163-82.

89.   Shi, H., X. Shi, and K.J. Liu, *Oxidative mechanism of arsenic toxicity and carcinogenesis.* Mol Cell Biochem, 2004. **255**(1-2): p. 67-78.

90.   Bertin, G. and D. Averbeck, *Cadmium: cellular effects, modifications of biomolecules, modulation of DNA repair and genotoxic consequences (a review).* Biochimie, 2006. **88**(11): p. 1549-59.

91.   Putney, J.W., Jr., *Capacitative calcium entry: sensing the calcium stores.* J Cell Biol, 2005. **169**(3): p. 381-2.

92.   Wu, W.S., *The signaling mechanism of ROS in tumor progression.* Cancer Metastasis Rev, 2006. **25**(4): p. 695-705.

93.   Klaunig, J.E., L.M. Kamendulis, and B.A. Hocevar, *Oxidative stress and oxidative damage in carcinogenesis.* Toxicol Pathol, 2010. **38**(1): p. 96-109.

94.   Kensler, T.W., N. Wakabayashi, and S. Biswal, *Cell survival responses to environmental stresses via the Keap1-Nrf2-ARE pathway.* Annu Rev Pharmacol Toxicol, 2007. **47**: p. 89-116.

95.   Pantano, C., et al., *Redox-sensitive kinases of the nuclear factor-kappaB signaling pathway.* Antioxid Redox Signal, 2006. **8**(9-10): p. 1791-806.

96.   Benhar, M., D. Engelberg, and A. Levitzki, *ROS, stress-activated kinases and stress signaling in cancer.* EMBO Rep, 2002. **3**(5): p. 420-5.

97.   Surh, Y.J., J.K. Kundu, and H.K. Na, *Nrf2 as a master redox switch in turning on the cellular signaling involved in the induction of cytoprotective genes by some chemopreventive phytochemicals.* Planta Med, 2008. **74**(13): p. 1526-39.

98.   Surh, Y.J. and H.K. Na, *NF-kappaB and Nrf2 as prime molecular targets for chemoprevention and cytoprotection with anti-inflammatory and antioxidant phytochemicals.* Genes Nutr, 2008. **2**(4): p. 313-7.

99.   Kim, H.J. and N.D. Vaziri, *Contribution of impaired Nrf2-Keap1 pathway to oxidative stress and inflammation in chronic renal failure.* Am J Physiol Renal Physiol, 2010. **298**(3): p. F662-71.

100. Motohashi, H. and M. Yamamoto, *Nrf2-Keap1 defines a physiologically important stress response mechanism.* Trends Mol Med, 2004. **10**(11): p. 549-57.

101. Lau, A., et al., *Dual roles of Nrf2 in cancer.* Pharmacol Res, 2008. **58**(5-6): p. 262-70.

102. Gloire, G., S. Legrand-Poels, and J. Piette, *NF-kappaB activation by reactive oxygen species: fifteen years later.* Biochem Pharmacol, 2006. **72**(11): p. 1493-505.

103. Habraken, Y. and J. Piette, *NF-kappaB activation by double-strand breaks.* Biochem Pharmacol, 2006. **72**(9): p. 1132-41.

104. Haefner, B., *NF-kappa B: arresting a major culprit in cancer.* Drug Discov Today, 2002. **7**(12): p. 653-63.

105. Pahl, H.L., *Activators and target genes of Rel/NF-kappaB transcription factors.* Oncogene, 1999. **18**(49): p. 6853-66.

106. Wu, Z.H. and S. Miyamoto, *Many faces of NF-kappaB signaling induced by genotoxic stress.* J Mol Med, 2007. **85**(11): p. 1187-202.

107. Burstein, E. and C.S. Duckett, *Dying for NF-kappaB? Control of cell death by transcriptional regulation of the apoptotic machinery.* Curr Opin Cell Biol, 2003. **15**(6): p. 732-7.

108. Luo, J.L., H. Kamata, and M. Karin, *IKK/NF-kappaB signaling: balancing life and death--a new approach to cancer therapy.* J Clin Invest, 2005. **115**(10): p. 2625-32.

109. Hockenbery, D.M., *Targeting mitochondria for cancer therapy.* Environ Mol Mutagen, 2010. **51**(5): p. 476-89.

110. Papa, S., et al., *The NF-kappaB-mediated control of the JNK cascade in the antagonism of programmed cell death in health and disease.* Cell Death Differ, 2006. **13**(5): p. 712-29.

111. Aggarwal, B.B., R.V. Vijayalekshmi, and B. Sung, *Targeting inflammatory pathways for prevention and therapy of cancer: short-term friend, long-term foe.* Clin Cancer Res, 2009. **15**(2): p. 425-30.

112. Mehdi, M.Z., Z.M. Azar, and A.K. Srivastava, *Role of receptor and nonreceptor protein tyrosine kinases in H2O2-induced PKB and ERK1/2 signaling.* Cell Biochem Biophys, 2007. **47**(1): p. 1-10.

113. Torres, M., *Mitogen-activated protein kinase pathways in redox signaling.* Front Biosci, 2003. **8**: p. d369-91.

114. Torres, M. and H.J. Forman, *Redox signaling and the MAP kinase pathways.* Biofactors, 2003. **17**(1-4): p. 287-96.

115. Hilger, R.A., M.E. Scheulen, and D. Strumberg, *The Ras-Raf-MEK-ERK pathway in the treatment of cancer.* Onkologie, 2002. **25**(6): p. 511-8.

116. Roberts, P.J. and C.J. Der, *Targeting the Raf-MEK-ERK mitogen-activated protein kinase cascade for the treatment of cancer.* Oncogene, 2007. **26**(22): p. 3291-310.

117. Lackner, M.R., et al., *A MAP kinase homolog, mpk-1, is involved in ras-mediated induction of vulval cell fates in Caenorhabditis elegans.* Genes Dev, 1994. **8**(2): p. 160-73.

118. Wu, Y., M. Han, and K.L. Guan, *MEK-2, a Caenorhabditis elegans MAP kinase kinase, functions in Ras-mediated vulval induction and other developmental events.* Genes Dev, 1995. **9**(6): p. 742-55.

119. Schaeffer, H.J. and M.J. Weber, *Mitogen-activated protein kinases: specific messages from ubiquitous messengers.* Mol Cell Biol, 1999. **19**(4): p. 2435-44.

120. Morrison, D.K. and R.E. Cutler, *The complexity of Raf-1 regulation.* Curr Opin Cell Biol, 1997. **9**(2): p. 174-9.

121. Seger, R., et al., *Purification and characterization of mitogen-activated protein kinase activator(s) from epidermal growth factor-stimulated A431 cells.* J Biol Chem, 1992. **267**(20): p. 14373-81.

122. de Borst, M.H., et al., *Specific MAP-kinase blockade protects against renal damage in homozygous TGR(mRen2)27 rats.* Lab Invest, 2003. **83**(12): p. 1761-70.

123. Wong, K.K., *Recent developments in anti-cancer agents targeting the Ras/Raf/ MEK/ERK pathway.* Recent Pat Anticancer Drug Discov, 2009. **4**(1): p. 28-35.

124. Mansour, S.J., et al., *Transformation of mammalian cells by constitutively active MAP kinase kinase.* Science, 1994. **265**(5174): p. 966-70.

125. Rossol-Haseroth, K., et al., *Mineralocorticoid receptor antagonists do not block rapid ERK activation by aldosterone.* Biochem Biophys Res Commun, 2004. **318**(1): p. 281-8.

126. Montagut, C. and J. Settleman, *Targeting the RAF-MEK-ERK pathway in cancer therapy.* Cancer Lett, 2009. **283**(2): p. 125-34.

127. Owuor, E.D. and A.N. Kong, *Antioxidants and oxidants regulated signal transduction pathways.* Biochem Pharmacol, 2002. **64**(5-6): p. 765-70.

128. Lewis, T.S., P.S. Shapiro, and N.G. Ahn, *Signal transduction through MAP kinase cascades.* Adv Cancer Res, 1998. **74**: p. 49-139.

129. McCubrey, J.A., et al., *Serine/threonine phosphorylation in cytokine signal transduction.* Leukemia, 2000. **14**(1): p. 9-21.

130. Shaywitz, A.J. and M.E. Greenberg, *CREB: a stimulus-induced transcription factor activated by a diverse array of extracellular signals.* Annu Rev Biochem, 1999. **68**: p. 821-61.

131. Bonni, A., et al., *Cell survival promoted by the Ras-MAPK signaling pathway by transcription-dependent and -independent mechanisms.* Science, 1999. **286**(5443): p. 1358-62.

132. Du, K. and M. Montminy, *CREB is a regulatory target for the protein kinase Akt/PKB.* J Biol Chem, 1998. **273**(49): p. 32377-9.

133. Mabuchi, T., et al., *Phosphorylation of cAMP response element-binding protein in hippocampal neurons as a protective response after exposure to glutamate in vitro and ischemia in vivo.* J Neurosci, 2001. **21**(23): p. 9204-13.

134. Xing, J., D.D. Ginty, and M.E. Greenberg, *Coupling of the RAS-MAPK pathway to gene activation by RSK2, a growth factor-regulated CREB kinase.* Science, 1996. **273**(5277): p. 959-63.

135. Darragh, J., et al., *MSKs are required for the transcription of the nuclear orphan receptors Nur77, Nurr1 and Nor1 downstream of MAPK signalling.* Biochem J, 2005. **390**(Pt 3): p. 749-59.

136. Arany, I., et al., *Activation of ERK or inhibition of JNK ameliorates H(2)O(2) cytotoxicity in mouse renal proximal tubule cells.* Kidney Int, 2004. **65**(4): p. 1231-9.

137. Arany, I., et al., *CREB mediates ERK-induced survival of mouse renal tubular cells after oxidant stress.* Kidney Int, 2005. **68**(4): p. 1573-82.

138. Bromberg, J. and X. Chen, *STAT proteins: signal tranducers and activators of transcription.* Methods Enzymol, 2001. **333**: p. 138-51.

139. Timofeeva, O.A., et al., *Serine-phosphorylated STAT1 is a prosurvival factor in Wilms' tumor pathogenesis.* Oncogene, 2006. **25**(58): p. 7555-64.

140. Calo, V., et al., *STAT proteins: from normal control of cellular events to tumorigenesis.* J Cell Physiol, 2003. **197**(2): p. 157-68.

141. Guo, C., et al., *Activation of Stat3 in renal tumors.* Am J Transl Res, 2009. **1**(3): p. 283-90.

142. Horiguchi, A., et al., *STAT3 inhibitor WP1066 as a novel therapeutic agent for renal cell carcinoma.* Br J Cancer, 2010. **102**(11): p. 1592-9.

143. Hui, Z., et al., *Radiosensitization by inhibiting STAT1 in renal cell carcinoma.* Int J Radiat Oncol Biol Phys, 2009. **73**(1): p. 288-95.

144. Bowman, T., et al., *STATs in oncogenesis.* Oncogene, 2000. **19**(21): p. 2474-88.

145. Khodarev, N.N., et al., *STAT1 is overexpressed in tumors selected for radioresistance and confers protection from radiation in transduced sensitive cells.* Proc Natl Acad Sci U S A, 2004. **101**(6): p. 1714-9.

146. Terui, K., et al., *Hypoxia/re-oxygenation-induced, redox-dependent activation of STAT1 (signal transducer and activator of transcription 1) confers resistance to apoptotic cell death via hsp70 induction.* Biochem J, 2004. **380**(Pt 1): p. 203-9.

147. Bromberg, J.F., et al., *Stat3 as an oncogene.* Cell, 1999. **98**(3): p. 295-303.

148. Aggarwal, B.B., et al., *Signal transducer and activator of transcription-3, inflammation, and cancer: how intimate is the relationship?* Ann N Y Acad Sci, 2009. **1171**: p. 59-76.

149. Kolkhof, P., A. Hillisch, and S. S., *Severe early-onset hypertension induced by a mineralocorticoid receptor (MR) gain-of-function mutation: differential effects of steroidal versus non-steroidal antagonists.* Eur Heart J, 2007. **28**(Supplement 1): p. 769.

150. Rozen, S. and H. Skaletsky, *Primer3 on the WWW for general users and for biologist programmers.* Methods Mol Biol, 2000. **132**: p. 365-86.

151. Rotman, B. and B.W. Papermaster, *Membrane properties of living mammalian cells as studied by enzymatic hydrolysis of fluorogenic esters.* Proc Natl Acad Sci U S A, 1966. **55**(1): p. 134-41.

152. Yang, H., et al., *In situ assessment of cell viability.* Cell Transplant, 1998. **7**(5): p. 443-51.

153. Collins, A.R., *The comet assay for DNA damage and repair: principles, applications, and limitations.* Mol Biotechnol, 2004. **26**(3): p. 249-61.

154. Stopper, H., et al., *Formation of micronuclei and inhibition of topoisomerase II in the comet assay in mammalian cells with altered DNA methylation.* Recent Results Cancer Res, 1997. **143**: p. 183-93.

155. Fenech, M., *The cytokinesis-block micronucleus technique and its application to genotoxicity studies in human populations.* Environ Health Perspect, 1993. **101 Suppl 3**: p. 101-7.

156. Murgia, E., et al., *Validation of micronuclei frequency in peripheral blood lymphocytes as early cancer risk biomarker in a nested case-control study.* Mutat Res, 2008. **639**(1-2): p. 27-34.

157. Fenech, M., *The in vitro micronucleus technique.* Mutat Res, 2000. **455**(1-2): p. 81-95.

158. Rasband, W.S., *ImageJ.* 1997-2008, U. S. National Institutes of Health Bethesda, Maryland, USA.

159. Valavanidis, A., T. Vlachogianni, and C. Fiotakis, *8-hydroxy-2' - deoxyguanosine (8-OHdG): A critical biomarker of oxidative stress and carcinogenesis.* J Environ Sci Health C Environ Carcinog Ecotoxicol Rev, 2009. **27**(2): p. 120-39.

160. Gratzner, H.G., *Monoclonal antibody to 5-bromo- and 5-iododeoxyuridine: A new reagent for detection of DNA replication.* Science, 1982. **218**(4571): p. 474-5.

161. Oli, R.G., et al., *No increased chromosomal damage in L-DOPA-treated patients with Parkinson's disease: a pilot study.* J Neural Transm, 2010. **117**(6): p. 737-46.

162. Chao, M.R., C.C. Yen, and C.W. Hu, *Prevention of artifactual oxidation in determination of cellular 8-oxo-7,8-dihydro-2'-deoxyguanosine by isotope-dilution LC-MS/MS with automated solid-phase extraction.* Free Radic Biol Med, 2008. **44**(3): p. 464-73.

163. Jones, D.P., et al., *Glutathione measurement in human plasma. Evaluation of sample collection, storage and derivatization conditions for analysis of dansyl derivatives by HPLC.* Clin Chim Acta, 1998. **275**(2): p. 175-84.

164. Kruger, N.J., *The Bradford method for protein quantitation.* Methods Mol Biol, 1994. **32**: p. 9-15.

165. Benzie, I.F. and J.J. Strain, *Ferric reducing/antioxidant power assay: direct measure of total antioxidant activity of biological fluids and modified version for simultaneous measurement of total antioxidant power and ascorbic acid concentration.* Methods Enzymol, 1999. **299**: p. 15-27.

166. Roy, S. and L. Packer, *Redox regulation of cell functions by alpha-lipoate: biochemical and molecular aspects.* Biofactors, 1998. **8**(1-2): p. 17-21.

167. Han, D., H.J. Tritschler, and L. Packer, *Alpha-lipoic acid increases intracellular glutathione in a human T-lymphocyte Jurkat cell line.* Biochem Biophys Res Commun, 1995. **207**(1): p. 258-64.

168. Zafarullah, M., et al., *Molecular mechanisms of N-acetylcysteine actions.* Cell Mol Life Sci, 2003. **60**(1): p. 6-20.

169. Wilcox, C.S. and A. Pearlman, *Chemistry and antihypertensive effects of tempol and other nitroxides.* Pharmacol Rev, 2008. **60**(4): p. 418-69.

170. Alam, J., et al., *Heme activates the heme oxygenase-1 gene in renal epithelial cells by stabilizing Nrf2.* Am J Physiol Renal Physiol, 2003. **284**(4): p. F743-52.

171. Kolkhof, P., A. Hillisch, and S. Schäfer, *Severe early-onset hypertension induced by a mineralocorticoid receptor (MR) gain-of-function mutation: differential effects of steroidal versus non-steroidal antagonists.* Eur Heart J, 2007. **28**: p. 769.

172. Fagart, J., et al., *A new mode of mineralocorticoid receptor antagonism by a potent and selective non-steroidal molecule.* J Biol Chem, 2010.

173. Park, Y.M., et al., *NAD(P)H oxidase inhibitor prevents blood pressure elevation and cardiovascular hypertrophy in aldosterone-infused rats.* Biochem Biophys Res Commun, 2004. **313**(3): p. 812-7.

174. ten Freyhaus, H., et al., *Novel Nox inhibitor VAS2870 attenuates PDGF-dependent smooth muscle cell chemotaxis, but not proliferation.* Cardiovasc Res, 2006. **71**(2): p. 331-41.

175. Nistala, R., et al., *Renin-angiotensin-aldosterone system-mediated redox effects in chronic kidney disease.* Transl Res, 2009. **153**(3): p. 102-13.

176. Weitzman, S.A., et al., *Phagocytes as carcinogens: malignant transformation produced by human neutrophils.* Science, 1985. **227**(4691): p. 1231-3.

177. Calo, L.A., et al., *Oxidative Stress Related Proteins in a Conn's Adenoma Tissue. Relevance for Aldosterone's Prooxidative and Proinflammatory Activity.* J Endocrinol Invest, 2009.

178. Burlinson, B., et al., *Fourth International Workgroup on Genotoxicity testing: results of the in vivo Comet assay workgroup.* Mutat Res, 2007. **627**(1): p. 31-5.

179. Brendler-Schwaab, S., et al., *The in vivo comet assay: use and status in genotoxicity testing.* Mutagenesis, 2005. **20**(4): p. 245-54.

180. Maluf, S.W., *Monitoring DNA damage following radiation exposure using cytokinesis-block micronucleus method and alkaline single-cell gel electrophoresis.* Clin Chim Acta, 2004. **347**(1-2): p. 15-24.

181. Decordier, I. and M. Kirsch-Volders, *The in vitro micronucleus test: from past to future.* Mutat Res, 2006. **607**(1): p. 2-4.

182. Patni, H., et al., *Aldosterone promotes proximal tubular cell apoptosis: role of oxidative stress.* Am J Physiol Renal Physiol, 2007. **293**(4): p. F1065-71.

183. Espinosa, O., et al., *Urinary 8-oxo-7,8-dihydro-2'-deoxyguanosine (8-oxo-dG), a reliable oxidative stress marker in hypertension.* Free Radic Res, 2007. **41**(5): p. 546-54.

184. Nakabeppu, Y., et al., *Mutagenesis and carcinogenesis caused by the oxidation of nucleic acids.* Biol Chem, 2006. **387**(4): p. 373-9.

185. Sun, Y., et al., *Aldosterone-induced inflammation in the rat heart : role of oxidative stress.* Am J Pathol, 2002. **161**(5): p. 1773-81.

186. Miyata, K., et al., *Aldosterone stimulates reactive oxygen species production through activation of NADPH oxidase in rat mesangial cells.* J Am Soc Nephrol, 2005. **16**(10): p. 2906-12.

187. Zhang, A., et al., *Aldosterone induces epithelial-mesenchymal transition via ROS of mitochondrial origin.* Am J Physiol Renal Physiol, 2007. **293**(3): p. F723-31.

188. Shibata, S., et al., *Podocyte as the target for aldosterone: roles of oxidative stress and Sgk1.* Hypertension, 2007. **49**(2): p. 355-64.

189. Hayashi, H., et al., *Aldosterone nongenomically produces NADPH oxidase-dependent reactive oxygen species and induces myocyte apoptosis.* Hypertens Res, 2008. **31**(2): p. 363-75.

190. Thomas, W., V. McEneaney, and B.J. Harvey, *Rapid responses to steroid hormones in the kidney.* Nephron Physiol, 2007. **107**(1): p. p1-9.

191. Aruoma, O.I., et al., *The antioxidant action of N-acetylcysteine: its reaction with hydrogen peroxide, hydroxyl radical, superoxide, and hypochlorous acid.* Free Radic Biol Med, 1989. **6**(6): p. 593-7.

192. Packer, L., E.H. Witt, and H.J. Tritschler, *alpha-Lipoic acid as a biological antioxidant.* Free Radic Biol Med, 1995. **19**(2): p. 227-50.

193. Krishna, M.C., et al., *Do nitroxide antioxidants act as scavengers of O2-. or as SOD mimics?* J Biol Chem, 1996. **271**(42): p. 26026-31.

194. Chatterjee, P.K., et al., *Tempol, a membrane-permeable radical scavenger, reduces oxidant stress-mediated renal dysfunction and injury in the rat.* Kidney Int, 2000. **58**(2): p. 658-73.

195. Lam, E.Y., et al., *Mineralocorticoid receptor blockade but not steroid withdrawal reverses renal fibrosis in deoxycorticosterone/salt rats.* Endocrinology, 2006. **147**(7): p. 3623-9.

196. Ishikawa, Y., et al., *Long-term administration of rho-kinase inhibitor ameliorates renal damage in malignant hypertensive rats.* Hypertension, 2006. **47**(6): p. 1075-83.

197. Ndisang, J.F., N. Lane, and A. Jadhav, *Crosstalk between the heme oxygenase system, aldosterone, and phospholipase C in hypertension.* J Hypertens, 2008. **26**(6): p. 1188-99.

198. Jin, L., et al., *Increased reactive oxygen species contributes to kidney injury in mineralocorticoid hypertensive rats.* J Physiol Pharmacol, 2006. **57**(3): p. 343-57.

199. Beswick, R.A., et al., *NADH/NADPH oxidase and enhanced superoxide production in the mineralocorticoid hypertensive rat.* Hypertension, 2001. **38**(5): p. 1107-11.

200. Schupp, N., et al., *Angiotensin II-induced genomic damage in renal cells can be prevented by angiotensin II type 1 receptor blockage or radical scavenging.* Am J Physiol Renal Physiol, 2007. **292**(5): p. F1427-34.

201. Schupp, N., et al., *Aldosterone Causes DNA Strand Breaks and Chromosomal Damage in Renal Cells, Which are Prevented by Mineralocorticoid Receptor Antagonists.* Horm Metab Res, 2010. **PMID: 20094972**.

202. Schmid, U., et al., *Angiotensin II induces DNA damage in the kidney.* Cancer Res, 2008. **68**(22): p. 9239-46.
203. Almeida, M.R., et al., *Genotoxic studies in hypertensive and normotensive rats treated with amiodarone.* Mutat Res, 2008. **657**(2): p. 155-9.
204. Park, E., et al., *Soy isoflavone supplementation alleviates oxidative stress and improves systolic blood pressure in male spontaneously hypertensive rats.* J Nutr Sci Vitaminol (Tokyo), 2005. **51**(4): p. 254-9.
205. Gur, M., et al., *Relationship between left ventricle geometric patterns and lymphocyte DNA damage in patients with untreated essential hypertension.* Clin Biochem, 2007. **40**(7): p. 454-9.
206. Bennett, E.J. and J.W. Harper, *DNA damage: ubiquitin marks the spot.* Nat Struct Mol Biol, 2008. **15**(1): p. 20-2.
207. Rothkamm, K., et al., *Pathways of DNA double-strand break repair during the mammalian cell cycle.* Mol Cell Biol, 2003. **23**(16): p. 5706-15.
208. Shrivastav, M., L.P. De Haro, and J.A. Nickoloff, *Regulation of DNA double-strand break repair pathway choice.* Cell Res, 2008. **18**(1): p. 134-47.
209. Ismail, I.H. and M.J. Hendzel, *The gamma-H2A.X: is it just a surrogate marker of double-strand breaks or much more?* Environ Mol Mutagen, 2008. **49**(1): p. 73-82.
210. Trapp, C., M. Schwarz, and B. Epe, *The peroxisome proliferator WY-14,643 promotes hepatocarcinogenesis caused by endogenously generated oxidative DNA base modifications in repair-deficient Csbm/m/Ogg1-/- mice.* Cancer Res, 2007. **67**(11): p. 5156-61.
211. Mathew, J.T., et al., *Aldosterone induces mesangial cell apoptosis both in vivo and in vitro.* Am J Physiol Renal Physiol, 2008. **295**(1): p. F73-81.
212. Iwazu, Y., et al., *Spironolactone suppresses peritubular capillary loss and prevents deoxycorticosterone acetate/salt-induced tubulointerstitial fibrosis.* Hypertension, 2008. **51**(3): p. 749-54.
213. Burniston, J.G., et al., *Aldosterone induces myocyte apoptosis in the heart and skeletal muscles of rats in vivo.* J Mol Cell Cardiol, 2005. **39**(2): p. 395-9.
214. Pietranera, L., et al., *Protective effects of estradiol in the brain of rats with genetic or mineralocorticoid-induced hypertension.* Psychoneuroendocrinology, 2008. **33**(3): p. 270-81.
215. Talalay, P., et al., *Chemoprotection against cancer by phase 2 enzyme induction.* Toxicol Lett, 1995. **82-83**: p. 173-9.
216. Gegg, M.E., et al., *Differential effect of nitric oxide on glutathione metabolism and mitochondrial function in astrocytes and neurones: implications for neuroprotection/neurodegeneration?* J Neurochem, 2003. **86**(1): p. 228-37.
217. Shih, A.Y., et al., *Coordinate regulation of glutathione biosynthesis and release by Nrf2-expressing glia potently protects neurons from oxidative stress.* J Neurosci, 2003. **23**(8): p. 3394-406.
218. McKinnon, P.J. and K.W. Caldecott, *DNA strand break repair and human genetic disease.* Annu Rev Genomics Hum Genet, 2007. **8**: p. 37-55.
219. Jeggo, P.A. and M. Lobrich, *DNA double-strand breaks: their cellular and clinical impact?* Oncogene, 2007. **26**(56): p. 7717-9.
220. Bonner, W.M., et al., *GammaH2AX and cancer.* Nat Rev Cancer, 2008. **8**(12): p. 957-67.
221. Cheng, K.C., et al., *8-Hydroxyguanine, an abundant form of oxidative DNA damage, causes G----T and A----C substitutions.* J Biol Chem, 1992. **267**(1): p. 166-72.

222. Cooke, M.S., R. Olinski, and M.D. Evans, *Does measurement of oxidative damage to DNA have clinical significance?* Clin Chim Acta, 2006. **365**(1-2): p. 30-49.

223. Aoki, Y., et al., *Accelerated DNA adduct formation in the lung of the Nrf2 knockout mouse exposed to diesel exhaust.* Toxicol Appl Pharmacol, 2001. **173**(3): p. 154-60.

224. Osburn, W.O. and T.W. Kensler, *Nrf2 signaling: an adaptive response pathway for protection against environmental toxic insults.* Mutat Res, 2008. **659**(1-2): p. 31-9.

225. Sethi, G., B. Sung, and B.B. Aggarwal, *Nuclear factor-kappaB activation: from bench to bedside.* Exp Biol Med (Maywood), 2008. **233**(1): p. 21-31.

226. Clement, J.F., S. Meloche, and M.J. Servant, *The IKK-related kinases: from innate immunity to oncogenesis.* Cell Res, 2008. **18**(9): p. 889-99.

227. Cachofeiro, V., et al., *Aldosterone and the vascular system.* J Steroid Biochem Mol Biol, 2008. **109**(3-5): p. 331-5.

228. Brzoska, K. and I. Szumiel, *Signalling loops and linear pathways: NF-kappaB activation in response to genotoxic stress.* Mutagenesis, 2009. **24**(1): p. 1-8.

229. Beswick, R.A., et al., *Long-term antioxidant administration attenuates mineralocorticoid hypertension and renal inflammatory response.* Hypertension, 2001. **37**(2 Part 2): p. 781-6.

230. Kang, Y.M., et al., *Brain nuclear factor-kappa B activation contributes to neurohumoral excitation in angiotensin II-induced hypertension.* Cardiovasc Res, 2009. **82**(3): p. 503-12.

231. Mackenzie, G.G., et al., *Curcumin induces cell-arrest and apoptosis in association with the inhibition of constitutively active NF-kappaB and STAT3 pathways in Hodgkin's lymphoma cells.* Int J Cancer, 2008. **123**(1): p. 56-65.

232. Manegold, J.C., et al., *Rapid aldosterone effects on tyrosine phosphorylation in vascular smooth muscle cells.* Cell Mol Biol (Noisy-le-grand), 1999. **45**(6): p. 805-13.

233. Meloche, S., et al., *Biphasic and synergistic activation of p44mapk (ERK1) by growth factors: correlation between late phase activation and mitogenicity.* Mol Endocrinol, 1992. **6**(5): p. 845-54.

234. Aplin, A.E., et al., *Integrin-mediated adhesion regulates ERK nuclear translocation and phosphorylation of Elk-1.* J Cell Biol, 2001. **153**(2): p. 273-82.

235. Ichiki, T., et al., *Cyclic AMP response element-binding protein mediates reactive oxygen species-induced c-fos expression.* Hypertension, 2003. **42**(2): p. 177-83.

236. Grossmann, C., et al., *Mineralocorticoid receptor inhibits CREB signaling by calcineurin activation.* FASEB J, 2010. **24**(6): p. 2010-9.

237. Marrero, M.B., et al., *Direct stimulation of Jak/STAT pathway by the angiotensin II AT1 receptor.* Nature, 1995. **375**(6528): p. 247-50.

238. Atkinson, G.P., S.E. Nozell, and E.T. Benveniste, *NF-kappaB and STAT3 signaling in glioma: targets for future therapies.* Expert Rev Neurother, 2010. **10**(4): p. 575-86.

239. Grivennikov, S.I. and M. Karin, *Dangerous liaisons: STAT3 and NF-kappaB collaboration and crosstalk in cancer.* Cytokine Growth Factor Rev, 2010. **21**(1): p. 11-9.

240. Hudelist, G., et al., *cDNA array analysis of cytobrush-collected normal and malignant cervical epithelial cells: a feasibility study.* Cancer Genet Cytogenet, 2005. **158**(1): p. 35-42.

241. Pansky, A., et al., *Defective Jak-STAT signal transduction pathway in melanoma cells resistant to growth inhibition by interferon-alpha.* Int J Cancer, 2000. **85**(5): p. 720-5.

242. McCubrey, J.A., et al., *Emerging MEK inhibitors.* Expert Opin Emerg Drugs, 2010. **15**(2): p. 203-23.

243. Losel, R.M., et al., *Nongenomic effects of aldosterone: cellular aspects and clinical implications.* Steroids, 2002. **67**(6): p. 493-8.

244. Gekle, M., et al., *Aldosterone interaction with epidermal growth factor receptor signaling in MDCK cells.* Am J Physiol Renal Physiol, 2002. **282**(4): p. F669-79.

245. Harvey, B.J. and M. Higgins, *Nongenomic effects of aldosterone on Ca2+ in M-1 cortical collecting duct cells.* Kidney Int, 2000. **57**(4): p. 1395-403.

246. Berridge, M.J., *Elementary and global aspects of calcium signalling.* J Physiol, 1997. **499 (Pt 2)**: p. 291-306.

247. Fan, Y.Y., et al., *Inhibitory effects of a dihydropyridine calcium channel blocker on renal injury in aldosterone-infused rats.* J Hypertens, 2009. **27**(9): p. 1855-62.

248. Yamamoto, E., et al., *Benidipine, a dihydropyridine L-type/T-type calcium channel blocker, affords additive benefits for prevention of cardiorenal injury in hypertensive rats.* J Hypertens.

249. Maruyama, T., et al., *2APB, 2-aminoethoxydiphenyl borate, a membrane-penetrable modulator of Ins(1,4,5)P3-induced Ca2+ release.* J Biochem, 1997. **122**(3): p. 498-505.

250. Prakriya, M. and R.S. Lewis, *Potentiation and inhibition of Ca(2+) release-activated Ca(2+) channels by 2-aminoethyldiphenyl borate (2-APB) occurs independently of IP(3) receptors.* J Physiol, 2001. **536**(Pt 1): p. 3-19.

251. Bootman, M.D., et al., *2-aminoethoxydiphenyl borate (2-APB) is a reliable blocker of store-operated Ca2+ entry but an inconsistent inhibitor of InsP3-induced Ca2+ release.* FASEB J, 2002. **16**(10): p. 1145-50.

252. Haque, M.Z. and D.S. Majid, *Assessment of renal functional phenotype in mice lacking gp91PHOX subunit of NAD(P)H oxidase.* Hypertension, 2004. **43**(2): p. 335-40.

253. Sachse, A. and G. Wolf, *Angiotensin II-induced reactive oxygen species and the kidney.* J Am Soc Nephrol, 2007. **18**(9): p. 2439-46.

254. Lambeth, J.D., *NOX enzymes and the biology of reactive oxygen.* Nat Rev Immunol, 2004. **4**(3): p. 181-9.

255. Han, W., et al., *Lipid rafts keep NADPH oxidase in the inactive state in human renal proximal tubule cells.* Hypertension, 2008. **51**(2): p. 481-7.

256. Noh, K.M. and J.Y. Koh, *Induction and activation by zinc of NADPH oxidase in cultured cortical neurons and astrocytes.* J Neurosci, 2000. **20**(23): p. RC111.

257. Siow, Y.L., et al., *Homocysteine stimulates phosphorylation of NADPH oxidase p47phox and p67phox subunits in monocytes via protein kinase Cbeta activation.* Biochem. J., 2006. **398**(1): p. 73-82.

258. Forbes, M.S., et al., *Lack of endothelial nitric-oxide synthase leads to progressive focal renal injury.* Am J Pathol, 2007. **170**(1): p. 87-99.

259. Heemskerk, S., et al., *Selective iNOS inhibition for the treatment of sepsis-induced acute kidney injury.* Nat Rev Nephrol, 2009. **5**(11): p. 629-40.

260. Cai, H. and D.G. Harrison, *Endothelial dysfunction in cardiovascular diseases: the role of oxidant stress.* Circ Res, 2000. **87**(10): p. 840-4.

261. Vaziri, N.D., *Roles of oxidative stress and antioxidant therapy in chronic kidney disease and hypertension.* Curr Opin Nephrol Hypertens, 2004. **13**(1): p. 93-9.

262. Laursen, J.B., et al., *Endothelial regulation of vasomotion in apoE-deficient mice: implications for interactions between peroxynitrite and tetrahydrobiopterin.* Circulation, 2001. **103**(9): p. 1282-8.

263. Nagata, D., et al., *Molecular mechanism of the inhibitory effect of aldosterone on endothelial NO synthase activity.* Hypertension, 2006. **48**(1): p. 165-71.

264. Jaiswal, M., N.F. LaRusso, and G.J. Gores, *Nitric oxide in gastrointestinal epithelial cell carcinogenesis: linking inflammation to oncogenesis.* Am J Physiol Gastrointest Liver Physiol, 2001. **281**(3): p. G626-34.

265. Rogerson, F.M., et al., *Differences in the determinants of eplerenone, spironolactone and aldosterone binding to the mineralocorticoid receptor.* Clin Exp Pharmacol Physiol, 2004. **31**(10): p. 704-9.

266. Muldowney, J.A., 3rd, J.A. Schoenhard, and C.D. Benge, *The clinical pharmacology of eplerenone.* Expert Opin Drug Metab Toxicol, 2009. **5**(4): p. 425-32.

267. Takeda, Y., *Effects of eplerenone, a selective mineralocorticoid receptor antagonist, on clinical and experimental salt-sensitive hypertension.* Hypertens Res, 2009. **32**(5): p. 321-4.

268. Gauer, S., V. Segitz, and M. Goppelt-Struebe, *Aldosterone induces CTGF in mesangial cells by activation of the glucocorticoid receptor.* Nephrol Dial Transplant, 2007. **22**(11): p. 3154-9.

269. Rogerson, F.M., et al., *A critical region in the mineralocorticoid receptor for aldosterone binding and activation by cortisol: evidence for a common mechanism governing ligand binding specificity in steroid hormone receptors.* Mol Endocrinol, 2007. **21**(4): p. 817-28.

270. Ames, B.N., M.K. Shigenaga, and T.M. Hagen, *Oxidants, antioxidants, and the degenerative diseases of aging.* Proc Natl Acad Sci U S A, 1993. **90**(17): p. 7915-22.

271. Collins, A.R., *Oxidative DNA damage, antioxidants, and cancer.* Bioessays, 1999. **21**(3): p. 238-46.

272. Paz-Elizur, T., et al., *DNA repair of oxidative DNA damage in human carcinogenesis: potential application for cancer risk assessment and prevention.* Cancer Lett, 2008. **266**(1): p. 60-72.

273. Liew, D. and H. Krum, *Aldosterone receptor antagonists for hypertension: what do they offer?* Drugs, 2003. **63**(19): p. 1963-72.

274. Kushibiki, M., et al., *Aldosterone causes vasoconstriction in coronary arterioles of rats via angiotensin II type-1 receptor: influence of hypertension.* Eur J Pharmacol, 2007. **572**(2-3): p. 182-8.

275. Florea, A.M., E.N. Yamoah, and E. Dopp, *Intracellular calcium disturbances induced by arsenic and its methylated derivatives in relation to genomic damage and apoptosis induction.* Environ Health Perspect, 2005. **113**(6): p. 659-64.

276. Dopp, E., et al., *Induction of genotoxic effects and modulation of the intracellular calcium level in syrian hamster embryo (SHE) fibroblasts caused by ochratoxin A.* Food Chem Toxicol, 1999. **37**(7): p. 713-21.

277. Xu, N., K.Q. Luo, and D.C. Chang, *Ca2+ signal blockers can inhibit M/A transition in mammalian cells by interfering with the spindle checkpoint.* Biochem Biophys Res Commun, 2003. **306**(3): p. 737-45.

278. Queisser, N., et al., *Aldosterone induces oxidative stress, oxidative DNA damage and NF-kappaB-activation in kidney tubule cells* 2010. Submitted.

279. Majander, A., M. Finel, and M. Wikstrom, *Diphenyleneiodonium inhibits reduction of iron-sulfur clusters in the mitochondrial NADH-ubiquinone oxidoreductase (Complex I).* J Biol Chem, 1994. **269**(33): p. 21037-42.

280. Lapperre, T.S., et al., *Apocynin increases glutathione synthesis and activates AP-1 in alveolar epithelial cells.* FEBS Lett, 1999. **443**(2): p. 235-9.

281. Stolk, J., et al., *Characteristics of the inhibition of NADPH oxidase activation in neutrophils by apocynin, a methoxy-substituted catechol.* Am J Respir Cell Mol Biol, 1994. **11**(1): p. 95-102.

282. Huang, Y.J., et al., *Nitrative and oxidative DNA damage as potential survival biomarkers for nasopharyngeal carcinoma.* Med Oncol, 2010.

283. Jaiswal, M., et al., *Nitric oxide-mediated inhibition of DNA repair potentiates oxidative DNA damage in cholangiocytes.* Gastroenterology, 2001. **120**(1): p. 190-9.

284. Burdette, D., M. Olivarez, and G. Waris, *Activation of transcription factor Nrf2 by hepatitis C virus induces the cell-survival pathway.* J Gen Virol, 2010. **91**(Pt 3): p. 681-90.

285. Gao, L. and G.E. Mann, *Vascular NAD(P)H oxidase activation in diabetes: a double-edged sword in redox signalling.* Cardiovasc Res, 2009. **82**(1): p. 9-20.

286. Huang, H.C., T. Nguyen, and C.B. Pickett, *Regulation of the antioxidant response element by protein kinase C-mediated phosphorylation of NF-E2-related factor 2.* Proc Natl Acad Sci U S A, 2000. **97**(23): p. 12475-80.

287. Dhakshinamoorthy, S. and A.G. Porter, *Nitric oxide-induced transcriptional up-regulation of protective genes by Nrf2 via the antioxidant response element counteracts apoptosis of neuroblastoma cells.* J Biol Chem, 2004. **279**(19): p. 20096-107.

288. Clark, J.D., et al., *Cytosolic phospholipase A2.* J Lipid Mediat Cell Signal, 1995. **12**(2-3): p. 83-117.

289. Shin, T.Y., et al., *Anti-allergic inflammatory activity of the fruit of Prunus persica: Role of calcium and NF-kappaB.* Food Chem Toxicol, 2010.

290. Khundmiri, S.J., et al., *Ouabain stimulates protein kinase B (Akt) phosphorylation in opossum kidney proximal tubule cells through an ERK-dependent pathway.* Am J Physiol Cell Physiol, 2007. **293**(3): p. C1171-80.

291. Ha, H. and H.B. Lee, *Reactive oxygen species amplify glucose signalling in renal cells cultured under high glucose and in diabetic kidney.* Nephrology (Carlton), 2005. **10 Suppl**: p. S7-10.

292. Matsunaga, Y., et al., *Involvement of activation of NADPH oxidase and extracellular signal-regulated kinase (ERK) in renal cell injury induced by zinc.* J Toxicol Sci, 2005. **30**(2): p. 135-44.

293. Go, Y.M., et al., *H2O2-dependent activation of GCLC-ARE4 reporter occurs by mitogen-activated protein kinase pathways without oxidation of cellular glutathione or thioredoxin-1.* J Biol Chem, 2004. **279**(7): p. 5837-45.

294. Cheng, H.F., M.Z. Zhang, and R.C. Harris, *Nitric oxide stimulates cyclooxygenase-2 in cultured cTAL cells through a p38-dependent pathway.* Am J Physiol Renal Physiol, 2006. **290**(6): p. F1391-7.

295. Meini, A., et al., *A nitric oxide/Ca(2+)/calmodulin/ERK1/2 mitogen-activated protein kinase pathway is involved in the mitogenic effect of IL-1beta in human astrocytoma cells.* Br J Pharmacol, 2008. **153**(8): p. 1706-17.

296. Espinosa, A., et al., *Myotube depolarization generates reactive oxygen species through NAD(P)H oxidase; ROS-elicited Ca2+ stimulates ERK, CREB, early genes.* J Cell Physiol, 2006. **209**(2): p. 379-88.

297. Schieffer, B., et al., *Role of NAD(P)H oxidase in angiotensin II-induced JAK/STAT signaling and cytokine induction.* Circ Res, 2000. **87**(12): p. 1195-201.

9 ACKNOWLEDGEMENTS

CURRICULUM VITAE

Nina Queisser
* November 5th 1981 in Ludwigsburg, Germany
Dettelbachergasse 3
97070 Würzburg

Education

07.2007 - present	Ph.D. thesis in toxicology at the Institute of Pharmacology and Toxicology, Department of Toxicology, University of Würzburg, Germany
09.2009 - 12.2009	Collaboration work at the Department of Nutrition and Department of Environmental Toxicology, University of California, Davis, USA
02.2009 - 05.2009	Collaboration work at the Department of Nutrition and Department of Environmental Toxicology, University of California, Davis, USA
04.2006 - 08.2006	Master thesis in nutrition at the Department of Nutrition and Department of Environmental Toxicology, University of California, Davis, USA
10.2004 - 03.2007	Master of Science in Nutritional Sciences at the University of Gießen, Germany
08.2004 – 09.2004	Bachelor thesis in nutrition at the University of Gießen, Germany
10.2001 – 09.2004	Bachelor of Science in Nutritional Sciences at the University of Gießen, Germany
08.1992 – 06.2001	Secondary school, Mörike-Gymnasium, Ludwigsburg, Germany Degree: General qualification for university entrance (Abitur)
08.1988 – 07.1992	Primary school, August-Lämmle-Schule, Ludwigsburg-Oßweil, Germany

PUBLICATIONS

1. published

Schupp N*, Kolkhof P*, **Queisser N***, Gärtner S, Schmid U, Kretschmer A, Hartmann E, Gnana O, Schäfer S, Stopper H:
>   Aldosterone causes DNA damage in kidneys of DOCA/salt-rats mediated by the mineralocorticoid receptor. FASEB Journal 2010, accepted

∗The first three authors contributed equally to this work

Queisser N, Oteiza P, Stopper H, Gnana O, Schupp N:
>   Aldosterone induces oxidative stress, oxidative DNA damage and NF-kappaB activation in kidney tubule cells. Molecular Carcinogenesis 2010, accepted

Queisser N, Fazeli G, Schupp N:
>   Superoxide anion and hydrogen peroxide-induced signaling and damage in angiotensin II and aldosterone action. Special Issue „Xenobiotics and Cell Signaling", Biological Chemistry 2010, accepted.

Schupp N*, **Queisser N***, Wolf M, Kolkhof P, Bärfacker L, Schäfer S, Heidland H, Stopper H:
>   Aldosterone causes DNA strand breaks and chromosomal damage in renal cells, which are prevented by mineralocorticoid receptor antagonists. Horm Metab Res. 2009;41:1-8

∗The first two authors contributed equally to this work.

Stopper H, Schupp N, Fazeli G, Dietel B, **Queisser N**, Walitza S, Gerlach M:
>   Genotoxicity of the neurotransmitter dopamine in vitro. Toxicol In Vitro. 2009 Jun; 23(4):640-6.

Schmid U, Stopper H, Schweda F, **Queisser N**, Schupp N:
>   Angiotensin II induces DNA damage in the kidney. Cancer Res 2008 Nov 15, 68(22)

Mackenzie GG*, **Queisser N***, Wolfson ML, Fraga CG, Adamo AM, Oteiza PI:
>   Curcumin induces cell-arrest and apoptosis in association with the inhibition of constitutively active NF-kappaB and STAT3 pathways in Hodgkin's lymphoma cells. Int J Cancer. 2008 Jul 1;123(1):56-65

∗The first two authors contributed equally to this work.

ABSTRACTS

Queisser N, Schupp N, Stopper H, Oteiza P:
> Aldosterone induces the activation of Nrf2 and NF-κB through the production of reactive oxygen and nitrogen species in kidney tubule cells. SFRR, September 2010, Oslo, Norway
> Oral presentation, Young investigator award

Queisser N, Stopper H, Schupp N:
> Aldosterone-caused DNA damage depends on the mineralocorticoid receptor inducing Ca^{2+} increase, leading to activation of PKC and finally NAD(P)H oxidase. SFRR, September 2010, Oslo, Norway

Schupp N; **Queisser N**; Oli G; Stopper H:
> Angiotensin II and aldosterone cause DNA damage and formation of the mutagenic 8-oxodG in kidney cells and animal models of elevated blood pressure. SFRR, September 2010, Oslo, Norway

Schupp N, **Queisser N**, Schweda F, Stopper H:
> DNA damage in kidney cells, in the isolated perfused kidney and in kidneys of rat models of elevated blood pressure by angiotensin II and aldosterone**.** XLVII ERA-EDTA Congress - II DGfN Congress, June 2010, Munich, Germany

Schupp N, Kolkhof P, **Queisser N**, Bärfacker L, Kretschmer A, Hartmann E, Schäfer S, Stopper H:
> Aldosterone causes DNA damage in vitro and in kidneys of DOCA/salt rats. DGPT, March 2010, Mainz, Germany
> Oral presentation

Queisser N, Schupp N, Stopper H, Oteiza P:
> Reactive oxygen species are involved in aldosterone-induced DNA damage and NF-κB activation in kidney cells. SFRBM, November 2009, San Francisco, USA

Schupp N, Kolkhof P, **Queisser N**, Bärfacker L, Kretschmer A, Hartmann E, Schäfer S, Stopper H:
> Aldosterone causes DNA damage in vitro and in kidneys of DOCA/salt rats, mediated by the mineralocorticoid receptor. 46th Congress of the European Societies of Toxicology, September 2009, Dresden, Germany
> Oral presentation

Queisser N, Schupp N, Stopper H, Oteiza P:
> Aldosterone activates NF-κB in kidney cells through NADPH oxidase-mediated oxidant production. SFRR, August 2009, Rome, Italy

Queisser N, Schupp N, Stopper H, Oteiza P:
> Aldosterone activates NF-κB in kidney cells through NADPH oxidase-mediated oxidant production. EEMS, August 2009, Florence, Italy

Queisser N, Stopper H, Kolkof P, Schäfer S, Heidland A, Schupp N:
Aldosterone-induced genomic damage is reduced by mineralocorticoid receptor antagonists. ASN, Renal week, November 2008, Philadelphia, USA

Schupp N, **Queisser N**, Schweda F, Stopper H:
Angiotensin II is genotoxic in vitro and causes DNA strand breaks in the isolated perfused kidney. ASN, Renal week, November 2008 Philadelphia, USA

Schupp N, **Queisser N**, Kolkhof P, Schäfer S, Heidland A, Stopper H:
Aldosterone-induced genomic damage is reduced by mineralocorticoid receptor antagonists. IV. Symposium on Cardiovascular Healing: Focus on Aldosterone (Leopoldina-Symposium), November 2008, Würzburg, Germany

Queisser N, Schmid U, Stopper H, Schupp N:
Aldosterone causes oxidative DNA damage. GUM Workshop, Oxidative stress and genomic damage, October 2008, Institute of Toxicology, Würzburg, Germany

Schupp N, **Queisser N**, Schweda F, Stopper H:
Angiotensin II and aldosterone cause DNA damage in vitro and in the isolated perfused mouse kidney via their receptors. Kongress für Nephrologie, September 2008, Tübingen, Germany

Queisser N, Schmid U, Stopper H, Schupp N:
Aldosterone causes oxidative DNA damage. DGPT, March 2008, Mainz, Germany

Stopper H, Schupp N, Fazeli G, **Queisser N**, Dietel B, Walitza S, Gerlach M:
Genotoxizität von Dopamin in vitro. DGPT, March 2008, Mainz, Germany

Schupp N, Schmid U, Kolkhof P, **Queisser N**, Schäfer S, Heidland A, Stopper H:
Aldosterone-induced genomic damage is reduced by mineralocorticoid receptor antagonists. Kongress Hypertonie, November 2007, Bochum, Germany

Queisser N, Mackenzie GG, Wolfson ML, Adamo AM, Oteiza PI:
Curcumin: a therapeutical agent in Hodgkin's lymphoma? 2nd Symposium International, Nutrition, Oxygen Biology and Medicine, April 2007, Paris, France

EHRENWÖRTLICHE ERKLÄRUNG

Hiermit erkläre ich, dass ich die Arbeit selbstständig verfasst habe und keine anderen als die von mir angegebenen Quellen und Hilfsmittel benutzt habe.

Ferner erkläre ich, dass ich nicht anderweitig mit oder ohne Erfolg versucht habe, diese Dissertation in gleicher oder ähnlicher Form einzureichen.

Ich habe keine Doktorprüfung an einer anderen Hochschule abgelegt oder endgültig nicht bestanden.

Würzburg, den 24.09.2010

Nina Queisser